

Molybdenum and Tungsten Enzymes

Bioinorganic Chemistry

RSC Metallobiology Series

Editor-in-Chief:

Professor C. David Garner, *University of Nottingham, UK*

Series Editors:

Professor Hongzhe Sun, *University of Hong Kong, China*

Professor Anthony Wedd, *University of Melbourne, Australia*

Professor Stefano L. Ciurli, *University of Bologna, Italy*

Editorial Advisor:

Professor Alison Butler, *University of California Santa Barbara, USA*

Titles in the Series:

- 1: Mechanisms and Metal Involvement in Neurodegenerative Diseases
- 2: Binding, Transport and Storage of Metal Ions in Biological Cells
- 3: 2-Oxoglutarate-Dependent Oxygenases
- 4: Heme Peroxidases
- 5: Molybdenum and Tungsten Enzymes: Biochemistry
- 6: Molybdenum and Tungsten Enzymes: Bioinorganic Chemistry

How to obtain future titles on publication:

A standing order plan is available for this series. A standing order will bring delivery of each new volume immediately on publication.

For further information please contact:

Book Sales Department, Royal Society of Chemistry, Thomas Graham House, Science Park, Milton Road, Cambridge, CB4 0WF, UK

Telephone: +44 (0)1223 420066, Fax: +44 (0)1223 420247,

Email: booksales@rsc.org

Visit our website at www.rsc.org/books

Molybdenum and Tungsten Enzymes

Bioinorganic Chemistry

Edited by

Russ Hille

University of California, Riverside, CA, USA

Email: russ.hille@ucr.edu

Carola Schulzke

University of Greifswald, Germany

Email: carola.schulzke@uni-greifswald.de

and

Martin L. Kirk

University of New Mexico, Albuquerque, NM, USA

Email: mkirk@unm.edu



RSC Metallobiology Series No. 6

Print ISBN: 978-1-78262-877-4

PDF eISBN: 978-1-78262-882-8

EPUB eISBN: 978-1-78262-883-5

Three-volume set print ISBN: 978-1-78262-879-8

ISSN: 2045-547X

A catalogue record for this book is available from the British Library

© The Royal Society of Chemistry 2017

All rights reserved

Apart from fair dealing for the purposes of research for non-commercial purposes or for private study, criticism or review, as permitted under the Copyright, Designs and Patents Act 1988 and the Copyright and Related Rights Regulations 2003, this publication may not be reproduced, stored or transmitted, in any form or by any means, without the prior permission in writing of The Royal Society of Chemistry or the copyright owner, or in the case of reproduction in accordance with the terms of licences issued by the Copyright Licensing Agency in the UK, or in accordance with the terms of the licences issued by the appropriate Reproduction Rights Organization outside the UK. Enquiries concerning reproduction outside the terms stated here should be sent to The Royal Society of Chemistry at the address printed on this page.

The RSC is not responsible for individual opinions expressed in this work.

The authors have sought to locate owners of all reproduced material not in their own possession and trust that no copyrights have been inadvertently infringed.

Published by The Royal Society of Chemistry,
Thomas Graham House, Science Park, Milton Road,
Cambridge CB4 0WF, UK

Registered Charity Number 207890

For further information see our website at www.rsc.org

Printed in the United Kingdom by CPI Group (UK) Ltd, Croydon, CR0 4YY, UK

Preface

In the late 1950s and early 1960s, evidence was accumulating that molybdenum was not simply present in the enzyme xanthine oxidase from cow's milk but that it was required for its activity and changed its oxidation state in the course of the reaction with substrate. In a *tour-de-force* isotopic substitution study reported in *Nature* in 1966, R.C. Bray and L.S. Meriwether demonstrated unequivocally that the EPR signals elicited by the enzyme upon treatment with xanthine arose from a molybdenum-containing active site. It is a happy coincidence but altogether fitting that this volume marks the 50th anniversary of this seminal work.

For many years, only five enzymes were recognized as possessing molybdenum in their active sites: nitrogenase from bacteria such as *Klebsiella pneumoniae* and *Azotobacter vinelandii*; xanthine oxidase from bovine milk (and other vertebrate sources); aldehyde oxidase from vertebrate as well as bacterial sources; the vertebrate sulfite oxidase; and the assimilatory nitrate reductase from plants (and algae and fungi). That began to change in the 1980s with the demonstration by K. V. Rajagopalan that an organic cofactor accompanied the molybdenum in the active sites of these enzymes (with the exception of nitrogenase), and with the contemporaneous discovery that tungsten was also found in the active sites of enzymes in certain bacteria.

There are now several dozen molybdenum- and tungsten-containing enzymes that have been crystallographically characterized, along with most of the enzymes responsible for the biosynthesis of the organic cofactor variously known as molybdopterin, tungstopterin and pyranopterin. The active site metal centres of these enzymes have proven to be fascinating and challenging targets for synthetic inorganic chemists, and both enzymes and synthetic models have proven fertile ground for the application of a range of physicochemical and spectroscopic methods probing their physical and electronic structures as well as their intrinsic reactivity. At present, well over

50 molybdenum- and tungsten-containing enzymes have been isolated and characterized, and these have been found to catalyze a broad range of oxidation-reduction reactions, and even reactions that (at least formally) do not involve oxidation-reduction of substrate. These enzymes are found in a wide range of metabolic pathways and play particularly prominent roles in the global cycling of nitrogen, sulfur and carbon. Many have vital roles in bacterial bioenergetics, catalyzing crucial energy-conserving reactions under a variety of growth conditions. Indeed, they seem to have been among the earliest enzyme systems to have arisen, as reflected in their near-universal distribution in the biosphere. Finally, genomics analyses have led to the identification of hundreds of genes encoding putative new proteins that are likely to possess one or another metal. These systems represent an enormous frontier of new enzymes that remains to be explored.

This title provides an up-to-date account of the state of our understanding of molybdenum and tungsten enzymes and is divided into three volumes, dealing with: (1) the enzymes themselves, along with pyranopterin cofactor biosynthesis and incorporation of the mature cofactor into apoprotein (*Molybdenum and Tungsten Enzymes: Biochemistry*), (2) inorganic complexes that model the structures and/or reactivity of the active sites of each major group of molybdenum and tungsten enzymes (*Molybdenum and Tungsten Enzymes: Inorganic Chemistry*) and (3) spectroscopic and related methods of physical chemistry (including computational work) that have been applied to both enzymes and model compounds (*Molybdenum and Tungsten Enzymes: Physical Methods*). Each volume is introduced by an overview chapter written by a leading expert in the field, followed by the individual chapters that detail specific topics associated with each volume. The intent of these overview chapters is to provide an overarching and unifying theme that places each of the three major subject areas in proper context.

We are deeply indebted to each of the contributors for their efforts, which lay out the current state of our understanding in each of the many subject areas considered. The coverage of these volumes is inevitably incomplete due to space constraints, however, and for this we apologize. However, the topics that are covered are presented to the reader in considerable detail; written in a style and spirit that will be fully accessible by current researchers in the field as well as those who wish to learn more about these fascinating metalloproteins. We sincerely hope that these volumes will underscore how rapid the progress has been over the past decade or so, and also how rapidly the field is expanding. The ultimate goal is to stimulate further research on molybdenum and tungsten enzymes, and especially to encourage new investigators to take up one or another aspect of these systems. It seems inevitable that many exciting new discoveries lie in wait.

Russ Hille
Carola Schulzke
Martin L. Kirk

Dedication



It is all too fitting that these volumes dealing with the bioinorganic chemistry of molybdenum and tungsten be dedicated to three outstanding chemists whose contributions to the field over many years continues to inform, illuminate and inspire: Richard H. Holm, C. David Garner and John H. Enemark.

Prof. Holm has over 500 research publications (cited over 35 000 times) covering a wide range of nickel, iron and molybdenum chemistry (among other transition metals). He is perhaps most widely recognized for studies, beginning in the 1970s, that describe the synthesis and characterization of iron-sulfur clusters. This work came to include modelling the M and P clusters of nitrogenase, which perhaps provided the motivation to investigate models of mononuclear molybdenum-containing enzymes. His molybdenum work achieved great success with the synthesis of MoO₂ models for enzymes of the sulfite oxidase, and later the DMSO reductase family, and the characterization of their properties as oxygen atom transfer catalysts. A key contribution was his use of bulky ligands to the metal that prevented μ-oxo

dimerization, which had long stymied work in the field. He is Higgins Professor of Chemistry at Harvard University, a member of the National Academy of Sciences and the recipient of many other awards.

Prof. Garner already had a strong track record in the synthesis of copper and molybdenum complexes when, beginning in the late 1970s, he became one of the first researchers to apply the then-new analytical method of X-ray absorption spectroscopy not only to models of molybdenum enzymes but also to the enzymes themselves. The discovery of thiolate-like sulfur, Mo=O and Mo=S ligands to the metal in the active sites of enzymes such as sulfite oxidase, xanthine oxidase and DMSO reductase was critical in establishing the molybdenum coordination environment in these enzymes and greatly focused efforts to synthesize accurate structural and functional mimics of the enzymes. With over 300 publications (having over 8000 citations), he is presently Professor Emeritus at the University of Nottingham and a Fellow of the Royal Society. He is also past President of the Royal Society of Chemistry.

Prof. Enemark was already well recognized for his work on metal nitrosyls and related systems when he began to exploit the tris-pyrazolylborate ligand as a scaffold on which to construct and study MoO₂ and MoO complexes. This work led to the synthesis and characterization of the first model that fully mimicked the catalytic cycle of oxotransferase enzymes such as sulfite oxidase. Enemark also played an instrumental role in the work that led to the first crystal structure of sulfite oxidase. Since that time, Enemark has pioneered the application of pulsed EPR methods to molybdenum enzymes and synthetic models of their active sites; work that has led to a deep understanding of not simply the physical but also the electronic structures of these systems. With over 250 publications and 10 000 citations, he is Regents Professor of Chemistry at the University of Arizona, a former Fulbright Scholar and recipient of the Humboldt Research Prize, among other national and international recognitions.

Contents

Chapter 1 An Overview of the Synthetic Strategies, Reaction Mechanisms and Kinetics of Model Compounds Relevant to Molybdenum- and Tungsten-Containing Enzymes	1
<i>Carola Schulzke</i>	
Introduction and Overview	1
Chapter 2 Pterin-Inspired Model Compounds of Molybdenum Enzymes	8
<i>Sharon J. Nieter Burgmayer, Benjamin R. Williams, and Partha Basu</i>	
2.1 Introduction	8
2.2 Unveiling the Pterin Component of Moco	10
2.2.1 The Pterin is Discovered	10
2.3 Development of Pterin-Inspired Models	15
2.3.1 First-Generation Models	15
2.3.2 Second-Generation Dithiolene Pterins and their Complexes	33
2.3.3 Third-Generation Dithiolene Pterins and their Complexes	43
2.3.4 Chemical Behavior of Dithiolenes Substituted by Pterin and N-Heterocycles	53
2.4 Unresolved Questions and Current Objectives	57
Acknowledgement	59
References	59

Chapter 3	Electron Transfer Mechanisms in Molybdenum and Tungsten Model Compounds	68
<i>Bholanath Pakhira, Rudra Sarkar, and Sabyasachi Sarkar</i>		
3.1	Introduction to Molybdenum and Tungsten	68
3.1.1	Role in Biology	69
3.2	Model Systems	70
3.3	Electron Transfer in Molybdoenzymes	78
3.3.1	Principle Involved in Electron Transfer Reactions	80
3.4	Conclusion	87
	References	88
Chapter 4	Comparative Kinetics of Enzymes and Models	94
<i>Christian Fischer and Lina Fischer</i>		
4.1	Active Sites of Molybdenum and Tungsten Enzymes	94
4.2	General Remarks on Michaelis–Menten Kinetics	96
4.2.1	Determination of Michaelis–Menten Parameters	100
4.2.2	Michaelis–Menten Kinetics for Oxygen Transfer Reactions – “Quo Vadis?”	103
4.3	Kinetic Aspects of Oxygen Transfer Reactions – Enzymes vs. Models	106
4.3.1	Oxygen Transfer Reactions Mediated by Enzymes	106
4.3.2	Studying Half-Reactions of Model Complexes	107
4.3.3	Selected Historical Steps in Functional Model Development	116
4.3.4	Half-Reaction Kinetics Applied to a Two-Substrate Catalytic Cycle – A Simulation	121
4.4	Dedication and Acknowledgements	124
	References	125
Chapter 5	Synthetic Models of the Nitrogenase Clusters	130
<i>Sonny C. Lee</i>		
5.1	Introduction	130
5.2	The Nitrogenase Metalloclusters: A Synthetic Perspective	131
5.2.1	The F-Cluster	132
5.2.2	The P-Cluster	132
5.2.3	The FeMo-Cofactor	133
5.3	Synthetic Considerations	134
5.4	F-Cluster Analogues: The All-Ferrous State	136

Contents

xi

5.5 Modeling the Nitrogenase Superclusters	137
5.5.1 Heterometallic Cores	137
5.5.2 Topological Analogues	141
5.5.3 Heteroligated Cores	148
5.6 Cluster Assembly Mechanisms: Chalcogen-Labeled Cores	154
5.7 Status and Prospects	158
Abbreviations	158
Acknowledgements	159
References	159
Chapter 6 Synthesis of Mono- and Bisdithiolene Molybdenum and Tungsten Model Compounds	166
<i>Hideki Sugimoto</i>	
6.1 Introduction	166
6.2 Model Compounds for the DMSOR Family	169
6.2.1 The Mo ^{VI} O ₂ and Mo ^{IV} O Couple	170
6.2.2 The Mo ^{VI} O and Mo ^{IV} Couple	176
6.2.3 Mo ^{VI} S(Se-R) and Mo ^{IV} S Couple	181
6.3 Model Compounds for the Sulfite Oxidase Family	182
6.4 Model Compounds for the Xanthine Oxidase Family	183
6.5 W-substituted Model Compounds for the DMSOR and Xanthine Oxidase Families	185
6.6 Model Compounds for Tungsten-Dependent Enzymes	186
6.6.1 The W ^{VI} O(S) Center	186
6.6.2 The W ^{VI} S(Se-R) Center	188
6.6.3 The W ^{VI} (CO/CN)(SR) Center	189
6.6.4 The Unidentified W Center	189
6.7 Conclusion	190
References	190
Chapter 7 Models for the Xanthine Oxidase Family of Enzymes	194
<i>Charles G. Young</i>	
7.1 Introduction	194
7.2 Molybdenum Hydroxylases	195
7.2.1 Overview of the Enzymes	195
7.2.2 Key Discoveries Informing Model Studies	196
7.2.3 Active Sites and Model Targets	199
7.3 Active Site Components: Synthetic Background	200
7.3.1 General Challenges	200
7.3.2 The Chalcogenido Components: Background, Synthetic Approaches and Reagents	201
7.3.3 The Mono(dithiolene) Component: Background and Synthetic Approaches	207
7.3.4 Maintaining Mononuclearity Post-Synthesis	209

7.4 Molybdenum Hydroxylase Models	211
7.4.1 Models of Enzymes Containing Oxosulfido and Oxo-selenido Active Sites	211
7.4.2 Models for the MoO(μ -S)Cu Active Site of CODH	223
7.5 Conclusion	226
Dedication and Acknowledgements	227
References	228
Subject Index	239

CHAPTER 1

An Overview of the Synthetic Strategies, Reaction Mechanisms and Kinetics of Model Compounds Relevant to Molybdenum- and Tungsten-Containing Enzymes

CAROLA SCHULZKE^a

^aInstitut für Biochemie, Ernst-Moritz-Arndt Universität Greifswald,
Felix-Hausdorff-Straße 4, D-17487 Greifswald, Germany

*E-mail: carola.schulzke@uni-greifswald.de

Introduction and Overview

Bioinorganic model chemistry in general comprises synthesizing complexes which resemble the natural active sites of metalloproteins with respect to either structure or function or (preferably) both and investigating their structural and spectroscopic characteristics and/or reactivity, most often in comparison with results from biological samples. This is important for a detailed understanding of the roles of metal, ligands and specific functional groups in the processes taking place at the active sites.

The following chapters in *Molybdenum and Tungsten Enzymes: Inorganic Chemistry* review advances in the field of molybdenum- and tungsten-dependent oxidoreductases and nitrogenase by bioinorganic model chemistry, or more precisely the synthetic and catalytic evaluation of model systems. All this falls into the core expertise of two of the three outstanding scientists to whom this book is dedicated. Both Richard H. Holm and C. David Garner have contributed formidably to the field of molybdenum and tungsten model chemistry for the respective molybdenum cofactor (Moco) and tungsten cofactor (Wco) bearing enzymes. Although with generally the same goal, *i.e.* furthering the understanding of the electronic and steric specifics of the respective active sites and their reactivity, the approaches of the two groups were quite distinct. Holm and coworkers created model systems for the immediate coordination spheres even of those enzymes that were most difficult to mimic, their chemical composition being rather uncommon in inorganic chemistry. Garner, often in cooperation with organic chemist John A. Joule, designed ligand model systems mimicking more of the rather complex natural ligand molybdopterin by synthesizing asymmetrically substituted dithiolene ligands bearing N-heterocyclic groups, even investigating different tautomeric forms thereof; all this in relation to the pterin part now presumed (based on protein structural findings) to play a substantial role for the reactivity of the oxidoreductases. Current work by the community attempts to unify these two approaches in order to accomplish the organic-inorganic synthesis of increasingly accurate Moco and Wco models with a perfect match still being elusive.

The authors of the following chapters have in their own work necessarily been inspired by the synthetic foundations of this field laid by Holm and Garner and some were even fortunate enough to have directly participated as their coworkers.

Holm has in addition for many years been involved in nitrogenase model chemistry. Pivotal work on the enzyme includes establishing the presence of the Fe₄S₄-ferredoxins in the α₂β₂ complex by their extrusion and characterization, utilizing ¹⁹F NMR spectroscopy for determining the magnetic moment of molybdenum in the M-Cluster at ambient temperature and investigating the binding of small molecules to the isolated M-Cluster. His synthetic contributions comprise the earliest syntheses of Fe–Mo–S clusters, the extension of this initial work to clusters with high nuclearity, double cubanes that served as topological models of the nitrogenase P-Cluster. This work included investigations of the reactivity of these model systems, demonstrating for example that it is possible to transform the alternate nitrogenase substrate acetylene to ethylene with model clusters. All this was indispensable in developing a molecular description of the metal sites in the nitrogenase. In his work, Holm always considered the “big picture”, meaning: instead of getting lost in utmost detail, he continued to question and investigate with perseverance the discrepancies observed between what was found in the proteins and what could be achieved in the chemical lab, still a key question for many areas of bioinorganic chemistry.

Today nitrogenase model chemistry has come quite a long way and some amazing science has been carried out. Still, we remain quite far away from being able to mimic the M-Cluster with all its features. This is partly due to the fact that for decades chemists tried to model a molybdenum–iron cluster, lacking an interstitial atom, now recognized to be carbon.

The structural model chemistry for both the nitrogenase and molybdopterin-containing cofactors is now well developed. At the same time, there are still important features of the active sites that await accurate modelling by bioinorganic chemists. This is what keeps this field challenging and interesting for the respective communities made up of scientists with vision and perseverance.

As will be laid out in the following chapters with respect to molybdopterin (MPT), a complex has been published by Sharon Burgmayer (co-author of Chapter 2 in this volume), which is the closest structural MPT-focused model for the active sites known today. There are only minimal differences (oxidation state of the nitrogen atoms in the pyrazine part, for instance) to the natural molecule, although these may have an important impact on reactivity. Incorporating this MPT model or another one developed by Partha Basu to a molybdenum or tungsten centre which more closely resembles the actual active site would be a fantastic achievement, although admittedly the respective chemistry is very difficult. In fact, a combination of model chemistry focusing on mimicking molybdopterin and of the immediate coordination sphere would actually involve merging Garner's and Holm's achievements and constitutes the most challenging aim of the respective bioinorganic community nowadays. Most likely it will be the active site of arsenite oxidase that will be modelled in all detail first, since in its reduced form it resembles molybdenum dithiolene complexes which are most common, *i.e.* mono-oxo bis-dithiolene molybdates (iv). For any other enzyme, model chemistry is more difficult as the active sites typically do not bear an oxo ligand together with two molybdopterins in their reduced form. Therefore, in addition to simply coordinating a more or less close molybdopterin model to molybdenum (and tungsten) it will also be necessary to fine-tune procedures allowing modification of such models, namely replacing the oxo ligand by ligands mimicking coordination to the peptide (alcoholates, thiolates *etc.*), replacing one dithiolene by a sulfido, oxo, hydroxide or hydrosulfido ligand, oxidizing the model to oxidation states v (intermediate in the catalytic cycle) and vi (the opposite end of the catalytic process) and to make the compounds water insensitive and water soluble. All this has been done before with complexes with simpler dithiolene ligands or with other ligand systems. Once the functional groups of MPT are present, however, the respective chemistry becomes unknown ground and very difficult. And this is not all. Even though a dithiolene ligand with all the functional groups of MPT is requisite for allowing detailed structure–function relationships to be studied, it will probably not be enough. In order to really understand the distinct function of a specific structural motif of MPT it will be necessary to compare the electronic states, the catalytic potential and the stability of models with and

without this specific motif. Eventually, the bioinorganic chemists' efforts will have to be united with those of the biologists. The models have to be tested with regard to being incorporated into the apoenzymes or recognized by the respective chaperones that can insert them into the enzymes.

Semisynthetic enzymes will have to be prepared and compared for their activity and need to be spectroscopically characterized. The requirements for models in a biological environment are high with respect to stability and solubility; another challenge for the bioinorganic chemist.

None of the above is trivial work and it is certainly impossible for one group only to address all these issues. Even though the community is not huge, the determination of its members is and the work of many contributors in this field is heading in one or another of the directions described above.

Only when looking at all the results of all the individual contributors to this field and combining these insights can we understand and describe the inorganic chemistry of the respective active sites really accurately.

As many cooperative efforts are required, the specific fields laid out in the following chapters, intended to inform in all needed detail, cannot be viewed completely independently from each other. Consequently there will be some overlap between the individual chapters, which should still provide a suitable reading experience for all types of readers.

In Chapter 6, Hideki Sugimoto reviews model systems for molybdenum and tungsten oxidoreductases which bear one (mimicking sulfite oxidase family, xanthine oxidoreductase family) or two (mimicking DMSO reductase family and tungsten enzymes) dithiolenes, and focuses to some extent on the first and second coordination shell of the enzymes. Sugimoto published the first structurally characterized model with dithiolene ligands bearing the pyrane ring of MPT, extending the respective model chemistry a bit farther out and contributing some interesting and detailed studies about the electronic properties of a variety of dithiolene model systems. Dithiolene ligands are special as they are non-innocent ligands, and can directly participate in oxidation-reduction reactions. This also means that it is not trivial working with these fascinating molecules. Both Garner and Holm developed procedures for the synthetic chemistry which are still widely applied today and without which there would hardly be any structural model chemistry of molybdenum and tungsten enzymes possible.

In Chapter 2, Partha Basu and Sharon Burgmayer detail the progress model chemistry has made with a focus on all the features of molybdopterin. Basu was a postdoc with John Enemark, the third outstanding scientist to whom this book is dedicated, whose work has focused on spectroscopy as much as synthesis. Burgmayer has received training in the group of Ed Stiefel, another founding father of the respective bioinorganic chemistry, and she was introduced to pterins early on in her career. Both Basu and Burgmayer have for many years, both independently and in collaboration, furthered the model chemistry of N-heterocyclic dithiolene chemistry. Burgmayer has developed the molybdenum bound model system which is most closely related to the natural molybdopterin today and is deeply involved in bringing pterin

chemistry together with pyrane and dithiolene chemistry. Basu follows different, complementing approaches towards the same goal and along the way managed to exploit the interesting chemistry these electronically flexible systems provide, for instance in the field of heavy metal ion sensing. Pterin chemistry *per se* is well understood, although elaborating pterins with pyrane and dithiolene moieties becomes incredibly complicated.

In Chapter 7, Charles G. Young outlines the bioinorganic efforts to understand enzymes of the xanthine oxidase family. These enzymes distinguish themselves from the other families in that (1) they do not catalyze the typical oxygen atom transfer reaction but rather the insertion of an oxygen atom into a C–H bond, *i.e.* they are hydroxylases; and (2), they bear a sulfido ligand in the active site which is crucial for catalytic activity. Young has worked for decades in this field and designed many model systems which have furthered our understanding of the sulfido ligand's role for the electronic states of the central metal and the complexes' (and hence enzymes') reactivity. The respective chemistry is very difficult, particularly when trying to address all ligands of the natural cofactors. Most often, for example, an auxiliary ligand system in place of the dithiolenes is used for stabilizing the respective complexes allowing the detailed investigations on the sulfide ligand's relevance to be carried out.

Young has extensively cooperated with many in the area of bioinorganic spectroscopy, including John Enemark, with whom he was a postdoc.

With respect to the catalytic evaluation of model compounds of the molybdenum and tungsten cofactors, it was Holm who first characterized a model system catalyzing oxygen atom transfer, *i.e.* the oxidation of triphenylphosphine by dimethyl sulfoxide. This model reaction is now an indispensable tool for the bioinorganic Moco/Wco community. The reaction takes place at ambient conditions only when catalyzed and it can be nicely followed by phosphorous NMR. Although DMSO actually is a natural substrate (as the DMSO reductase family evidences), triphenylphosphine is not and recent and current efforts have focused on more physiologically relevant reactions with the most difficult task of employing water as solvent and/or substrate. The authors of the two chapters dealing with catalysis and kinetics are involved in the respective developments. In particular, Sabyasachi Sarkar has been responsible for some of the most exciting findings in this field by employing a comparatively simple model system which turned out to be a fabulous work horse.

In Chapter 3, Sabyasachi Sarkar describes the achievements that were made in applying model systems in catalytic processes mimicking natural enzymatic substrate transformations and in understanding the respective mechanisms in detail. Among other achievements in this area he discovered the catalytic potential of comparatively simple dithiolene-bearing model compounds employing maleonitrile ligands $[MO_x(mnt)_2]^{2-}$ ($M = Mo, W; x = 1, 2$). He coaxed some surprising substrate transformations out of these small complexes by fine-tuning the respective reaction conditions. Reactions described by Sarkar and coworkers include transformation of hydrogensulfite

to hydrogensulfate relevant for sulfite oxidase, the reduction of hydrogencarbonate to formate at pH 7.5, *i.e.* basically transformation of CO₂ and relevant for tungsten-formate dehydrogenase, the oxidation of aldehydes to carboxylic acids relevant for aldehyde oxidase and the transformation of acetylene to acetaldehyde relevant for the extraordinary tungsten-dependent acetylene hydratase plus various non-natural substrates like phosphanes.

Sarkar too has cooperated with John Enemark in the past, emphasizing that many specialists with different expertise are needed in order to understand the molybdenum and tungsten oxidoreductases in detail, in particular when it comes to reactivity.

In Chapter 4, Christian Fischer reviews catalytic properties of models and enzymes more specifically. This chapter includes a detailed kinetic evaluation of the catalytic systems. As a young academic Fischer has only recently started working in the field of molybdenum- and tungsten-dependent enzymes. He has graduated from the Leibnitz Institute of Catalysis led by Matthias Beller and is an expert in the field of catalysis. His involvement will hopefully extend what we know about the kinetics of models and enzymes continuing Holm's excellent work in this field. Notably, Fischer has already developed and investigated the first catalytic system being able to operate in pure water.

In the case of the bioinorganic chemistry relevant for nitrogenase, the determination of the presence of an interstitial carbon at the centre of the M-Cluster of nitrogenase has fuelled much new model chemistry. At present, there are only three variants known of the M-Cluster with vanadium or iron in place of the molybdenum but no variation of the general cluster structure or coordination environment. Therefore structural models are rather scarce, particularly when compared with the Moco or Wco chemistry. When it comes to functional models, the achievements in particular of the last years are impressive. Many molybdenum systems and now even a few iron complexes are known which can catalytically reduce the rather inert elemental nitrogen to ammonia. These model systems are intended to mimic the natural process because it would be industrially immensely important being able to split the nitrogen triple bond catalytically at mild conditions. More importantly, from a bioinorganic point of view it would be very important to reliably identify the place on the M-Cluster where nitrogen is bound and transformed. Although recent work of Dean, Hoffman and Seefeldt strongly supports binding of N₂ on the Fe_{2,3,6,7} face of the M-Cluster, nitrogenase has still not been "caught in the act" of nitrogen binding crystallographically. Advocates of molybdenum- and iron-based chemistry have been fighting over this for decades and we still do not know with absolute certainty what happens at the active site of this intriguing, long-known and yet mysterious enzyme. In Chapter 5, Sonny Lee, a former coworker of Holm in this particular field, has taken on the huge task to guide the reader through the various fundamental and recent developments in the bioinorganic model chemistry of nitrogenase.

The work of each of the authors contributing to this volume has been seminal with respect to developing the most accurate models of molybdopterin and for the structures and functions of the molybdenum- and

tungsten-containing centres of nitrogenase and oxidoreductase, the best of the latter being able to catalyze biologically relevant reactions. Most of the authors have been directly involved in the outstanding achievements of those this book is dedicated to.

I am thankful to all of them for having expertly detailed the fundamental and the recent advancements in the field of molybdenum and tungsten bioinorganic chemistry. Further, I am immensely grateful to C. David Garner and Richard H. Holm in particular, and also to John Enemark for having inspired me at the beginning of my independent academic work to an extent that it was actually their work that made me choose my scientific home in this field of research.

CHAPTER 2

Pterin-Inspired Model Compounds of Molybdenum Enzymes

SHARON J. NIETER BURGMAYER^{*a}, BENJAMIN R. WILLIAMS^a,
AND PARTHA BASU^{*b†}

^aDepartment, of Chemistry, Bryn Mawr College, Bryn Mawr, PA 19010, USA;

^bDepartment of Chemistry and Biochemistry, Duquesne University,
Pittsburgh, PA 15282, USA

*E-mail: sburgmay@brynmawr.edu, brwilliams@brynmawr.edu

2.1 Introduction

The molybdenum cofactor (Moco) is an extraordinary molecule in biology. As a small metal-containing compound, it has the unprecedented combination of a dithiolene chelate for metal binding and a pterin appended to a pyran ring. The resultant cofactor is electronically nimble due to the presence of three redox active moieties, *i.e.* the molybdenum atom, the dithiolene and the pterin, which in concert can support a range of redox events.

The long history of modeling Moco dates back nearly 50 years.¹ The early models were developed before the pterin in Moco was identified and before

[†]Present address: Department of Chemistry and Chemical Biology, Indiana University Purdue University at Indianapolis, Indianapolis, IN 46202, Email: basup@iupui.edu.

a structure of Moco had been determined by X-ray crystallography. Yet these early models provided a base of knowledge from which an understanding of possible mechanisms and of the electronic environment within the Mo inner coordination sphere was built. The chapters in this second volume discuss the contributions made by others that enhanced our knowledge of the function of molybdenum and tungsten enzymes.

The discovery of the pterin-substituted dithiolene ligand in Moco established a specific target for modeling chemists, albeit a target of considerable synthetic difficulty. There have been concerted efforts to reproduce aspects of the pterin-dithiolene ligand in Moco and their synthetic model systems have evolved over the past 30 years.^{1a,2} The complexity of pterin and pyranopterin chemistry starts with the different numbering systems used, and these are shown in Figure 2.1 for the pterin and pteridine ring systems, the fully reduced, open form initially proposed for Moco and two numbering systems used for the reduced pyranopterin forms of Moco.³

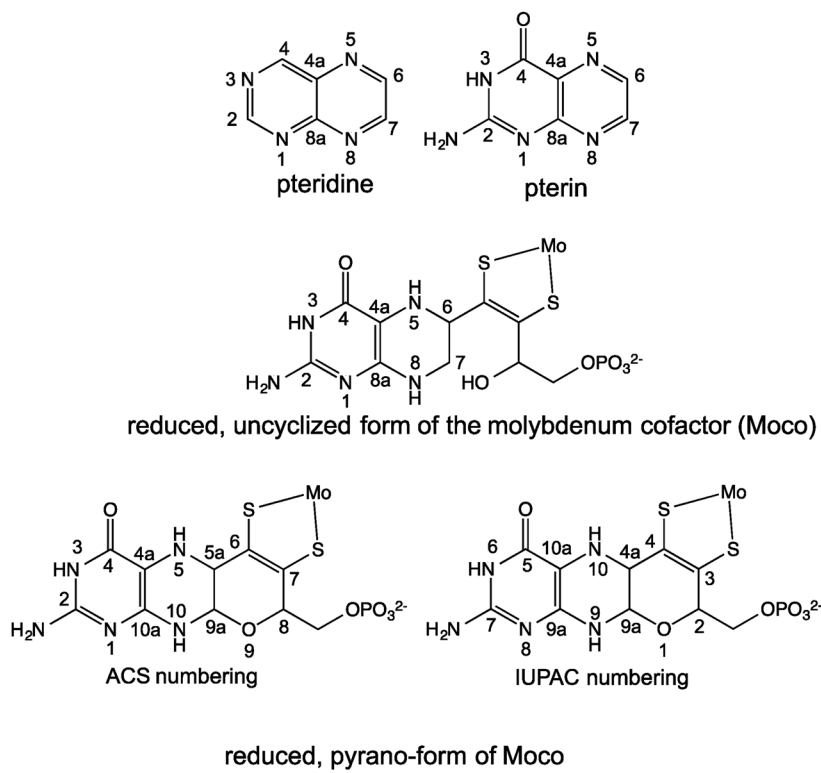


Figure 2.1 Numbering systems for pterin, a derivative of the pteridine ring system (top), in an uncyclized and fully reduced form initially proposed for Moco (middle) and as the cyclized and reduced pyranopterin form observed by crystallography in the majority of molybdenum enzymes (bottom).

The scope of this chapter is to review the model work directed towards the pterin aspects of the molybdenum cofactor. Our objective is to provide a detailed description of model work involving pterin, pteridine and related N-heterocycle systems that have been specifically developed to mimic features of Moco, as well as the study of these molecules in the absence of metal. Because the evolution of pterin models parallels the progress of revealing the pterin component of Moco, the chapter begins with a review of the key developments that unveiled the pterin ligand of Moco.

2.2 Unveiling the Pterin Component of Moco

In this section, an overview is of studies presented that revealed the presence of a pterin in molybdenum enzymes and eventually the structure of the pterin-dithiolene ligand of Moco. This background provides the context for pterin-inspired model work over the past three decades and highlights how the making of synthetic models for metal sites in enzymes follows acquisition of experimental data obtained from the metal site in the proteins.

Prior to the discovery of the molybdopterin, it had already been established that the molybdenum catalytic center of the molybdenum enzymes was part of a dissociable cofactor. Reconstitution of a Moco-deficient mutant of *Neurospora crassa nit-1* by the dissociated molybdenum cofactor from a variety of molybdoenzymes regenerated nitrate reductase activity in nit-1 further confirming that molybdenum and a particular ligand set comprised Moco.⁴ Spectroscopic studies, primarily electron paramagnetic resonance (EPR) spectroscopy and extended X-ray absorption fine structure (EXAFS) spectroscopy, had suggested both oxo and sulfur coordination in the dissociated Moco samples,^{2b,5} but the pterin component remained invisible in these studies. It was not until 1980, when fluorescence was detected in degraded Moco-containing protein samples, that an indication of the presence of a pterin emerged.⁶

2.2.1 The Pterin is Discovered

The investigation of the pterin component of Moco was a focus of Rajagopalan and his coworkers.⁷ Initially, various oxidative treatments of Moco were shown to yield different pterin species, each having distinctive fluorescence and electronic spectral signatures, and each pterin species substituted at the C6 position on the pterin system. One of these degradation products, Form B (**1**), was proposed to have a thiophene structure similar to urothione (**2**). Urothione was found to be a metabolite of Moco in humans.⁸ The sulfur atoms in **2** became the starting point for hypothesizing a dithiolene chelate attached at C6, and the dithiolene hypothesis was eventually confirmed through alkylation and trapping the dithiolene-substituted pterin.⁹ The trapped pterin-dithiolene molecule also provided further support for the reduced state of the pterin. A tetrahydropterin had been suspected from the lack of fluorescent behavior of Moco, whereas oxidative degradation of Moco containing enzyme produced highly fluorescent oxidized pterins. A pictorial summary of the pterin studies is shown in Figure 2.2.

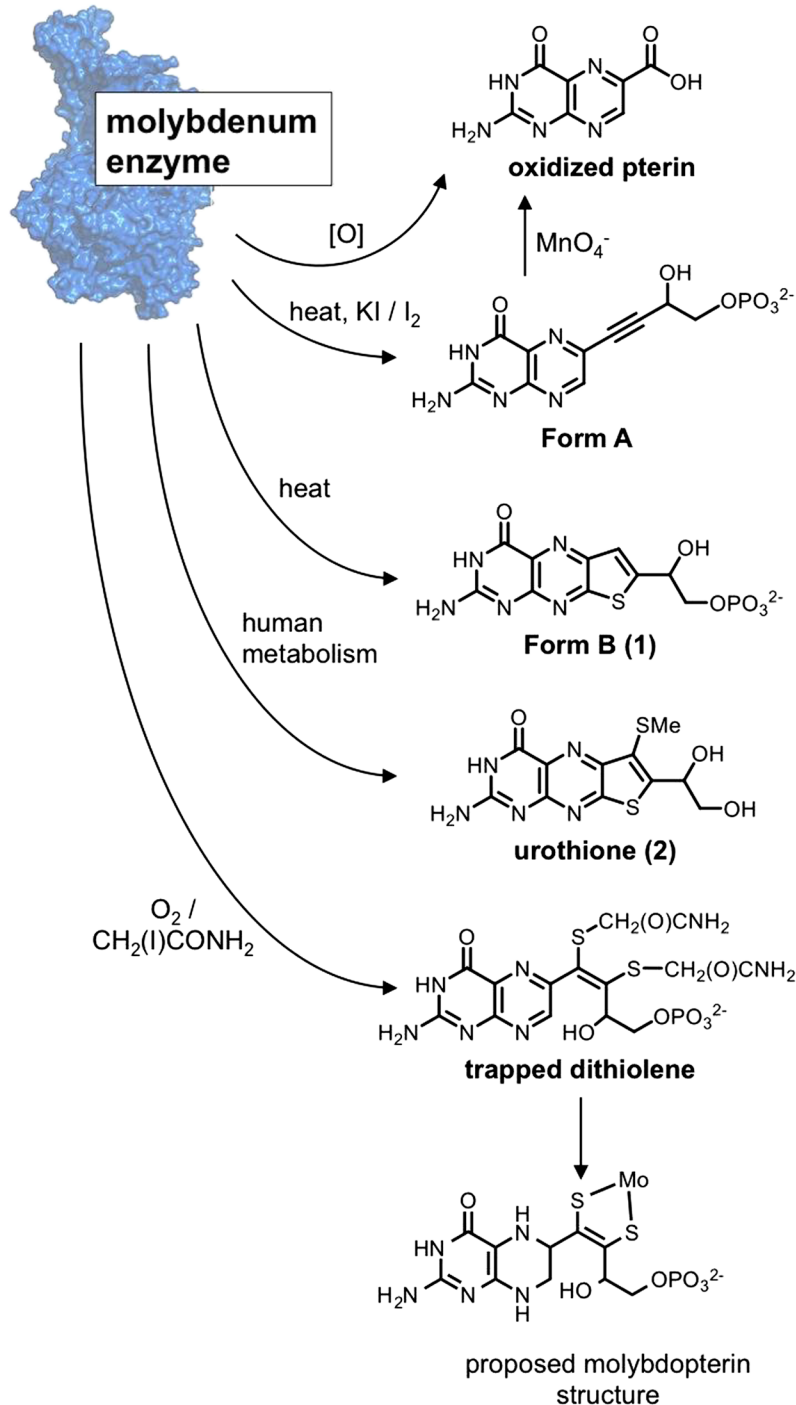


Figure 2.2 A summary of key experiments that revealed the pterin and dithiolene groups, and led Rajagopalan to propose the bottom structure for Moco.

In 1982, the culmination of these studies led to the proposal that the hidden ligand on Moco was a reduced tetrahydropterin substituted at C6 by a four-carbon chain having a dithiolene chelate at the α - and β -carbons, a hydroxyl group at the γ -carbon and terminated with a phosphate (Figure 2.1, center).^{8,10} This ligand was initially named molybdopterin for “the special ligand on molybdenum”, abbreviated as MPT. Since then, other names have been sought and used for this ligand, especially since the pterin-dithiolene ligand also is the special ligand in tungsten enzymes.^{3,11}

The tetrahydropterin-dithiolene ligand generated considerable excitement and speculation. It was unique in biochemistry, and is unusual in chemistry. While dithiolenes were well-known ligands for molybdenum and other metals, this was the first time a dithiolene was proposed to play a role in biochemistry. On the other hand, tetrahydropterins were already known molecules in biochemical processes, such as the tetrahydrobiopterin cofactor used by aromatic amino acid hydroxylases and tetrahydrofolate in C1 transfer in methionine synthesis (Figure 2.3). Certainly, this was the first time a pterin was found to be in combination with a dithiolene anywhere in chemistry.

The known redox roles of tetrahydropterins in biochemistry led Rajagopalan to investigate the redox behavior of the pterin unit of Moco. They titrated Moco within molybdoproteins (XO and SO) with two different oxidants, ferrocyanide and the redox dye dichlorophenol indophenol (DCIP),¹² and obtained unexpected results: two electron equivalents of either oxidant produced the spectral signature of a fully oxidized pterin (Scheme 2.1), a result only consistent with the pterin in Moco starting at the dihydro oxidation state rather than the tetrahydro state as initially proposed. The interpretation at the time was that the pterin in Moco, instead of the initially proposed tetrahydropterin structure, was a dihydropterin in an unusual tautomeric form.

Prior to the discovery of the pterin portion of Moco, it was assumed that all molybdenum enzymes (except nitrogenase) used the same cofactor, since

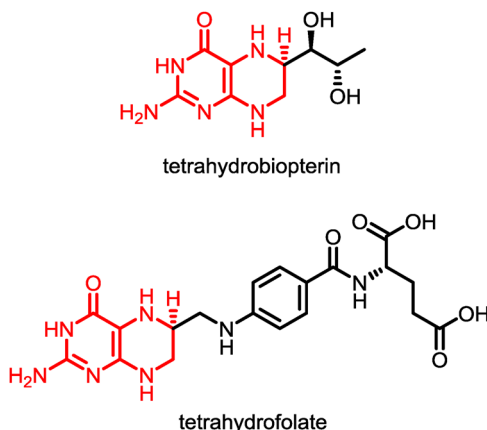
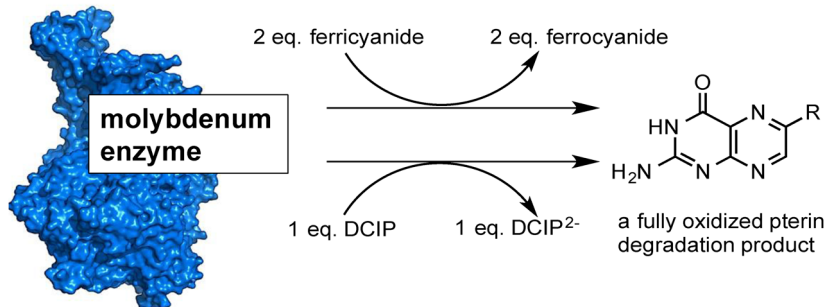


Figure 2.3 Structures of other pterins used in biochemical catalysis.



Scheme 2.1 The results of redox titration experiments on molybdoenzymes.

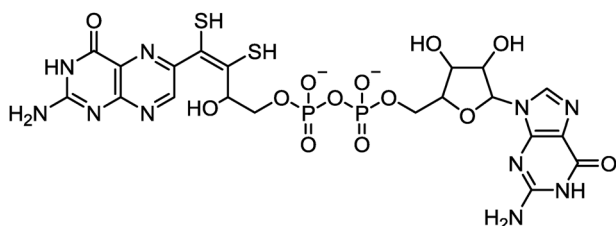


Figure 2.4 Proposed structure of MGT with appended guanosine nucleotide.

isolated Moco solutions could regenerate nitrate reductase activity in the *Neurospora crassa nit-1* mutant.^{4b,4c} Krüger *et al.*¹³ challenged the notion that the proposed Moco in Figure 2.2 was the universal structure in all molybdoenzymes in 1986 when they proposed a larger structure with a second phosphorylated aromatic unit. Rajagopalan's group's definitive analytical work on DMSOR from *Rhodobacter sphaeroides* proved that it possessed a modified MPT, described as a phosphoric anhydride of MPT and 5'-GMP (Figure 2.4), which they called MGD for molybdopterin guanosine dinucleotide.¹⁴ They noted that the relationship of MPT to MGD was analogous to that between FMN and FAD.⁷ By 1992 additional variants of MPT with adenine, cytosine, inosine dinucleotides were identified. Dinucleotide substitution on the side chain is restricted to Moco from prokaryotic sources.

After years of speculation, in 1995, the unique structure of molybdopterin was revealed by X-ray crystallography, first in the tungsten enzyme, aldehyde ferredoxin oxidoreductase isolated from the hyperthermophile *Pyrococcus furiosus*,¹⁵ and later as part of Moco in aldehyde oxidoreductase isolated from *Desulfovibrio gigas*.¹⁶ These structures confirmed most of Rajagopalan's proposal with one exception: both structures showed that the dithiolene formed a third ring, a six-membered pyran ring fused to the pterin structure, presumably through a cyclization reaction involving the side chain hydroxyl group (Figure 2.5). Since these first two structures of Mo and W proteins were reported, dozens of X-ray structures have been determined and all the structures have shown the same pyranopterin-dithiolene structure for molybdopterin, with two exceptions. The first exception was observed in 2003 for a membrane bound dissimilatory nitrate

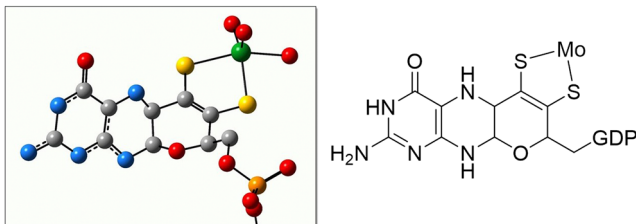


Figure 2.5 The pyranopterin structure within MPT determined by protein X-ray crystallography of aldehyde oxidoreductase from *Desulfovibrio gigas* (PDB 1DGJ, guanosine not shown).

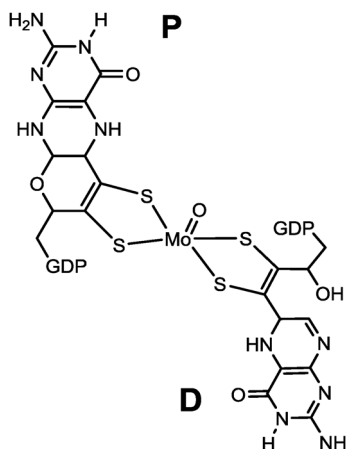


Figure 2.6 Structure of Moco found in *E. coli* dissimilatory nitrate reductase.

reductase (Nar) isolated from *Escherichia coli*.¹⁷ Moco in this protein has two MPT ligands displaying two different structures (Figure 2.6). The proximal MPT, *i.e.* the pterindithiolene closest to the Fe₄S₄ cluster involved in the electron transport chain, has the expected pyranopterin structure, but the distal MPT no longer has a pyran ring. Pyran ring cleavage had been shown to be a facile reaction in a model compound (see section 2.3.3.4) and this reaction was considered a possible role for the MPT ligand. In this regard, the Nar structure was pivotal in providing evidence that ring opening might occur in the protein. Soon after, a second example of a cleaved pyran structure at the distal MPT was available in the X-ray structure of ethylbenzene dehydrogenase isolated from *Aromatoleum aromaticum*.¹⁸

In 1993, Wuebbens and Rajagopalan reported a molecule called precursor Z (**3**)¹⁹ as a biosynthetic precursor of Moco.²⁰ This was the first stable intermediate identified in Moco biosynthesis, and soon afterwards the involvement of GTP in Moco biosynthesis in *E. coli* was reported.²¹ In 1997 a parallel scheme for plants was reported by Mendel *et al.*²² While several structures for **3** were proposed in the literature, in 2004, based on ¹H NMR data

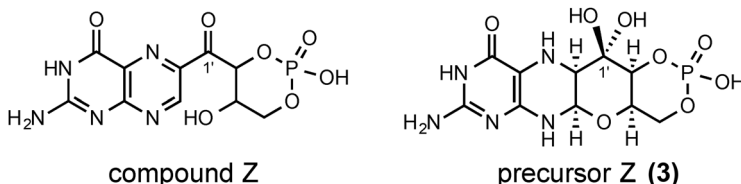


Figure 2.7 Structures of the biosynthetic precursor to MPT, precursor Z, and compound Z as the first isolated form of precursor Z.

Santamaria-Araujo *et al.* proved that 3 was a pyranopterin in the reduced state with a geminal diol formed by hydration at the C1' position (Figure 2.7).²³ By 2006 a more complete picture of Moco biosynthesis emerged.²⁴

2.3 Development of Pterin-Inspired Models

Pterin-inspired models have evolved in response to the acquisition and interpretation of new data from Moco, both from holoenzymes and from dissociated, isolated Moco samples. The key events punctuating the growing knowledge of the nature of the pterin in Moco were described in the preceding section and are graphically presented as a timeline in Figure 2.8. The development of pterin models can be appreciated and understood when compared to this timeline. For the purposes of this chapter, the pterin model evolution presented below is partitioned into three sections, described as three generations of models.

2.3.1 First-Generation Models

The earliest period of work on pterin models for Moco followed the discovery of the pterin unit within Moco, and occurred prior to the confirmation of the dithiolene chelate. These early studies explored the coordination chemistry between molybdenum and pterins or other structurally related molecules such as pteridines (Figure 2.1, top). The resulting themes of this body of work include the favorable coordination by molybdenum in several oxidation states to the O₄, N₅ chelate site in pterin (see Figure 2.1 for numbering), a variety of reactivities exhibited by Mo^{VI}-tetrahydropterin systems and the highly delocalized electronic structures in molybdenum-pterin complexes that defy formal oxidation state assignments to Mo and pterin.

2.3.1.1 Models Where Molybdenum is Coordinated Directly to Pterins

The pterin component of Moco has been fascinating – why did Nature make such a complicated heterocyclic substituent for the dithiolene tether to molybdenum? The original molybdopterin structure (Figure 2.1, center structure)

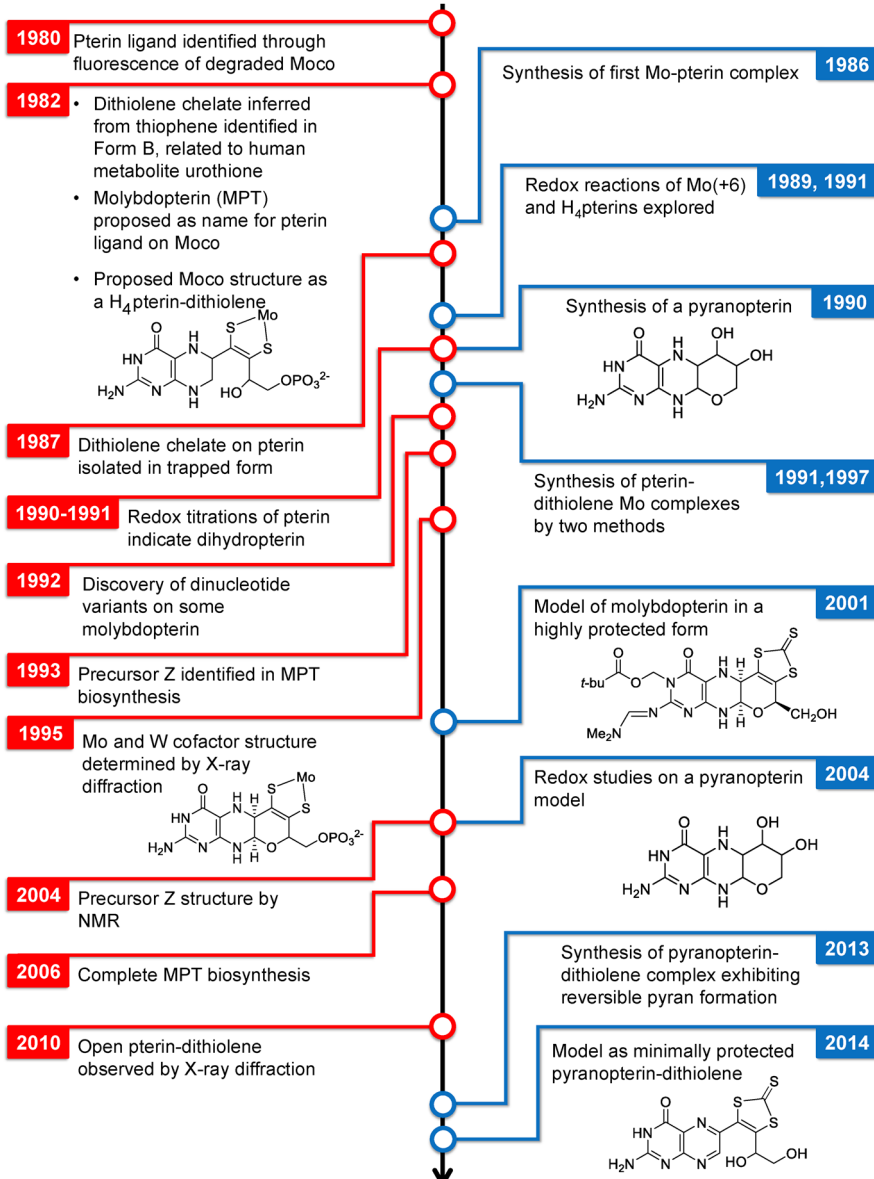


Figure 2.8 Timeline illustrating the progress in defining the identity of the pterin ligand in Moco, and the development of selected pterin model compounds.

proposed by Rajagopalan, suggested several metal binding sites in addition to the pterin-dithiylene (Figure 2.9) and prompted the notion that the pterin could present alternative coordination environments for molybdenum.

The first example of pterin coordination to Mo was reported in 1986. Xanthopterin under basic conditions reacted with molybdate to produce a

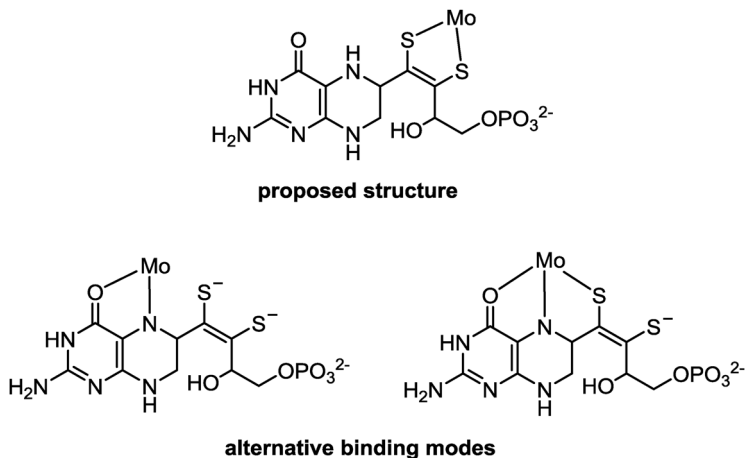


Figure 2.9 The proposed structure of Moco after Rajagopalan, and alternative molybdenum binding modes to molybdopterin.

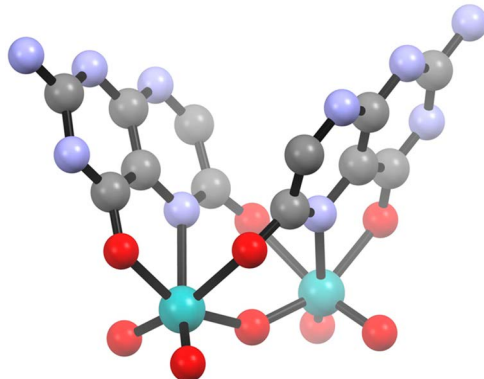


Figure 2.10 Ball-and-stick drawing of a pterin chelating molybdenum complex $[\text{Mo}_2\text{O}_5(\text{xanthopterinate})_2]^{2-}$. Red, oxygen; green, molybdenum; blue, nitrogen; grey, carbon.

dimeric species $[\text{Mo}_2\text{O}_5(\text{xanthopterinate})_2]^{2-}$ (Figure 2.10) where, amusingly, the yellow butterfly pigment xanthopterin produced a dimeric Mo₂-bis(xanthopterinate) compound with a butterfly conformation of the two bridging pterin chelates.²⁵ The significance of this system was that Mo^{VI} in the biologically relevant form of molybdenum $[\text{MoO}_4]^{2-}$, reacted with a pterin chelated through the O4, N5 donor atoms. In the specific case of xanthopterin, a second carbonyl functionality serves as a bridge to another Mo atom to structurally reinforce the common $[\text{Mo}_2\text{O}_5]^{2+}$ core. Although free xanthopterin fluoresces strongly as is typical of oxidized pterins, coordination to Mo completely quenches its inherent fluorescence.

2.3.1.2 Model Exploration of Redox Processes Between Mo and Pterin

Subsequent Mo-pterin model investigations addressed a second provocative aspect of Rajagopalan's proposed Moco structure. The 1982 proposal for Moco paired an oxidized Mo^{VI} center with a reduced tetrahydropterin – a juxtaposition of the highest molybdenum oxidation state with the most reduced form of pterin – that seemed incompatible and implied possible redox reactions between the metal and the organic cofactor. This section describes studies directed at exploring whether molybdenum and pterin redox reactions might occur. These studies were conducted from 1989 to 1999 and include reactivity studies of oxidized molybdenum(vi) with reduced pterins, and studies of reduced molybdenum(iv) with oxidized pterins and pteridines.

Interpreting the results from these experiments was surprisingly difficult but a broad range of approaches eventually led to the view that the molybdenum-pterin duo joined the growing numbers of examples of complexes that defy formal oxidation state assignments. These complexes, sometimes referred to as valence isomers, typically have redox-active metals and ligands, and are characterized by highly covalent interactions. The ligands in these complexes are also called “non-innocent” to allude to their ability to participate in electron transfer involving the metal.

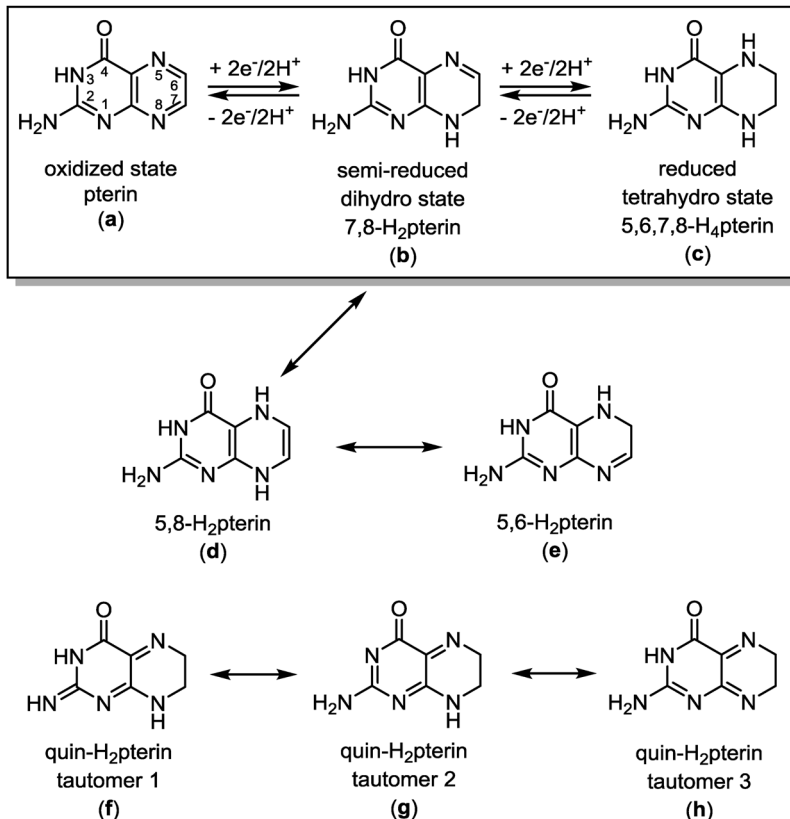
A brief summary of pterin redox chemistry is presented first to provide the necessary context for understanding the interpretations of the redox studies, followed by discussions of a series of studies pursuing the outcomes of oxo-Mo^{VI} and Mo^{IV} complexes reacted with tetrahydropterins and pterins.

2.3.1.2.1 Pterin Redox Chemistry.

Participation in redox processes is one of the fundamental roles of pteridines in biology, and pterins most often appear in biological systems as a redox component of a catalytic process. Their redox reactivity is a consequence of their nitrogen heterocyclic structure that can support several reduction levels and multiple tautomeric forms. The N-heterocyclic structure of the bicyclic pterin system exhibits a wealth of redox reactions in ways similar to the related N-heterocycle isoalloxazine in FAD. Unlike FAD where redox reactions are limited to $2e^-$, $2H^+$ processes, pterins are able to transfer up to $4e^-$, $4H^+$ units in sequential reactions.

The fully oxidized state, the semi-reduced or dihydro state and the fully reduced or tetrahydro state (Scheme 2.2a–c) are the three main redox states of pterins interconverted by $2e^-$, $2H^+$ reactions. The complexity of pterin redox chemistry results from many tautomeric forms of the semi-reduced state (Scheme 2.2d–h), which, unless highly substituted, will eventually rearrange to the most thermodynamically stable form, *ca.* the 7,8-dihydropterin (Scheme 2.2b)

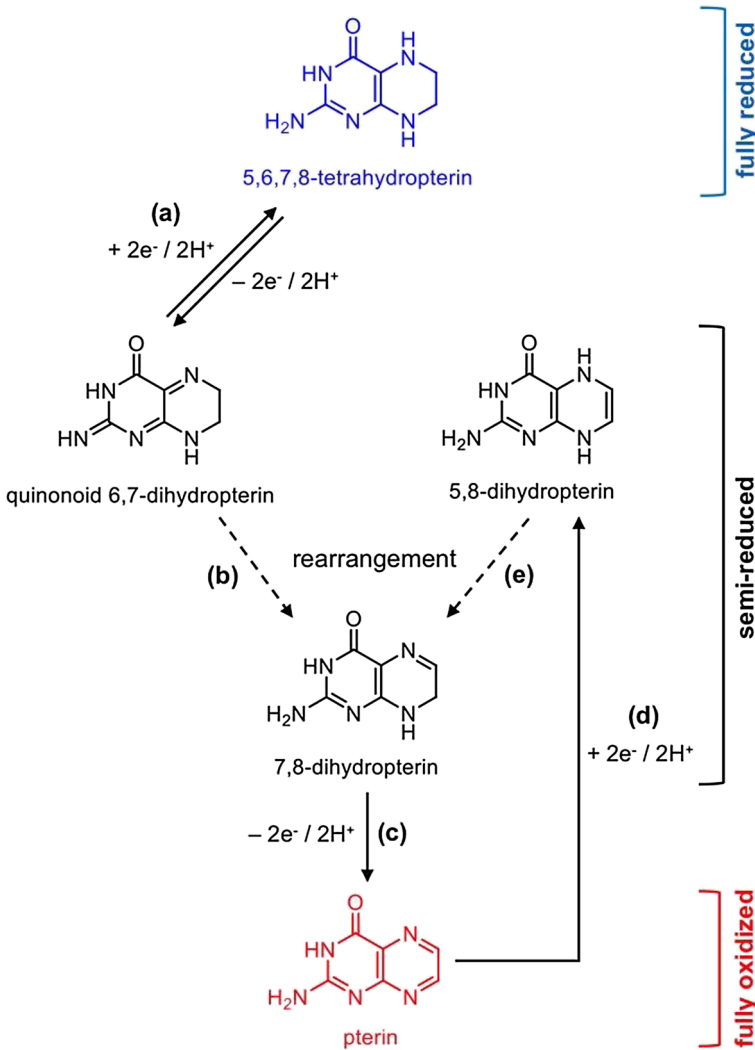
A thorough investigation using voltammetry revealed the key features of pterin redox chemistry that are generally applicable for simple pterins such as 6- and 6,7-methylated pterins.²⁶ These key features are illustrated for unsubstituted pterin in Scheme 2.3. The scheme is arranged with the



Scheme 2.2 The three oxidation states of pterin (a–c, top row) and the multiple dihydropterin tautomers (d–h) that are less thermodynamically stable.

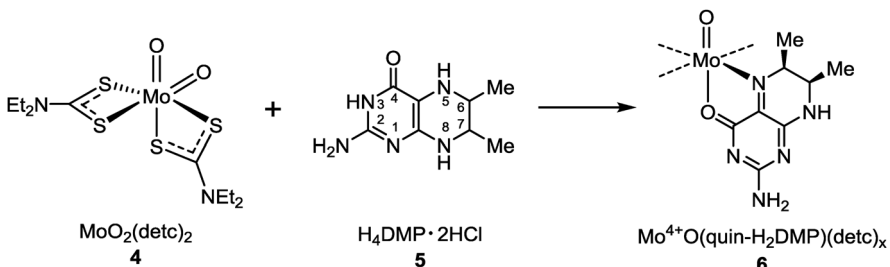
most reduced species at the top, the most oxidized species at the bottom and semi-reduced species in the middle of the diagram.

The only reversible redox process observed under rapid scanning of potential in the entire scheme occurs between tetrahydropterin and the quinonoid tautomer of dihydropterin in step (a) (Scheme 2.3). All other redox processes in the scheme lead to unstable dihydropterin forms that rapidly rearrange to the most stable tautomer, 7,8-dihydro dihydropterin in step (b). While 7,8-dihydropterin can be oxidized to pterin in step (c), it is a much less favorable oxidation process requiring potentials ~500 mV more positive than that for the reversible tetrahydro/quinonoid oxidation. Likewise 7,8-dihydropterin is reducible to tetrahydropterin but at potentials over 1 V more negative than reversible quinonoid/tetrahydro reduction. Such a low reduction potential accounts for unlikely participation of simple 7,8-H₂pterins in any redox step of Moco catalysis. Reduction of fully oxidized pterin also generates an unstable 5,8-dihydropterin tautomer, which rearranges to the 7,8-dihydro tautomer step (d) before further reduction to tetrahydropterin can occur.



Scheme 2.3 Reaction scheme relating the various redox species generated from unsubstituted pterin. (a) Reversible redox reaction; (b) and (d) tautomerization; (c) irreversible oxidation; (d) irreversible reduction.

2.3.1.2.2 Pterin-Molybdenum Redox Chemistry. The early studies focused on Mo(VI) and tetrahydropterin reagents to closely mimic the Mo and pterin portions of Moco. These studies showed that a variety of dioxo-Mo(VI) complexes reacted with tetrahydropterins to produce intensely colored mono-oxo Mo complexes, but the reports offered different interpretations of what reaction had occurred and what resulting oxidation states of molybdenum and pterin had been produced, even when X-ray structures of the product Mo-pterin complexes were available. A clear picture of the electronic structure was eventually developed from redox titrations, reactivity studies, theoretical calculations and X-ray photoelectron spectroscopy (XPS) studies.

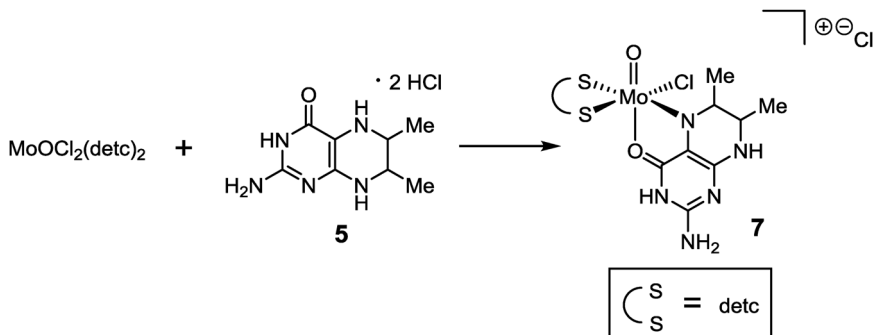


Scheme 2.4 Reaction of a dioxo-Mo(vi) complex with dimethyl-tetrahydropterin.

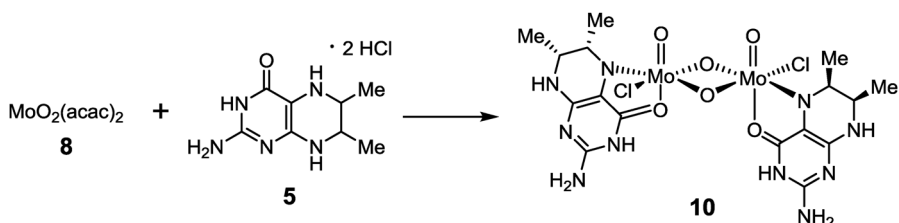
In 1989 Burgmayer's group reported a molybdenum–pterin redox reaction between a known oxygen atom donor complex, MoO₂(detc)₂ (**4**), and 6,7-dimethyltetrahydropterin (H₄dmp, **5**) (Scheme 2.4).²⁷ A fast reaction indicated by rapid color change from yellow (**4**) to purple was consistent with molybdenum reduction in known molybdenum-oxo chemistry. The ¹H NMR resonances from the purple complex generated *in situ* resembled those of a quinonoid tautomer of 6,7-dimethyldihydropterin (quin-H₂dmp). These two pieces of spectroscopic data led to the conclusion that a two-electron redox reaction occurred yielding complex **6** containing a Mo^{IV} atom coordinated by a quinonoid tautomer, quin-H₂dmp, at atoms O₄ and N₅ as shown in Scheme 2.4. This result was significant in Moco modeling for two reasons. First, it confirmed that Mo^{VI} combined with a tetrahydropterin would react and, second, that quinonoid dihydropterin coordinated to Mo imparted an unusual stability, which prevented the expected rearrangement of the unstable quinonoid dihydropterin to the 7,8-dihydro isomer (see Scheme 2.3). Unfortunately, compound **6** was not isolated and its exact structure remained unknown until 1996 when a different preparative method was developed.²⁸ This later method replaced **4** with Mo^{VI}OCl₂(detc)₂ in the reaction with **5** (Scheme 2.5) and reproduced the same spectral data observed for Scheme 2.4 as well as crystalline material for X-ray analysis to prove the stoichiometry of the purple product from either reaction (Scheme 2.5) as [MoOCl(detc)(H₂dmpH)]Cl (**7**).²⁸

Reactions of other dioxo-Mo^{VI} reagents with reduced H₄pterins were investigated to determine if quinonoid dihydropterin formation and coordination was a general feature.²⁹ Burgmayer showed Mo^{VI} reagents MoO₂(acac)₂ (**8**, acac = acetylacetone) and MoO₂Cl₂ (**9**) reacted with **5** to produce similar purple species with the characteristic downfield ¹H NMR resonances of quinonoid dihydropterin (Schemes 2.6 and 2.7).^{29b} Simultaneously, Fischer observed that tetrahydrobiopterin (**11b**) reacted with MoO₂Cl₂ to generate a red-purple material (Scheme 2.7).^{29c} All the Mo-pterin products exhibited $\nu(\text{Mo}=\text{O})$ in a region of 960–990 cm⁻¹, typical for oxo-Mo^{IV} centers.

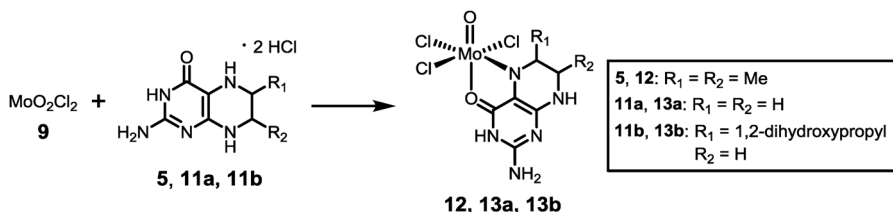
The products **6**, **7**, **10**, **12** and **13a–b** (Schemes 2.4–2.7) were characterized by X-ray crystallography, which confirmed pterin chelation at the O₄, N₅-site and clearly showed saturation at atoms C₆ and C₇ as expected for a quinonoid isomer of dihydropterin. Each compound also showed a proton at N₈.



Scheme 2.5 Reaction of a monooxo-Mo(VI) complex with dimethyl-tetrahydropterin.

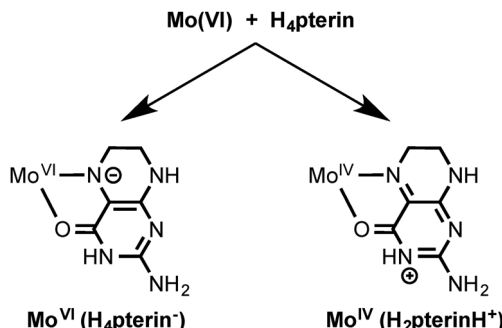


Scheme 2.6 Reaction of a dioxo-Mo(VI) complex with dimethyl-tetrahydropterin leading to a dimeric product.



Scheme 2.7 Reaction of dichloro-dioxo-Mo(VI) with various tetrahydropterins.

However, despite the similarity of pterin coordination, the molybdenum and pterin oxidation states in all the products from Schemes 2.4–2.7 were assigned differently. For **10**, the long Mo···Mo distance of 3.01 Å was inconsistent with a bonding interaction between the two Mo atoms as expected for a Mo(IV) dimer, but it was entirely consistent with the Mo_2O_4 core of a Mo(VI) dimer. Assigning a $\text{Mo}(\text{VI})_2\text{O}_4$ -core required that, for charge balance in the neutral dimer, the coordinated tetrahydropterin existed in a deprotonated form ($\text{H}_4\text{pterinate}$ or H_4dmp^-), thus leading to a dimer formulation as $\text{Mo}(\text{VI})_2\text{O}_4\text{Cl}_2(\text{H}_4\text{dmp}^-)_2$. Because **12** had similar bond distances within the Mo-pterin unit, it was also described as $\text{Mo}(\text{VI})\text{OCl}_3(\text{H}_4\text{dmp}^-)$. In contrast, Fischer's report of **13b** considered the product a Mo(IV) complex of a protonated form of quinonoid tautomer of $\text{H}_2\text{biopterin}$, $\text{Mo}(\text{IV})\text{OCl}_3(\text{quin-H}_2\text{biopterinH}^+)$.

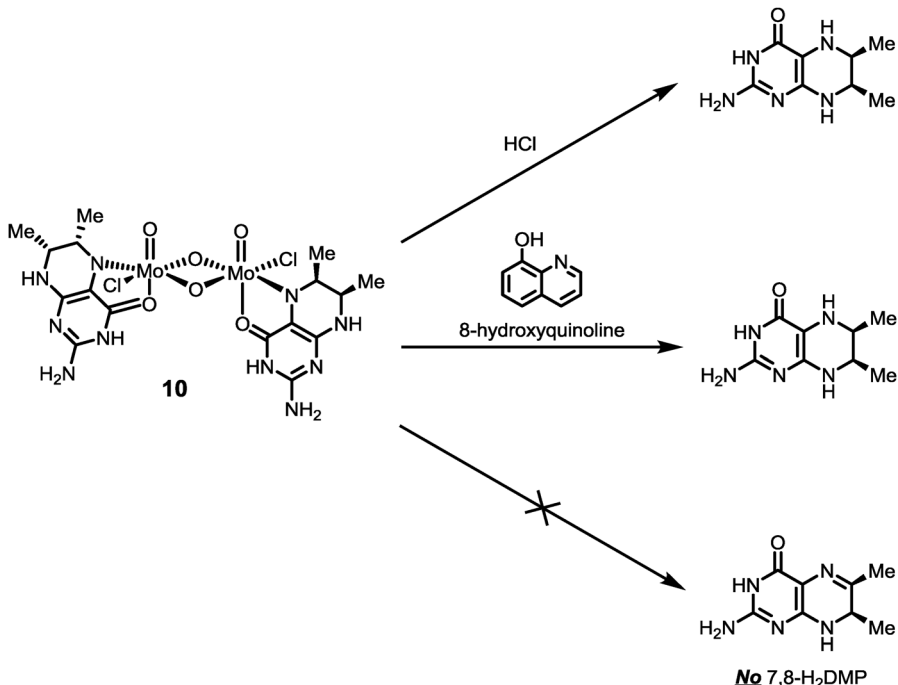


Scheme 2.8 Different formulations for the Mo-pterin products produced from reactions between Mo(vi) reagents and tetrahydropterins.

In short, these examples of Mo(vi) reactions with tetrahydropterins were described by one research group as simple ligand substitution and by another research group as two-electron redox reactions (Scheme 2.8).

2.3.1.2.3 Reactivity of Molybdenum Complexes of Reduced Pterins. To reconcile the contradictory Mo and pterin oxidation state assignments, several experiments were designed to reveal the formal oxidation state. The first was to induce dissociation of the reduced pterin ligand and observe the free ligand by ¹H NMR spectroscopy. If the complexes were Mo^{VI} ions coordinated by tetrahydropterinate chelates (structure on left of Scheme 2.8), then pterin dissociation would simply result in formation of free tetrahydropterin. However, if the complexes consisted of a reduced Mo^{IV} bound to a (quinonoid-H₂pterinH⁺) ligand (right structure in Scheme 2.8), dissociation of the unstable quinonoid-H₂pterin would be expected to cause its tautomerization to the stable 7,8-dihydropterin isomer. These two outcomes were easily distinguished using ¹H NMR spectra. Pterin dissociation was accomplished by the addition of either 8-hydroxyquinoline or hydrochloric acid. The results for dimeric **10** shown in Scheme 2.9 were the same for all the Mo-pterin products from Schemes 2.4–2.7. Because only free tetrahydropterin was detected and no 7,8-dihydropterin was observed, the results were consistent with the formulation of the complexes as Mo(vi)-(H₄pterinate) where *no* complete transfer of two electrons from pterin to molybdenum had occurred. An alternate possibility of Mo being in +5 oxidation state, discussed later, is consistent with the XPS data.

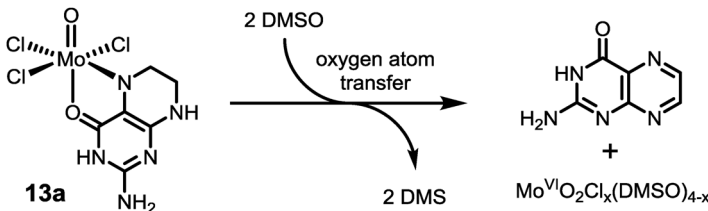
The second method of establishing oxidation states employed redox titration using the redox dye dichlorophenolindophenol (DCIP) based on the knowledge that tetrahydropterins reduce DCIP instantaneously while quinonoid dihydropterins react slowly and 7,8-dihydropterins do not reduce DCIP at all.³⁰ As previously mentioned in this chapter, DCIP oxidation of Moco within several molybdoenzymes was determined to be a two-electron process, suggesting a dihydropterin reduction state that was speculated to be the quinonoid tautomer. The results of stoichiometric additions of DCIP to the molybdenum complexes of reduced pterins showed that no oxidation of



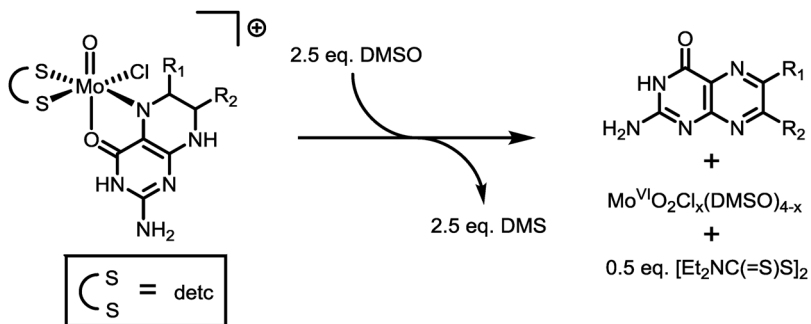
Scheme 2.9 Pterin dissociation produces only free tetrahydropterin.

coordinated pterin occurred in DMF solvent where all complexes remained intact, though in one case proton transfer had occurred. The uniform lack of reactivity of any intact molybdenum complex with DCIP could be explained by several arguments: (a) coordination of a tetrahydropterinate stabilizes the pterin towards oxidation by DCIP; (b) the coordinated pterin is, in fact, a partially oxidized dihydropterin; or (c) the coordinated pterin is bound as a partially oxidized pterin where ownership of the two electrons is shared by both the molybdenum and the pterin. X-ray photoelectron spectroscopy would confirm (*vide infra*) that option (c) is the most accurate description.

2.3.1.2.4 DMSO Reduction. Model compounds for the molybdenum cofactor are often developed to be capable of mimicking biological activity.^{2c,31} The ability of synthetic Mo-pterin model complexes to demonstrate oxygen atom transfer (OAT) was examined by reduction of dimethylsulfoxide (DMSO) to dimethyl sulfide (DMS). The ambiguity surrounding the molybdenum oxidation state in the pterin complexes **7**, **10**, **12** and **13** was addressed by testing each complex for its ability to reduce DMSO. The outcomes were mixed; two complexes did not undergo any oxygen atom transfer (OAT) activity with DMSO while the remaining two underwent OAT reactivity, yielding dimethylsulfide and an unknown Mo^{VI} species, and free, oxidized pterin. The dimer **10** was unreactive towards DMSO when monitored by electronic spectroscopy for 2 days. Likewise **12** did not reduce DMSO, but did undergo



Scheme 2.10 DMSO reduction by complex **13a**.

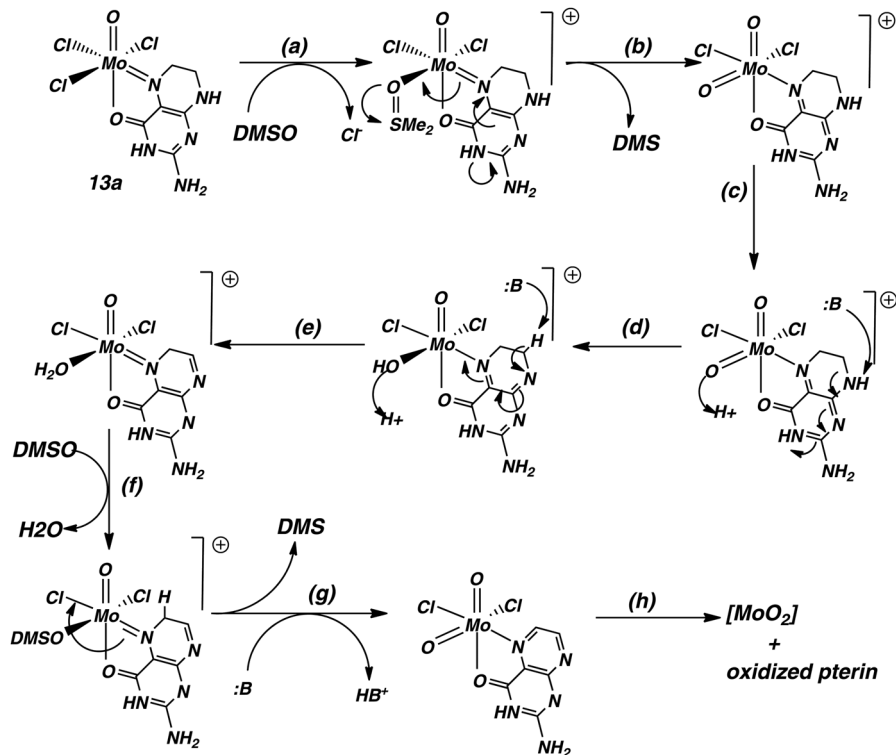


Scheme 2.11 DMSO reduction by complexes **7a** and **7b**.

substitution of the chloride ligand by DMSO. In contrast, **13a** reduces two equivalents DMSO to yield an oxidized $\text{Mo}^{\text{VI}}\text{O}_2$ species and fully oxidized pterin (Scheme 2.10). There is no apparent difference in the bond distances between complexes **12**, **13a** and **13b** that would offer a simple explanation as to why only one reduces DMSO, however it may be related to the much greater insolubility of unsubstituted pterin that drives the reaction forward. Complexes **7a** and **7b** react slowly with DMSO and consume three equivalents DMSO to produce the oxidized pterin, a $\text{Mo}^{\text{VI}}\text{O}_2$ core and oxidized dithiocarbamate (Scheme 2.11).

The ability of certain complexes to reduce DMSO but not other complexes may be related to the ancillary sulfur ligands in view of previous studies demonstrating an easier oxidation of Mo^{IV} when complexed to sulfur ligands.^{2c,31b}

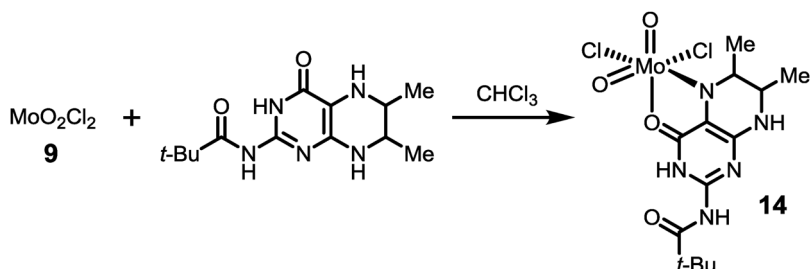
A mechanism proposed for DMSO reduction by **13a** is shown in Scheme 2.12. The first step (a), DMSO substitution for chloride, is supported by spectroscopic and conductivity data observed for **7a** and **12** in DMSO solution.^{29b} The X-ray structure of **12** reveals that DMSO coordinates to Mo, *cis* to N5 of the pterin. DMSO coordinates to the molybdenum center, *cis* to the pterin nitrogen N5 since the *cis*-Cl site has the longest, and presumably weakest, Mo–Cl bond based on the X-ray structure of **12**. The transfer of an oxygen atom in step (b) from DMSO to Mo may be viewed as the result of a two-electron transfer from the Mo=N5 bond to the incipient Mo=O bond. Prior to further oxidation, the



Scheme 2.12 A possible mechanism for the reduction of two molecules of DMSO by one molecule **13a**.

pterin loses two protons to a base designated:**B** in Scheme 2.12 (steps c and d). Species capable of proton abstraction are the **Mo=O** group, as used in Scheme 2.12, or another pterin molecule. The **Mo=O** group is sequentially converted from an oxo ligand *via* a hydroxo to an aquo group on **Mo(VI)** simultaneous with the further oxidation of pterin *via* electron transfer to molybdenum, which regenerates a **Mo(IV)** oxidation state. Substitution of the water ligand by a second **DMSO** molecule in step (f) precedes the reduction step (g) of a second **DMSO**. Overall the reaction is a four-electron oxidation of the molybdenum-pterin complex coupled to the four-electron reduction of two molecules **DMSO** (h). The six-electron oxidation observed for complex **[MoOCl(detc)(H₄dmp)]Cl** can be imagined to proceed similarly to the reactions (a–h) in Scheme 2.12, where reduction of two **DMSO** molecules again consumes four electrons from the **Mo** atom and the pterin, while two additional electrons are produced from oxidation of two dithiocarbamate ligands to a disulfide.

Several general conclusions may be made regarding synthesis of reduced pterin complexes of molybdenum. The stability of these complexes depends on formation of a **Mo=N** bond, which, electronically, replaces one of the two **Mo=O** groups of the reagent as detailed in Scheme 2.12. Loss of an oxo ligand is facilitated by protonation by the two equivalents of **HCl** associated with



Scheme 2.13 Proposed unstable dioxo-Mo(vi)-tetrahydropterin complex **14**.

the pterin reagents. If reaction conditions prevent formation of this bond, no pterin coordination is observed. Hence the syntheses fail in basic media and when two equivalents of triethylamine are added to the reaction mixture to neutralize the two equivalents of HCl; under these conditions no pterin coordination can be observed spectroscopically. When synthesis is attempted under neutral, aprotic reaction conditions using the solubilized pterin shown in Scheme 2.13, a highly reactive $\text{MoO}_2(\text{H}_4\text{pterin})$ complex (**14**) forms that rapidly decomposes in any coordinating solvent.

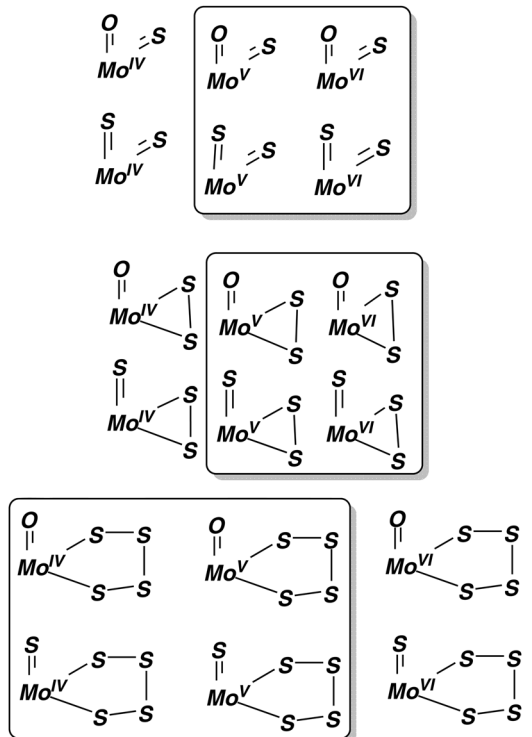
The failure to form a stable dioxo-Mo-(H_4pterin) complex can be attributed to competition between the two extant $\text{Mo}=\text{O}$ groups on the molybdenum reagent with the incipient $\text{Mo}=\text{N}5$ bond to the pterin. The competition is relieved in protic environments where one oxo ligand can be protonated and removed as water. One may consider that the $\text{Mo}(=\text{O})(=\text{N}5)$ unit of the molybdenum pterin complexes substitutes for the common $\text{Mo}(=\text{O})_2$ core frequently observed in Mo(vi) complexes.

2.3.1.2.5 Molybdenum(IV) Reactions with Oxidized Pterins. Long before a pteridine was discovered in Moco, the reaction of Mo(IV) and flavin was reported in 1974 (Scheme 2.14), yielding oxo-Mo^{IV}OCl₃(flavinH) (**15**) complex, which was characterized by spectroscopic and analytical data.³² This research was called into question shortly after its publication.³³

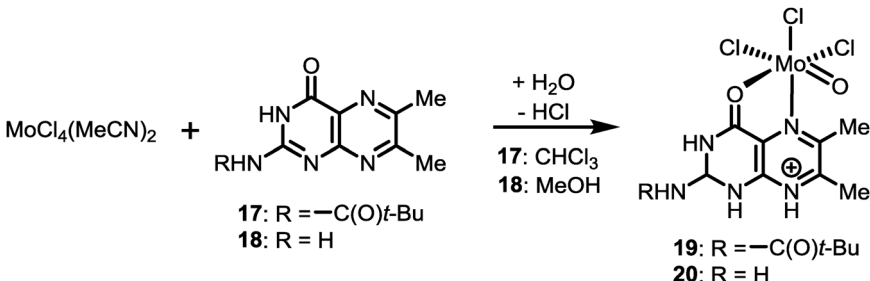
On reinvestigating this reaction, the Burgmayer group verified the accuracy of the original interpretation.^{29a} In addition to reproducing the synthesis and the spectroscopic data, an X-ray crystal structure of MoOCl₃(tmazH) (**16**) (tmaz=tetramethylalloxazine) confirmed the original formulation of a Mo^{IV} complex of protonated flavin. The same preparative method yielded additional examples of Mo^{IV} bound to oxidized pterins (piv-dmp, **17**, and dmp, **18**) (Scheme 2.15).

All of these red-purple Mo(IV)-pterin complexes exhibit strong MLCT absorptions. X-ray diffraction of one of these, **19**, proved the pterin coordinates through the same O4, N5 chelation site previously observed in Mo^{VI} complexes of reduced pterins and that the oxidized pterin is protonated at N8.

A striking feature of Mo(IV)-oxidized pterin systems is that metal chelation is coupled to pteridine protonation. This protonation is evidence of a change in the electronic structure within the Mo-pterin unit, where electron density is increased in the pteridine system through delocalization *via*

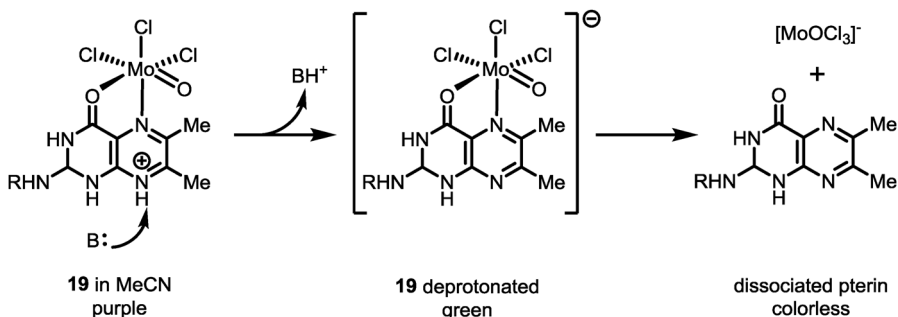


Scheme 2.14 Reaction between Mo(IV) and flavin.



Scheme 2.15 Reaction between Mo(IV) and dimethylpterin.

π -bonding from Mo. Viewed another way, the pterin moiety is effectively partially reduced by incomplete oxidation of the metal. The solution behavior of the molybdenum-flavin and -pterin complexes supports the idea that protonation is coupled to electron delocalization. While Mo(IV)-pterin complexes produce relatively stable purple solutions in acetonitrile or acetone, dissolution in a more basic solvent like DMF or addition of triethylamine causes an immediate color change to green followed by rapid bleaching. This is interpreted as pterin deprotonation at site N8 to produce an anionic



Scheme 2.16 Deprotonation of **19** leads to pterin dissociation.

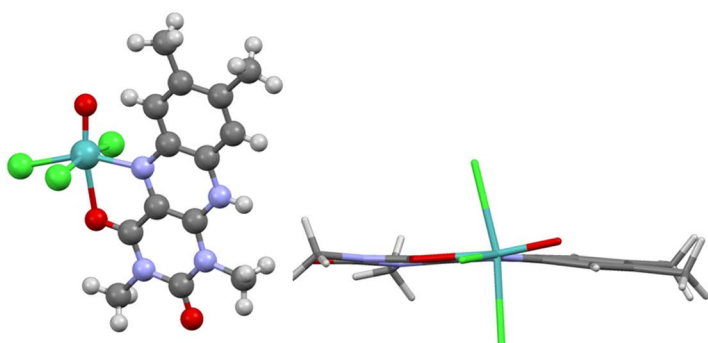


Figure 2.11 A ball-and-stick drawing of **16** (left) and depiction of its bent alloxazine ligand TMAZH.

green species $[\text{MoOCl}_3(\text{pteridine})]^-$, followed by the dissociation of the neutral pterin, which can be detected by ^1H NMR spectroscopy (Scheme 2.16).

This hypothesis leads to the prediction that oxidized forms of pterin and pteridine will favorably coordinate to metal ions specifically under acidic conditions. In a related work involving pterin complexes of ruthenium, Clarke *et al.* determined the pK_a s for pterin protons at various positions in several ruthenium–pterin complexes.³⁴ From these data it was concluded that the site of greatest basicity shifted from N1 to N8 upon coordination of the pterin to the ruthenium.

Partial pteridine reduction favored by its protonation is further suggested by a structural feature of **16**, which exhibits a distinct bending of the flavin along the N5–N10 axis (Figure 2.11). Flavin bending was also observed in a ruthenium–flavin complex and used as one of the criteria to support the notion that coordinated flavin was partially reduced and that the Ru-flavin complex was best described as a delocalized system of flavin semiquinone coordinated to ruthenium(III).³⁵ Applying the same argument to explain the non-planarity of tmaz in **1** leads to assigned formal oxidation states of Mo(v) and (tmazH^\cdot) radical. Interestingly, the Mo(v) oxidation state is consistent with XPS data (*vide infra*).

Having structures of both oxidized and reduced pterin complexes, such as the pair **19** and **20**, allows a detailed examination of the effect of metal

coordination on oxidized and reduced tetrahydropterin geometries. The major difference between these two complexes is the length of the Mo-N5 bonds. The shorter Mo-N5 bond in **20** corresponds to a greater electron transfer from H₄dmp to Mo(vi) as compared to the electron transfer from Mo(iv) to piv-dmp in **19**. In addition, the longer C4a-C8a bond in the reduced pterin complex **12** indicates a redistribution of π -electron density producing a π -quinonoid dihydropterin structure. The conclusion can be made that metal-mediated pterin reduction enables the initial formation of a 5,8-dihydropterin.

2.3.1.2.6 Formal Oxidation States in Molybdenum-Pterin Complexes. These molybdenum-pterin complexes share a theme: all complexes provide evidence of considerable electronic delocalization between molybdenum and pterin and, therefore, a change in the effective charge on molybdenum. In the case of the Mo complexes with reduced pterins, the disagreement about the correct formal oxidation state assignments as described earlier in Section 2.3.1.2.2 was eventually resolved through two methods: application of the bond valence sum (BVS) method and measurement of core Mo 3d binding energies by X-ray photoelectron spectroscopy (XPS).³⁶ The BVS method is based on the observation that as the unit charge on the metal increases, the bond length to ligated atoms decreases.³⁷ An illustration of this trend is in the series of neutral fragments M-OH₂, M-OH, M=O where the metal bears no charge, +1 and +2 units of charge, respectively, in parallel with decreasing Mo-O distances to the neutral, anionic and dianionic ligands. The empirical BVS method was previously used to estimate oxidation states on metal ions in enzymes.³⁸

The bond valence sum (BVS) method produced calculated charges on molybdenum in the Mo-reduced pterin complexes from Schemes 2.4–2.7 that were most consistent with a Mo^V assignment. The approach used a set of 17 molybdenum complexes as “standards” spanning oxidation states IV to VI, where these had a variety of donor atoms ligands including thiolate, tris(pyrazolyl)hydroborate, chloride and oxo ligands. The BVS calculations for the standard complexes gave formal oxidation states of Mo grouped in distinct ranges. The set of Mo^{VI} standard complexes had Mo charges calculated by the BVS method in the range 6.12–5.32, whereas the Mo^V and the Mo^{IV} standard complexes gave charges in the ranges 5.43–5.03 and 4.78–4.22, respectively. The Mo-pterin complexes produced BVS charges in the range 4.9–5.6, thus best matching the range for the standard Mo(v) complexes (Figure 2.12).

The conclusion that the Mo-pterin complexes best fit a Mo^V assignment was confirmed by XPS.³⁶ The same technique was used to investigate the effective charge on molybdenum through comparison of Mo 3d binding energies (B.E.) in the Mo-pterin complexes with B.E. as measured in series of standard molybdenum complexes (Figure 2.13). Surprisingly, Mo coordinated by both reduced pterin as well as oxidized pterin had binding energies that matched the range of BE values observed for the standard Mo^V complexes.

Both BVS and XPS methods, although different in approach, converge on the same conclusion: the molybdenum pterin complexes, as a group, are most consistent with an oxidation state assignment of +5 for molybdenum. To

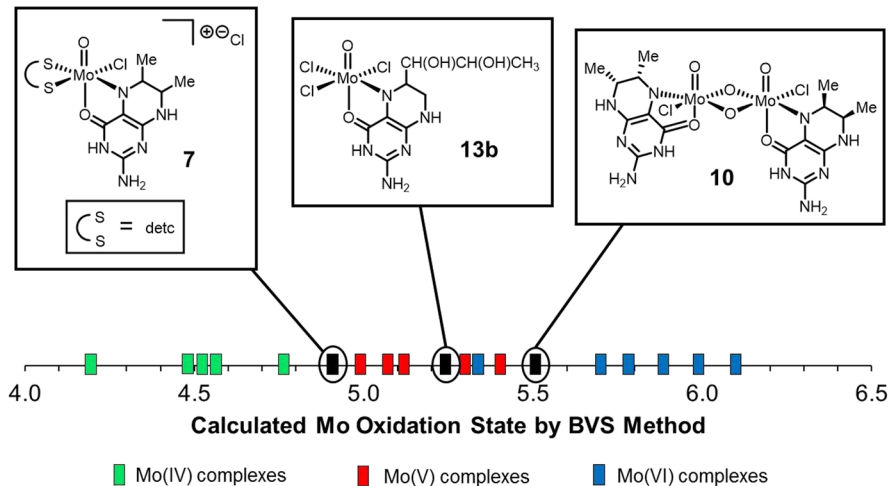


Figure 2.12 A graphical display of the results of Bond Valence Sum calculations.

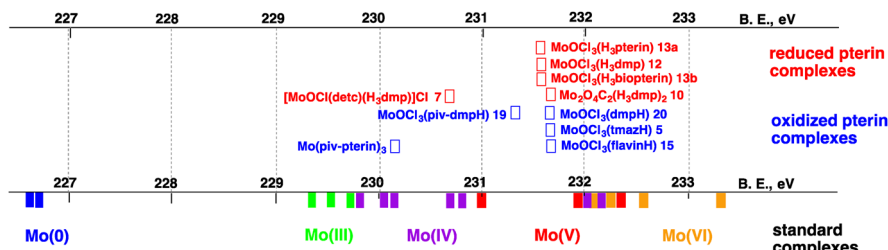
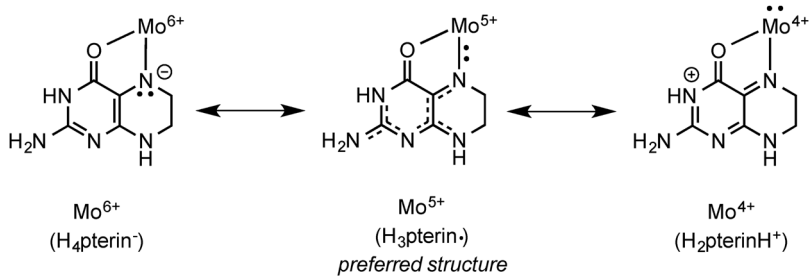


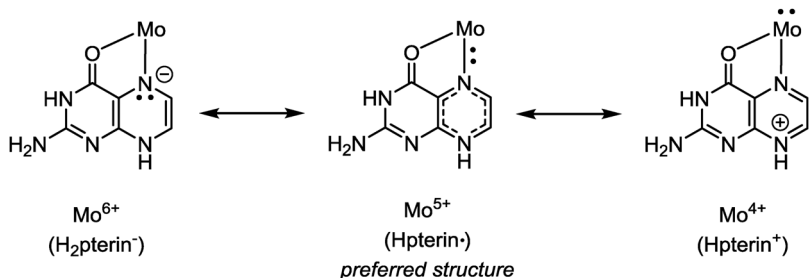
Figure 2.13 The binding energies (B.E., eV) for Mo complexes of reduced (red) and oxidized pterins (blue) compared to a series of standard Mo complexes in oxidation states 0–VI as determined from XPS studies.

understand this result, it is helpful to consider the Schemes 2.17 and 2.18. For Mo(vi) reacted with tetrahydropterins, the limiting oxidation assignments are Mo(vi) coordinated by a deprotonated tetrahydropterin ($\text{H}_4\text{pterin}^-$) (Scheme 2.17, left structure) and Mo(iv) coordinated by protonated quinonoid dihydropertin ($\text{H}_2\text{pterinH}^+$) (Scheme 2.17, right structure). The pterin redox state appropriate to pair with a Mo(v) center is thus the intermediate option between these limiting scenarios, corresponding to a neutral, *trihydropterin radical* (Scheme 2.17, center structure). This structure indicates the pair of π -electrons donated by the deprotonated N5 atom as delocalized over the Mo–N5 bond and available to either Mo or the pterin, depending on the environment. This assignment is interesting in light of a trihydropterin radical observed in three different aldehyde dehydrogenases as detected by EPR.³⁹

The Mo^V-trihydropterin radical view accommodates all the experimental data observed for the Mo complexes of reduced pterins. For example, tetrahydropterin ligand dissociation suggests a heterolytic cleavage of the Mo-N5 bond with the pterin regaining its original lone pair electrons. The lack of



Scheme 2.17 Resonance structures for molybdenum coordinated to reduced pterin. Note the location of the pair of electrons depicted near Mo and N5 shifts in the three structures.



Scheme 2.18 Resonance structures for molybdenum coordinated to oxidized pterin. Note how the location of the pair of electrons depicted near the Mo–N5 bond shifts in the three structures.

reactivity of molybdenum pterin complexes **7**, **10**, **12** and **13** with the mild oxidant DCIP is consistent with a deactivated tetrahydropterin through partial electron delocalization onto the molybdenum. The ability of molybdenum pterin complexes to reduce DMSO can be interpreted as the result of a subtle shift of the electron pair between Mo and N5 in response to changing ligand fields of ancillary ligands on Mo.

In the case of molybdenum complexes of oxidized pterin and pteridine ligands, a similar argument leads to the formulation of these complexes as Mo(v) bound to a protonated, one-electron reduced pteridine radical, or Mo^{v-}(Hpterin[•]) (Scheme 2.18). This interpretation is consonant with earlier work on Ru^{II}-flavin complexes. Radical character on flavin arising from intramolecular electron transfer was consistent with a structural distortion of flavin observed crystallographically, interpreted as partial Ru^{III}-flavinsemiquinone character.^{34,40} Similarly, the Mo complexes of oxidized pterins and pteridines display short M=N5 bonds and bent flavin or pterin planes, consistent with a similar delocalized electronic structure.

2.3.1.2.7 Evidence for the Non-innocent Nature of Pterin Ligands. The sum of experimental and computational results emphasizes that the electron flow between molybdenum and pterin is bidirectional, and that there is

an apparent preference of the molybdenum atom to acquire the equivalent of a Mo(v) oxidation state regardless of the oxidation state of the coordinated pterin ligand. Pterins and pteridines join a growing number of other redox-active ligands that are well known for their redox “non-innocent” behavior in coordination chemistry.⁴¹ Non-innocent ligands exhibit the same preferences with respect to matching ligand and metal oxidation states, where the reduced and electron rich form of the ligand (*e.g.* tetrahydropterin, catechol, dithiolene) prefer coordination to metals in high oxidation states, whereas the oxidized and electron-deficient form of the ligand (*e.g.* pterin, quinone, dithione) preferentially reacts with lower valent metals.⁴² The complexes formed in either of these two extreme cases are characterized by substantial electron delocalization over the redox-active ligand/metal framework as they seek to attain electroneutrality.

It required a decade of study to develop a clear understanding of the principles and outcome of pterin reactions to molybdenum. The results summarized here tell the story of non-innocent ligand behavior of pterin and pteridine ligands. During this period the first crystal structure of molybdenum enzymes emerged from which the dithiolene chelation of molybdopterin was proved. While protein structures unequivocally confirmed the dithiolene coordination to molybdenum, the alternative coordination mode described in this section underscores the electronic flexibility of the pterin system partnered with molybdenum.

2.3.2 Second-Generation Dithiolene Pterins and their Complexes

Following the proposal for a dithiolene tether on molybdopterin to bind Mo, many synthetic dithiolene model complexes having simple substituents, such as methyl,^{31a} cyanide^{2d,43} or where dithiolene is part of a ring system (*e.g.* 1,2-benzenedithiolate, bdt),⁴⁴ were studied to establish how a dithiolene chelate influences Mo reactivity. However, a dithiolene chelate substituted by pterin introduces additional electronic flexibility such as conjugation between the pterin and the dithiolene, in addition to proton-coupled redox processes. To address the question of how pterin further modulates the dithiolene, a few research groups began developing strategies for placing a pterin on a dithiolene chelate to create a ligand having the essential components of molybdopterin.

In this section, second-generation models are reviewed. Here we define second-generation models as those that combine a pterin with a dithiolene chelate. Often an N-heterocycle similar to pterin, such as quinoxaline, was used in the exploratory work. Significant efforts went into the development of chemistry to prepare more structurally faithful functionally competent complexes incorporating the three components of the cofactor, *i.e.* the dithiolene, the pterin, and the metal. First presented are the various strategies used to synthesize Mo-dithiolene complexes bearing pterin or pterin-like substituents. This work is followed by a description of methodologies developed to access sulfur-containing pterin molecules not attached to metals.

2.3.2.1 Synthesis of Mo-Dithiolene Complexes in Reactions of Alkynes and Metal Polysulfides

In the early 1980s the Coucoubanis group explored the reactivity of polythio molybdenum anions such as $[\text{MoS}_4]^{2-}$ and $[\text{MoO}_{4-n}\text{S}_n]^{2-}$ with elemental sulfur (Figure 2.14).⁴⁵ The facile conversions of thiomolybdates are thought to proceed *via* intramolecular electron transfer due to a close energy matching of the S 3p and Mo 4d orbitals.

The polysulfide species $[\text{Mo=S}(\text{S}_4)_2]^{2-}$ (**20** in Scheme 2.19) was reported to react with an alkyne producing a metal dithiolene unit *in situ*.⁴⁷ The metal insertion reaction proceeds *via* electrophilic attack by dimethylacetylene-carboxylate (DMAC). It was observed that replacing the sulfido ligand with an oxo makes the tetrasulfide ligand less reactive towards the electrophilic attack by DMAC and changes the product of the reaction of DMAC and complexes possessing a $\text{Mo}(\text{S}_4)$ as shown in Scheme 2.19.

This methodology of reacting a metal tetrasulfide with an acetylene to introduce a metal dithiolene unit has been frequently used to generate models for Moco.^{46,48} The Burgmayer group reported that this method produced a tris-quinoxalylidithiolene-Mo complex in 1991 (**21**, Scheme 2.20).⁶⁸ An important result from this study was that the iodine oxidation of the product

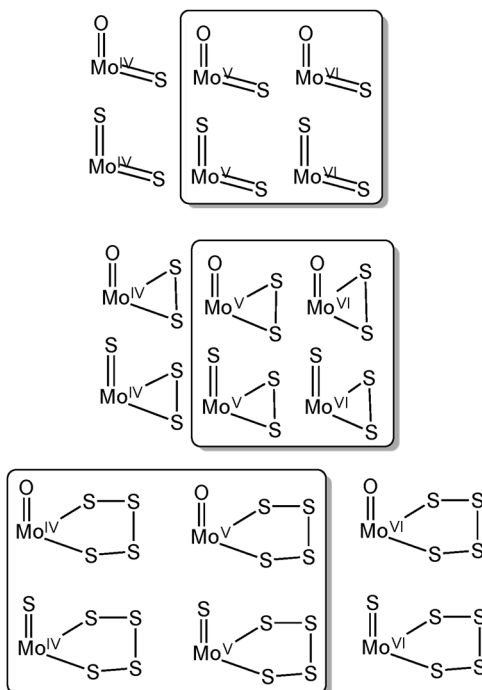
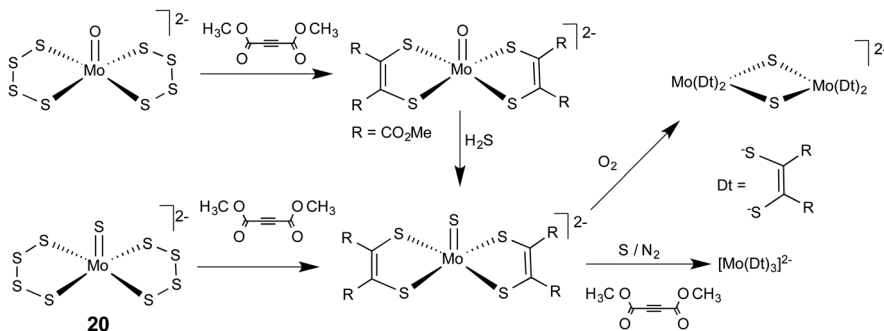
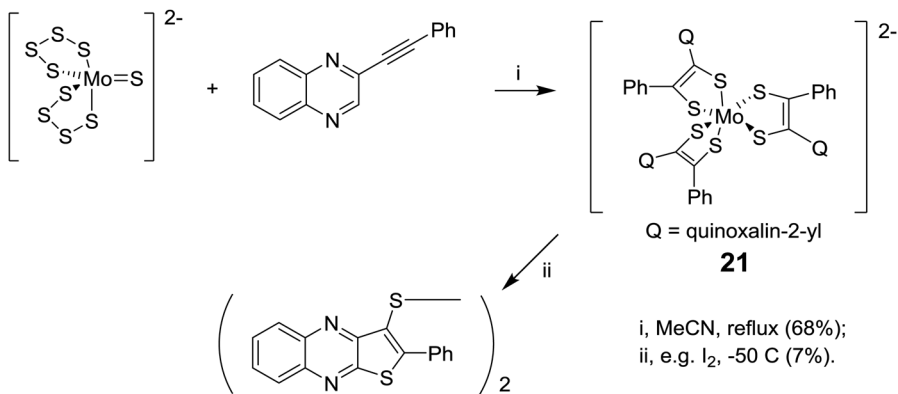


Figure 2.14 Selected functional groups used in preparing thio-Mo(IV/V/VI) complexes with known groups are in frames. Adapted from ref. 46.



Scheme 2.19 Formation of oxo/thiomolybdenum dithiolenes from acetylene derivatives.

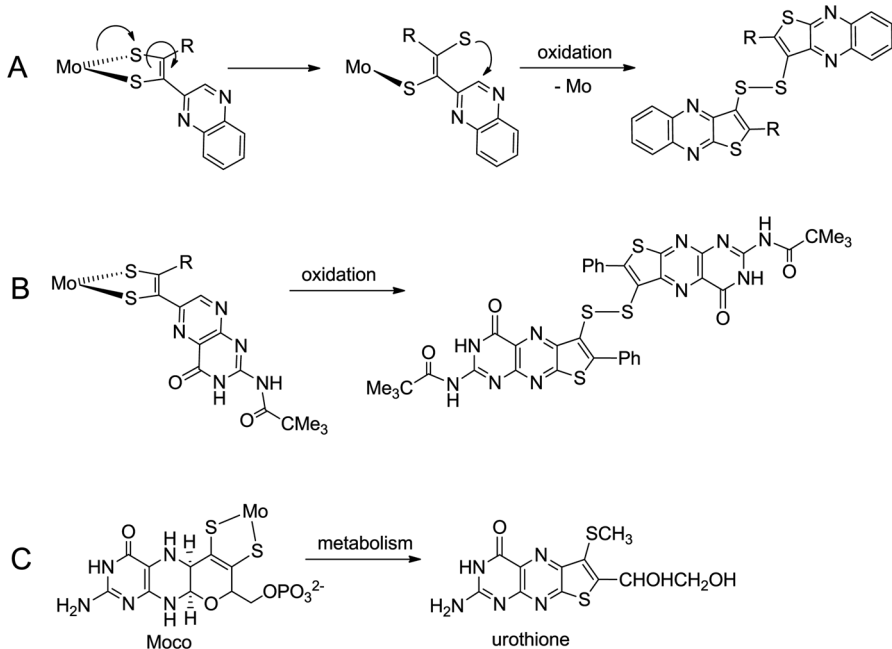


Scheme 2.20 Formation of tris-molybdenum dithiolene through acetylene activation and its degradation to a thiophene derivative.

complex $[\text{Mo}(\text{quinoxalinedithiolate})_3]^{2-}$ **21** resulted in dithiolene ligand dissociation and degradation forming a thiophene.

The mechanism leading to thiophene formation is presumed to involve dissociation of one sulfur atom of a dithiolene chelate followed by sulfur attack on a pyrazine carbon, cyclization and oxidation to form a thiophene ring (A in Scheme 2.21). When the dithiolene-forming reaction in Scheme 2.20 employed a pterinyl alkyne, no tris-pterinyldithiolene complex could be isolated. However, pterinyldithiophene formation was implied by the isolation of a pterin thiophene whose identity was confirmed by X-ray crystallographic determination (B in Scheme 2.21). This observation was an early confirmation of the correctness of the proposed pterin-dithiophene in Moco prior to any available X-ray protein structures. These thiophene products were reminiscent of Moco oxidation products **1** and the natural metabolite of Moco, urothione **2** (see Figure 2.2), studied by Rajagopalan (C in Scheme 2.21).

Simultaneously, Stiefel and Taylor were exploiting this methodology of cyclo-addition of quinoxalyl and pteridinyl acetylenes with a Mo-(S₄) reagent **22**



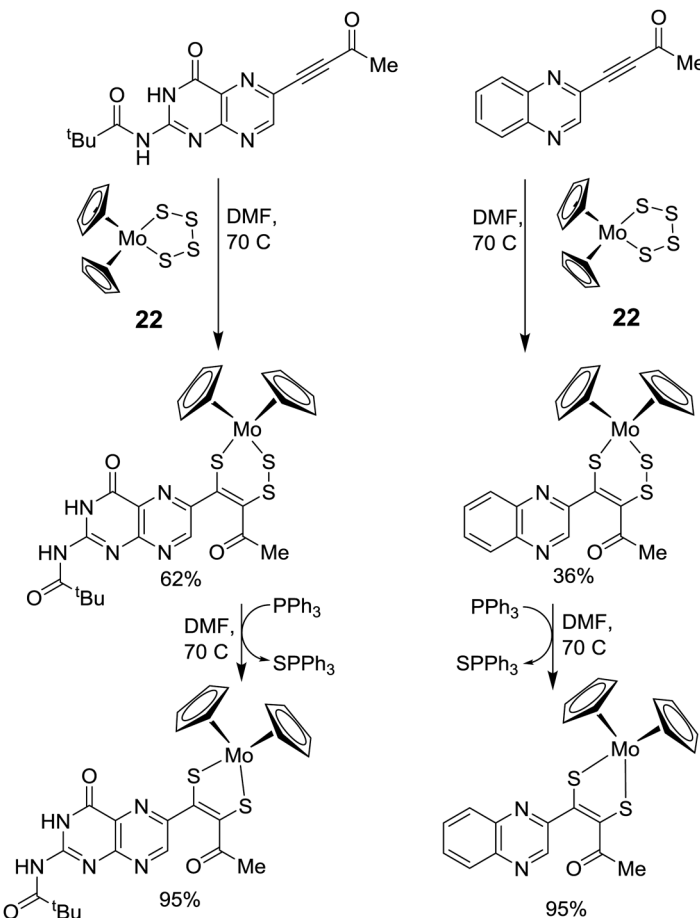
Scheme 2.21 Oxidative products of quinoxaline (A) and pterin dithiolene (B and C) originating from dechelation of the metal and the metabolic product of the cofactor degradation.

to generate *mono*-dithiolene complexes of molybdenum(IV) (Scheme 2.22).⁴⁹ In their system it was discovered that a trithiolene species was the initial cycloaddition product, and was readily converted to the target dithiolene complex *via* a sulfur atom transfer reaction to PPh_3 . An important strategy of this model system was the use of cyclopentadienide ligand (Cp) to block coordination sites of the metal center to ensure formation of the mono-dithiolene complex. A disadvantage of this $\text{Cp}_2\text{Mo}(\text{S}_4)$ entry into pterin-dithiolene models was limited further development of the system.

More recently the Burgmayer group applied the same method to generate a variety of monooxo-mono-pterin-dithiolene Mo complexes on a tris(3,5-di-methylpyrazolyl)hydroborate (Tp^*) framework. One example is presented in Scheme 2.23. Notably the Tp^*Mo -based model system allows synthesis of both sulfido and oxo forms of $\text{Tp}^*\text{MoO}(\text{pterin-dithiolene})$ complexes in both biologically relevant IV and V oxidation states.⁵⁰

2.3.2.2 Synthesis of Dithiolene Ligands and Complexes from Protected Dithiolene Precursors

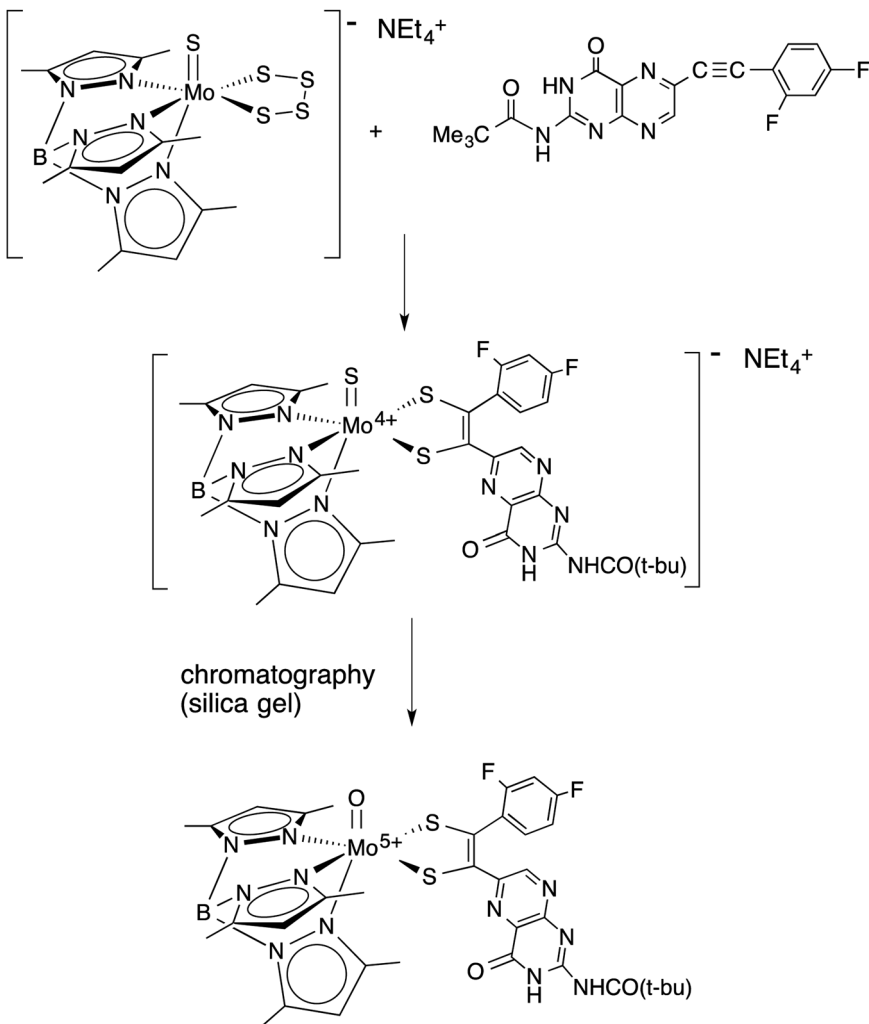
Insertion of a metal into a dithiolene ligand has been investigated for decades. In the preceding section we discussed accessing dithiolenes through reaction metal polysulfide species with appropriately substituted alkynes. In this



Scheme 2.22 Synthetic strategy for preparing molybdenum pterin dithiolene complex.

section, syntheses of new heterocyclic dithiolene ligands are discussed, whose inherent reactivity at the dithiolene moiety required more complicated synthetic schemes to protect this reactive unit. The protective group at the dithiolene was removed at a later stage when the metal insertion is desired. In this section we briefly discuss some of the strategies that are important in the context of heterocyclic dithiolene ligands.

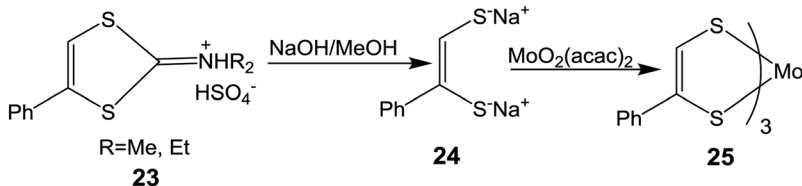
Garner and Joule developed methodologies for preparing protected dithiolene ligand precursors. The precedence for this chemistry lies in the reports of deMayo⁵¹ and Rauchfuss.⁵² The first example reported by Garner and Joule was the synthesis of an unprotected dithiolene from base-catalyzed hydrolysis of an unsymmetrical, styrene-1,2-dithiolate **23** yielding the dialkylamino-1,3-dithiolium salt **24** (Scheme 2.24).⁵³ While the free ligand could not be isolated, it reacted with $\text{MoO}_2(\text{acac})_2$ producing a tris-dithiolene complex **25** (Scheme 2.24). The base hydrolysis of protected dithiolene precursor molecules remains an



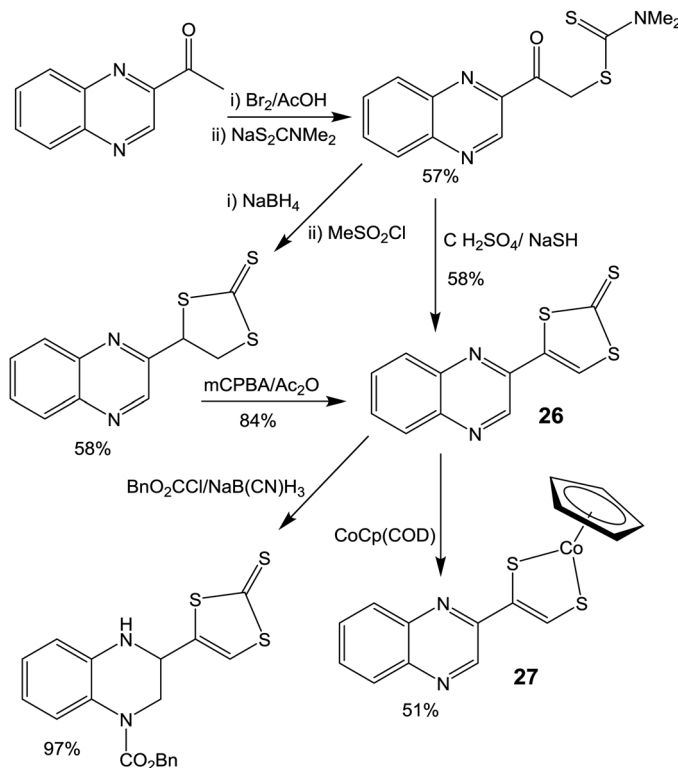
Scheme 2.23 Cycloaddition reaction of molybdenum thiolate and acetylene derivative forming molybdenum dithiolene complex.

important strategy for developing new model species where different types of base such as alkoxide, NaOH, CsOH and Et₄NOH are successfully used.

Garner and Joule next adapted the protected dithiolene strategy to target heterocyclic dithiolene complexes. This approach, first reported in 1988 by Larsen *et al.*,⁵⁴ is illustrated in Scheme 2.25 with the formation of a cobalt quinoxalyldithiolene complex. Reaction of [CoCp(COD)] (COD = 1,5-cyclooctadiene) with 4-(quinoxalin-2-yl)-1,3-dithiole-2-thione (**26**) affords a quinoxaline dithiolene complex (**27**) that has been structurally characterized.⁵⁵ This cobalt complex undergoes extensive proton-coupled electron transfer process (see Section 2.3.4). This system was further elaborated when the pyrazine ring in 4-(quinoxalin-2-yl)-1,3-dithiole-2-thione **26** was selectively



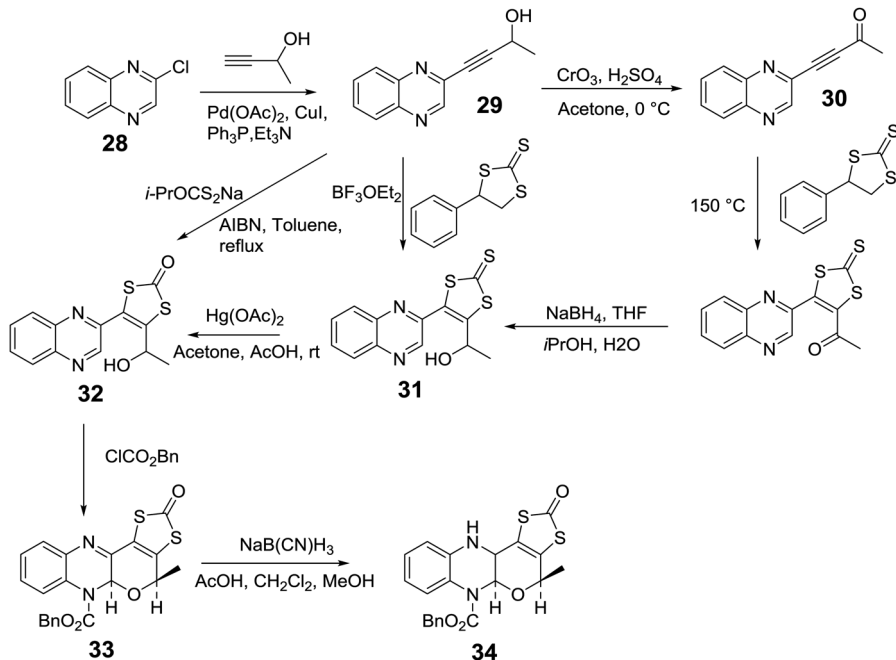
Scheme 2.24 Garner and Joule's method of preparing unprotected dithiolene, and its molybdenum complex.



Scheme 2.25 Synthesis of cobalt complex coordinated by a single dithiolene ligand.

and quantitatively reduced by $\text{NaB}(\text{CN})\text{H}_3$, without reduction of the dithiolene moiety, generating a structure similar to the tetrahydro form of pterin. However, this reduced product is very air sensitive and susceptible to rapid oxidation to the aromatic quinoxaline. This procedure opened an avenue for synthesizing reduced pterin similar to the cofactor without reducing the dithiolene unit. The Joule–Garner group has done extensive work on fundamental chemistry of this system leading to an analog of urothione.⁵⁶

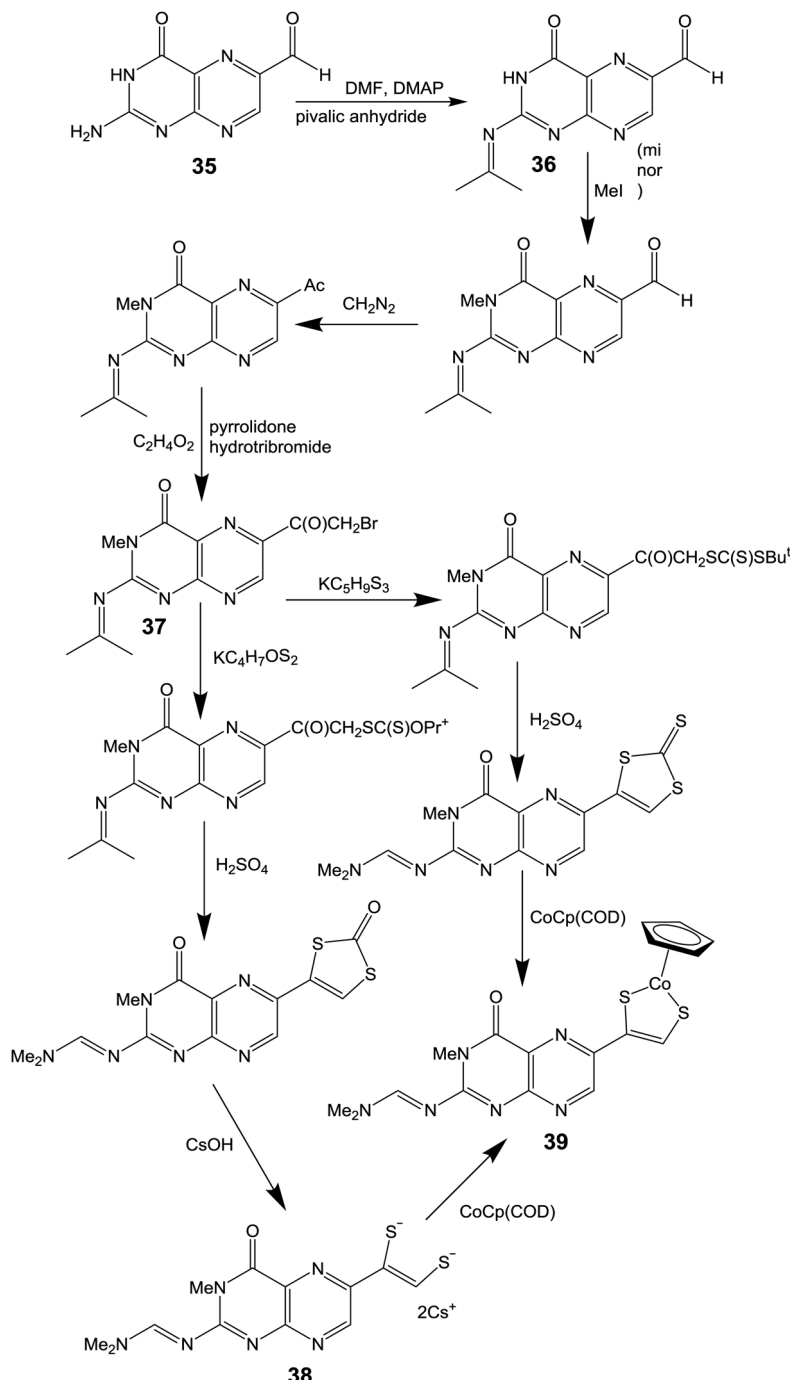
In a related system (Scheme 2.26), Bradshaw *et al.*⁵⁷ coupled 2-chloroquinoxaline (**28**) with but-3-yn-2-ol using a palladium-catalyzed Sonogashira



Scheme 2.26 Synthetic strategy for reduced quinoxalinepyran dithiolene ligand.

coupling. Oxidation of the alcohol (**29**) by CrO₃ produced the corresponding ketone (**30**), which reacted with 4-phenyl-1,3-dithiolane-3-thione to introduce the protected dithiolene moiety, a reaction known⁵⁷ to be favored with alkynes bearing an electron-withdrawing substituent such as a quinoxaline.⁵⁷ The dithiolene insertion reaction has also been achieved by treating with xanthate in the presence of AIBN (azobisisobutyronitrile).⁵⁸ Subsequent selective reduction of the ketone functionality with NaBH₄ reformed the alcohol group in **31**; conversion to 1,3-dithiol-2-one (**32**) was then achieved with mercuric acetate. Treatment of this compound with benzyl chloroformate in the absence of solvent or added base resulted in the cyclized, pyrano- product **33** with no O-acylation. Reduction of the remaining imine unit was achieved by treating with sodium cyanoborohydride, forming product **34**. Hydrolysis of the ketone of 1,3-dithiol-2-one with aqueous CsOH deprotects the dithiolene, which was reacted with cyclopentadienyl(diiodo)cobalt *in situ* resulting in the formation of a dithiolene coordinated Co complex.⁵⁷ The structural and electronic properties of this system have recently been investigated in detail.⁵⁹ The same ligand has been reacted⁶⁰ with K₄[Mo^{IV}O₂(CN)₄]·6H₂O yielding [Mo^{IV}O(dithiolene)]²⁻.

This approach was extended to prepare a more faithful structural analog of molybdopterin (Scheme 2.27).⁶¹ The synthetic scheme begins with the convenient reagent pterin-6-aldehyde **35** that is produced by degradation of folic acid. Solubility of the pterin can be increased through N2-pivaloylation or by forming 2-N,N-dimethylamino methyleneaminopteridine (**36**) by treating pterin-6-aldehyde with Bredereck's reagent. The N-3 was protected through

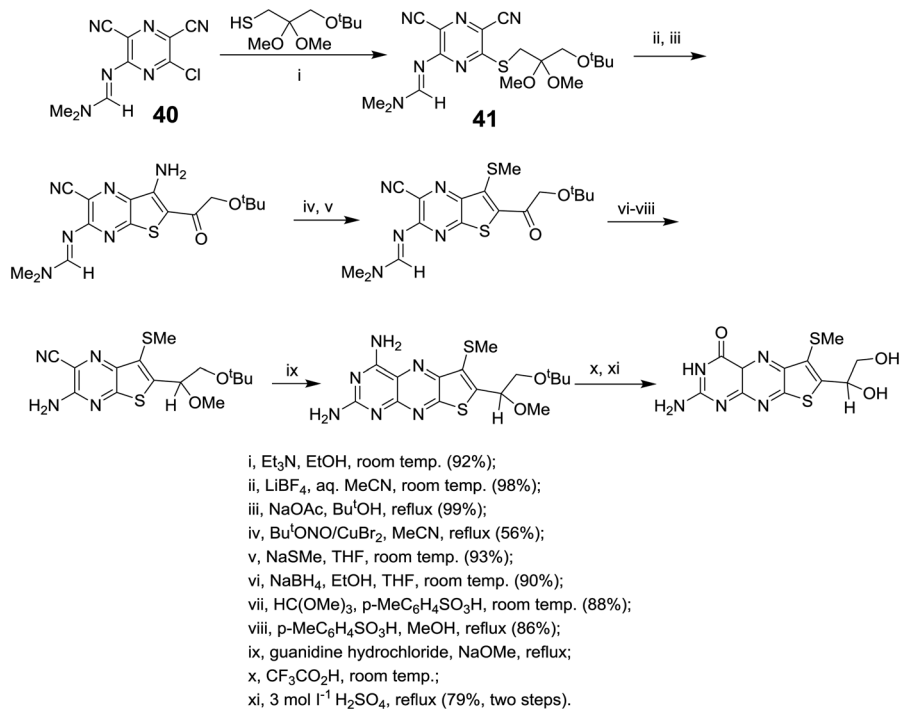


Scheme 2.27 Synthesis of a cobalt complex of a pterindithiolene ligand.

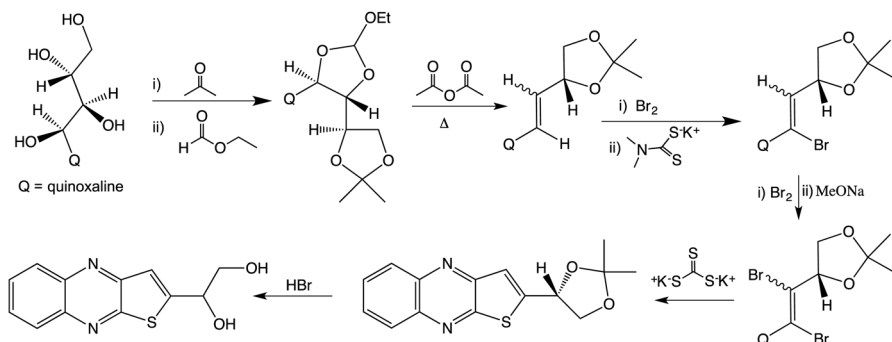
alkylation with diazabicycloundecane (DBU). Following formation of an α -bromo ketone on the side chain (37), modification of the α -bromo ketone could introduce the dithiolene unit through a variety of reagents *e.g.* dialkyldithiocarbamate, or tertbutyltrithiocarbonate.⁶² Hydrolysis with a base (*e.g.* CsOH) removed the dithiolene protection allowing the dithiolate (38) form to react with $\text{CpCo}^{\text{III}}\text{I}_2$ to yield the Co-pterin-dithiolene complex 39, which was characterized structurally.⁶³

2.3.2.3 Synthesis of Sulfur-Containing Pterin Molecules

2.3.2.3.1 Chemical Synthesis of the Moco Metabolite Urothione. In 1982, Johnson and Rajagopalan published¹⁰ their seminal paper proposing the structure of molybdenum cofactor, and its degradation product urothione 2, a thienopterin. Urothione was first isolated from human urine in 1940.⁶⁴ Its structure and total synthesis were described by Goto.⁶⁵ A more robust total synthesis of the deoxyurothione was also reported in 1982 by Taylor.⁶⁶ The regioselective synthesis of the pteridine is shown in Scheme 2.28. An important point of Taylor's scheme is that the pterin ring is formed after construction of the thiophene ring. The starting point was a suitable pyrazine molecule (**40**) for the annulation of the thiophene and pyrimidine rings.



Scheme 2.28 Synthesis of urothione from pyrazine.



Scheme 2.29 Synthesis of quinoxaline model of form B.

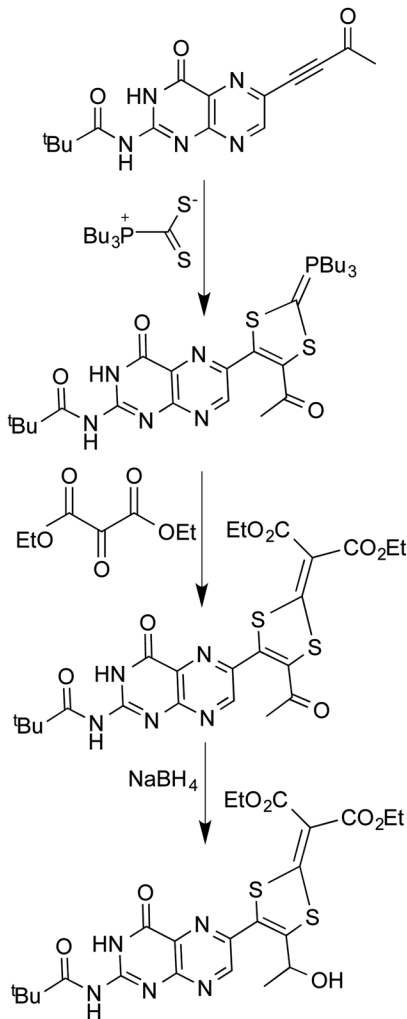
Condensation of 6-chloro-3,5-dicyano-2-(dimethylamino)methylenelaminopyrazine with α -mercaptopropionyl chloride or 1-mercaptopropanone introduces C-S bond formation between the C7 of the pyrazine ring, forming **41**, which can then be cyclized under basic conditions.

From the cofactor structure, we now know that the thiol sulfurs are not directly connected to the pterin ring; rather, they are appended from the pyran ring. Therefore, formation of urothione from the molybdenum cofactor must involve a cyclization step, and a similar process may also be involved in the formation of form B (**1**). Such reactions have been “modeled” through oxidation of quinoxaline dithiolene ligand (Scheme 2.29)⁶⁷ as well as in complexes (see Scheme 2.20 above).⁶⁸

2.3.2.3.2 Synthesis of Pterin Dithiolene Ligand. In 1971, Hartzler communicated that an ylide can be formed by reacting an activated alkyne with betainic tributylphosphine-carbon disulfide compound, converting the alkyne into a dithiolene moiety.⁶⁹ The antiaromaticity (8π -electrons) of the five-membered ylides makes them very reactive, and they readily undergo the Wittig reaction with an aldehyde forming a C=C bond. Taylor's use of this interesting reaction with a pteridinyl ketone resulted in a pterin dithiolene (Scheme 2.30). However, attempts to cleave the dithiolene ring releasing unprotected dithiolene were unsuccessful.⁷⁰ Interestingly, treatment with NaBH_4 reduced the keto group without reducing the pyrazine ring.

2.3.3 Third-Generation Dithiolene Pterins and their Complexes

As described in the previous section, model chemistry had succeeded in making pterinylidene complexes of Mo. However, a remaining challenge was to position an alcohol group on the dithiolene side chain for cyclization to a pyran ring thereby forming the entire pyranopterinylidene found in Moco. This section presents a variety of approaches and results from studies aimed to prepare and understand dithiolenes fused to pyran rings as well as the behavior of the pyranopterin unit itself.

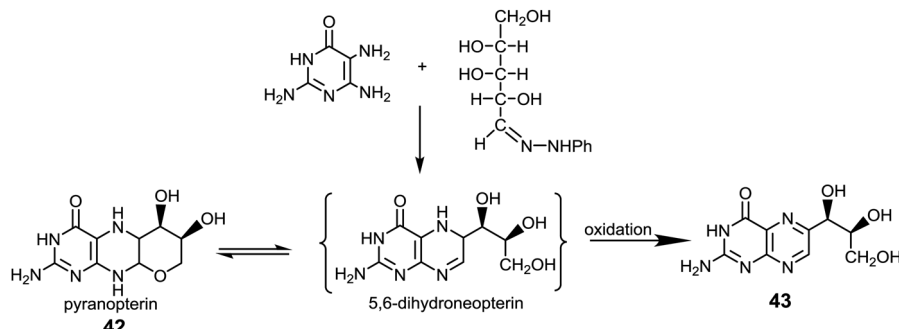


Scheme 2.30 Synthesis of pterin dithiolene protected as an ylide.

2.3.3.1 A Route to a Synthetic Pyranopterin Leads to Molybdopterin in Protected Form

Based on the well-established reaction of *o*-phenylenediamine and sugars,^{71,72} Soyka *et al.*⁷³ sought to prepare 5,6-dihydropterins from the reaction of 5,6-diaminopyrimidine and the phenylcarbazone of arabinose. However, pyranopterin **42** was the major product formed, as shown in Scheme 2.31. The pyranopterin could be viewed as the stabilized form of the target but unstable 5,6-dihydro tautomer, which easily oxidizes to neopterin **43**.

This condensation approach was successfully applied by the Manchester group to synthesize the pyranopterin cofactor in a highly protected form as

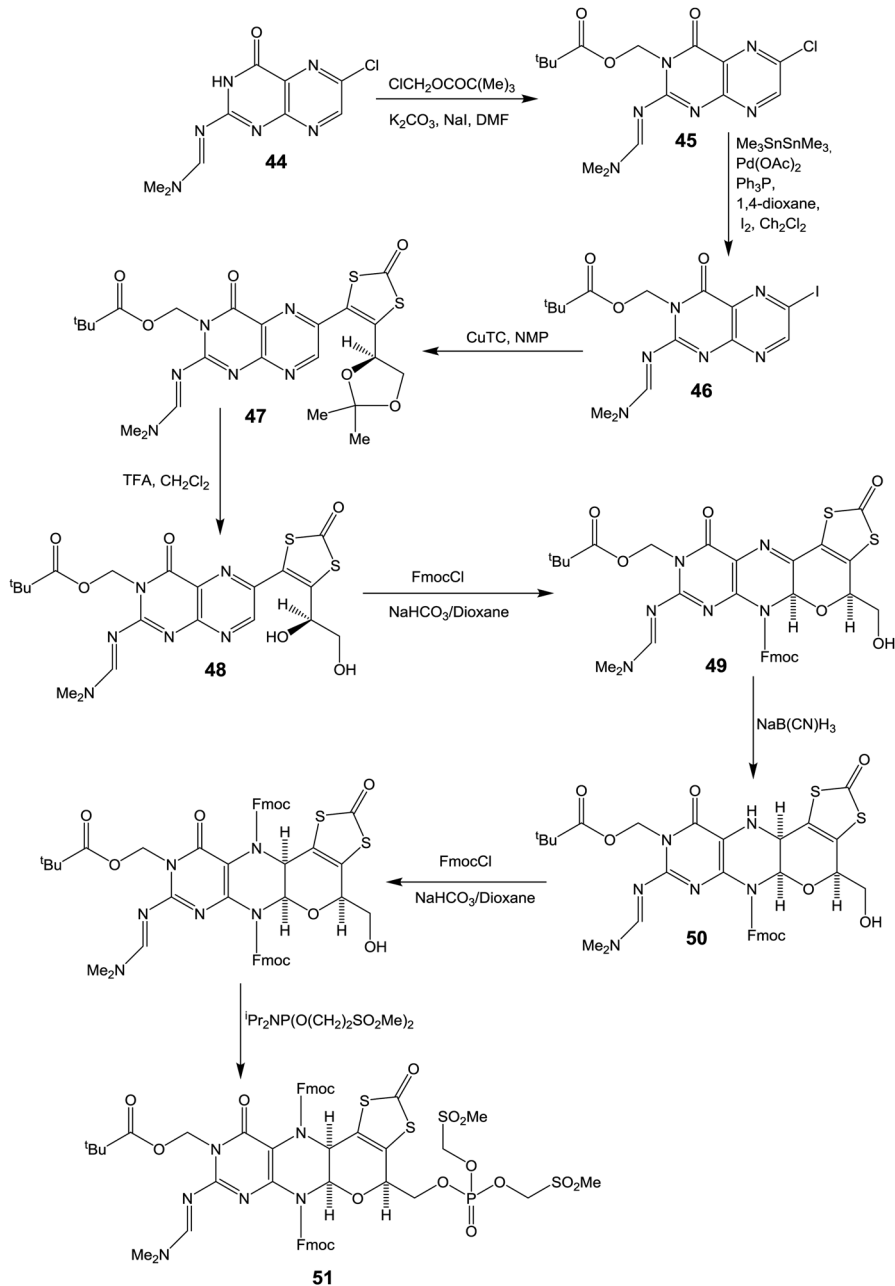


Scheme 2.31 Synthesis of pyranopterin by condensing a sugar molecule with a diaminopyrimidine.

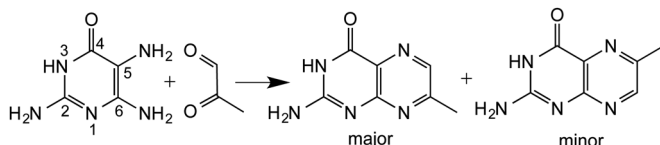
described by Bradshaw *et al.* (Scheme 2.32).⁷⁴ In this lengthy procedure, protection of the 2-NH₂ group and the N3 atom in 44 precedes replacement of the 6-chloro atom in 45 by a more reactive iodo group in 46. Coupling this compound with 4-(2,2-dimethyl-1,3-dioxolan-4-yl)-5-(tributylstannyl)-1,3-dithiol-2-one using copper thiophene-2-carboxylate (CuTC) occurred in moderately high yield positioning the protected diol (47) to be coupled with the pterin ring. The diol group in 47 was subsequently hydrolyzed to the corresponding diol 48. Treatment of this compound with 9H-fluoren-9-ylmethyl chloroformate (FmocCl) leads to ring closure and the formation of two isomeric Fmoc protected pyranopteridines in 49, where the two hydrogens at 5a- and 4-positions are either *cis* or *trans* configuration. The compound was reduced stereospecifically with NaB(CN)H₃, resulting in the reduced pyranopterin compound 50. The alcohol group was converted to a phosphate group with treatment of *i*Pr₂NP(O(CH₂)₂SO₂Me)₂ and accomplished the chemical synthesis of molybdopterin ligand of Moco, although in highly protected form 51.

The above methodologies for synthesis of pyranopterins involve the functionalization of an existing pterin. Substituted pterins can be prepared by Isay–Gabriel–Colman reaction, where 5,6-pyrimidinediamine is condensed with compounds containing a dicarbonyl functionality. One of the major problems with this reaction is the preferential formation of the undesired 7-stereoisomer when an asymmetric dicarbonyl reagent is used (Scheme 2.33). Different aspects of this approach were discussed extensively in a recent review article.⁷⁵ Very recently, the Basu group⁷⁶ have demonstrated that the Isay coupling reaction can be controlled by varying solvent and additives, which influences the nucleophilicity of carbonyl functionality. Furthermore, sluggishness of the Isay condensations can be addressed by including an osone derivative.

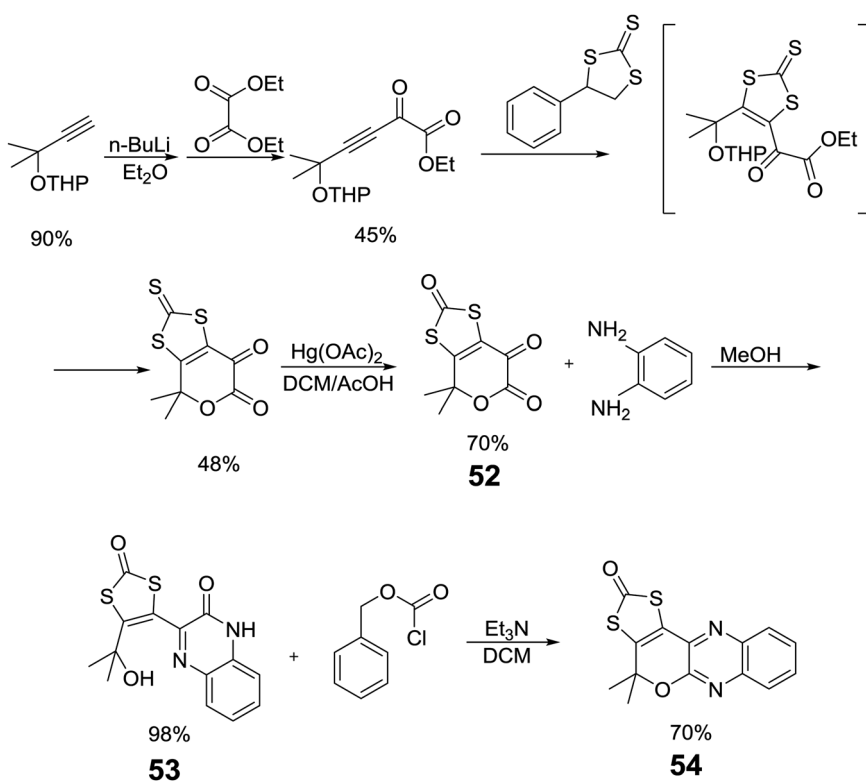
In order to better understand the reactivity of N-heterocycle, the Basu group⁷⁷ have utilized the Isay–Gabriel–Colman reaction in preparation of pyranoquinoxaline dithiolene compounds (Scheme 2.34). In these studies a pyran dithiolene diketone (52) was synthesized from a protected alkyne using the sulfur insertion methodology developed by Joule and Garner. The diketone was coupled with *o*-phenylenediamine, which results primarily in an open ring compound 53. The pyran ring can be formed through treatment of benzylchloroformate. The



Scheme 2.32 Bradshaw *et al.* synthesis of reduced pyranopterin dithiolene ligand in a highly protected form.



Scheme 2.33 Stereoselective Isay coupling reaction.

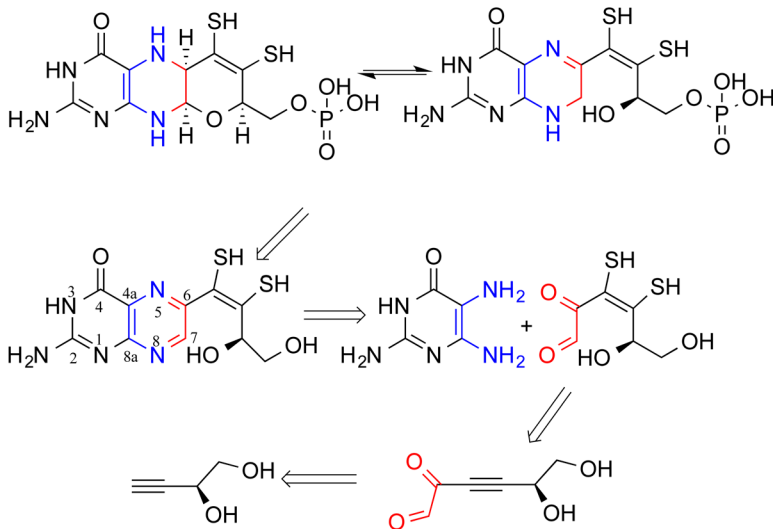


Scheme 2.34 A new synthetic scheme for pyranoquinoxaline dithiolene derivative using a protected dithiolene.

resulting product 54 is fluorescent and the dithiolene moiety can be deprotected with a base, and the ensuing ligand binds a variety of metal ions.

2.3.3.2 A Retrosynthetic Analysis Approach

In a different approach, a retrosynthetic analysis of MPT suggested a potential starting point for synthesizing the molybdopterin cofactor.⁷⁸ The retrosynthetic analysis, shown in Scheme 2.35, of the MPT provides a conceptual framework for this investigation. The fragile N8-C7-O moiety of the MPT can be oxidatively cleaved under acidic conditions, yielding a fully oxidized pyrazine ring, concomitantly opening the pyran ring by breaking the C7-O

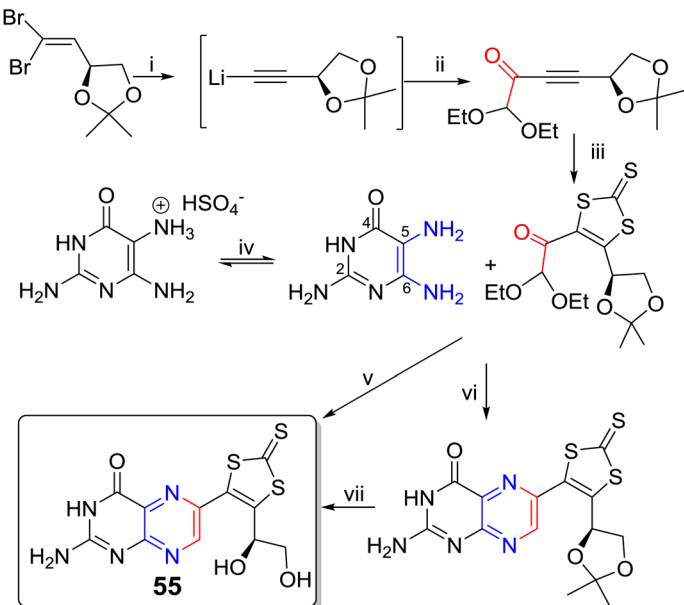


Scheme 2.35 A retrosynthetic scheme for molybdopterin.

bond. The N8–C7–O moiety can be reconstructed by nucleophilic addition of the alcohol to an *N*-acetylated pyrazine ring, which can be formed by treating the pterin with chloroformate reagents that can subsequently be reduced by NaBH₃CN. It is now known that both the open and closed forms exist in equilibrium,⁷⁹ and the open form can be oxidized to fully oxidized pterin. Pimkov *et al.*⁷⁸ suggested that the pyrazine ring of the oxidized molybdopterin can be constructed *via* the condensation of an α -keto aldehyde, with 2,5,6-triamino-3,4-dihydropyrimidin-4-one. The retrosynthetic analysis highlights α -keto aldehyde as a key precursor to MPT, which is an “osone” harboring a dithiolene moiety. A protected form of dithiolene was achieved from an activated acetylene derivative to which a dithiolene was introduced. The keto group adjacent to acetylene activates the alkyne, which was prepared from an acetylene through a nucleophilic addition reaction (Scheme 2.36) methodology, which yielded a minimally protected molybdopterin. The condensation reaction of oxo-aldehyde with the triaminohydroxy pyrimidine was conducted in a regioselective manner to obtain the desired 6-substituted regiosomer 55. In this case, the pterin functionality bears no protection; the only protection is in the dithiolene unit, which can be modified to introduce metal ions. This molecule has all the components of the dephospho MPT and can serve as a spectroscopic benchmark for future studies.

2.3.3.3 Spontaneous Pyran Ring Cyclization Within a Pterin Dithiolene Complex

Building on their strategy of preparing pterin dithiolene complexes through coupling [Tp*Mo(S)(S₄)][–] with pterinyl alkynes (see Scheme 2.23), Burgmayer’s group employed a pterinyl alkyne nearly identical to Form A to generate a



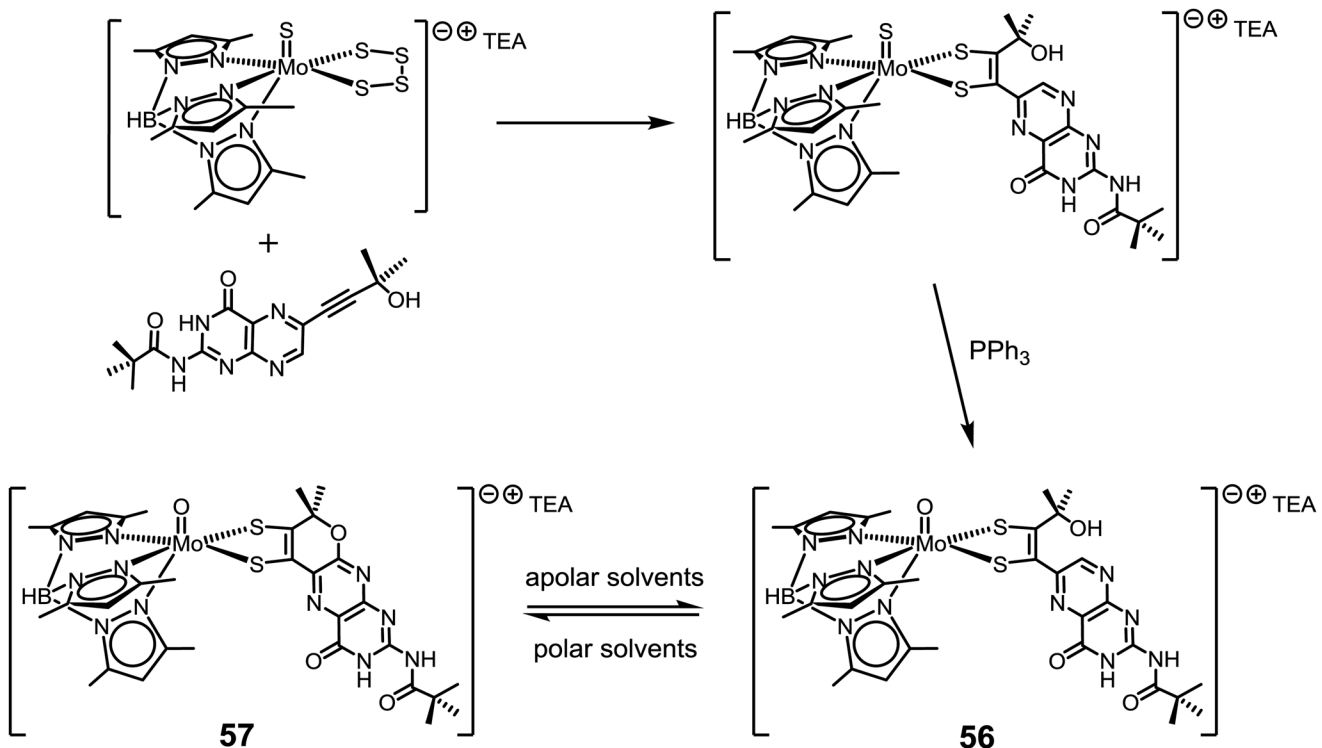
(i) ⁷BuLi, Et₂O at -78 °C, room temperature; (ii) ethyl 2,2-diethoxyacetate at -78 °C, room temperature (31%); (iii) phenyl-1,3-dithiolane-2-thione at 130 °C (58%); (iv) Na₂SO₃, DMSO; (v) 150 °C, Na₂SO₃, DMSO (24%); (vi) 120 °C, 2-mercaptoethanol, DMSO (31%) (vii) CF₃COOH, DMF at 60 °C (82%).

Scheme 2.36 Design of an activated dithiolene and its condensation with pyrimidine forming dephospho molybdopterin with protected dithiolene.

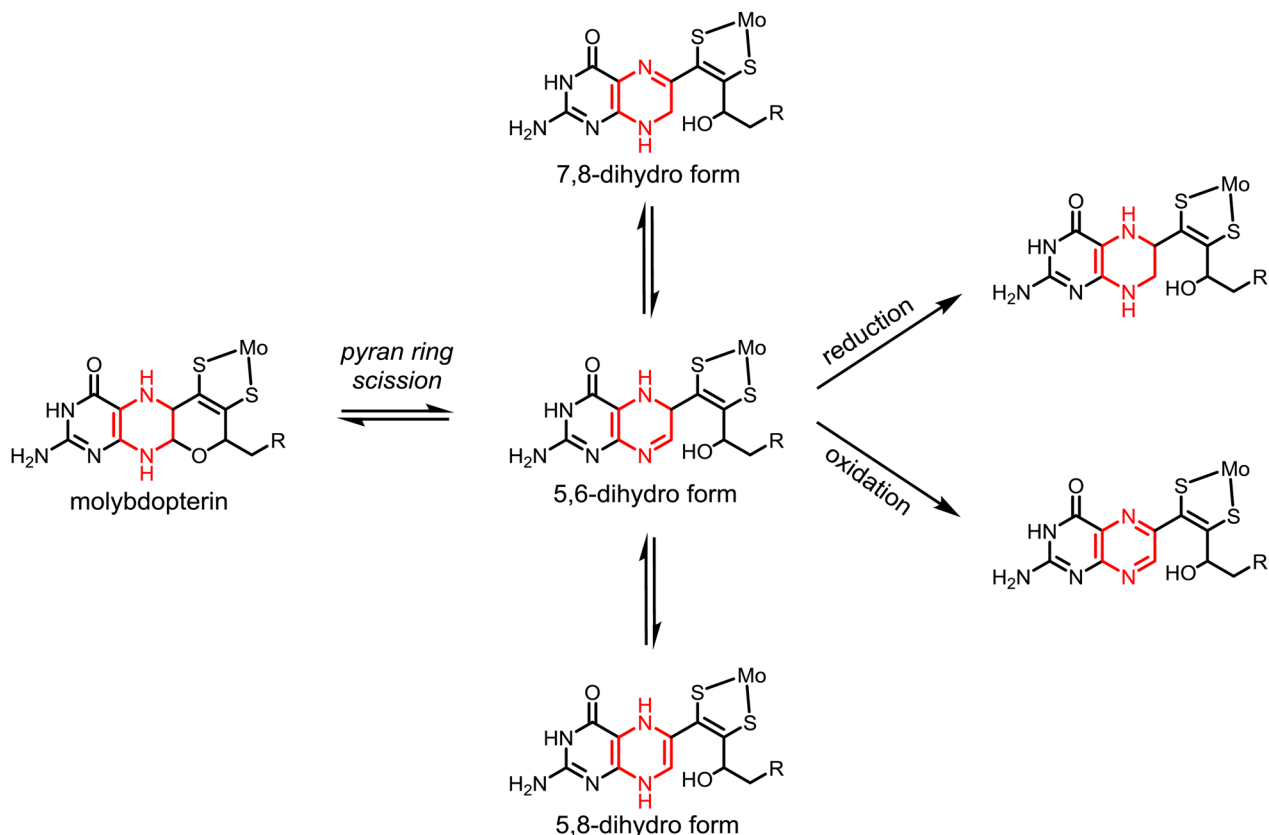
pterinyldithiolene complex **56** having a hydroxyl group positioned to cyclize to a pyran (Scheme 2.37).⁷⁹ In fact, they discovered that pyran cyclization occurred spontaneously following dithiolene ligand formation. Subsequent studies revealed the pyran cyclization was reversible where the pyranopterin form (**57**) exists in equilibrium with the uncyclized or open form. Solvent characteristics, especially the solvent dielectric constant, determined whether the pyranopterin or the open pterin predominates. Apolar solvents favor the open pterin structure whereas more polar solvents favor the pyranopterin form. Van't Hoff analysis of this equilibrium yielded thermodynamic parameters and showed the reversible cyclization had a low energy barrier of less than 10 kJ mol⁻¹.⁸⁰

2.3.3.4 Determining the Redox State of the Pyranopterin System

After acquiring the structural identity of the pyranopterin ligand in Moco by protein crystallography, there was confusion about its redox state. The saturated, quaternary carbons of the middle pyrazine ring in the pyranopterin seem similar to the structure of a tetrahydropterin but scission of the pyran ring reveals a 5,6-dihydropterin (Scheme 2.38). The ring-opened, 5,6-dihydropterin form of molybdopterin might then be anticipated to tautomerize to other dihydro- structures, and in principle could be further reduced to a true



Scheme 2.37 Spontaneous pyranopterin formation.



Scheme 2.38 A few of many possible outcomes of redox reactions at molybdopterin after pyran ring scission.

tetrahydropterin, or further oxidized to an oxidized pterin. Scheme 2.38 shows possible molybdopterin inter-conversions based on known pterin chemistry, suggesting a variety of reaction possibilities. The interpretation of the pyranopterin structure as a protected form of a 5,6-dihydropterin is intriguing since it is consistent with Rajagopalan's conclusion that Moco contained a dihydro-, not tetrahydro-, pterin as discussed in Section 2.3.1.

The availability of a pyranopterin model compound from the reaction reported by Soyka *et al.*⁷⁴ (Scheme 2.31) allowed the Burgmayer group to establish the redox state of pyranopterin **58** and confirmed that pyranopterin behaves as a dihydropterin under oxidative conditions where it undergoes a two-electron, two-proton oxidation to yield the fully oxidized neopterin **59** (Figure 2.15).⁸¹ Kinetic analysis showed this oxidation of **58** to **59** was slower than tetrahydropterin oxidation to 7,8-dihydropterin, thereby confirming that the fused pyran ring contributes a stabilizing effect. The oxidation reaction of pyranopterin exhibits a minimal pH and solvent dependence, in marked contrast to tetrahydropterin oxidation that is strongly pH and solvent dependent. The pyranopterin **58** resisted further reduction to tetrahydropterin **60** using a variety of reducing agents known to reduce oxidized and 7,8-dihydropterins to tetrahydropterins. This experimental work proves that pyranopterin possesses a distinct redox chemistry, unlike that of an unsubstituted pterin, and it may be critical to its use as part of the molybdopterin ligand for molybdenum and tungsten in enzymes. The reduced pyranopterin is often referred to as a tetrahydropyranopterin in the literature, based on its saturated pyrazine, but it is functionally a dihydropterin.

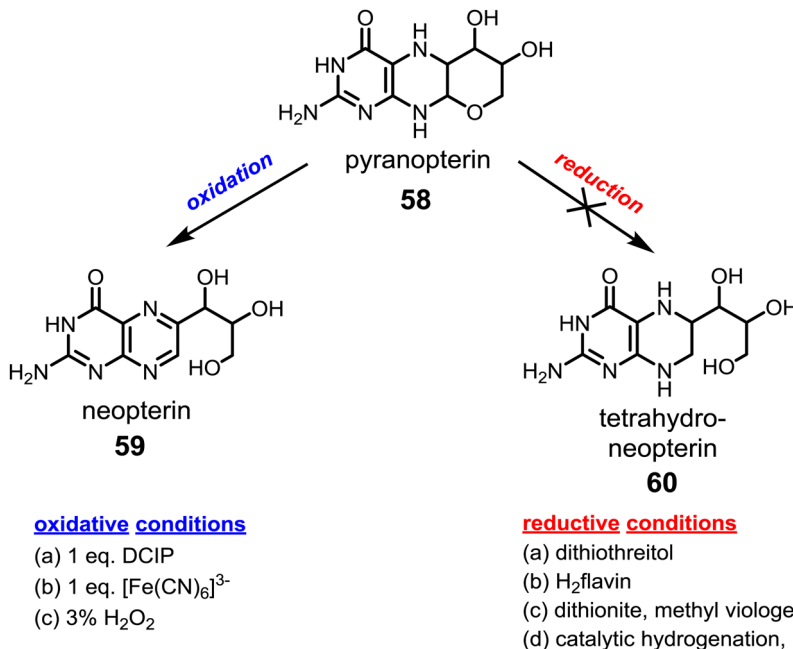


Figure 2.15 The redox reactivity of a model pyranopterin.

2.3.4 Chemical Behavior of Dithiolenes Substituted by Pterin and N-Heterocycles

The effect of a pterin (or quinoxaline) on a dithiolene molybdenum complex has been studied spectroscopically (EPR, electronic spectroscopy, magnetic circular dichroism), using cyclic voltammetry, chemical reactivity and probed through computations. The Mo(v) forms of the two pterin-dithiolene model systems $[Cp_2Mo(v)(\text{pterin}-\text{dithiolene})]^{+}$ and $Tp^*\text{Mo}(v)\text{O}(\text{pterin}-\text{dithiolene})$ can be generated by oxidation of the initial Mo(iv) product with ferrocenium or iodine.^{49,50} These Mo(v) species are suitable for analysis by EPR and magnetic circular dichroism (MCD). Comparison of EPR data obtained from the $Tp^*\text{MoO}(\text{pterin}-\text{dithiolene})$ and $[Cp_2\text{Mo}(\text{pterin}-\text{dithiolene})]^{+}$ model complexes shows the electronic flexibility of the pteridinyldithiolene ligand. $Tp^*\text{MoO}(\text{pterin}-\text{dithiolene})$ complexes have $^{95,97}\text{Mo}$ hyperfine values considerably larger ($A_{\text{ave}} = 37 \text{ G}$) than observed for $Cp_2\text{Mo}(\text{pterin}-\text{dithiolene})$ ($A_{\text{ave}} = 11 \text{ G}$).⁸² The smaller $^{95,97}\text{Mo}$ A value in $Cp_2\text{Mo}(\text{pterin}-\text{dithiolene})$ has been interpreted as reflecting the composition of the HOMO being localized on the dithiolene sulfur and carbon atoms allowing delocalization of substantial spin density from the Mo(v) center onto the dithiolene chelate. An unexpected result from spectroscopic analysis was that the EPR and MCD parameters for $Tp^*\text{MoO}(\text{pterin}-\text{dithiolene})$ model complexes were nearly identical to those exhibited by $Tp^*\text{MoO}(\text{bdt})$ ($\text{bdt} = 1,2\text{-benzenedithiolate}$) suggesting the electronic effect of the pterin on the Mo atom was minimal.

Cyclic voltammetry (CV) is useful to probe the electronic effect of pterin and quinoxaline groups on the $\text{Mo}^{\text{V}/\text{IV}}$ reduction potential and this method was applied to a series of $Tp^*\text{MoO}(\text{dithiolene})$ complexes. The results are graphically summarized in Figure 2.16. Within a series of $Tp^*\text{MoO}(\text{dithiolenes})$, it is clear that pterin (or quinoxaline) substitution causes a significant shift in the $\text{Mo}^{\text{V}/\text{IV}}$ redox potential to more positive values compared to simpler dithiolenes like benzenedithiolate (bdt) or ethanedithiolate (edt). This conclusion seems to contradict the results from EPR and MCD studies of $Tp^*\text{MoO}(\text{pterin}-\text{dithiolene})$ vs. $Tp^*\text{MoO}(\text{bdt})$, which, as noted above, failed to reveal any differences among the dithiolene complexes.

Cyclic voltammetry was also a good reporter of a significant electronic effect produced by N-heterocycle protonation. The earliest report concerned $\text{Mo}^{\text{V}/\text{IV}}$ tris-dithiolene complexes of 2,3-quinoxalyldithiolate (qdt).⁸³ Subsequently, the effect of N-heterocycle protonation on the electronic structure of dithiolene was revisited in several studies of Mo dithiolenes substituted with quinoxaline, pyrazine and pyridines.⁸⁴ All these studies showed that protonation at quinoxaline made reduction processes more favorable and caused a reorganization of electron density throughout the heterocycle in conjugation with the dithiolene that is consistent with the scheme shown in Scheme 2.39. In certain cases the one-electron reduced species were best described as quinoxalyldithiolene radicals.

Tautomers B and C in Scheme 2.39 illustrate one of the most significant consequences of a pterin or quinoxaline substituent on a dithiolene. Protonating a ring N atom induces a subtle shift of electron density from either the

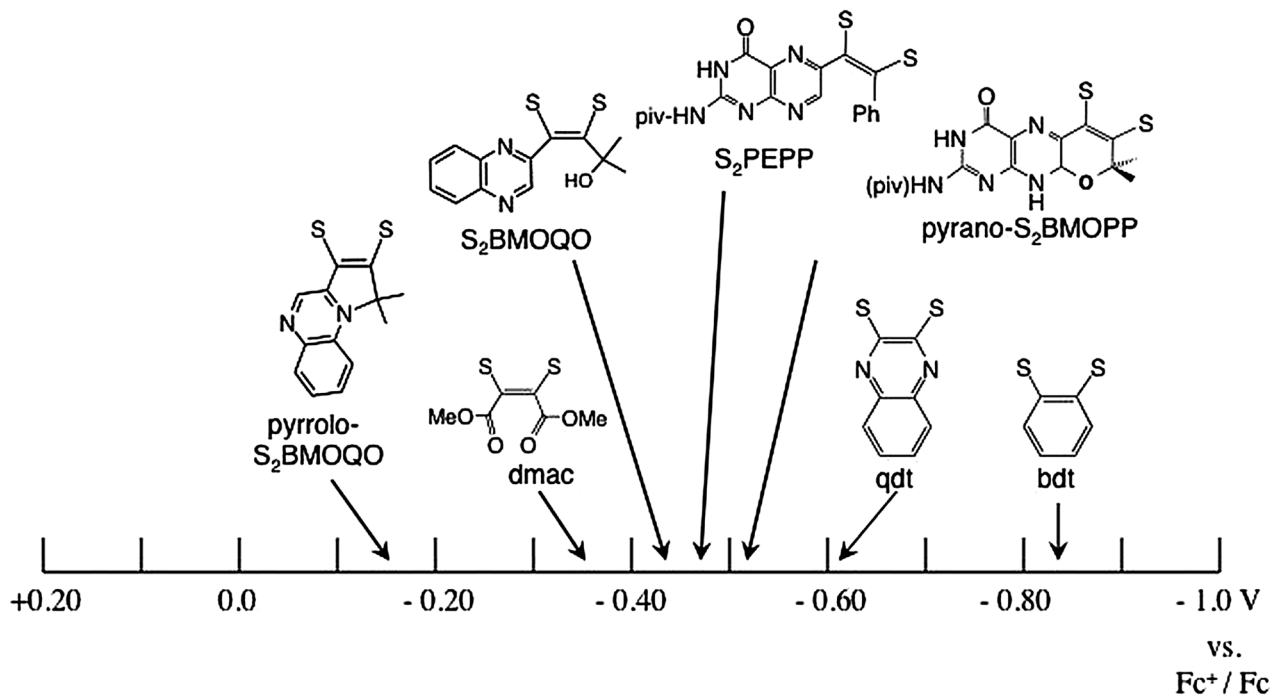
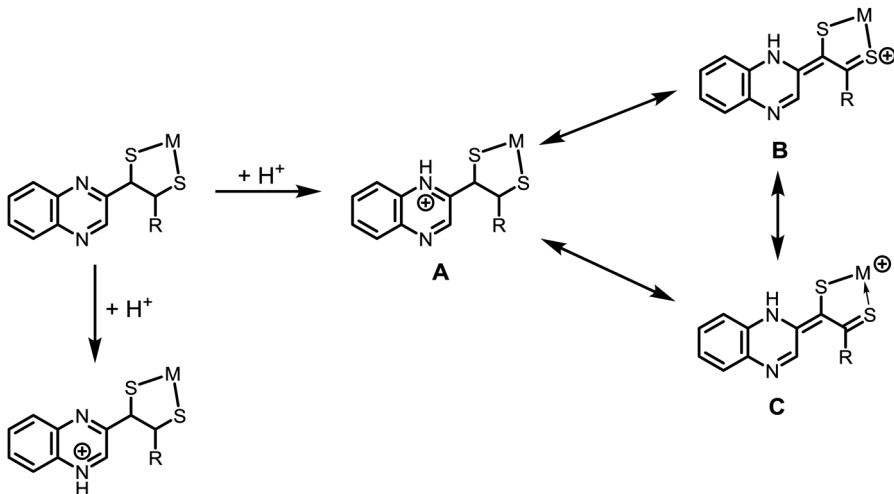


Figure 2.16 Comparison of $\text{Mo}^{\text{VII}/\text{IV}}$ reduction potentials in a series of $\text{Tp}^*\text{MoO}(\text{dithiolene})$ complexes where the specific dithiolene is shown on the plot. Potentials were measured by CV and are shown *vs.* the ferrocenium/ferrocene couple.



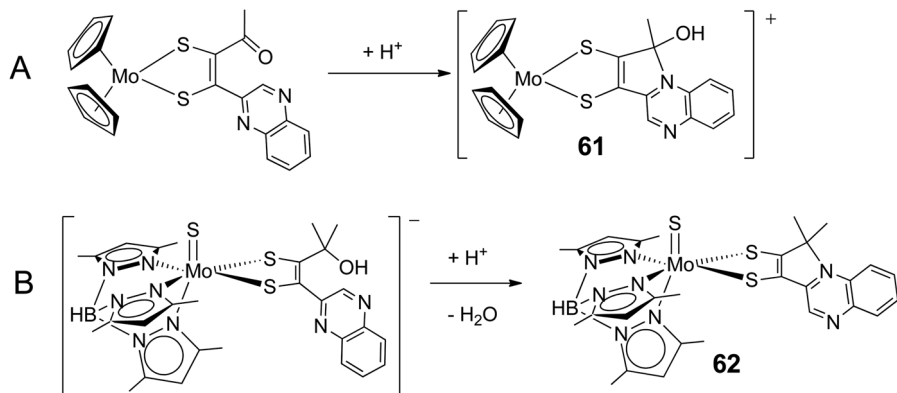
Scheme 2.39 Quinoxaline protonation can access other resonance forms including thiolate, thione chelates on Mo.

S atom in tautomer B or the Mo atom in tautomer C resulting in two thione-chelates oxidized compared to the dithiolene (or ene-dithiolate) in tautomer A. A detailed electrochemical study of Cp₂Co(S₂C₂H(quin)) (Cp = cyclopentadienide; quin = 2-quinoxaline) provided evidence for multiple tautomers of protonated quinoxaline N atoms.⁸⁵

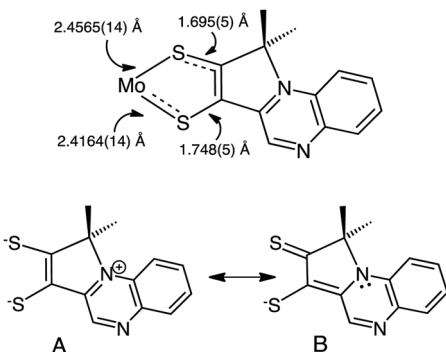
The introduction of pterin- and quinoxaline-substituents on dithiolenes induces reactivity at the pyrazine N atoms. In both Cp₂Mo(quinoxalyldithiylene) (**61**, in reaction A) and Tp^{*}MoO(quinoxalyldithiylene) (**62**, in reaction B) complexes, electrophilic attack at atom N1 of the pyrazine ring results in an intramolecular cyclization producing a pyrrole-like ring (Scheme 2.40).⁸⁶ X-ray structures of both **61** and **62** reveal that the dithiylene chelate is asymmetrically bound, exhibiting asymmetric Mo-S and S-C bond lengths.

An analysis of the electronic structure in these complexes using Resonance Raman, EPR and Density Functional Theory (DFT) calculations provide evidence for tautomers depicted in Scheme 2.41 as an admixture of a thione-thiolate structure, which can be considered to result from electron density distributed into the quinoxaline structure from partial thiolate to thione oxidation (Scheme 2.41).⁸⁶

Electronic delocalization from the dithiylene into the quinoxaline system makes structure B (Scheme 2.41) significantly electron-withdrawing, as compared to the structure A, which has the effect of stabilizing the Mo(IV) state. A stabilized Mo(IV) is indicated by a 300 mV positive shift in the Mo(V/IV) reduction potential, as shown in Figure 2.16. Both of the cyclized quinoxaline dithiylene complexes in Scheme 2.40 are characterized by intense absorptions in the visible electronic spectrum that have been assigned to intramolecular ligand charge transfer transitions. The electronic reorganization



Scheme 2.40 Electrophilic reactions of quinoxalyl-dithiolenes cause intramolecular cyclization.

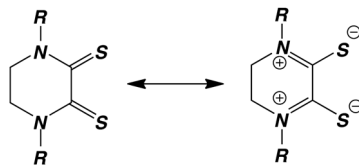


Scheme 2.41 Asymmetry of the dithiolen chelates explained by an admixture of resonance forms, the thione-thiolate (structure B) and the dithiolate (structure A).

depicted in Scheme 2.41 in addition to the protonation effects illustrated in Scheme 2.39 hints at the rich chemistry possible when a N-heterocycle is appended to a dithiolen on a redox active metal.

Investigation of N-cycle protonation (N-cycle is either quinoxaline or pyridine) in the $\text{Cp}^*\text{Mo}(\text{S}_2\text{C}_2\text{H}(\text{N}-\text{cycle}))$ system shows that the pK_a values increase by 1–3 units as compared to the free heterocycles due to the resonance stabilization by the metallo-1,2-enedithiolate.^{84a} N-heterocycle protonation also has a strong effect on electronic transitions in these complexes where the relative energies of d-based and ligand-based unoccupied orbitals can be switching, accessing luminescent emissive Inter Ligand Charge Transfer (ILCT) excited states.^{84b}

The above examples underline that the dithiolen unit can also be an important redox component of the molybdenum cofactor. Much of the discussion in this chapter has focused on the redox chemistry of pterin and its



Scheme 2.42 The structure of dithione ligand (left) and its dizwitterionic resonance form (right).

interaction with molybdenum. The details of the redox chemistry of dithiolene are covered in Chapter 3. However, it is instructive to point out that the dithiolene chelate can be present in fully reduced dithiolene, fully oxidized dithione or in between one electron reduced thioquinone state.⁸⁷ From the early discovery of the dithiolene piece of MPT, it was assumed that it was in the fully reduced dithiolene state in all oxidation states of Mo. While protein crystal structures unequivocally establish that both sulfur donors of the dithiolene ligand coordinate to the metal center, they have not provided evidence for other redox states of the dithiolene unit.⁸⁸

Another heterocycle, piperazine, has been used in developing the chemistry of the oxidized form of the dithiolene. Thus chemistry of the *N,N'*-dialkylpiperazine-2,3-dithione has been explored to understand the basic chemistry of the unit. Because the piperazine ring is fully reduced, electron delocalization can only occur through a keto-enol type tautomerism of the dithione (Scheme 2.42, left) to the dithiolene (Scheme 2.42, right) involving the nitrogen in the heterocycle. The dithione (Dt0) moiety of this ligand represents the two-electron oxidized form of the dithiolene ligand.

Interestingly, the chemistry of the oxidized dithione ligand has not been explored in depth even though redox non-innocence of the ligand was well established.⁸⁹ The dithiolene moiety in these ligands behave as π -acceptors rather than π -donors. Consequently, they stabilize low valent metal centers, *e.g.* a Mo carbonyl species.⁹⁰ However, oxo-molybdenum complexes of this ligand has been synthesized and structurally characterized.^{90b} A resonance Raman study of $[\text{MoOCl}(\text{Dt0})_2](\text{PF}_6)$ showed the ground state description of the complex is an admixture of dithiolene and dithione forms with 37% exhibiting enol form.^{90c} This investigation underscores the complexity of the molybdenum cofactor as it can exist in different redox forms, which is particularly difficult to discern in the native proteins.

2.4 Unresolved Questions and Current Objectives

In the last three decades, significant progress has been made in devising synthetic methodology to obtain closer analogs of MPT and the molybdenum cofactor. These include methodologies for synthesizing pterin, functionalizing a pterin to harbor a dithiolene moiety and metal coordination of both pterin-dithiolenes and pyranopterin dithiolenes. With these molecules in hand, one may ask detailed questions about reactivity, electronic structure and

geometric propensity. We will soon be in a position to say how a fused pyran ring on the pterin affects pterin redox chemistry and how this will affect the electronic environment of the appended dithiolene group and the molybdenum center. In addition, specific details of how the pterin system responds to oxidation state changes at the molybdenum can be known. As this information is considered with corresponding information gained from protein crystallography and spectroscopy, we will attain a more precise understanding of Moco.

There remain large gaps in knowledge in regards to substrate reactions. For example, it is not clear how the pterin cofactor might enhance the rate of substrate transformations that are typically orders of magnitude higher than those determined from model compounds. Protein crystallography has revealed extensive hydrogen bonding of the pterin cofactor with the protein backbone and typically the cofactor is buried deep ($\sim 15 \text{ \AA}$) inside the protein.⁹¹ Such a feature has been modeled by sterically encumbered dendritic ligand architecture that has been shown to influence the electronic structure⁹² as well as the solvent polarity at the vicinity of the metal center.⁹³ Together both factors influence the redox chemistry. Recently, we have suggested that the extended H-bonded structure imposed by the pterin cofactor may poised the electronic states such that minimum reorganization energy is spent, a condition reminiscent of the entatic state discussed extensively in copper enzymes.⁹⁴ Current functional models for Moco undergo significant reorganization during the oxygen atom transfer step. A future goal for Moco model systems is to build pterin and pyranopterin dithiolene complexes capable of substrate reactions to closely investigate the relationship of environment on reactivity.

There are fundamental aspects of Moco within the proteins that will need exploration to complete our insight into the function of this important class of enzymes. Protein crystallography may not be sufficient to provide the information. Despite the many X-ray structures showing reduced pterin in Moco, there remains uncertainty in the exact nature of redox state of the components of the Moco.⁹⁵ In our view, one of the objectives in the field is to understand clearly how the redox equivalents are distributed, as there are several competent units that can shuttle electrons. One can take this a step further and ask the questions: are the redox equivalents distributed equally in all molybdoproteins in the resting state? Do they change during the course of catalysis? The former seems unlikely since there is a great deal of variation not only in the cofactor composition but also in their structure. A recent analysis of the crystallographically determined cofactor structure revealed that the distortions within the cofactor vary significantly, and these distortions may be related to the electron transfer pathway.⁹⁵ The second question is more difficult to assess and one would assume that electron distribution would change during catalysis, which may be a consequence of the electron transfer through pterin backbone. Another important objective is to evaluate whether different redox states of the pterin can affect the substrate transformation of the system. This will require well-characterized compounds with different pterin redox states. As we have outlined in this review, pterin chemistry is inherently challenging, but we are hopeful that with the success of the past decades, the next decade will be more rewarding.

Acknowledgement

We are thankful to numerous coworkers who have contributed significantly in the development of the chemistry in our laboratories. Financial support from the National Institutes of Health (GM 061555 to PB and GM 081848 to SB) is gratefully acknowledged.

References

1. (a) E. I. Stiefel, The coordination and bioinorganic chemistry of molybdenum, *Prog. Inorg. Chem.*, 1977, **22**, 1–223; (b) J. T. Spence, Modeling the molybdenum centers of the molybdenum hydroxylases, *Coord. Chem. Rev.*, 1983, **48**, 59–82.
2. (a) J. H. Enemark, J. J. A. Cooney, J.-J. Wang and R. H. Holm, Synthetic Analogues and Reaction Systems Relevant to the Molybdenum and Tungsten Oxotransferases, *Chem. Rev.*, 2004, **104**, 1175–1200; (b) J. H. Enemark and C. G. Young, Bioinorganic chemistry of pterin-containing molybdenum and tungsten enzymes, *Adv. Inorg. Chem.*, 1994, **40**, 1–88; (c) R. H. Holm, The biologically relevant oxygen atom transfer chemistry of molybdenum: from synthetic analog systems to enzymes, *Coord. Chem. Rev.*, 1990, **100**, 183–221; (d) A. Majumdar and S. Sarkar, Bioinorganic chemistry of molybdenum and tungsten enzymes: A structural-functional modeling approach, *Coord. Chem. Rev.*, 2011, **255**, 1039–1054.
3. B. Fischer, J. H. Enemark and P. Basu, A chemical approach to systematically designate the pyranopterin centers of molybdenum and tungsten enzymes and synthetic models, *J. Inorg. Biochem.*, 1998, **72**, 13–21.
4. (a) P. A. Ketchum, H. Y. Cambier, W. A. Frazier III, C. H. Madansky and A. Nason, In vitro assembly of Neurospora assimilatory nitrate reductase from protein subunits of a Neurospora mutant and the xanthine oxidizing or aldehyde oxidase systems of high animals, *Proc. Natl. Acad. Sci. U. S. A.*, 1970, **66**, 1016–1023; (b) A. Nason, A. D. Antoine, P. A. Ketchum, W. A. Frazier III and D. K. Lee, Formation of assimilatory nitrate reductase by in vitro intercistronic complementation in *Neurospora crassa*, *Proc. Natl. Acad. Sci. U. S. A.*, 1970, **65**, 137–144; (c) A. Nason, K.-Y. Lee, S.-S. Pan, P. A. Ketchum, A. Lamberti and J. DeVries, In vitro formation of assimilatory reduced nicotinamide adenine dinucleotide phosphate: nitrate reductase from a *Neurospora* mutant and a component of molybdenum-enzymes, *Proc. Natl. Acad. Sci. U. S. A.*, 1971, **68**, 3242–3246.
5. E. I. Stiefel, *The structures and spectra of molybdoenzyme active sites and their models*, Pergamon, 1980, pp. 41–98.
6. J. L. Johnson, B. E. Hainline and K. V. Rajagopalan, Characterization of the molybdenum cofactor of sulfite oxidase, xanthine oxidase, and nitrate reductase. Identification of a pteridine as a structural component, *J. Biol. Chem.*, 1980, **255**, 1783–1786.
7. K. V. Rajagopalan, Novel aspects of the biochemistry of the molybdenum cofactor, *Adv. Enzymol. Relat. Areas. Mol. Biol.*, 1991, **64**, 215–290.

8. J. L. Johnson, B. E. Hainline, K. V. Rajagopalan and B. H. Arison, The Pterin Component of the Molybdenum Cofactor Structural characterization of two fluorescent derivatives, *J. Biol. Chem.*, 1984, **259**, 5414–5422.
9. S. P. Kramer, J. L. Johnson, A. A. Ribeiro, D. S. Millington and K. V. Rajagopalan, The structure of the molybdenum cofactor. Characterization of di-(carboxamidomethyl)molybdopterin from sulfite oxidase and xanthine oxidase, *J. Biol. Chem.*, 1987, **262**, 16357–16363.
10. J. L. Johnson and K. V. Rajagopalan, Structural and metabolic relationship between the molybdenum cofactor and urothione, *Proc. Natl. Acad. Sci. U. S. A.*, 1982, **79**, 6856–6860.
11. J. H. Enemark and C. D. Garner, The coordination chemistry and function of the molybdenum centers of the oxomolybdoenzymes, *JBIC, J. Biol. Inorg. Chem.*, 1997, **2**, 817–822.
12. (a) S. Gardlik, M. J. Barber and K. V. Rajagopalan, A molybdopterin-free form of xanthine oxidase, *Arch. Biochem. Biophys.*, 1987, **259**, 363–371; (b) S. Gardlik and K. V. Rajagopalan, The state of reduction of molybdopterin in xanthine oxidase and sulfite oxidase, *J. Biol. Chem.*, 1990, **265**, 13047–13054.
13. B. Kruger and O. Meyer, The pterin (bactopterin) of carbon monoxide dehydrogenase from *Pseudomonas carboxydoflava*, *Eur. J. Biochem.*, 1986, **157**, 121–128.
14. J. L. Johnson, N. R. Bastian and K. V. Rajagopalan, Molybdopterin guanine dinucleotide: a modified form of molybdopterin identified in the molybdenum cofactor of dimethyl sulfoxide reductase from *Rhodobacter sphaeroides forma specialis denitrificans*, *Proc. Natl. Acad. Sci. U. S. A.*, 1990, **87**, 3190–3194.
15. M. K. Chan, S. Mukund, A. Kletzin, M. W. W. Adams and D. C. Rees, Structure of a hyperthermophilic tungstopterin enzyme, aldehyde ferredoxin oxidoreductase, *Science*, 1995, **267**, 1463–1469.
16. (a) R. Huber, P. Hof, R. O. Duarte, J. J. G. Moura, I. Moura, M.-Y. Liu, J. LeGall, R. Hille, M. Archer and M. J. Romao, A structure-based catalytic mechanism for the xanthine oxidase family of molybdenum enzymes, *Proc. Natl. Acad. Sci. U. S. A.*, 1996, **93**, 8846–8851; (b) M. J. Romao, M. Archer, I. Moura, J. J. G. Moura, J. LeGall, R. Engh, M. Schneider, P. Hof and R. Huber, Crystal structure of the xanthine oxidase-related aldehyde oido-reductase from *D. gigas*, *Science*, 1995, **270**, 1170–1176.
17. M. G. Bertero, R. A. Rothery, M. Palak, C. Hou, D. Lim, F. Blasco, J. H. Weiner and N. C. J. Strynadka, Insights into the respiratory electron transfer pathway from the structure of nitrate reductase A, *Nat. Struct. Biol.*, 2003, **10**, 681–687.
18. D. P. Kloer, C. Hagel, J. Heider and G. E. Schulz, Crystal structure of ethylbenzene dehydrogenase from *Aromatoleum aromaticum*, *Structure*, 2006, **14**, 1377–1388.
19. M. M. Wuebbens and K. V. Rajagopalan, Structural characterization of a molybdopterin precursor, *J. Biol. Chem.*, 1993, **268**, 13493–13498.

20. J. L. Johnson, M. M. Wuebbens and K. V. Rajagopalan, The structure of a molybdopterin precursor. Characterization of a stable, oxidized derivative, *J. Biol. Chem.*, 1989, **264**, 13440–13447.
21. K. V. Rajagopalan, Biosynthesis and processing of the molybdenum cofactors, *Biochem. Soc. Trans.*, 1997, **25**, 757–761.
22. R. R. Mendel, Molybdenum cofactor of higher plants: biosynthesis and molecular biology, *Planta*, 1997, **203**, 399–405.
23. J. A. Santamaria-Araujo, B. Fischer, T. Otte, M. Nimtz, R. R. Mendel, V. Wray and G. Schwarz, The Tetrahydropyranopterin Structure of the Sulfur-free and Metal-free Molybdenum Cofactor Precursor, *J. Biol. Chem.*, 2004, **279**, 15994–15999.
24. G. Schwarz, R. R. Mendel and M. W. Ribbe, Molybdenum cofactors, enzymes and pathways, *Nature*, 2009, **460**, 839–847.
25. S. J. N. Burgmayer and E. I. Stiefel, Synthesis and structure of the first molybdenum-pterin complex, *J. Am. Chem. Soc.*, 1986, **108**, 8310–8311.
26. (a) R. Raghavan and G. Dryhurst, Redox chemistry of reduced pterin species, *J. Electroanal. Chem. Interfacial Electrochem.*, 1981, **129**, 189–212; (b) D. Ege-Serpkenci and G. Dryhurst, Electrochemistry of 6,7-dimethylpterins, *Bioelectrochem. Bioenerg.*, 1982, **9**, 175–195; (c) L. G. Karber and G. Dryhurst, Electrochemistry of 6-methyl-5,6,7,8-tetrahydropterin, *J. Electroanal. Chem. Interfacial Electrochem.*, 1982, **136**, 271–289; (d) D. Ege-Serpkenci, R. Raghavan and G. Dryhurst, Oxidation of methylated tetrahydropterins. Structure of the initial quinonoid-dihydropterin intermediate, *Bioelectrochem. Bioenerg.*, 1983, **10**, 357–376; (e) L. G. Karber and G. Dryhurst, Electrochemical oxidation of 5-methyl-5,6,7,8-tetrahydropterin, *J. Electroanal. Chem. Interfacial Electrochem.*, 1984, **160**, 141–157.
27. S. J. N. Burgmayer, A. Baruch, K. Kerr and K. Yoon, A model reaction for molybdenum(VI) reduction by molybdopterin, *J. Am. Chem. Soc.*, 1989, **111**, 4982–4984.
28. H. L. Kaufmann, L. Liable-Sands, A. L. Rheingold and S. J. N. Burgmayer, Molybdenum-Pterin Chemistry. 1. The Five-Electron Oxidation of an Oxo Molybdenum Dithiolate Complex of a Reduced Pterin, *Inorg. Chem.*, 1999, **38**, 2592–2599.
29. (a) H. L. Kaufmann, P. J. Carroll and S. J. N. Burgmayer, Molybdenum-Pterin Chemistry. 2. Reinvestigation of Molybdenum(IV) Coordination by Flavin Gives Evidence for Partial Pteridine Reduction, *Inorg. Chem.*, 1999, **38**, 2600–2606; (b) S. J. N. Burgmayer, M. R. Arkin, L. Bostick, S. Dempster, K. M. Everett, H. L. Layton, K. E. Paul, C. Rogge and A. L. Rheingold, Tetrahydropterin Reactions of Dioxo-Molybdenum(6+) Complexes: Does Redox Occur?, *J. Am. Chem. Soc.*, 1995, **117**, 5812–5823; (c) B. Fischer, J. Straehle and M. Viscontini, Pterin chemistry. 90. Synthesis and crystal structure of the first quinoid dihydropterinmolybdenum(IV) complex, *Helv. Chim. Acta*, 1991, **74**, 1544–1554.
30. S. Kaufman, *J. Biol. Chem.*, 1961, **36**, 804–810.

31. (a) R. H. Holm, E. I. Solomon, A. Majumdar and A. Tenderholt, Comparative molecular chemistry of molybdenum and tungsten and its relation to hydroxylase and oxotransferase enzymes, *Coord. Chem. Rev.*, 2011, **255**, 993–1015; (b) R. H. Holm, Metal-centered oxygen atom transfer reactions, *Chem. Rev.*, 1987, **87**, 1401–1449; (c) P. Basu, B. W. Kail, A. K. Adams and V. N. Nemykin, Quantitation of the ligand effect in oxo-transfer reactions of dioxo-Mo(VI) tris(pyrazolyl)borate complexes, *Dalton Trans.*, 2013, **42**, 3071–3081; (d) P. Basu, B. W. Kail and C. G. Young, Influence of the Oxygen Atom Acceptor on the Reaction Coordinate and Mechanism of Oxygen Atom Transfer From the Dioxo-Mo(VI) Complex, $\text{Tp}^{\text{iPr}}\text{MoO}_2(\text{OPh})$, to Tertiary Phosphines, *Inorg. Chem.*, 2010, **49**, 4895–4900; (e) P. Basu, V. N. Nemykin and R. S. Sengar, Substituent Effect on Oxygen Atom Transfer Reactivity from Oxomolybdenum Centers: Synthesis, Structure, Electrochemistry, and Mechanism, *Inorg. Chem.*, 2009, **48**, 6303–6313; (f) B. W. Kail, L. M. Perez, S. D. Zaric, A. J. Millar, C. G. Young, M. B. Hall and P. Basu, Mechanistic investigation of the oxygen-atom-transfer reactivity of dioxo-molybdenum(VI) complexes, *Chem.-Eur. J.*, 2006, **12**, 7501–7509; (g) V. N. Nemykin and P. Basu, Oxygen Atom Transfer Reactivity from a Dioxo-Mo(VI) Complex to Tertiary Phosphines: Synthesis, Characterization, and Structure of Phosphoryl Intermediate Complexes, *Inorg. Chem.*, 2005, **44**, 7494–7502; (h) A. J. Millar, C. J. Doonan, P. D. Smith, V. N. Nemykin, P. Basu and C. G. Young, Oxygen atom transfer in models for molybdenum enzymes: isolation and structural, spectroscopic, and computational studies of intermediates in oxygen atom transfer from molybdenum(VI) to phosphorus(III), *Chem.-Eur. J.*, 2005, **11**, 3255–3267; (i) V. N. Nemykin, J. Laskin and P. Basu, Isolation, Characterization of an Intermediate in an Oxygen Atom-Transfer Reaction, and the Determination of the Bond Dissociation Energy, *J. Am. Chem. Soc.*, 2004, **126**, 8604–8605; (j) V. N. Nemykin and P. Basu, A bifurcated pathway of oxygen atom transfer reactions from a monooxo molybdenum(VI) complex under electrospray ionization mass spectrometric conditions, *Dalton Trans.*, 2004, 1928–1933; (k) P. D. Smith, A. J. Millar, C. G. Young, A. Ghosh and P. Basu, Detection, Isolation, and Characterization of Intermediates in Oxygen Atom Transfer Reactions in Molybdoenzyme Model Systems, *J. Am. Chem. Soc.*, 2000, **122**, 9298–9299.
32. J. Selbin, J. Sherrill and C. H. Bigger, Model compounds of biological molybdenum. Flavin and mixed-ligand complexes of molybdenum(IV) and (V), *Inorg. Chem.*, 1974, **13**, 2544–2549.
33. D. T. Sawyer and W. H. Doub Jr, Formation of model compounds of biological molybdenum(IV), *Inorg. Chem.*, 1975, **14**, 1736–1737.
34. A. Abelleira, R. D. Galang and M. J. Clarke, Synthesis and electrochemistry of pterins coordinated to tetraammineruthenium(II), *Inorg. Chem.*, 1990, **29**, 633–639.
35. M. J. Clarke and M. G. Dowling, Cyclic voltammetry studies of metalloflavin complexes in aqueous solution, *Inorg. Chem.*, 1981, **20**, 3506–3514.
36. S. J. N. Burgmayer, H. L. Kaufmann, G. Fortunato, P. Hug and B. Fischer, Molybdenum-Pterin Chemistry. 3. Use of X-ray Photoelectron

- Spectroscopy To Assign Oxidation States in Metal Complexes of Noninnocent Ligands, *Inorg. Chem.*, 1999, **38**, 2607–2613.
37. I. D. Brown and D. Altermatt, Bond-valence parameters obtained from a systematic analysis of the inorganic crystal structure database, *Acta Crystallogr., Sect. B: Struct. Sci.*, 1985, **B41**, 244–247.
38. (a) H. H. Thorp, Bond valence sum analysis of metal-ligand bond lengths in metalloenzymes and model complexes, *Inorg. Chem.*, 1992, **31**, 1585–1588; (b) W. Liu and H. H. Thorp, Bond valence sum analysis of metal-ligand bond lengths in metalloenzymes and model complexes. 2. Refined distances and other enzymes, *Inorg. Chem.*, 1993, **32**, 4102–4105.
39. D. M. A. M. Luykx, J. A. Duine and S. de Vries, Molybdopterin Radical in Bacterial Aldehyde Dehydrogenases, *Biochemistry*, 1998, **37**, 11366–11375.
40. M. J. Clarke, M. G. Dowling, A. R. Garafalo and T. F. Brennan, Structural and electronic effects resulting from metal-flavin ligation, *J. Biol. Chem.*, 1980, **255**, 3472–3481.
41. P. J. Chirik, Preface: Forum on Redox-Active Ligands, *Inorg. Chem.*, 2011, **50**, 9737–9740.
42. C. G. Pierpont, Ligand Redox Activity and Mixed Valency in First-Row Transition-Metal Complexes Containing Tetrachlorocatecholate and Radical Tetrachlorosemiquinonate Ligands, *Inorg. Chem.*, 2011, **50**, 9766–9772.
43. S. K. Das, P. K. Chaudhury, D. Biswas and S. Sarkar, Modeling for the Active Site of Sulfite Oxidase: Synthesis, Characterization, and Reactivity of $[\text{Mo}^{\text{VI}}\text{O}_2(\text{mnt})_2]^{2-}$ (mnt^{2-} = 1,2-Dicyanoethylenedithiolate), *J. Am. Chem. Soc.*, 1994, **116**, 9061–9070.
44. (a) R. L. McNaughton, M. E. Helton, N. D. Rubie and M. L. Kirk, The Oxo-Gate Hypothesis and DMSO Reductase: Implications for a Pseudo- σ Bonding Interaction Involved in Enzymatic Electron Transfer, *Inorg. Chem.*, 2000, **39**, 4386–4387; (b) M. E. Helton, N. E. Gruhn, R. L. McNaughton and M. L. Kirk, Control of Oxo-Molybdenum Reduction and Ionization Potentials by Dithiolate Donors, *Inorg. Chem.*, 2000, **39**, 2273–2278.
45. M. Draganjac, E. Simhon, L. T. Chan, M. Kanatzidis, N. C. Baenziger and D. Coucouvanis, Synthesis, interconversions, and structural characterization of the $[(\text{S}_4)_2\text{MoS}]^{2-}$, $[(\text{S}_4)_2\text{MoO}]^{2-}$, $(\text{Mo}_2\text{S}_{10})^{2-}$, and $(\text{Mo}_2\text{S}_{12})^{2-}$ anions, *Inorg. Chem.*, 1982, **21**, 3321–3332.
46. D. Coucouvanis, A. Hadjikyriacou, A. Toupadakis, S. M. Koo, O. Ileperuma, M. Draganjac and A. Salifoglou, Studies of the reactivity of binary thio- and tertiary oxothiomolybdates toward electrophiles. Reactions with dicarbomethoxyacetylene and the synthesis and structures of the $[\text{Et}_4\text{N}]_2[\text{MoO}(\text{L})_2]$, anti- $[\text{Et}_4\text{N}]_2[\text{Mo}_2\text{O}_2\text{S}_2(\text{L})_2]$, syn- $[\text{Ph}_4\text{P}]_2[\text{Mo}_2\text{O}_2\text{S}_2(\text{L})_2]\cdot 2\text{DMF}$, $[\text{Ph}_4\text{P}]_2[\text{Mo}(\text{L}_3)]\text{DMF}\cdot \text{C}_6\text{H}_6$, and $[\text{Ph}_4\text{P}]_2[\text{Mo}_2\text{S}_2(\text{L})_2]\text{CH}_2\text{Cl}_2$ complexes (L = 1,2-dicarbomethoxy-1,2-ethylenedithiolate), *Inorg. Chem.*, 1991, **30**, 754–767.
47. M. Draganjac and D. Coucouvanis, Reaction of MoS_9^{2-} with bis-carboxymethyl)acetylene. The crystal and molecular structure of $(\text{Ph}_4\text{P})_2\text{Mo}[\text{S}_2\text{C}_2(\text{COOMe})_2]_3$: a trigonal prismatic complex with a new dithiolene ligand, *J. Am. Chem. Soc.*, 1983, **105**, 139–140.

48. D. Coucouvanis, Syntheses, structures, and reactions of binary and tertiary thiomolybdate complexes containing the (O)Mo(S_x) and (S)Mo(S_x) functional groups (x = 1, 2, 4), *Adv. Inorg. Chem.*, 1998, **45**, 1–73.
49. R. S. Pilato, K. A. Eriksen, M. A. Greaney, E. I. Stiefel, S. Goswami, L. Kilpatrick, T. G. Spiro, E. C. Taylor and A. L. Rheingold, Model complexes for molybdopterin-containing enzymes: preparation and crystallographic characterization of a molybdenum ene-1-perthiolate-2-thiolate (trithiolate) complex, *J. Am. Chem. Soc.*, 1991, **113**, 9372–9374.
50. S. J. N. Burgmayer, M. Kim, R. Petit, A. Rothkopf, A. Kim, S. BelHam-dounia, Y. Hou, A. Somogyi, D. Habel-Rodriguez, A. Williams and M. L. Kirk, Synthesis, characterization, and spectroscopy of model molybdopterin complexes, *J. Inorg. Biochem.*, 2007, **101**, 1601–1616.
51. W. Kusters and P. De Mayo, Photochemical synthesis. 56. Thione photochemistry. 15. Preparation and properties of the α -dithione system, *J. Am. Chem. Soc.*, 1974, **96**, 3502–3511.
52. X. Yang, G. K. W. Freeman, T. B. Rauchfuss and S. R. Wilson, The Dithiocarbonate Route to 1,2-Dithiolene Complexes of Molybdenum and Tungsten, *Inorg. Chem.*, 1991, **30**, 3034–3038.
53. S. Boyde, C. D. Garner, J. A. Joule and D. J. Rowe, New synthetic route to transition-metal complexes of unsymmetrically substituted dithiolenes: evidence for a metalladithiolene ring current, *J. Chem. Soc., Chem. Commun.*, 1987, **11**, 800–801.
54. L. Larsen, D. J. Rowe, C. D. Garner and J. A. Joule, Synthesis of 1-(quinoxalin-2-yl)-alkane-1,2-dithiols and -alkene-1,2-dithiols of relevance to the molybdoenzyme cofactor, Moco, *Tetrahedron Lett.*, 1988, **29**, 1453–1456.
55. C. D. Garner, E. M. Armstrong, M. J. Ashcroft, M. S. Austerberry, J. H. Birks, D. Collison, A. J. Goodwin, L. Larsen, D. J. Rowe and J. R. Russell, Strategies for the synthesis of the cofactor of the oxomolybdoenzymes (Molybdenum Enzymes, Cofactors, and Model Systems), *ACS Symp. Ser.*, 1993, **535**, 98–113.
56. L. Larsen, C. D. Garner and J. A. Joule, Model studies related to the cofactor of oxomolybdoenzymes. Part 2. Quinoxalin-2-yl ethane- and -ethene-1,2-dithiols, *J. Chem. Soc., Perkin Trans. 1*, 1989, **12**, 2311–2316.
57. B. Bradshaw, A. Dinsmore, C. D. Garner and J. A. Joule, Synthesis of a cobalt complex of a pyrano[2,3-b]quinoxaline-3,4-dithiolate related to molybdopterin, *Chem. Commun.*, 1998, **3**, 417–418.
58. B. Bradshaw, A. Dinsmore, D. Collison, C. D. Garner and J. A. Joule, The synthesis of pyrano[2,3-b]quinoxalines related to molybdopterin, *J. Chem. Soc., Perkin Trans.*, 2001, **24**, 3232–3238.
59. J. P. Dicks, M. Zubair, E. S. Davies, C. D. Garner, C. Schulzke, C. Wilson and J. McMaster, Synthesis, Structure and Redox Properties of Asymmetric (Cyclopentadienyl)(ene-1,2-dithiolate)cobalt(III) Complexes Containing Phenyl, Pyridyl and Pyrazinyl Units, *Eur. J. Inorg. Chem.*, 2015, 3550–3561.

60. E. S. Davies, R. L. Beddoes, D. Collison, A. Dinsmore, A. Doerat, J. A. Joule, C. R. Wilson and C. D. Garner, Synthesis of oxomolybdenum bis(dithiolene) complexes related to the cofactor of the oxomolybdoenzymes, *J. Chem. Soc., Dalton Trans.*, 1997, **21**, 3985–3996.
61. A. Dinsmore, J. H. Birks, C. D. Garner and J. A. Joule, Synthesis of (η^5 -cyclopentadienyl)-1-(4-benzyloxycarbonyl-3,4-dihydroquinoxalin-2-yl) ethene-1,2-dithiolatocobalt(III) and (η^5 -cyclopentadienyl)-1-[2-(N,N-dimethylaminomethyleneamino)-3-methyl-4-oxopteridin-6-yl]ethene-1,2-dithiolatocobalt(III), *J. Chem. Soc., Perkin Trans. 1*, 1997, **6**, 801–807.
62. E. S. Davies, A. Dinsmore, C. D. Garner and J. A. Joule, Synthetic approaches to molybdenum cofactors, *Chem. Biol. Pteridines Folates*, 1997, 693–696; Proceedings of the International Symposium on Pteridines and Folates, 11th, Berchtesgaden, Germany, June 15–20, 1997.
63. R. L. Beddoes, A. Dinsmore, M. Helliwell, C. D. Garner and J. A. Joule, A pteridin-6-yl alkene-1,2-dithiolate complex of cobalt, *Acta Crystallogr., Sect. C: Cryst. Struct. Commun.*, 1997, **53**, 213–215.
64. (a) W. Koschara, Urothion, a yellow sulfur-rich pigment from human urine, *Z. Physiol. Chem.*, 1940, **263**, 78–79; (b) W. Koschara, Isolation of urothion, *Hoppe-Seyler's Z. Physiol. Chem.*, 1943, **277**, 284–287; (c) W. Koschara, Urothion, a pterin derivative with a terminal glycol group, *Hoppe-Seyler's Z. Physiol. Chem.*, 1943, **279**, 44–52.
65. (a) M. Goto, A. Sakurai, K. Ohta and H. Yamakami, Pteridine. II. Structure of urothion, *J. Biochem.*, 1969, **65**, 611–620; (b) A. Sakurai and M. Goto, Urothione synthesis, *Tetrahedron Lett.*, 1968, **25**, 2941–2944; (c) M. Goto, A. Sakurai, K. Ohta and H. Yamakami, Structure of urothione, *Tetrahedron Lett.*, 1967, **45**, 4507–4511.
66. E. C. Taylor and L. A. Reiter, Pteridines. 50. Unequivocal total synthesis of deoxyurothione, *J. Org. Chem.*, 1982, **47**, 528–531.
67. L. Larsen, D. J. Rowe, C. D. Garner and J. A. Joule, Model studies related to the cofactor of oxomolybdoenzymes. Part 3, *J. Chem. Soc., Perkin Trans.*, 1989, **12**, 2317–2327.
68. C. L. Soricelli, V. A. Szalai and S. J. N. Burgmayer, Oxidation of molybdenum dithiolene complexes yields thiophene analogs of urothione and molybdopterin form B, *J. Am. Chem. Soc.*, 1991, **113**, 9877–9878.
69. H. D. Hartzler, 2-Benzylidene-1,3-dithioles. Remarkably rapid Wittig reaction, *J. Am. Chem. Soc.*, 1971, **93**, 4961–4962.
70. E. C. Taylor and R. Doetzer, Model studies directed toward the molybdenum cofactor: 2-alkylidene- and 2-(phenylimino)-1,3-dithioles from acetylenes, *J. Org. Chem.*, 1991, **56**, 1816–1822.
71. (a) S. Gerchakov, P. J. Whitman and H. P. Schultz, Quinoxaline studies. XIII. N-(2-Quinoxaloyl)- α -amino acids, *J. Med. Chem.*, 1966, **9**, 266–268; (b) D. Horton and M. J. Miller, Structure of 2-(D-arabino-tetrahydroxybutyl)quinoxaline, *J. Org. Chem.*, 1965, **30**, 2457–2459; (c) S. Goswami and A. K. Adak, A one-pot synthesis of cyclic pyrido[1,2-a]quinoxaline phosphate, a new molecule of biological importance from a quinoxaline derivative of sugar, *Chem. Lett.*, 2003, **32**, 678–679.

72. (a) P. Griess and G. Harrow, Action of aromatic diamines on sugars, *Chem. Ber.*, 1887, **20**, 2205–2213; (b) P. Griess and G. Harrow, Action of aromatic diamines on sugars, *Chem. Ber.*, 1887, **20**, 281–282.
73. R. Soyka, W. Pfleiderer and R. Prewo, Pteridines. Part XCIV. Synthesis and characteristics of 5,6-dihydro-6-(1,2,3-trihydroxypropyl)pteridines. Covalent intramolecular adducts, *Helv. Chim. Acta*, 1990, **73**, 808–826.
74. B. Bradshaw, A. Dinsmore, W. Ajana, D. Collison, C. D. Garner and J. A. Joule, Synthesis of the organic ligand of the molybdenum cofactor, in protected form, *J. Chem. Soc., Perkin Trans.*, 2001, **24**, 3239–3244.
75. P. Basu and S. J. N. Burgmayer, Pterin chemistry and its relationship to the molybdenum cofactor, *Coord. Chem. Rev.*, 2011, **255**, 1016–1038.
76. I. V. Pimkov, B. Serli-Mitasev, A. A. Peterson, S. C. Ratvasky, B. Hammann and P. Basu, Designing the Molybdopterin Core through Regioselective Coupling of Building Blocks, *Chem.-Eur. J.*, 2015, **21**, 17057–17072.
77. L. Marbella, B. Serli-Mitasev and P. Basu, Development of a Fluorescent Pb²⁺ Sensor, *Angew. Chem., Int. Ed.*, 2009, **48**, 3996–3998, S3996/1-S3996/4.
78. I. V. Pimkov, A. A. Peterson, D. N. Vaccarello and P. Basu, A regioselective synthesis of the dephospho dithiolene protected molybdopterin, *RSC Adv.*, 2014, **4**, 19072–19076.
79. B. R. Williams, Y. Fu, G. P. A. Yap and S. J. N. Burgmayer, Structure and Reversible Pyran Formation in Molybdenum Pyranopterin Dithiolene Models of the Molybdenum Cofactor, *J. Am. Chem. Soc.*, 2012, **134**, 19584–19587.
80. B. R. Williams, D. Gisewhite, A. Kalinsky, A. Esmail and S. J. N. Burgmayer, Solvent-Dependent Pyranopterin Cyclization in Molybdenum Cofactor Model Complexes, *Inorg. Chem.*, 2015, **54**, 8214–8222.
81. S. J. N. Burgmayer, D. L. Pearsall, S. Blaney, E. Moore and C. Sauk-Schubert, Redox Reactions of the Pyranopterin System of the Molybdenum Cofactor, *J. Biol. Inorg. Chem.*, 2004, **9**, 59–66.
82. R. S. Pilato, K. Eriksen, M. A. Greaney, Y. Gea, E. C. Taylor, S. Goswami, L. Kilpatrick, T. G. Spiro, A. L. Rheingold and E. I. Stiefel, *ACS Symp. Ser.*, 1993, **535**, 83.
83. S. Boyde and C. D. Garner, *J. Chem. Soc., Dalton Trans.*, 1991, 713.
84. (a) J. K. Hsu, C. J. Bonangolino, S. P. Kaiwar C. M. Boggs, J. C. Fettinger and R. S. Pilato, *Inorg. Chem.*, 1996, **35**, 4743; (b) S. P. Kaiwar, A. Vodacek, N. V. Blough and R. S. Pilato, *J. Am. Chem. Soc.*, 1997, **119**, 9211; (c) K. A. Van Houten, C. M. Boggs and R. S. Pilato, *Tetrahedron*, 1998, **54**, 10973.
85. E. M. Armstrong, M. S. Austerberry, J. H. Birks, R. L. Beddoes, M. Hellier, J. A. Joule and C. D. Garner, *Heterocycles*, 1993, **35**, 563.
86. (a) K. G. Matz, R. P. Mtei, B. Leung, S. J. N. Burgmayer and M. L. Kirk, *J. Am. Chem. Soc.*, 2010, **132**, 7830; (b) K. G. Matz, R. P. Mtei, R. Rothstein, M. L. Kirk and S. J. N. Burgmayer, *Inorg. Chem.*, 2011, **50**, 9804.
87. M. L. Kirk, R. L. McNaughton and M. E. Helton, The electronic structure and spectroscopy of metallo-dithiolene complexes, *Prog. Inorg. Chem.*, 2003, **52**, 111–212.

88. M. J. Romao, Molybdenum and tungsten enzymes: A crystallographic and mechanistic overview, *Dalton Trans.*, 2009, **21**, 4053–4068.
89. R. Eisenberg and H. B. Gray, Noninnocence in Metal Complexes: A Dithiolene Dawn, *Inorg. Chem.*, 2011, **50**, 9741–9751.
90. (a) V. N. Nemykin, J. G. Olsen, E. Perera and P. Basu, Synthesis, Molecular and Electronic Structure, and TDDFT and TDDFT-PCM Study of the Solvatochromic Properties of (Me_2Pipdt) $\text{Mo}(\text{CO})_4$ Complex (Me_2Pipdt = N,N'-Dimethylpiperazine-2,3-dithione), *Inorg. Chem.*, 2006, **45**, 3557–3568; (b) E. Perera and P. Basu, Synthesis, characterization and structure of a low coordinate desoxomolybdenum cluster stabilized by a dithione ligand, *Dalton Trans.*, 2009, 5023–5028; (c) R. P. Mtei, E. Perera, B. Mogesa, B. Stein, P. Basu and M. L. Kirk, A Valence Bond Description of Dizwitterionic Dithiolene Character in an Oxomolybdenum-Bis(dithione) Complex, *Eur. J. Inorg. Chem.*, 2011, **2011**, 5467–5470; (d) B. Mogesa, E. Perera, H. M. Rhoda, J. K. Gibson, J. Oomens, G. Berden, M. J. van Stipdonk, V. N. Nemykin and P. Basu, Solution, Solid, and Gas Phase Studies on a Nickel Dithiolene System: Spectator Metal and Reactor Ligand, *Inorg. Chem.*, 2015, **54**, 7703–7716.
91. J. Dias, M. Than, A. Humm, G. P. Bourenkov, H. D. Bartunik, S. Bursakov, J. Calvete, J. Caldeira, C. Carneiro, J. J. Moura, I. Moura and M. J. Romao, Crystal structure of the first dissimilatory nitrate reductase at 1.9 Å solved by MAD methods, *Structure*, 1999, **7**, 65–79.
92. R. L. McNaughton, S. Mondal, V. N. Nemykin, P. Basu and M. L. Kirk, Oxomolybdenum Tetrathiolates with Sterically Encumbering Ligands: Modeling the Effect of a Protein Matrix on Electronic Structure and Reduction Potentials, *Inorg. Chem.*, 2005, **44**, 8216–8222.
93. (a) S. Mondal and P. Basu, Dendrimer Encapsulation of [Mo^VOS₄] Cores: Implications for the DMSO Reductase Family of Enzymes, *Inorg. Chem.*, 2001, **40**, 192–193; (b) R. S. Sengar, V. N. Nemykin and P. Basu, Electronic properties of para-substituted thiophenols and disulfides from ¹³C NMR spectroscopy and *ab initio* calculations: relations to the Hammett parameters and atomic charges, *New J. Chem.*, 2003, **27**, 1115–1123; (c) R. S. Sengar and P. Basu, Design, synthesis, and characterization of a sterically encumbered dioxo molybdenum(VI) core, *Inorg. Chim. Acta*, 2007, **360**, 2092–2099.
94. P. Basu, V. N. Nemykin and R. S. Sengar, Syntheses, Spectroscopy, and Redox Chemistry of Encapsulated Oxo-Mo(V) Centers: Implications for Pyranopterin-Containing Molybdoenzymes, *Inorg. Chem.*, 2003, **42**, 7489–7501.
95. R. A. Rothery, B. Stein, M. Solomonson, M. L. Kirk and J. H. Weiner, Pyranopterin conformation defines the function of molybdenum and tungsten enzymes, *Proc. Natl. Acad. Sci. U. S. A.*, 2012, **109**, 14773–14778.

CHAPTER 3

Electron Transfer Mechanisms in Molybdenum and Tungsten Model Compounds

BHOLANATH PAKHIRA^a, RUDRA SARKAR^a, AND SABYASACHI SARKAR^{*a}

^aNano Science and Synthetic Leaf Laboratory, Department of Chemistry, Indian Institute of Engineering Science and Technology, Shibpur, Botanic Garden-711103, Howrah, West Bengal, India

*E-mail: aby@iitk.ac.in, sabby@chem.iests.ac.in

3.1 Introduction to Molybdenum and Tungsten

The element molybdenum (Mo) forms several fascinating compounds in contemporary chemistry ranging from unique molybdenum blues to aesthetically pleasant giant inorganic fullerene shape molecules named Keplarates and compounds used in hydrodesulphurization catalysts. The other facet of Mo chemistry comprises compounds with Mo–Mo bonds of different multiplicities along with the facile formation of higher nuclearity homo- and hetero-metallic cluster compounds in its different oxidation states. Another aspect of molybdenum compounds is their use as catalysts in chemical transformations.^{1–3} Finally, its most exciting involvement is related to its adaptation by Nature to develop biological processes from the beginning of evolution and conserving its role even in human physiology.

RSC Metallobiology Series No. 6

Molybdenum and Tungsten Enzymes: Bioinorganic Chemistry

Edited by Russ Hille, Carola Schulzke, and Martin L. Kirk

© The Royal Society of Chemistry 2017

Published by the Royal Society of Chemistry, www.rsc.org

Its higher congener, tungsten (W), displays similar chemical properties to molybdenum by virtue of its position in the same group, yet there are differences related to the variation in the kinetics and thermodynamic properties in these. Such differences were meticulously exploited by Nature in complementary fashion during her marathon race in creating this living world from the start of the juvenile, hyperthermophilic and anaerobic Earth to its latest aerobic and mesophilic form. From the inorganic chemist's point of view the most exciting properties of Mo and W shall be highlighted, which are crucial to assimilate them and assign the role they play in the biosystem.

3.1.1 Role in Biology

The availability of these metals as oxometallates, MO_4^{2-} ($\text{M} = \text{Mo}, \text{W}$) ions, in water under normal biological pH is important in contrast to their relatively low abundance on Earth. For all the transition metals involved in biology, Mo and W are the only active metals from the 4d and 5d series. Their relative abundance in Earth's crust is very low; however, in sea water their presence in the form of water-soluble MO_4^{2-} made the available concentration of these elements comparable to iron.⁴ Such availability in water induces their ready participation in biology. The other important characteristic displayed by these metals is their unique reduction–oxidation (redox) chemistry. The easy interplay of the oxidation states from VI to IV is spectacular as two-electron redox reactions can be achieved directly assisted by oxygen atom transfer or in a stepwise fashion involving sequential one-electron change coupled with proton transfer hopping through the intermediate oxidation state, v. There is no other bioactive metal that can perform such one-step, two-electron redox reactions and may conveniently switch over to sequential one-electron redox reactions when needed by the system. It is only iron that, under very specific conditions, transiently displays such two-electron redox reactions. These are related to oxo-transfer iron enzymes like cytochrome P₄₅₀, NO-synthase, peroxidase, catalase and also cytochrome c-oxidase class of enzymes.⁵ However, these lack the versatility to use the alternative or complementary proton-coupled sequential one-electron redox reaction operating on the same metalloprotein. Another important facet of these metals is related to the flexibility of the coordination geometry where varied coordination numbers are accessible with little difference in energy. This characteristic is essential for creating a site for the substrate to bind, which is an important requirement for any enzymatic reaction.

From the synthetic chemistry perspective it is not an easy task to stabilize a monomeric Mo (W is even more difficult) complex in the +v or +IV oxidation state but in biological reactions the participation of Mo (or W) in these oxidation states is routine and takes place easily. In Nature the readily available form of Mo or W is the MO_4^{2-} ion. Details of the incorporation of these metals into apo-enzymes to develop holo-enzymes is not in the focus of this review but certain qualification of these elements related to their chemistry should be highlighted. It is rather difficult to reduce MO_4^{2-} in basic to

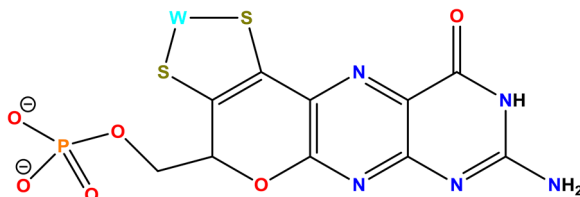


Figure 3.1 The structure of the molybdenum cofactor (in W-protein Mo is replaced by W, cyan = Mo or W, orange = P, rest = standard colour code).

neutral media but under acidic conditions protonation of the coordinated oxo ligand, together with raising the coordination number by hydration in water, facilitates the reduction process. However, once in contact with acidic media oxo-molybdates and -tungstates typically form polyoxometallates and for tungsten this polymerization leads to quantitative precipitation of polymeric $\text{WO}_3 \cdot 2\text{H}_2\text{O}$.^{3,6} Thus, to chemically allow these metals to keep their mononuclear form, a preformed mononuclear Mo (or W) compound is generally used as starting material applied in an organic solvent for synthesizing the respective model compound.

Another important aspect regarding modelling is the choice of the ligand(s), which should help the central Mo (W) atom adopting the desired coordination geometry as required for a mimic of the molybdenum or tungsten cofactor. The model chemistry for the molybdenum and tungsten dependent enzymes drastically shifted when, in 1987, the presence of molybdopterin as ligand and, hence, part of the Mo-cofactor (or Moco) bound to the central molybdenum atom *via* two sulfur donor atoms was spectroscopically established.⁷ Based on this information, post-1987 syntheses of model compounds are dominated by the necessary ene-dithiolate coordination as found in molybdopterin in the cofactor of molybdo- and tungstoenzymes. It took several years until in 1996 the first X-ray structure of a W-protein of hyperthermophilic origin revealed the precise structure of such molybdopterin ligand as a pyranopterindithiolate entity⁸ (Figure 3.1) (pyranopterindithiolate entity was also earlier referred to as molybdopterin or sometimes pterindithiolene), verifying the proposed essential ene-dithiolate moiety being attached to the central W.

3.2 Model Systems

In the light of enzymatic structures and reactions, when model compounds are explored then one should generally define and address the required qualification for a synthetic compound in order to be called a structural and/or functional model. A pedagogical representation of the different model compounds may be given using the example of a steam locomotive engine.

Figure 3.2 illustrates the formal presence of a simple structural model of a locomotive engine, which does not have any function, and a functional

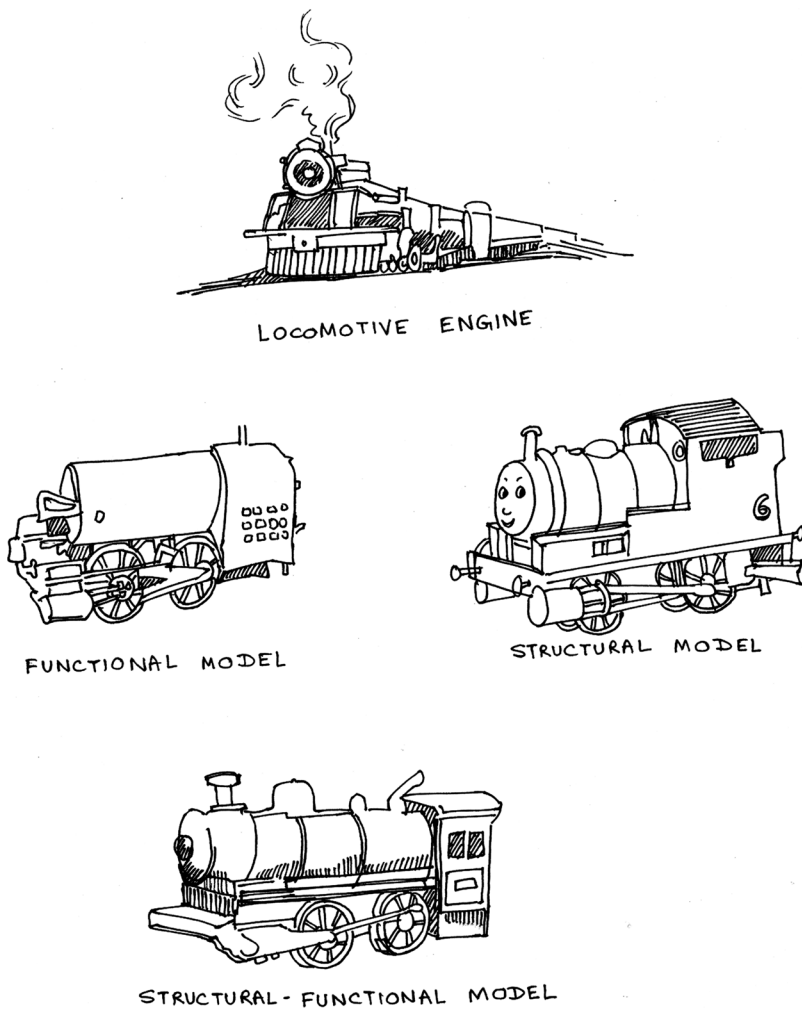


Figure 3.2 Illustrating the different model characters using the example of a locomotive engine.

model, which may have all the intriguing inner arrangements to function but may differ from the structural model. Finally, the best and most realistic model that can be considered is a precise replica of the locomotive engine addressing both characteristics, structure and function. The structural-functional model is the miniature form of the real locomotive engine that may pound the rails once energy is supplied. Considering that in the enzymes the large apo-protein protects the active site, and that the central molybdenum or tungsten in synthetic model compounds are typically only bound by rather small ligands, it is debatable how good chemical models of the enzymes actually are. Typically a model compound would be closely

mimicking the atomic arrangement near the central atom comprising the active site only and generally one may consider this part as a prosthetic group (Moco) attached to the apo-protein. Thus if a model could be made with the arrangement very similar to the Moco then achieving such thermodynamical arrangements would respond to functional reaction similar to the native proteins possessing such Moco. The stability of only Moco without the peripheral apo-enzyme support should be considered first to model a replica of such a system. However, isolating and stabilizing the intact Moco is problematic due to its inherent instability once separated from the apo-protein. In addition the old definition of one “universal cofactor” in the molybdenum and tungsten enzymes is no longer valid as per Hille’s classification of all the molybdoenzymes⁹ (Figure 3.3). We can now understand the differences and similarities in different cofactors and the ease with which they reconstitute under the provision of the most suitable *N. Crassa* Nit-1 variant of nitrate reductase. Here the presence of molybdopterin ligand is enough to rebuild the holoenzyme in the presence of external molybdate and thiol.¹⁰ According to Hille’s classification, the mononuclear molybdoenzymes have been most reasonably categorized into three main families, which are the sulfite oxidase, xanthine oxidase and DMSO reductase families. This classification along with the active site structures for the members of these three families are shown in Figure 3.3. Though there are other versions as shown in Figure 3.3, the essential grouping is based on the presence of either one pyranopterindithiolate coordinated *via* the dithiolene moiety in sulfite or xanthine oxidase or two dithiolenes for all the other enzymes. Members of the xanthine oxidase family are characterized by one pyranopterindithiolate entity, which gives a five-membered ene-1,2-dithiolate metallacycle, and the *cis*-Mo^{VI}O₂ moiety. The family is represented by aldehyde oxidoreductase^{11,12} and xanthine oxidase/dehydrogenase.^{13–16} A simple change in *cis*-[Mo^{VI}O₂] moiety led to the sulfite oxidase class of enzymes.¹⁷

Further, another member of this family is carbon monoxide dehydrogenase. Here the sulfido ligand is additionally coordinated by Cu^I in what is thus far a unique structure in biology.¹⁸ The extensively studied sulfite oxidase (SO) isolated from chicken liver is characterized by one pyranopterindithiolate, a *cis*-Mo^{VI}O₂ group and a highly conserved cysteinate residue as ligand in SOs obtained from other sources.^{19–21} Other than sulfite oxidase itself, the SO family also includes assimilatory nitrate reductase.²² Members of the DMSO reductase family bind two pyranopterindithiolate ligands and in the oxidized form has one residue from the protein as ligand, which is variable, and a terminal oxo or hydroxo ligand.^{23,24}

In the late 1970s synthetic chemists were eagerly awaiting information regarding the immediate neighbour atoms around the central molybdenum of a molybdoenzyme. In the absence of detailed X-ray structures, initially, the Extended Absorption X-ray Fine Structure (EXAFS) analysis provided information regarding the nearest atoms around the molybdenum centre. It was the foresight of chemists like Williams, Stiefel, Holm and Garner that drove the model chemistry for the molybdenum- and tungsten-dependent

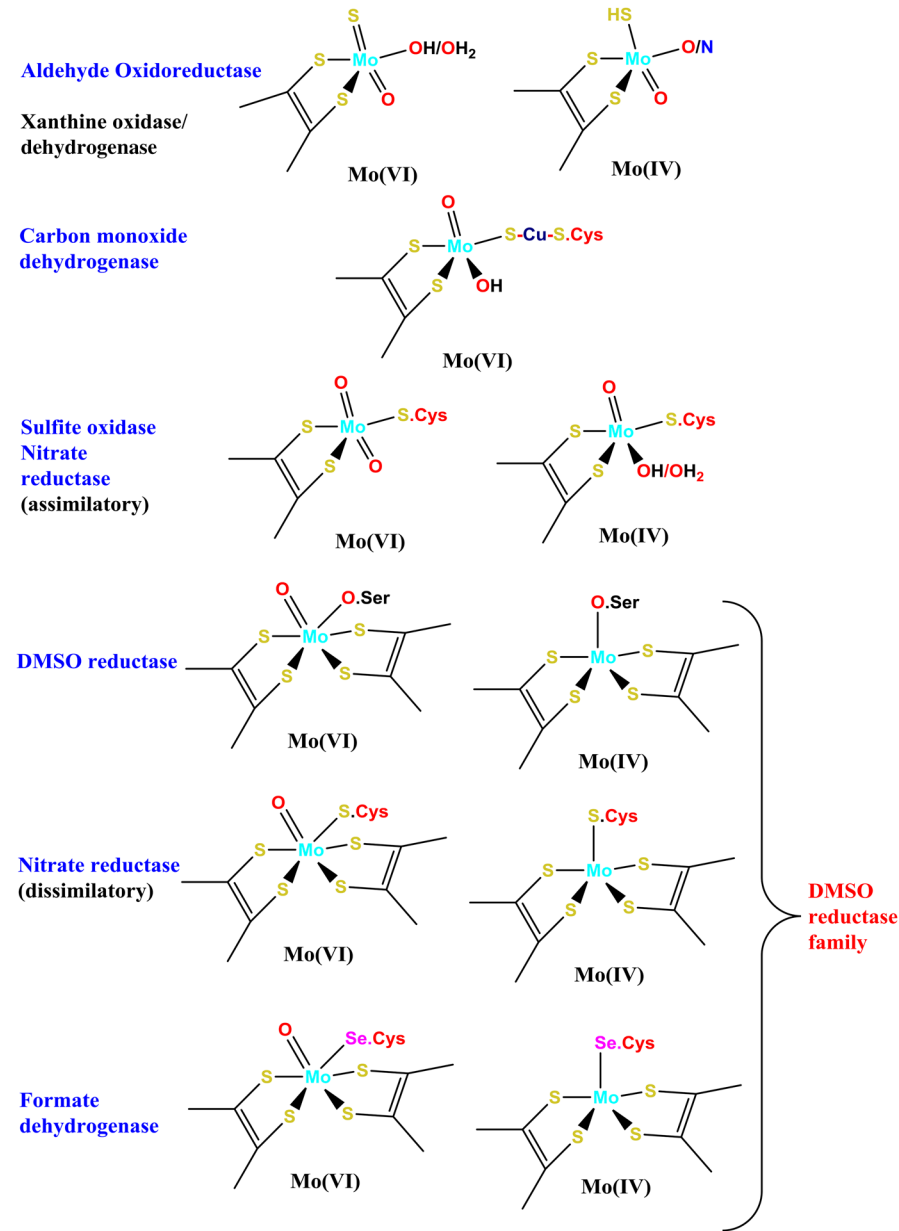


Figure 3.3 Hille's classification of Mo cofactor present in different Mo enzymes. (W enzymes have very similar cofactor with W in place of Mo, the main difference is with one or two dithiolene coordination where one terminal oxo group is retained in the oxidized form.)

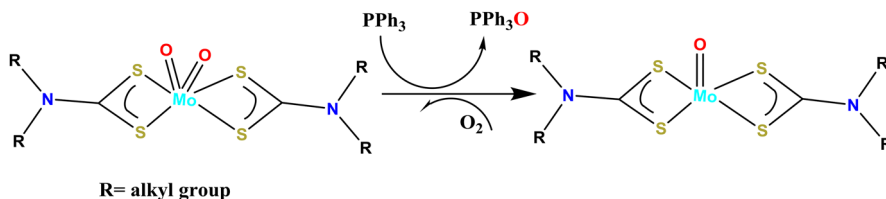


Figure 3.4 $[\text{MoO}_2(\text{DTC})_2]$ and its forward and backward oxo-transfer reaction.

oxidoreductases and provided insight into the enzymatic structure and reactivity. They were able to extract relevant information addressing the basic need of the presence of one to two oxo groups and two to four sulfur atoms around the central molybdenum and created the first set of compounds appropriately defined as models. Representative examples of such model chemistry in relevance to molybdoenzymes have been extensively described in the well-referred literature.^{25–31} In the initial period, two compounds, the $[\text{MoO}_2(\text{DTC})_2]$ (DTC = dialkylthiocarbamate, R_2NCS_2^- , R = alkyl)³² and $[\text{MoO}_2(-\text{NS})_2]$ ^{33,34} ($-\text{NS}_2^-$ = 2,6-bis-(2,2-diphenyl-2-thioethyl)pyridinate²⁻) demonstrated oxo-transfer activity with the possibility of completing catalytic cycles. It is the DTC compound that was shown to be an oxo-transfer agent using the substrate PPh_3 .³² Interestingly, the reduced $[\text{MoO}(\text{DTC})_2]$ readily reacts with oxygen to regenerate the oxidized catalyst species (Figure 3.4).

It was more than a decade later that Holm³⁴ (1986) put such reactivity into the context of molybdoenzymes. He exploited PPh_3 as a model substrate and its oxo-acceptor nature for a reaction with the synthesized complex $[\text{MoO}_2(\text{NS})_2]$ demonstrating, hence, that a synthetic complex may respond to the presence of a suitable substrate by an oxo-transfer reaction similar to the molybdoenzymes. This reactivity was extended to the backward reaction where DMSO was used as the second substrate to regenerate the oxidized $[\text{MoO}_2(-\text{NS})_2]$ from the reduced $[\text{MoO}(-\text{NS})_2]$ species (Figure 3.5).

However, this reaction was later found to be not clean as was initially perceived.³⁵ This is due to the inherent chemistry of molybdenum complexes where disproportionation and comproportionation reactions are typical and very common between the oxidation states IV, V and VI. Thus, the reduced $[\text{MoO}(-\text{NS})_2]$ species once formed in the course of the catalytic transformation comproportionates with the available unreacted $[\text{MoO}_2(-\text{NS})_2]$ in the reaction mixture yielding $[\text{Mo}_2\text{O}_3(-\text{NS})_4]$. This necessarily leads to competing kinetic reactions during the progress of the main oxo-transfer reaction. However, the end product in this case was the reduced $[\text{MoO}(-\text{NS})_2]$ species in the presence of excess of PPh_3 or the oxidized $[\text{MoO}_2(-\text{NS})_2]$ species when an excess of DMSO was used. Following this discovery, there has been a surge of publications of similar oxo-transfer reactions using PPh_3 and several other phosphines as the oxo-abstraction substrate. Essentially, those reactions were mainly concerned with the effectiveness of varied phosphines to be used as the oxo-abstracting agent with several newly created model

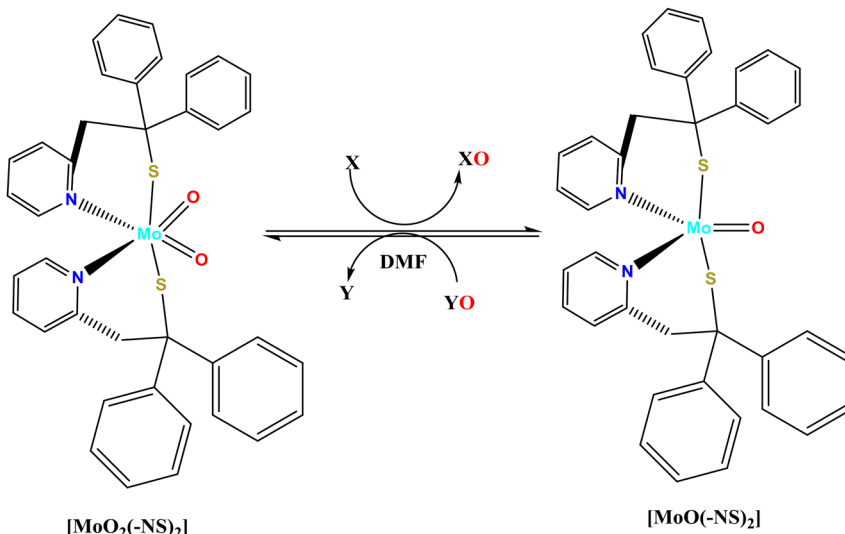


Figure 3.5 The first demonstration of two-directional oxo-transfer reaction in reference to molybdoenzymes.

compounds.^{32,36–58} The main challenge addressed by these early model compounds was to retain the $[\text{MoO}_2]^{2+}$ core with assorted donor atoms like N, O and S. In the absence of X-ray structure data the local geometry around Mo in the molybdoenzymes was not known at the time these experiments took place. Enemark and coworkers used a series of trispyrazoleborate ligands (Figure 3.6) to study the catalytic oxo-transfer model reaction with phosphine-type substrates. The complex $[\text{TpMo}^{\text{VI}}\text{O}_2(\text{S-C}_6\text{H}_5)]$ (Tp = hydrotris-(3,5-dimethylpyrazolyl)borate) was reduced to the $[\text{TpMo}^{\text{IV}}\text{O}(\text{py})(\text{S-C}_4\text{H}_5)]$ species by PPh_3 in the presence of pyridine⁴⁸ demonstrating the complex's reducibility by means of oxo-transfer. The catalytic oxidation of phosphine species (PR_3 , R = alkyl, aryl) by Moco and Wco models as established by Holm and coworkers and as later exploited by Enemark and coworkers was and still is very frequently used to evaluate the oxo-transfer properties of model compounds. This emphasizes the fundamental importance of this conveniently applied and monitored model substrate and its oxidative transformation.^{48,51,54,59–82}

The seminal work of Rajagopalan and coworkers⁷ (1987) discovering molybdopterin as ligand to bind the central molybdenum by the ene-dithiolate functional group provoked a paradigm shift in the search for and the design of suitable model compounds for the molybdenum and tungsten cofactors. Employing ene-dithiolate coordination as present in the pyranopterindithiolate (molybdopterin) ligand (Figure 3.1) in native proteins the comparably long waiting period in the synthesis of actually realistic model compounds was eventually tackled. It was immediately recognized that the remaining organic part of pyranopterindithiolate not involved in binding the metal can and most likely in principle is used for electron flow, promoting

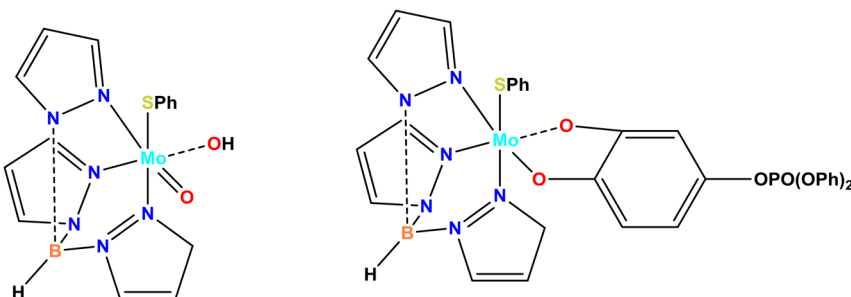


Figure 3.6 Pyrazoleborate capped model compounds developed by the Enemark group.

the redox turnover between different domains in these proteins. This also provides greater stability of the cofactor anchoring it within the pocket of the apo-protein. Thus model compounds started to appear using ene-dithiolates as sulfur donor ligands in combination with the prevalent $[\text{MoO}_2]^{2+}$ or $[\text{MoO}]^{2+}$ moiety.

From the synthetic standpoint one has to consider the total number of donor atoms to be attached to the central molybdenum or tungsten, when designing a structural model. If one resolves to retain a *cis* $[\text{MoO}_2]^{2+}$ or $[\text{MoOS}]^{2-}$ moiety to build a model compound, then, based on cofactor structure as shown in Figure 3.3, one has to adapt for adding one or two dithiolene ligands in order to build a mononuclear model. Creating a bis-dithiolene coordinated complex retaining the $[\text{MoO}]^{2+}$ moiety may not be very difficult to achieve but the use of only one dithiolene to attempt modelling xanthine or sulfite oxidase is challenging given the inherent instability of such four-fold coordinated species (Figure 3.7(b)). This is so because if one considers the Moco of these enzymes without the contribution of apo-enzyme then a *cis* $[\text{MoO}_2]^{2+}$ or $[\text{MoOS}]^{2-}$ moiety will be associated with only one ene-dithiolate ligand. However, work-up in a solvent may temporarily increase the coordination number of the tetra-coordinated species upon coordination of the solvent gaining stability, but that increased coordination will render the central Mo more vulnerable for reduction, which is well known when the relevant water molecule is the solvent ligand. The chemical combination of highly oxidized molybdenum species, *i.e.* Mo(vi), with reduced sulfur functional groups, *i.e.* S(ii⁻) is in general very difficult to achieve and control as it is prone to internal redox reactions. This is also true for dithiolene coordination, which is able to provoke Mo \leftarrow S (dithiolene) electron transfer reactions resulting in the reduction of Mo(vi) to Mo(v). In the presence of additional thiols available as reducing agents without any stabilizing or protecting chelating properties as dithiolenes have, the system can even proceed to further reduction to the Mo(iv) state plus, typically, the generation of disulfide species ($-\text{S}(\text{i}^-)-\text{S}(\text{i}^-)-$). The simultaneous presence of Mo(vi) and Mo(iv) states together with a limited proportion of dithiolene ligand (*i.e.* one dithiolene per Mo) in order to achieve extra stability will drive the system to comproportionate leading to the formation of a dimeric species

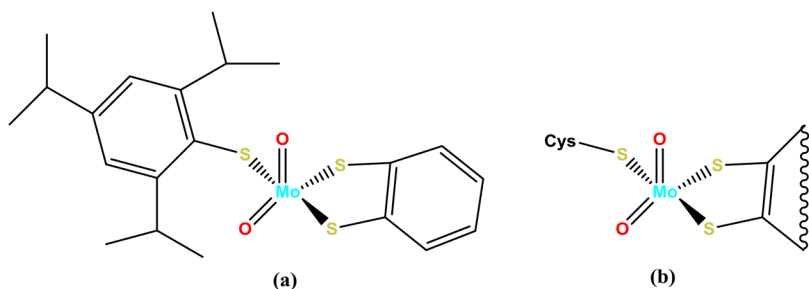


Figure 3.7 (a) A structural analogue of SO by Holm, (b) active site structure of SO.

of general formula $[(dt)Mo^V(O)\mu(O)Mo^V(O) (dt)]^{2-}$ (dt = dithiolene ligand, the oxo ligand may be replaced by a sulfide ligand).⁸³ It may be precisely this chemistry that is the reason for the considerable instability encountered when Moco was isolated from molybdoenzymes in which just one molybdopterin ligand is present. In an environment with reducing conditions and proper pH the dimeric Mo(v) species may be hydrolyzed followed by reduction to yield Mo(iv) species, which had been routinely utilized earlier for the reconstitution of the nitrate reductase.¹⁰ Therefore, without a protein matrix environment, keeping two monomeric coordinately unsaturated molybdenum complexes apart is challenging and thus modelling such a cofactor as a stable compound having one dithiolene ligand is difficult. To circumvent such difficulties Holm and coworkers⁸⁴ utilized some bulky thiol ligands, mimicking the cysteinate residue of the protein, to model sulfite oxidase. One of the best representative structural analogues of the sulfite oxidase cofactor based on such a strategy of preventing dimerization by steric hindrance is shown in Figure 3.7(a).

Unfortunately such a complex has no functionality with respect to transforming any substrate of relevance. The situation becomes even worse when it comes to modelling xanthine oxidase because stabilizing a $[MoOS]^{2+}$ moiety is even more difficult. This is again due to the inherent instability based on intramolecular redox processes of species combining reduced sulfur donor ligands and oxidized molybdenum centre. A comprehensive and detailed account of XO model chemistry is provided in Chapter 6. of this book. Modelling the reduced state of xanthine or sulfite oxidase has been approached for instance by preventing the dimerization process utilizing some site blocking co-ligands without resemblance to the natural coordination environment of molybdenum.^{85,86} Such complexes may not be called actual models from the purist's point of view but some relevant chemistry may be investigated, for example the reaction of reduced xanthine oxidase in air (oxygen).⁸⁵

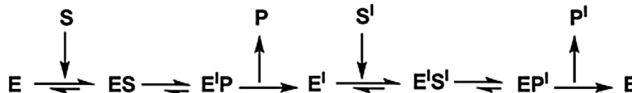
Boyde *et al.*⁸⁷ synthesized $(Et_4N)_2[Mo^{IV}O(bdt)_2]$ and $(Ph_4P)[Mo^V O(bdt)_2]$, [$bdt = C_6H_4S_2^{2-}$] in 1986 and these early archetypes were followed by more than two dozen bis(dithiolene) Mo^{IV}O compounds.^{42,46,84,88-94} Strategies for the synthesis of asymmetric oxo-molybdenum dithiolene complexes made from, 1,3-dithiol-2-one precursors were reported by Garner and coworkers.⁹⁵⁻⁹⁷ This development was important because other than the bdt- the ene-dithiolene

in pyranopterindithiolate in enzymes is unsymmetrically coordinated using different hydrogen bonding network and the ene-moiety is not a part of an aromatic ring. In contrast to the reduced complexes with an $[Mo^{IV}O]$ core, bis(dithiolene) compounds with the $[Mo^{VI}O_2]$ moiety are much more difficult to stabilize and most often defied isolation because of the intramolecular electron transfer between Mo(VI) and coordinated dithiolene. Yoshinaga *et al.*⁹⁸ prepared $(Et_4N)_2[Mo^{VI}O_2(bdt)_2]$ from the reduced $Mo^{IV}O$ species using Me_3NO as the oxidizing agent especially in aprotic solvent. Only very few other examples using mnt^{90,99} and bdtCl₂ ligands were reported with crystallographically characterized bis(dithiolene) $Mo^{VI}O_2/Mo^{IV}O$ compounds.^{91,92,100,101} There are several reports^{49,102,103} available about utilizing Me_3NO as a good oxo-transfer reagent for synthesizing dioxoMo(vi) complexes from the corresponding Mo(iv) monoxo species by simple oxo-transfer reaction. However, varied kinetics of such reaction were reported and this method is not universally applicable. Ueyama and coworkers suggested that these oxo-transfer reactions are promoted by N-H-S-bonding and, notably, the reaction rates were found to be faster when the respective H-bonding is intramolecular rather than intermolecular.¹⁰⁴ It was also proposed that such a reaction involves a *cis* attack of Me_3NO on the Mo centre, which is the rate determining step being followed by product formation and without the occurrence of any *cis-trans* rearrangement.^{105–108} Sugimoto *et al.* reported the synthesis of dioxo Mo(vi) species from a mono-oxo Mo(iv) complex with two structurally different dithiolenes and the reported kinetics of this reaction was determined to be of second order.¹⁰¹ The structurally characterized *cis*-dioxo-molybdenum(vi) complexes, with varied dithiolenes, were again basically synthesized from the corresponding molybdenum(iv) and W(rv) complexes using Me_3NO ¹⁰¹ as the oxidizing agent just as first described by Ueyama and coworkers. The desoxo-molybdenum(iv) complexes $[Mo(OSiR_3)(S_2C_2-(COOMe)_2)_2]$ [where $R_3 = ^iPr_3, ^tBuPh_2; S_2C_2(COOMe)_2 = 1,2\text{-dicarbomethoxyethylene-1,2-dithiolate}$] reacted smoothly with Me_3NO following first-order kinetics whereas the corresponding reaction with Me_2SO (DMSO) was too slow.¹⁰⁹

Holm and coworkers synthesized desoxo-bisdithiolene complexes mimicking the ligand environment in further analogues of the DMSO family of enzymes,^{33,47,60,63–67} and all these complexes invariably follow second-order kinetics. Though the bisdithiolene model complexes are easily formed especially in the reduced state, the mono dithiolene relatives are difficult to stabilize in the solid state, hence hardly suitable for isolation.

3.3 Electron Transfer in Molybdoenzymes

The fundamental single electron transfer reaction (*i.e.* $A + e^- \rightarrow A^-$) is prevalent in Nature, performed by electron transfer metalloproteins like cytochromes (heme-iron) or iron-sulfur proteins. Such proteins remain associated to the catalytically active sub-units in the form of additional domains, together constituting the molybdoenzymes. These electron transfer domains



Scheme 3.1 Oxo-transfer reaction steps in the catalytic cycles of molybdoenzymes.

help shuttling the electron flow throughout the holoenzyme connecting the central domain bearing the molybdenum cofactor with extrinsic redox equivalents. The electron flow to and/or from the active site is essential for completing the redox reaction in the catalytic cycle. However, at the active sites of molybdoenzymes such electron transfer also remains associated with oxygen atom transfer, which cannot be addressed by a simple straightforward electron transfer reaction alone.

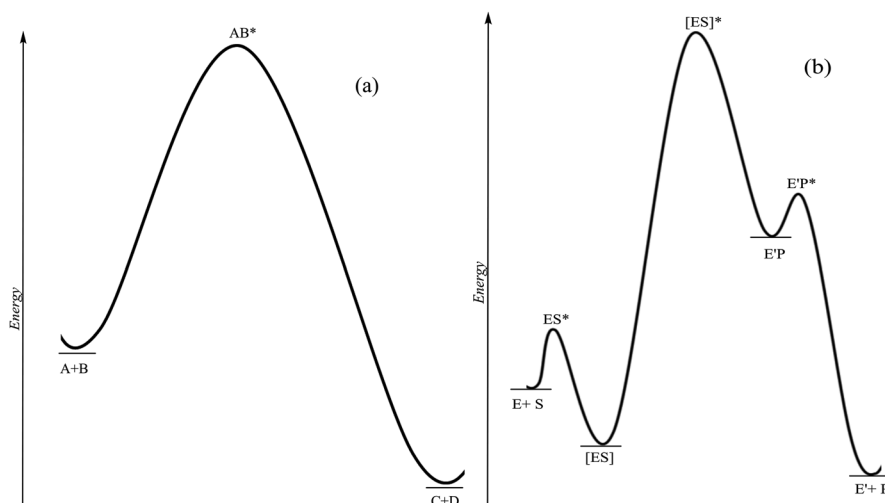
A realistic model chemistry must follow the mechanism of oxo-transfer reaction prevalent in this class of molybdoenzymes. To understand the unique feature of oxo-transfer reaction of a molybdoenzyme the overall catalytic process may briefly be summarized as schematically shown in Scheme 3.1.⁹⁵

Here E represents the Mo centre of the enzyme, S the substrate, ES the all-important enzyme–substrate complex, E'P is the product bound to the Mo centre (E'), the redox state of which and effective atom coordination arrangement around it is changed from the starting E. Next comes the product release stage where upon releasing the product, P, the E' form completes the forward reaction. The next reaction is almost started at this stage where the second substrate, S', used for regenerating the E state of the enzyme, comes in creating another enzyme substrate complex (E'S'). Such enzymatic reaction is classically known as hybrid ping-pong mechanism¹¹⁰ and operative in two substrates based oxidoreductase class of molybdoenzymes. Now the intramolecular electron (atom transfer, often proton coupled) transfer in E'S' takes place regenerating E in completing the catalytic cycle. For a specific example the enzyme, hepatic sulfite-cytochrome-*c* oxidoreductase (SO) may be considered here. In the reductive half-reaction it is the named substrate, sulfite (or bisulfite) that gets oxidized resulting in the reduction of $\{\text{Mo}^{\text{VI}}\text{O}_2\}^{2+}$ (E) to $\{\text{Mo}^{\text{IV}}\text{O}\}^{2+}$ (E'). This reaction is coupled with the oxidative half-reaction by cytochrome *c* as the electron acceptor to regenerate $\{\text{Mo}^{\text{VI}}\text{O}_2\}^{2+}$ (E) from $\{\text{Mo}^{\text{IV}}\text{O}\}^{2+}$ (E'). It is in the regeneration stage, one water molecule is coordinated at the Mo centre of the reduced E'. The reactive species now $\{\text{Mo}^{\text{IV}}\text{O}(\text{H}_2\text{O})\}^{2+}$ responds to two sequential one electron oxidation (coupled with proton elimination like $\{\text{Mo}^{\text{IV}}\text{O}(\text{H}_2\text{O})\}^{2+} \rightarrow \{\text{Mo}^{\text{V}}\text{O}(\text{OH})\}^{2+} \rightarrow \{\text{Mo}^{\text{VI}}\text{O}_2\}^{2+}$). Such oxidative half-reaction involves two consecutive proton-coupled electron transfer (PCET) reactions (in the reaction Scheme 3.1, for simplicity only one step is shown). This hybrid ping-pong mechanism^{111,112} comprising both the reductive half-reaction and oxidative half-reaction completes the catalytic cycle and demonstrates that the oxygen atom that is transferred to the substrate is essentially supplied by water.^{113,114} For any catalytic model reaction all these aspects should be taken into account. Normally, demonstrating such a complete cycle is rather difficult depending on the reactivity and stability of a small synthetic molecule.

However, a response of the model related to the main forward reaction is generally considered a good model reaction.

3.3.1 Principle Involved in Electron Transfer Reactions

Most of the reactions falling under the purview of enzymatic transformations by molybdoenzymes are reduction–oxidation (redox) reactions. Chemical redox reactions in general are very diverse in nature. Biochemical reactions basically adopt a specific reaction mechanism exploiting the inherent thermodynamics and kinetics of these systems. It is to be understood clearly that there is a subtle difference between the enzymatic oxygen atom transfer reaction catalyzed by molybdoenzymes and well-established classical oxo atom transfer reaction in inorganic chemistry. The simplest kind of redox reaction involving electron transfer from one centre to another can be classified as outer-sphere electron transfer reaction where the coordination sphere of the oxidant and the reductant remains intact in the course of electron transfer (*i.e.* no formal bond breaking or bond making takes place).¹¹⁵ Such simple redox activity can be exemplified by the electron transfer between cytochrome *c* and cytochrome *b*₅, the two electron carrier domains present in the enzyme sulfite oxidase. More relevant for substrate transformation, however, is the redox reaction involving the active site. The respective redox process may be best described as following an inner-sphere electron transfer mechanism, which is accompanied by the formation of a bridged intermediate finally resulting in atom ligand exchange.¹¹⁶ Initially, a binuclear precursor complex is formed with a bridging atom; subsequently electron transfer is mediated *via* the bridge forming a successor complex, which collapses yielding the final products of the reaction. The mechanism of chemical inner-sphere electron transfer was first demonstrated by Henry Taube.¹¹⁷ These reactions mainly occur in the activated state following classical oxo-transfer reaction or atom transfer reaction. These reactions follow an established kinetics following second-order rate constant and even under pseudo first-order conditions these reaction do not show the well-known enzymatic saturation kinetics behaviour.¹¹⁸ One has to understand the difference between oxo-transfer reaction from a classical inorganic point of view and enzymatic oxo-transfer reaction, where the mechanism of such reactions differ. The subtle difference in the reaction mechanism is related to second-order kinetics followed in classical oxo-transfer reaction *vis à vis* the saturation kinetics of enzymatic oxo-transfer reaction. In the enzymatic oxo-transfer reaction of molybdoenzymes the formation of the Michaelis–Menten (enzyme–substrate) complex is a prerequisite in the ground state where this complex is the unique reactant and not the enzyme and the substrate as two individual and separate entities. The enzymatic reaction differs on the count that it is the newly formed enzyme–substrate complex that responds to reaction. This led to saturation kinetics behaviour, which is different from the classical oxo-transfer reaction. The difference in the kinetic profile between inorganic oxo-transfer and enzymatic oxo-transfer reactions is shown in Scheme 3.2.



Scheme 3.2 Energy profile of (a) inorganic oxo-transfer and (b) enzymatic oxo-transfer reactions.¹¹⁶

Example of a non-classical oxo-transfer reaction¹¹⁹ is rare where a relatively stable complex mimicking the role of enzyme-substrate adduct could be isolated. However, the complex $[\text{MoO}(3,5\text{-DBCat})_2(\text{Opy})]$ ¹¹⁹ may be treated as a complex of similar nature. This complex in solution responds to intramolecular reaction where the coordinated pyO gets deoxygenated and released as simple pyridine. The oxygen is now attached to the molybdenum centre.

This type of electron transfer reaction can be induced by physical or chemical stimuli. By a simple electron bookkeeping formalism, in such a reaction, by the action of an external redox system, a species A is converted to B with its associated ligand carrying an odd electron; the internal electron transfer may ensure the internal oxidation whereby the metal oxidation state changes. Regeneration of enzymes like reduced xanthine oxidase (XO) in air (molecular oxygen) involves stepwise oxidation of the active site with the intermediate formation of O_2^- .¹²⁰ Hughes and coworkers¹²¹ have shown that the electron transfer from substrate to the molybdenum centre in XO is a concerted process; this involves flavin and iron-sulfur clusters functioning concomitantly with the molybdenum cofactor in an elaborate electron flow. Here Mo in its reduced, *i.e.* IV, state in principle might affect the reduction of molecular oxygen by two electrons, yet the involvement of flavin participating in this redox process is reminiscent of an induction process where molecular oxygen might play the role of an external oxidant inducing electron transfer *via* flavin and Fe-S proteins to the molybdenum centre *via* the Moco entity.^{110,122}

The well-known coordination chemistry of molybdenum suggests a distinct relationship between acid-base and redox properties of molybdenum complexes and that a coupled electron-proton transfer (to or from the substrate) may be mediated by molybdoenzymes. Simple molecular mechanisms

embodying coupled electron–proton transfer can explain many key steps in the catalytic cycle of molybdenum enzymes, especially at the regeneration stage of the enzyme like xanthine oxidase, aldehyde oxidase or sulfite oxidase. If a complex reacts by losing one electron, then it is more prone to lose a proton from the coordinating oxygen atom of water as the electron density is shifted from the donor-atom hydrogen bond to the donor-atom metal centre bond. Thus, simple proton and electron transfer reactions can be and very often are coupled. Such a reaction, overall, is important for removing the tightly coordinated terminal oxo group that may be accomplished easily (in a thermodynamic sense) using a couple of protons and thus eliminating the attached terminal oxo group in the form of water. Conversely, the $\{\text{Mo}^{\text{IV}}-\text{OH}_2\}$ moiety releases in a stepwise fashion a proton coupled with the removal of one electron to yield first the intermediate $\{\text{Mo}^{\text{V}}-\text{OH}\}$ group and eventually the final $\{\text{Mo}^{\text{VI}}=\text{O}\}$ moiety. These reactions are essentially called proton coupled electron transfer (PCET) reactions.

The interpretation of enzymatic kinetics based on the reactivity of the enzyme–substrate complex, where the free enzyme does not participate in the said reaction, leading to product formation may be viewed as oxidative addition and reductive elimination reactions. Therefore the enzymatic oxo-transfer reactions may involve redox reactions different from the classical oxo-transfer reaction. It is known that all such enzymatic reactions (atom transfer) of molybdoenzymes follow saturation kinetics. Initially such a reaction starts with a bimolecular reaction between E (enzyme) and S (substrate) but under high concentration of S (saturation) the ES (enzyme–substrate or Michaelis–Menten) complex is formed.¹¹⁸ Once such a complex is generated the typical rate-determining enzymatic step follows as a single catalytic step with an apparent unimolecular rate constant. Under such substrate saturation conditions it is the instability of the ES complex that leads to the reaction forming E'P. One can readily compare the characteristics of such ES complex with the precursor complex and of E'P with the successor complex in Taube's inner sphere mechanism but the salient difference may be noted that the classical atom transfer reactions involve such intermediates in the activated states. In contrast, at least, the precursor complex in enzymatic reaction is a thermodynamic stable entity generally noted as ES complex, which could be similar to the starting complex shown in Figure 3.8. The reactivity of ES disintegrating into E' and P is based on its inherent instability. The disintegration follows a step in which the new bond is strengthened and the old bond is weakened in the {E–O–S} moiety (E is the Mo part of the enzyme and “O” is the oxo donor atom of the substrate, S) that is similar to the successor complex formation in the inner sphere mechanism. At the product release stage of the successor complex the enzymatic reaction can be viewed as a rare combination of the oxidative addition based on E (Mo(IV)) and the reductive elimination based on S (for example DMSO for the DMSO reductase family of enzymes) in a concerted manner. Considering E, the formation of E' can best be described as an oxidative addition reaction where Mo(IV) gets oxidized by two units to Mo(VI) along with the expansion of its coordination number by one oxo group with a double bond (this is equivalent to two single

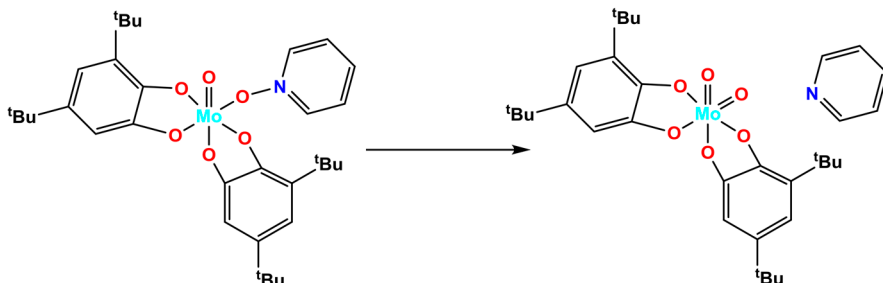
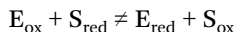


Figure 3.8 Non-classical oxo-transfer reaction resembling the chemistry of enzyme–substrate complex.

bonds). Interestingly, based on S the reaction can be viewed as the reductive elimination to yield P where the central atom of S is virtually reduced by two units along with the loss of the oxo group (equivalent to two coordination number; however, here the central representative element will follow the octet rule whereas the metal centre would follow the 18 electron rule). A similar description may be applied to the oxidase class of enzyme where the metal centred reaction can be viewed as responding to reductive elimination and for the central atom of the substrate it is the oxidative addition reaction. Thus the ES complex of the enzyme sulfite oxidase would respond in the form of a reductive elimination and the sulfur of the attached sulfite (or bisulfite) would face oxidative addition upon which the sulfate ion is formed as product (for sulfur the effective atomic number rule may be governed by the octet rule). However, the necessity of retaining 18 electron configuration³ may not strictly be followed in these oxo-transfer metalloenzymes. This is because both the oxidized and the reduced forms of an enzyme must not be very stable but relatively active, so that the oxidized and reduced states can oscillate back and forth completing the catalytic cycle preferentially with high turnover numbers, which stable species would prevent. These molybdoenzymes are, hence, involved in various types of redox reactions as known from general chemistry. Thus for oxo-transfer enzymes the redox reactions transforming the substrates are two-electron atom transfer reactions involving reactive intermediate ES complex types. A simple enzyme (E) and substrate (S) redox process like:



does not take place in these enzymatic reactions but in reality the intramolecular electronic readjustment in the light of ES.



predicts the $ES \leftrightarrow E'P$ interconversion and the product release reaction is similar to the oxidative addition and reductive elimination reactions prevalent in several well-known inorganic and organometallic catalytic reactions. There

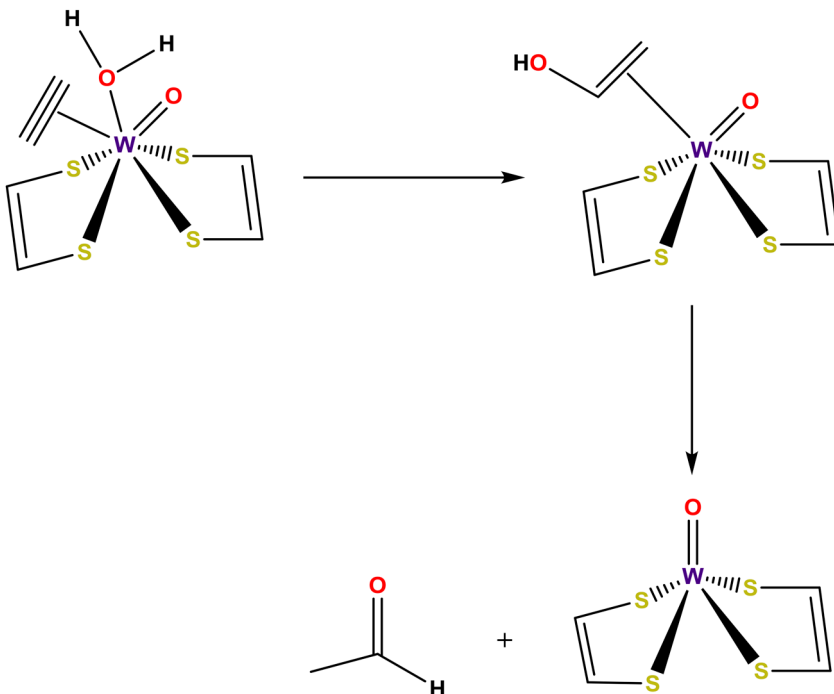


Figure 3.9 The proposed catalytic/enzymatic hydration of acetylene.¹²²

is only one class of pterin-based non-redox tungstoenzymes known today: acetylene hydratase, which catalyzes the hydration of acetylene. Respective molybdenum versions are known from different strains.¹²³ A demonstration of such hydration chemistry was made using a synthetic structural and functional model.¹²⁴ The proposed reaction mechanism is shown in Figure 3.9.

For the enzymatic model reaction one should expect a behaviour expressing saturation kinetics. Only a few model compounds were subjected to kinetic evaluation and both classes of enzymatic model compounds, oxidizing and reducing, were tested. For the substrate used with the oxidizing models, barring one case where the native hydrogensulfite ion (the reaction of SO takes place in the IM space of mitochondria where the pH of medium is below 7 where thermodynamically SO_3^{2-} is not stable and HSO_3^- is the substrate of choice^{111,112}) was used for the sulfite oxidase model reaction, the rest of the reactions utilized the proxy substrate, PPh_3 , and its numerous variations where the phenyl (Ph) group is replaced by several types of substituents. All these reactions show straightforward second-order kinetics. Interestingly, the sulfite oxidase model complex responding with saturation kinetics⁹⁰ to the hydrogensulfite ion demonstrates a clean reaction. In addition this reaction has been shown to respond to inhibition by different patterns similar to native sulfite oxidase.¹²⁵ As the model contains two dithiolene ligands instead of one and one thiol ligand mimicking cysteine as observed in the native SO, the model compound can be viewed as formally

being a good structural model in one respect and a not so good model in another. Interestingly, density functional theory showed that in the activated complex one sulfur coordination from one of the dithiolenes became very weak with the eventual distance limited to simple van der Waals interactions suggesting it to have a role as blocker to a site of the Mo complex preventing its decomposition by the process of dimerization.¹²⁶ When tested with PPh_3 as substrate this complex ion $[\text{Mo}(\text{O})_2(\text{mnt})_2]^{2-}$ (mnt = maleonitriledithiolate) does not follow saturation kinetics but rather shows the commonly observed second-order kinetics following classical oxo-transfer reaction.⁸⁸ This suggests that the reaction mechanism involving the hydrogensulfite ion and PPh_3 as substrate differs. To understand this difference a reaction profile investigation by density functional theory (DFT) between the Mo-cofactor with HSO_3^- and PPh_3 as substrates reveals the difference in frontier orbital interaction (FMO) between them.¹²⁶ The interaction (Figure 3.10) between molecular orbitals of Moco (LUMO) and of HSO_3^- (HOMO (middle)), where arrows indicate the FMO interaction of the same phase, corresponds to the interaction between Mo (dxy) and O₋ (p) of HSO_3^- (a), and to the interaction between O_{eq} and the S atom of HSO_3^- (b). The HOMO (right) of PPh_3 shows only one possible interaction.¹²⁶

Therefore an exact mimicking of the electronic effects may not be expected when proxy substrates like phosphines are used in order to understand the reaction profiles of model reactions. Holm, in a detailed paper,¹²⁷ presented the essence of reaction kinetics of a series of complexes of W with bisdithiobenzene coordination representing models for iso-enzymes of DMSO reductase (Figure 3.11). The corresponding Mo model systems are much more reactive, hence it is difficult to observe smooth kinetics for their reactions. The mechanistic description of the catalyzed reaction with the tungsten model involves $\text{W}^{\text{IV}}-\text{O}-\text{S}$ bond-making followed by substantial weakening of the O-S bond. Such behaviour is typical for inner sphere mechanisms and reminiscent of oxidative additions as enumerated earlier. Interestingly, it was concluded that the reaction is intrinsic to the used complexes and substrate. In proteins such properties would be influenced by the protein structure and the active site environment. Therefore any data or kinetic pattern extracted

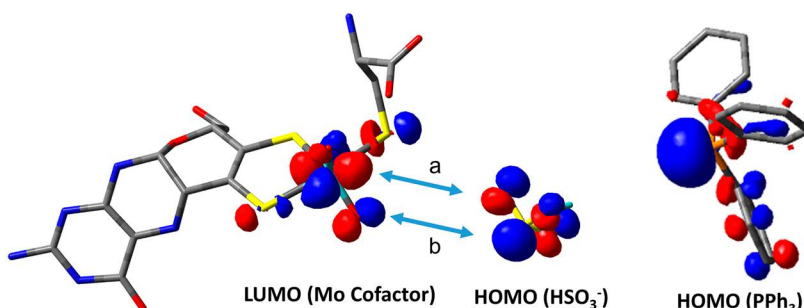


Figure 3.10 The difference in HOMO-LUMO interaction of Moco with HSO_3^- or PPh_3 .¹²⁶ Reproduced with permission from ref. 126. © Wiley-VCH Verlag GmbH & Co. KGaA, Weinheim.

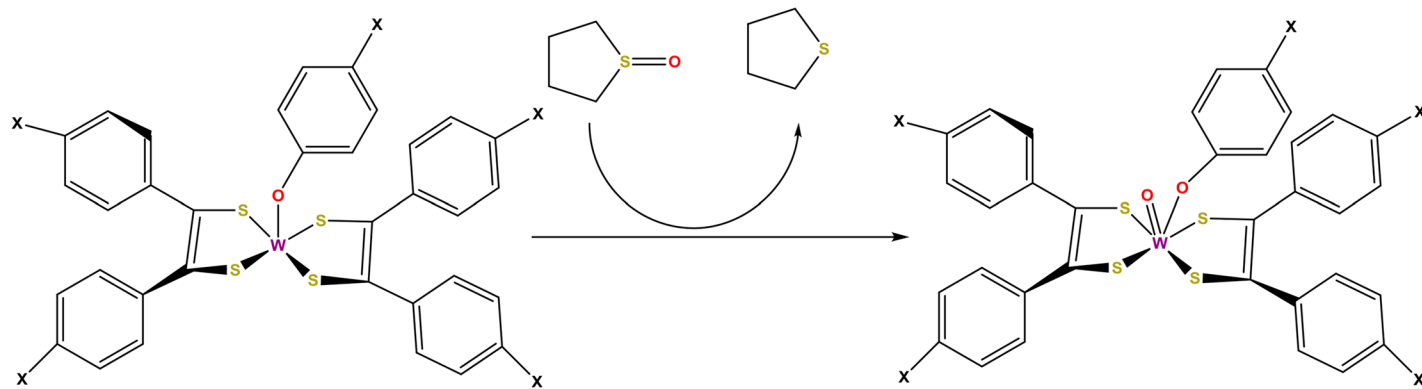


Figure 3.11 Oxygen atom transfer reactions of *S*-oxides mediated by bis(dithiolene) W complexes.

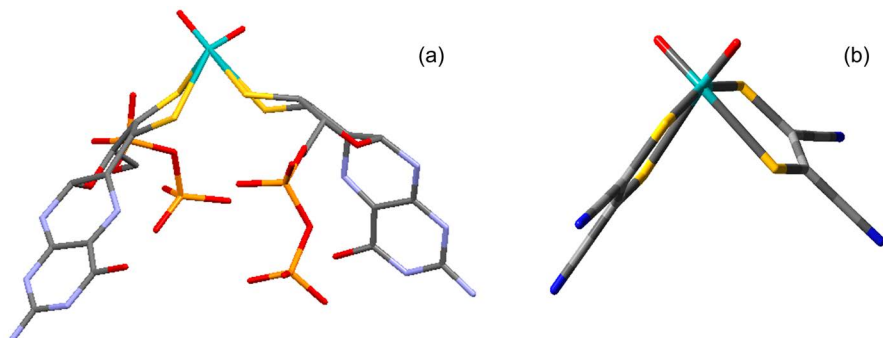


Figure 3.12 The active site structure of the oxidized native protein (a) and model complex, $[\text{MoO}_2(\text{mnt})_2]^{2-}$ (b). Reproduced with permission from M. Czjzek, J. Dos Santos, J. Pommier, G. Giordano, V. Mejean and R. Hasser, Crystal structure of oxidized trimethylamine N-oxide reductase from *Shewanella massilia* at 2.5 Å resolution, *Journal of Molecular Biology*, 284(2), 435–447. Copyright 1998 with permission from Elsevier.

from model systems has to be taken with caution as it may not be to the tune of the reaction systems of the native enzymes.

The structural analogy of trimethylamine *N*-oxide reductase (TMANOR) with the synthetic complex may be visualized by comparing the X-ray structures of the active site of the oxidized native protein from *Shewanella massilia*¹²⁸ and of the model (Figure 3.12).

A detailed kinetic investigation of bis-dithiolene MoO complexes coordinated with two different dithiolene ligands (asymmetric) demonstrates saturation kinetics using the native substrate, TMANO.¹²⁹ Interestingly, it was observed that in complexes like $[\text{pyH}_2][\text{MoO}(\text{mnt})_2]$ the so-called lone oxo group, which may be viewed as the preserved “spectator oxo group”¹³⁰ from its oxidized dioxo redox partner, is hydrogen bonded. H-bonding leads to a lengthening of the Mo=O bond,⁷⁵ which raises the respective reaction rate towards substrate (TMANO) transformation. The asymmetric bis-dithiolene MoO complexes also showed a variation in Mo=O bond lengths¹²⁹ in these complexes, which directly influence their reactivity in oxo-transfer reactions with the substrate TMANO. There was, hence, a direct correlation found between bond length and reaction rate. Such investigations raise questions about the role of the “spectator oxo group” of the oxo-molybdenum moiety, which, in reality, may not be a silent spectator but rather silently modulating the electron (atom) transfer reaction.

3.4 Conclusion

Since the identification of XO in 1891,²⁰ understanding the enzymatic reactions advanced up to the molecular level with the availability of X-ray structural data for several oxo-molybdoenzymes and oxo-tungstoenzymes. The

challenge of synthesizing models for such complicated assemblages was taken up by synthetic chemists aiming to mimic the structure and function of these biological molecules. Based on the made observations this review tried to explain the reactivity of oxo-transfer involving the ES complex using the theoretical paradigm of concerted oxidative addition and reductive elimination reaction. The salient difference between the classical oxo-transfer reaction and the enzymatic oxo-transfer reaction has now been addressed. The knowledge gained by the synthetic model approach is now used to create newer systems which may not be necessarily structural replica of enzymes but may catalyze with ease similar transformation as the enzymes using modified arrangements *via* bio-inspired chemistry. The routine use of density functional theory these days on these systems substantially furthers our understanding of the electronic arrangement and helps explain key characteristics of the electron transfer reactions, which again generates a feedback governing the design of even more suitable biomimetic model complexes.

References

1. S. Sarkar, in *Molybdenum and its Compounds: Applications, Electrochemical Properties and Geological Implications*, ed. V. S. Saji and S. I. Lopatin, Nova Scientific Publisher, 2014, ch. 1, pp. 3–8.
2. A. Müller, S. Sarkar, S. Q. N. Shah, H. Bögge, M. Schmidtmann, S. Sarkar, P. Kögerler, B. Hauptfleisch, A. X. Trautwein and V. Schünemann, *Angew. Chem., Int. Ed.*, 1999, **38**, 3238–3241.
3. F. A. Cotton, G. Wilkinson, C. A. Murillo and M. Bochmann, *Advanced Inorganic Chemistry*, Wiley Interscience, 6th edn, 1999.
4. *Molybdenum and Molybdenum containing Enzymes*, ed. M. P. Coughlan, Pergamon Press, London, 1980.
5. J. M. Nocek, J. S. Zhou, S. De Forest, S. Priyadarshy, D. N. Beratan, J. N. Onuchic and B. M. Hoffman, *Chem. Rev.*, 1996, **96**, 2459–2490.
6. M. T. Pope, E. R. Still and R. J. P. Williams, in *Molybdenum and Molybdenum containing Enzymes*, ed. M. P. Coughlan, Pergamon Press, London, 1980, ch. 1, pp. 1–40.
7. S. P. Kramer, J. L. Johnson, A. A. Ribeiro, D. S. Millington and K. V. Rajagopalan, *J. Biol. Chem.*, 1987, **262**, 16357–16363.
8. H. Schindelin, C. Kisker, J. Hilton, K. V. Rajagopalan and D. C. Rees, *Science*, 1996, **272**, 1615–1621.
9. R. Hille, *Chem. Rev.*, 1996, **96**, 2757–2816.
10. J. L. Johnson, in *Molybdenum and Molybdenum containing Enzymes*, ed. M. P. Coughlan, Pergamon Press, London, 1980, ch. 10, pp. 345–384.
11. J. Rebelo, S. Macieira, J. M. Dias, R. Huber, C. S. Ascenso, F. Rusnak, J. J. Moura, I. Moura and M. J. Romao, *J. Mol. Biol.*, 2000, **297**, 135–146.
12. M. J. Romão, M. Archer, I. Moura, J. J. G. Moura, J. LeGall, R. Engh, M. Schneider, P. Hof and R. Huber, *Science*, 1995, **270**, 1170–1176.
13. J. J. Truglio, K. Theis, S. Leimkuhler, R. Rappa, K. V. Rajagopalan and C. Kisker, *Structure*, 2002, **10**, 115–125.

14. C. Enroth, B. T. Eger, K. Okamoto, T. Nishino, T. Nishino and E. F. Pai, *Proc. Natl. Acad. Sci. U. S. A.*, 2000, **97**, 10723–10728.
15. R. Hille, G. N. George, M. K. Eidsness and S. P. Cramer, *Inorg. Chem.*, 1989, **28**, 4018–4022.
16. R. Huber, P. Hof, R. O. Duarte, J. J. Moura, I. Moura, M. Y. Liu, J. LeGall, R. Hille, M. Archer and M. J. Romao, *Proc. Natl. Acad. Sci. U. S. A.*, 1996, **93**, 8846–8851.
17. K. V. Rajagopalan, in *Molybdenum and Molybdenum-containing Enzymes*, ed. M. P. Coughlan, Pergamon Press, London, 1980, ch. 7, pp. 241–272.
18. H. Dobbek, L. Gremer, R. Kiefersauer, R. Huber and O. Meyer, *Proc. Natl. Acad. Sci. U. S. A.*, 2002, **99**, 15971–15976.
19. G. N. George, R. M. Garrett, R. C. Prince and K. V. Rajagopalan, *J. Am. Chem. Soc.*, 1996, **118**, 8588–8592.
20. G. N. George, I. J. Pickering and C. Kisker, *Inorg. Chem.*, 1999, **38**, 2539–2540.
21. C. Kisker, H. Schindelin, A. Pacheco, W. A. Wehbi, R. M. Garrett, K. V. Rajagopalan, J. H. Enemark and D. C. Rees, *Cell*, 1997, **91**, 973–983.
22. G. N. George, J. A. Mertens and W. H. Campbell, *J. Am. Chem. Soc.*, 1999, **121**, 9730–9731.
23. R. Hille, *Dalton Trans.*, 2013, **42**, 3029–3042.
24. A. G. McEwan, J. P. Ridge, C. A. McDevitt and P. Hugenholtz, *Geomicrobiol. J.*, 2002, **19**, 3–21.
25. *Molybdenum Enzyme*, ed. T. G. Spiro, Wiley-Interscience, 1985.
26. C. A. McAuliffe, *Techniques and topics in Bioinorganic Chemistry*, Macmillan Press Ltd, 1975.
27. *Molybdenum and Molybdenum-containing Enzyme*, ed. M. P. Coughlan, Pergamon Press, 1980.
28. R. Hille, J. Hall and P. Basu, *Chem. Rev.*, 2014, **114**, 3963–4038.
29. R. Hille, *Molybdenum Enzymes*, 1999, **34**, 125–137.
30. *Molybdenum Enzymes, Cofactors, and Model Systems*, ed. E. I. Stiefel, D. Coucouvanis and W. E. Newton, ACS Symposium Series, 1993.
31. *Molybdenum*, ed. R. R. Mendel and R. Hille, *Coord. Chem. Rev.*, 2011.
32. R. Barral, C. Bocard, I. S. de Roch and L. Sajus, *Tetrahedron Lett.*, 1972, **13**, 1693–1696.
33. M. S. Reynolds, J. M. Berg and R. H. Holm, *Inorg. Chem.*, 1984, **23**, 3057–3062.
34. E. W. Harlan, J. M. Berg and R. H. Holm, *J. Am. Chem. Soc.*, 1986, **108**, 6992–7000.
35. C. J. Doonan, D. A. Slizys and C. G. Young, *J. Am. Chem. Soc.*, 1999, **121**, 6430–6436.
36. H. Sugimoto, S. Tatemoto, K. Toyota, K. Ashikari, M. Kubo, T. Ogura and S. Itoh, *Chem. Commun.*, 2013, **49**, 4358–4360.
37. H. Sugimoto, K. Hatakeyama, K. Toyota, S. Tatemoto, M. Kubo, T. Ogura and S. Itoh, *Dalton Trans.*, 2013, **42**, 3059–3070.
38. M. Volpe and N. C. Mösch-Zanetti, *Inorg. Chem.*, 2012, **51**, 1440–1449.
39. N. Nguyen, A. J. Lough and U. Fekl, *Inorg. Chem.*, 2012, **51**, 6446–6448.

40. A. Cervilla, F. Pérez-Pla, E. Llopis and M. Piles, *Inorg. Chem.*, 2006, **45**, 7357–7366.
41. K. Baba, T. A. Okamura, H. Yamamoto, T. Yamamoto, M. Ohama and N. Ueyama, *Inorg. Chem.*, 2006, **45**, 8365–8371.
42. H. Sugimoto, M. Tarumizu, K. Tanaka, H. Miyake and H. Tsukube, *Dalton Trans.*, 2005, 3558–3565, DOI: 10.1039/B503828F.
43. C. J. Doonan, A. J. Millar, D. J. Nielsen and C. G. Young, *Inorg. Chem.*, 2005, **44**, 4506–4514.
44. D. R. Evans, M. Huang, J. C. Fettinger and T. L. Williams, *Inorg. Chem.*, 2002, **41**, 5986–6000.
45. K. Heffron, C. Léger, R. A. Rothery, J. H. Weiner and F. A. Armstrong, *Biochemistry*, 2001, **40**, 3117–3126.
46. J. P. Donahue, C. R. Goldsmith, U. Nadiminti and R. H. Holm, *J. Am. Chem. Soc.*, 1998, **120**, 12869–12881.
47. F. A. Cotton and G. Schmid, *Inorg. Chem.*, 1997, **36**, 2267–2278.
48. Z. Xiao, M. A. Bruck, J. H. Enemark, C. G. Young and A. G. Wedd, *Inorg. Chem.*, 1996, **35**, 7508–7515.
49. N. Ueyama, H. Oku, M. Kondo, T.-a. Okamura, N. Yoshinaga and A. Nakamura, *Inorg. Chem.*, 1996, **35**, 643–650.
50. M. A. Pietsch, M. Couty and M. B. Hall, *J. Phys. Chem.*, 1995, **99**, 16315–16319.
51. Z. Xiao, M. A. Bruck, J. H. Enemark, C. G. Young and A. G. Wedd, *Inorg. Chem.*, 1993, **35**, 7508–7515.
52. H. Masanobu and M. Yasushi, in *Molybdenum Enzymes, Cofactors, and Model Systems*, American Chemical Society, 1993, ch. 22, vol. 535, pp. 346–362.
53. J. M. Charnock, S. Bristow, J. R. Nicholson, C. D. Garner and W. Clegg, *J. Chem. Soc., Dalton Trans.*, 1987, 303–306, DOI: 10.1039/DT9870000303.
54. W. E. Newton, J. W. McDonald, K. Yamanouchi and J. H. Enemark, *Inorg. Chem.*, 1979, **18**, 1621–1626.
55. N. Nguyen, A. J. Lough and U. Fekl, *Inorg. Chem.*, 1977, **51**, 6446–6448.
56. J. P. Donahue, C. R. Goldsmith, U. Nadiminti and R. H. Holm, *J. Am. Chem. Soc.*, 1977, **120**, 12869–12881.
57. A. Cervilla, F. Pérez-Pla, E. Llopis and M. Piles, *Inorg. Chem.*, 1977, **45**, 7357–7366.
58. J. Leppin, C. Förster and K. Heinze, *Inorg. Chem.*, 2014, **53**, 12416–12427.
59. C. A. Kipke, W. E. Cleland, Jnr, S. A. Roberts and J. H. Enemark, *Acta Crystallogr., Sect. A*, 1989, **45**, 870–872.
60. C.-S. J. Chang, T. J. Pecci, M. D. Carducci and J. H. Enemark, *Acta Crystallogr., Sect. A*, 1992, **48**, 1096–1097.
61. C. S. J. Chang, D. Collison, F. E. Mabbs and J. H. Enemark, *Inorg. Chem.*, 1990, **29**, 2261–2267.
62. J. I. Gelder and J. H. Enemark, *Inorg. Chem.*, 1976, **15**, 1839–1843.
63. C. G. Young, D. Collison, F. E. Mabbs and J. H. Enemark, *Inorg. Chem.*, 1987, **26**, 2925–2927.
64. Z. Xiao, M. A. Bruck, C. Doyle, J. H. Enemark, C. Grittini, R. W. Gable, A. G. Wedd and C. G. Young, *Inorg. Chem.*, 1995, **34**, 5950–5962.

65. I. K. Dhawan, A. Pacheco and J. H. Enemark, *J. Am. Chem. Soc.*, 1994, **116**, 7911–7912.
66. C. J. Hinshaw, G. Peng, R. Singh, J. T. Spence, J. H. Enemark, M. Bruck, J. Kristofzski, S. L. Merbs, R. B. Ortega and P. A. Wexler, *Inorg. Chem.*, 1989, **28**, 4483–4491.
67. D. Dowerah, J. T. Spence, R. Singh, A. G. Wedd, G. L. Wilson, F. Farchione, J. H. Enemark, J. Kristofzski and M. Bruck, *J. Am. Chem. Soc.*, 1987, **109**, 5655–5665.
68. I. K. Dhawan and J. H. Enemark, *Inorg. Chem.*, 1996, **35**, 4873–4882.
69. V. V. Kurshev, L. Kevan, P. Basu and J. Enemark, *J. Phys. Chem.*, 1995, **99**, 11288–11291.
70. B. B. Kaul, J. H. Enemark, S. L. Merbs and J. T. Spence, *J. Am. Chem. Soc.*, 1985, **107**, 2885–2891.
71. B. L. Westcott, N. E. Gruhn and J. H. Enemark, *J. Am. Chem. Soc.*, 1998, **120**, 3382–3386.
72. I. K. Dhawan, M. A. Bruck, B. Schilling, C. Grittini and J. H. Enemark, *Inorg. Chem.*, 1995, **34**, 3801–3808.
73. Z. Xiao, J. H. Enemark, A. G. Wedd and C. G. Young, *Inorg. Chem.*, 1994, **33**, 3438–3441.
74. K. R. Barnard, M. Bruck, S. Huber, C. Grittini, J. H. Enemark, R. W. Gable and A. G. Wedd, *Inorg. Chem.*, 1997, **36**, 637–649.
75. M. L. Mader, M. D. Carducci and J. H. Enemark, *Inorg. Chem.*, 2000, **39**, 525–531.
76. H. K. Joshi and J. H. Enemark, *J. Am. Chem. Soc.*, 2004, **126**, 11784–11785.
77. P. Subramanian, J. T. Spence, R. Ortega and J. H. Enemark, *Inorg. Chem.*, 1984, **23**, 2564–2572.
78. M. Minelli, J. H. Enemark, K. Wieghardt and M. Hahn, *Inorg. Chem.*, 1983, **22**, 3952–3953.
79. D. C. Bravard, W. E. Newton, J. T. Huneke, K. Yamanouchi and J. H. Enemark, *Inorg. Chem.*, 1982, **21**, 3795–3798.
80. K. Yamanouchi and J. H. Enemark, *Inorg. Chem.*, 1979, **18**, 1626–1633.
81. K. Yamanouchi and J. H. Enemark, *Inorg. Chem.*, 1978, **17**, 1981–1986.
82. K. Yamanouchi and J. H. Enemark, *Inorg. Chem.*, 1978, **17**, 2911–2917.
83. K. Pal, R. Maiti, P. K. Chaudhury and S. Sarkar, *Inorg. Chim. Acta*, 2007, **360**, 2721–2733.
84. B. S. Lim, M. W. Willer, M. Miao and R. H. Holm, *J. Am. Chem. Soc.*, 2001, **123**, 8343–8349.
85. J. Mitra and S. Sarkar, *Dalton Trans.*, 2013, **42**, 3050–3058.
86. J. Mitra and S. Sarkar, *Inorg. Chem.*, 2013, **52**, 3032–3042.
87. S. Boyde, S. R. Ellis, C. D. Garner and W. Clegg, *J. Chem. Soc., Chem. Commun.*, 1986, 1541–1543, DOI: 10.1039/C39860001541.
88. J. H. Enemark, J. J. A. Cooney, J.-J. Wang and R. H. Holm, *Chem. Rev.*, 2004, **104**, 1175–1200.
89. J. McMaster, J. M. Tunney and C. D. Garner, in *Dithiolene Chemistry*, John Wiley & Sons, Inc., 2004, pp. 539–583.
90. S. K. Das, P. K. Chaudhury, D. Biswas and S. Sarkar, *J. Am. Chem. Soc.*, 1994, **116**, 9061–9070.

91. H. Sugimoto, K. Suyama, K. Sugimoto, H. Miyake, I. Takahashi, S. Hirota and S. Itoh, *Inorg. Chem.*, 2008, **47**, 10150–10157.
92. H. Sugimoto, T. Sakurai, H. Miyake, K. Tanaka and H. Tsukube, *Inorg. Chem.*, 2005, **44**, 6927–6929.
93. H. Sugimoto, M. Harihara, M. Shiro, K. Sugimoto, K. Tanaka, H. Miyake and H. Tsukube, *Inorg. Chem.*, 2005, **44**, 6386–6392.
94. B. S. Lim and R. H. Holm, *J. Am. Chem. Soc.*, 2001, **123**, 1920–1930.
95. B. Bradshaw, D. Collison, C. D. Garner and J. A. Joule, *Org. Biomol. Chem.*, 2003, **1**, 129–133.
96. E. Stephen Davies, G. M. Aston, R. L. Beddoes, D. Collison, A. Dinsmore, A. Docrat, J. A. Joule, C. R. Wilson and C. David Garner, *J. Chem. Soc., Dalton Trans.*, 1998, 3647–3656, DOI: 10.1039/A805688I.
97. E. Stephen Davies, R. L. Beddoes, D. Collison, A. Dinsmore, A. Docrat, J. A. Joule, C. R. Wilson and C. David Garner, *J. Chem. Soc., Dalton Trans.*, 1997, 3985–3996, DOI: 10.1039/A703682E.
98. N. Yoshinaga, N. Ueyama, T.-a. Okamura and A. Nakamura, *Chem. Lett.*, 1990, **19**, 1655–1656.
99. S. K. Das, D. Biswas, R. Maiti and S. Sarkar, *J. Am. Chem. Soc.*, 1996, **118**, 1387–1397.
100. H. Tano, R. Tajima, H. Miyake, S. Itoh and H. Sugimoto, *Inorg. Chem.*, 2008, **47**, 7465–7467.
101. H. Sugimoto, S. Tatemoto, K. Suyama, H. Miyake, S. Itoh, C. Dong, J. Yang and M. L. Kirk, *Inorg. Chem.*, 2009, **48**, 10581–10590.
102. H. Oku, N. Ueyama, M. Kondo and A. Nakamura, *Inorg. Chem.*, 1994, **33**, 209–216.
103. B. S. Lim, K.-M. Sung and R. H. Holm, *J. Am. Chem. Soc.*, 2000, **122**, 7410–7411.
104. K. Baba, T.-a. Okamura, C. Suzuki, H. Yamamoto, T. Yamamoto, M. Ohama and N. Ueyama, *Inorg. Chem.*, 2006, **45**, 894–901.
105. T.-a. Okamura, M. Tatsumi, Y. Omi, H. Yamamoto and K. Onitsuka, *Inorg. Chem.*, 2012, **51**, 11688–11697.
106. T.-a. Okamura, Y. Ushijima, Y. Omi and K. Onitsuka, *Inorg. Chem.*, 2013, **52**, 381–394.
107. A. T.-a. Okamura, Y. Omi, M. Fujii, M. Tatsumi and K. Onitsuka, *Dalton Trans.*, 2015, **44**, 18090–18100.
108. Y. Hasenaka, T.-a. Okamura, M. Tatsumi, N. Inazumi and K. Onitsuka, *Dalton Trans.*, 2014, **43**, 15491–15502.
109. H. Sugimoto, S. Tatemoto, K. Suyama, H. Miyake, R. P. Mtei, S. Itoh and M. L. Kirk, *Inorg. Chem.*, 2010, **49**, 5368–5370.
110. M. P. Coughlan, in *Molybdenum and Molybdenum containing Enzymes*, ed. M. P. Coughlan, Pergamon Press, London, 1980, ch. 4, pp. 119–186.
111. N. Schrader, K. Fischer, K. Theis, R. R. Mendel, G. Schwarz and C. Kisker, *Structure*, 2003, **11**, 1251–1263.
112. U. Kappler, *Biochim. Biophys. Acta, Bioenerg.*, 2011, **1807**, 1–10.
113. R. Hille, T. Nishino and F. Bittner, *Coord. Chem. Rev.*, 2011, **255**, 1179–1205.

114. R. Hille and R. F. Anderson, *J. Biol. Chem.*, 2001, **276**, 31193–31201.
115. R. D. Cannon, *Electron Transfer Reactions*, Butterworth and Co publisher Ltd., London, 1980.
116. D. Astruc, *Electron Transfer and Radical Processes in Transition Metal Chemistry*, Willy-VCH, 1985.
117. H. Taube, *Electron-Transfer Reactions of Complex Ions in Solution*, Academic Press, New York, 1970.
118. E. C. W. M. Dixon, C. J. R. Thorne and K. F. Tipton, *Enzymes*, Longmans, Green & Co., London, and Academic Press, New York, 3rd edn, 1971.
119. T. Marshall-Roth, S. C. Liebscher, K. Rickert, N. J. Seewald, A. G. Oliver and S. N. Brown, *Chem. Commun.*, 2012, **48**, 7826–7828.
120. J. S. Olson, D. P. Ballou, G. Palmer and V. Massey, *J. Biol. Chem.*, 1974, **249**, 4363–4382.
121. *The Inorganic Chemistry of Biological Processes*, ed. M. N. Hughes, John Wiley and Sons, Chichester, 1984.
122. G. Palmer and J. S. Olson, in *Molybdenum and Molybdenum containing Enzymes*, ed. M. P. Coughlan, Pergamon Press, London, 1980, ch. 5, pp. 187–220.
123. B. M. Rosner, F. A. Rainey, R. M. Kroppenstedt and B. Schink, *FEMS Microbiol. Lett.*, 1997, **148**, 175–180.
124. J. Yadav, S. K. Das and S. Sarkar, *J. Am. Chem. Soc.*, 1997, **119**, 4315–4316.
125. P. K. Chaudhury, S. K. Das and S. Sarkar, *Biochem. J.*, 1996, **319**, 953–959.
126. K. Pal, P. K. Chaudhury and S. Sarkar, *Chem.-Asian J.*, 2007, **2**, 956–964.
127. K.-M. Sung and R. H. Holm, *J. Am. Chem. Soc.*, 2002, **124**, 4312–4320.
128. M. Czjzek, J.-P. Dos Santos, J. Pommier, G. Giordano, V. Méjean and R. Haser, *J. Mol. Biol.*, 1998, **284**, 435–447.
129. G. Moula, M. Bose and S. Sarkar, *Inorg. Chem.*, 2013, **52**, 5316–5327.
130. A. K. Rappe and W. A. Goddard, *J. Am. Chem. Soc.*, 1982, **104**, 3287–3294.

CHAPTER 4

Comparative Kinetics of Enzymes and Models

CHRISTIAN FISCHER^{*a} AND LINA FISCHER^a

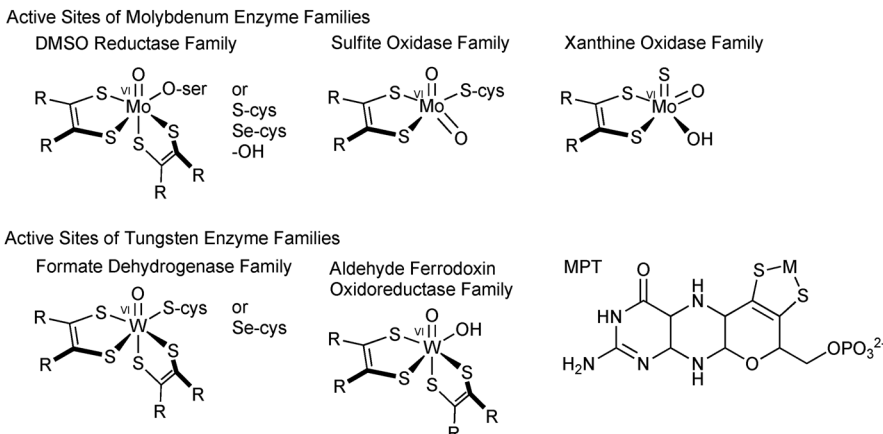
^aInstitut für Biochemie, Bioanorganische Chemie, Felix-Hausdorff-Straße 4,
17487 Greifswald, Germany

*E-mail: christian.fischer@uni-greifswald.de

4.1 Active Sites of Molybdenum and Tungsten Enzymes

All known molybdenum- and tungsten-containing enzymes catalyse reduction–oxidation reactions. The oxidation state of the metal centre can vary between IV, V and VI, hence one- and two-electron transfer reaction steps are possible. In Nature two different ways exist to control the catalytic power and the oxidation state of the metal centre of molybdenum enzymes.¹ One is a mononuclear metal centre, which consists of sulfur and oxygen atoms as coordination sphere around molybdenum and the other is the multinuclear metal centre in which the molybdenum is part of an iron–sulfur cluster, which is only known for bacterial nitroge-nase enzymes.²

In mononuclear metal centres, molybdenum is coordinated by one or two special ligands named molybdopterin (furthermore abbreviated as MPT; see



Scheme 4.1 Active sites of molybdenum and tungsten enzyme families and structure of MPT.

Scheme 4.1).[†] Later it was found that MPT binds tungsten as well. Until today chemists were not able to synthesize molybdenum or tungsten complexes with the complete MPT ligand, although some research groups are close to the target compound.⁵

By now more than 50 different enzymes containing mononuclear molybdenum centres are known.^{6–8} These enzymes can be grouped into three families based on the reactions they catalyse and the structures of their active sites⁹ (Scheme 4.1). Enzymes of the xanthine oxidase family comprise the first group with an (MPT)Mo^{VI}OS(OH) core in the oxidized state and with only one MPT ligand in the cofactor. These enzymes catalyse the hydroxylation of carbon atoms. One exception is the carbon monoxide dehydrogenase from *Oligotropha carboxidovorans*, which oxidizes CO to CO₂ and has a distinct chemical structure with a sulfide bridging molybdenum and a copper atom, which is not present in any other active site of these enzymes.¹⁰ Sulfite oxidase and some nitrate reductases are members of the second family. In the oxidized state they have an (MPT)Mo^{VI}O₂(S-Cys) core and catalyse the formal transfer of oxygen atoms. The atoms can be passed to or abstracted from a substrate. Common to the third family is the presence of two molybdopterin ligands and one oxygen atom bound to molybdenum in the oxidized form (Mo^{VI}). The sixth coordination site, X in (MPT)₂Mo^{VI}OX, can constitute a direct covalent link to the peptide *via* serinate, cysteinate, selenocysteinate or aspartate. Examples where X is an oxo ligand or possibly hydroxide/water are also known. These enzymes catalyse oxygen atom transfer (again, to or

[†]Pyranopterin ene-1,2-dithiolate is the full name for the ligand which consists of a pterin, with pyrimidine and pyrazine rings, and a pyran ring with an ene-1,2-dithiolate and a -CH₂OPO₃²⁻ group.³ The dithiolene unit binds the metal as a bidentate ligand and the phosphate group is a linker to the enzyme *via* hydrogen bonding. Dithiolene ligands as synthetic analogues simulate structural and electronic features of the active sites of the enzymes.⁴

from substrate depending on the enzyme's specificity) or dehydrogenation reactions.

Tungsten-containing enzymes can be classified into two groups according to the coordination sphere of the metal centre and the reactions the enzymes catalyse: the aldehyde oxidoreductases and the formate dehydrogenases.¹¹ Tungsten, in any case known to date, is coordinated by two MPTs. In aldehyde oxidoreductases the MPT unit is in a mononucleotide form while in enzymes of the formate dehydrogenase family a guanine monophosphate is attached to each MPT. In contrast to the first tungsten family no direct link *via* coordination of an amino acid residue to tungsten has been observed for enzymes of this family. Enzymes of the aldehyde oxidoreductase family catalyse the oxidation of aldehydes to carboxylic acids; enzymes of the formate dehydrogenases family catalyse the oxidation of formate to carbon dioxide. A third "family" consists of only one enzyme: the acetylene hydratase from *Pelobacter acetylenicus*, which catalyses the hydration of acetylene to acetaldehyde.¹²

The general approach for developing a suitable model compound is to analyze the enzyme by spectroscopic methods and ideally to obtain a crystal structure by X-ray diffraction. Based on the obtained analytical information a target compound can be designed and synthesized.¹³ Depending on the questions a researcher can either focus on structural or on functional modelling.¹⁴ Ideally, models with a structural similarity with the active sites are also active in substrate transformation. For a kinetic comparison the model compound should catalyse the same reaction as the corresponding enzyme. Enzymes are very complex systems with many "invisible" reaction steps. The benefit of using model compounds is to survey these reactions independently. Consequently single model compounds should and typically do mimic accurately just one part of the complex function of enzymes. To separate the reactions is a way to simplify the process and to accumulate information gained from several different model compounds. The strategies towards synthesizing suitable model compounds will be described later in Section 4.3.3.

Many molybdenum and tungsten complexes have been synthesized to date, mimicking oxygen, sulfur and selenium transfer reactions. Studying their kinetic characteristics can be undertaken *via* several alternative routes and procedures. These methodologies and their respective results are presented in the following parts of this chapter.

4.2 General Remarks on Michaelis–Menten Kinetics

Most enzyme kinetics and with them the corresponding catalytic cycles are characterized by the fact that there is always a rate-determining step. Prior to this step several intermediates are coupled in pre-equilibria between the enzyme and the substrates. For that reason Michaelis–Menten kinetics as a simplification of the real underlying elemental reactions were established in the early years of the last century.¹⁵ Presented in its simplest form in Scheme 4.2, this sequence and



Scheme 4.2 Reaction sequence of the simplest case of Michaelis-Menten kinetics. E=enzyme; S=substrate; ES=enzyme-substrate complex; P = product.

its kinetic derivation are of fundamental importance not only for enzyme kinetics but also for homogenous catalysis in general.[‡]

As shown in Scheme 4.2, the enzyme first reacts with the substrate to give the enzyme-substrate complex followed by a first-order step in which the product is formed and the enzyme is released to continue with the next cycle.

Most of the observed enzyme-mediated oxo-transfer reactions follow this pattern^{13,16} and some model reactions do as well. To properly compare the kinetics of enzymes with those of model catalysts it is obviously of high relevance to examine the Michaelis-Menten equation in a bit more detail.

Independent of the approximation chosen to solve the differential equations resulting from Scheme 4.2 for $d[P]/dt$ the well-known target form always is the same, see eqn (4.1) (with [P] – product concentration; [S] – substrate concentration; [E] – enzyme concentration; K_m – Michaelis-Menten constant; V_{sat} – maximum rate under saturation conditions).

$$\frac{d[P]}{dt} = \frac{V_{\text{sat}} \cdot [S]}{K_m + [S]} = \frac{k_2 \cdot [E]_0 \cdot [S]}{K_m + [S]} \quad (4.1)$$

The derivation mathematics are detailed in many publications dealing with enzyme kinetics.¹⁷⁻²³ The Michaelis-Menten constant K_m is, however, due to the individual approximation used, not always the same. The simplest values result from the implementation of the equilibrium approximation in which K_m represents the inverse equilibrium constant (eqn (4.2(a))).¹⁵ A more common method is the steady-state approach for which Briggs and Haldane assumed that a steady state would be reached in which the concentration of the intermediate was constant (eqn (4.2(b))).²⁴ The last important approach, which should be mentioned, is the assumption of an irreversible formation of the substrate complex ($k_{-1} = 0$) (eqn (4.2(c))),²⁵ which is of course very unlikely. In real enzyme reactions and even in modelled oxo-transfer reactions, this seems not to be the case.

$$(a) K_m = \frac{k_{-1}}{k_1} \quad (b) K_m = \frac{k_{-1} + k_2}{k_1} \quad (c) K_m = \frac{k_2}{k_1} \quad (4.2)$$

Beside K_m the Michaelis-Menten equation is characterized by another constant, V_{sat} , which represents the maximum rate of product formation. This

[‡]This importance becomes apparent when considering that even the derivation of much more complicated mechanisms by using the King-Altman or the Christiansen method in many cases leads to the standard form of the Michaelis-Menten equation.

characterizes a state in which all of the active sites of the enzyme are occupied by substrate and this situation is termed “saturated”. In the simplest case V_{sat} represents the rate constant for the reaction of the catalyst–substrate complex to the product multiplied by the total enzyme concentration.

Please note, these approximations are all dealing with the simple reaction sequence from Scheme 4.2. The application of e.g. the King–Altman method for multistep reactions will lead to the Michaelis–Menten equation in its typical form but with much more complex values for K_m and V_{sat} .

The typical curve resulting from applying eqn (4.1) with $K_m = V_{\text{sat}} = 1$ is shown in Figure 4.1 adapted from ref. 26.

Independent of the approximation used, the Michaelis–Menten constant has the dimension of a concentration and characterizes the substrate concentration at which the rate has reached half of its limiting value. Or in other words: half of the enzyme is in the form of the enzyme–substrate complex and the other half is in its free form. This can be carried on and results for

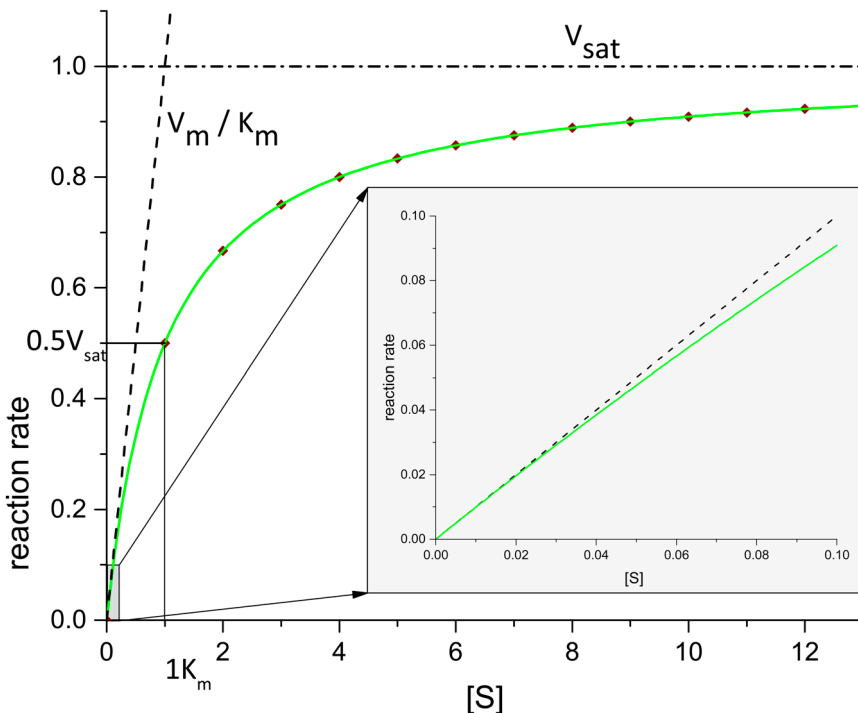


Figure 4.1 Typical Michaelis–Menten graph which shows the dependency of the reaction rate on the substrate concentration for $K_m = V_{\text{sat}} = 1$ (adapted from ref. 26). Notably, a substrate concentration equal to $1 K_m$ is the exact concentration at which the enzyme reaches half of its maximum rate ($0.5 V_{\text{sat}}$). The insertion represents a detail from the very onset of the curve and thus very low substrate concentrations. It typifies the boundary case for a first-order reaction.

instance in 83% of V_{sat} at a substrate concentration equalling $5 K_m$ and in 95% of V_{sat} at $20 K_m$. The substrate concentration $[S]$ expressed in terms of multiple units of K_m leads to eqn (4.3) exemplified for $[S] = 20 K_m$.

$$\frac{d[P]}{dt} = \frac{V_{\text{sat}} \cdot 20K_m}{K_m + 20K_m} = \frac{20}{21} V_{\text{sat}} \quad (4.3)$$

Considering Figure 4.1, which shows a declining increase of the rate with increasing substrate concentration, and also when applying eqn (4.3) it becomes clear that the velocity can never reach its limiting value no matter how much substrate is available. Even at a concentration one-hundred-fold the value of K_m the velocity is at only 99% of its theoretical maximum (V_{sat}). Still, at very large substrate concentrations or with very small Michaelis-Menten constants, the denominator of eqn (4.1) becomes mathematically almost independent of K_m . In such cases a reduced form of the Michaelis-Menten equation can be used:

$$\frac{d[P]}{dt} = V_{\text{sat}} = k_2 \cdot [E]_0 \quad (4.4)$$

The conditions given above for allowing such reduction of the equation cause the enzyme to work at its maximum activity and the reaction corresponds now to a zero-order reaction with respect to the substrate. This limiting case of eqn (4.1) is easily fulfilled by applying very high substrate concentrations. Additionally it leads to the well-known Turn-Over-Frequency (TOF), which equals k_2 in eqn (4.4) and is given in the unit of mol L⁻¹ s⁻¹. In other words, the TOF corresponds to the number of catalytic cycles per time, a fact which makes it a very appropriate value for the comparison of different enzymes. However straightforward it may seem, calculating TOF values should be done carefully and only for those cases for which the activity is definitely independent of the employed substrate concentration (see eqn (4.3) and (4.4)).

The condition for the opposite limiting case is fulfilled when very low substrate concentrations are utilized (or very large Michaelis-Menten constants observed). Here $[S]$ in eqn (4.1) becomes so small in comparison to K_m that it can be neglected in the denominator and eqn (4.1) can again be simplified (see eqn (4.5)).

$$\frac{d[P]}{dt} = V_{\text{sat}} = \frac{k_2 \cdot [E]_0}{K_m} \cdot [S] = \frac{k_2}{K_m} \cdot [E]_0 \cdot [S] \quad (4.5)$$

The Michaelis-Menten equation for these conditions has been reduced to a second-order reaction, which is first order with respect to the substrate and first order with respect to the total enzyme concentration. The quotient of k_2 and K_m now becomes a very fundamental value. It is sometimes called catalytic efficiency or specificity constant.²⁰ It can be determined from the initial

slope of the plot in Figure 4.1 as V_{sat}/K_m or from a suitably varied plot derived from this initial slope. This specificity constant makes sense in relation to the biological environment in the cell. Under physiological conditions the enzyme almost never reaches its maximum rate because the substrates are always restored and the enzymes are never saturated with the substrate. It follows that the reaction rate in these cases is not only dependent on k_2 but also on the pre-equilibrium between the free enzyme and the substrate with the substrate complex, specified by the Michaelis–Menten constant. A high reaction rate constant k_2 together with a large value for K_m may give a slower overall reaction than a moderate rate constant together with a very small K_m .

The catalytic specificity seems to be the best choice for comparing enzymes with model catalysts when the utilized substrates are the same. Unfortunately, two major drawbacks have to be emphasized. Firstly, in cases when the reaction follows zero-order kinetics (eqn (4.4)) the Michaelis–Menten constant cannot be determined. Conversely it is not easy to identify whether one is observing a real first-order reaction at the limiting case for first-order reactions or one is observing the typical Michaelis–Menten case near the boundary condition.[§] And secondly, as Eisenthal *et al.* pointed out, a higher specificity constant can lead to higher reaction rates at low substrate concentrations in contrast to slower reaction rates at high substrate concentrations, especially compared to a system with a smaller specificity constant.²⁷ This is simply caused by the fact that the specificity constant is mathematically a quotient of the two values k_2 (or V_{sat}) and K_m and the consequence becomes apparent when looking at the graphs in Figure 4.2.

4.2.1 Determination of Michaelis–Menten Parameters

Most common Michaelis–Menten analytics are associated with the typical linearization plots namely Lineweaver–Burk²⁸ (or double-reciprocal plot), Eadie–Hofstee^{28–31} and Hanes³² plots. All three have in common that they are using the experimental differential values of either product formation or substrate uptake. Very often these values cannot be determined directly and must be differentiated from the corresponding concentration–time values numerically. This can naturally cause large errors, in particular when the measured data are very noisy and/or just a very low number of data points exist. Nevertheless, the Hanes plot is the most favoured one due to its much more uniform error distribution (see eqn (4.6) with $v = d[P]/dt$).

$$\text{Hanes: } \frac{[S]}{v} = \frac{K_m}{V_{\text{sat}}} + \frac{1}{V_{\text{sat}}} \cdot [S] \quad (4.6)$$

Unfortunately, the least suitable Lineweaver–Burk (eqn (4.7)) plot is the most commonly used one despite the fact that the inventors themselves,

[§]As a reminder: both limiting cases are just assumptions leading to approximations(!). In the same way that the maximum rate in the zero-order case can never be reached as outlined above, even at very low substrate concentrations the calculated velocity from eqn (4.1) will never exactly match the specificity constant (see also the inset of Figure 4.1)!

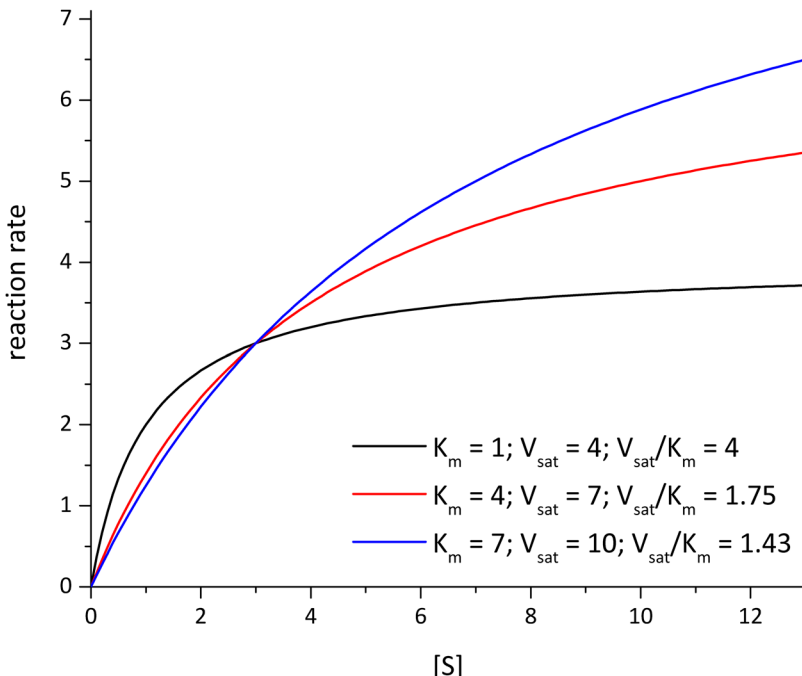


Figure 4.2 Is the catalytic specificity an appropriate value for the comparison of different enzymes? Michaelis-Menten graphs for different K_m -values with $V_{sat}(i) = K_m(i) + 3$ (the value of 3 was arbitrarily chosen) and thus different specificity constants adapted from ref. 18.

Hans Lineweaver and Dean Burk, emphasized the uncertainty of large $1/\nu$ values and suggested to apply smaller weightings for these values.²⁸ Problems arise specifically for small substrate concentrations resulting in slow reaction rates. When the reaction rates are particularly small ($\ll 1$) the reciprocal value becomes very large, as does the error of this value.

$$\text{Lineweaver-Burk: } \frac{1}{\nu} = \frac{K_m}{V_{sat}} \cdot \frac{1}{[S]} + \frac{1}{V_{sat}} \quad (4.7)$$

In general, the discussed linearization plots and others can be used to obtain initial data for a much more appropriate analysis. Determining the needed constants can be carried out by applying nonlinear regression procedures based on eqn (4.1). This can be done with the values obtained from many "initial rate" experiments but it is, notably, also possible by using the numerically differentiated values of just one experiment.

"An analysis of the product formation [or substrate consumption] is, in principle, not limited to the initial range of rates, however."²⁶ Laidler investigated the problem of the transient phase before the steady-state equilibrium is established.³³ In cases when this transition phase is a relatively short period, the pre-equilibrium is thus rapidly established and the Michaelis-Menten

equation will be obeyed with high accuracy. The most important condition to keep the transient phase short is probably $[S]_0 \gg [E]_0$ because it can be applied easily.[¶] If the total reaction was irreversible, each point in a measured concentration–time diagram would correspond to an initial rate experiment while the velocity of substrate consumption ($d[S]/dt$) is calculated numerically.^{||}

The convention in the field of chemical kinetics to use integrated rate equations whenever possible does not usually suit the field of enzyme kinetics. The main reason, obviously, lies in the complexity of biological systems. Reversible product formation, side reactions and/or inhibition phenomena are all reduced to a minimum by the “initial rate” method. Beside these advantages the major disadvantage is of course that a large number of experiments have to be performed, which is naturally very time consuming.

In the same manner that the target constants K_m and V_{sat} are calculable from just one concentration–time diagram by differentiating the values obtained as outlined above, it is also feasible to utilize the integrated Michaelis–Menten equation with the time-dependent values directly. Eqn (4.8) and its detailed integration from eqn (4.1) can be found in the literature.^{34,35}

$$\frac{1}{t} \cdot \ln \frac{[S]_0}{[S]_t} = \frac{[S]_t}{K_m \cdot t} + \frac{V_{sat}}{K_m} \quad (4.8)$$

This can be expressed in terms of the Lambert-W function.^{**} A detailed derivation has been described by Williams.³⁵

$$[S]_t = K_m \cdot W \left\{ \frac{[S]_0}{K_m} \cdot e^{\left(\frac{[S]_0 - V_{sat} \cdot t}{K_m} \right)} \right\} \quad (4.9)$$

The implementation of this equation in a commercial program like *MatLab* or *Mathematica*,^{††} which is able to perform nonlinear optimization routines to minimize the function of eqn (4.10) allows determining the numerical values for K_m and V_{sat} with comparable ease.³⁹

$$F(K_m, V_{sat}) = \sum_i ([S]_i^{obsd}(t_i) - [S]_i^{calcd}(t_i))^2 \quad (4.10)$$

[¶]Other possible conditions mentioned by Laidler are: $[E]_0 \gg [S]_0$, $k_{-1} + k_2 \gg k_1 \cdot [E]_0$, $k_{-1} + k_2 \gg k_1 \cdot [S]_0$

^{||}In some cases it is possible to obtain differential values directly. This is the case for instance when a gaseous substrate is used, then flow-meters are able to measure the current flow rate directly.²⁶

^{**}The Lambert-W function (also called omega function) is actually a set of functions of the inverse relation of the function $f(x) = xe^x$.

^{††}If the intrigued user did not have one of the programs aforementioned at his/her disposal, the free FORTRAN libraries NL2SOL³⁶ (nonlinear optimization procedure) and TOMS443 (evaluation of the Lambert-W function)^{37,38} are highly recommended. An implementation of both in a small program will provide the same results.

Remarkably, this closed-form solution is no longer dependent on the substrate concentration but it is expressed as a function of time. Again, the boundary condition $[E]_0 \ll ([S]_0 + K_m)$, which validates the steady-state approximation, has to be complied with.

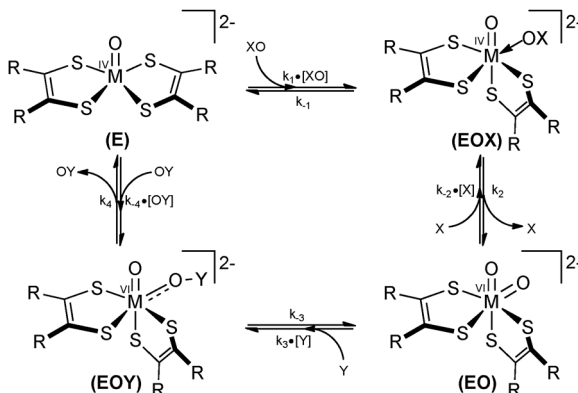
In summary both presented methods are dealing with time-dependent substrate concentration data. While the first one ("initial rate" method) uses differentiated values, the other approach uses integrated values. Both have in common that they are not suitable for analysing a reversible Michaelis-Menten mechanism. However, if the reaction conditions are obeying the conditions required for kinetic analysis *via* eqn (4.9) and (4.10), this method is highly recommended since it is most reliable and in practice very comfortable compared to the time-consuming initial rate experiments. All one has to do is to make sure that either sufficiently high substrate or enzyme/catalyst concentrations are applied.

4.2.2 Michaelis–Menten Kinetics for Oxygen Transfer Reactions – “*Quo Vadis?*”

The mathematical kinetic treatments outlined above are based on the simplest case of Michaelis–Menten enzyme kinetics. Transferred to oxygen atom transfer reactions, the simplest case only corresponds to a half-reaction of the real catalytic cycle. This becomes apparent when considering a famous catalytic oxygen atom transfer model reaction, *e.g.* the oxidation of hydrogensulfite catalysed by $[\text{Bu}_4\text{N}]_2[\text{Mo}^{\text{VI}}\text{O}_2(\text{mnt})_2]$. Das *et al.* were the first to investigate this model reaction and found that the catalyst follows a typical simple Michaelis–Menten mechanism with $k_2 = 0.87 \text{ s}^{-1}$ and $K_m = 0.01 \text{ L mol}^{-1}$.^{40,41} The re-oxidation of the now reduced form of the catalyst $[\text{Bu}_4\text{N}]_2[\text{Mo}^{\text{IV}}\text{O}(\text{mnt})_2]$ was originally realized by oxidation with $\text{K}_3[\text{Fe}(\text{CN})_6]$. As better oxidation agents for this type of molybdenum complexes *N*-oxides like Me_3NO and PyNO have been established. The respective oxidation reactions with Me_3NO for instance have been examined in a plethora of varieties predominantly by the Holm group (see also Tables 4.2 and 4.3).^{42,43} However, saturation kinetics for this re-oxidation have been confirmed very seldom for different reasons, which will be discussed later. Nevertheless, it is legitimate to presume a similar reaction sequence for this back reaction as for the forward one. The combination of both half-reactions then corresponds to the catalytic cycle presented in Scheme 4.3.

The depicted cycle starts for instance with the oxidized form of the catalyst/enzyme (EO; lower right in Scheme 4.3) from which the intermediate (EOY) is formed through coordination of the substrate (Y) to one metal bonded oxygen atom. After the reductive elimination of the product (YO) the enzyme is now in its reduced form. These two steps are in accordance with the proposed reaction cycle of sulfite oxidase.⁴⁴ The re-oxidation then takes

⁴⁰A later investigation confirmed the mechanism but determined different parameters ($k_2 = 1.02 \text{ s}^{-1}$; $K_m = 0.039 \text{ L mol}^{-1}$).⁴⁰



Scheme 4.3 Substituted enzyme mechanism transferred to oxygen atom transfer catalysis ($M = \text{Mo}, \text{W}$). In principle, this represents two coupled half-reactions with a pre-equilibrium at each half-reaction. This is the favoured mechanism due to the negative activation entropies observed for this type of reaction.

place in two steps. The first step is the formation of the intermediate by the coordination of an oxygen-bearing substrate *via* its oxygen atom to the metal centre. In a second step the reduced product (X) is eliminated and the metal is now in the oxidation state +vi. Every step in this reaction pathway is considered reversible with the special case of some back reactions in which a product is formed ($\text{EOY} \rightarrow \text{E}/\text{EOX} \rightarrow \text{EO}$). Obviously these back reactions are dependent on the amount of the product produced in the forward reaction. In enzyme kinetics this phenomenon is often called product inhibition.

The depicted mechanism is of course much more complex than the simple Michaelis–Menten scheme, but it can be simplified by employing the steady state approximation. This may be done in a relatively simple manner by applying either the King–Altman⁴⁵ method or the less well-known Christiansen formalism.^{46–48} Applying the King–Altman method to the catalytic cycle given in Scheme 4.3 leads to a rate equation that is equal to the substituted-enzyme mechanism, the detailed derivation of which was debated by Cornish-Bowden.²⁰

At the very beginning of the reaction and assuming that both substrates are of higher concentration than the total enzyme concentration, the amount of the products produced (YO, X) equals almost zero. Therefore all terms containing these products can be removed. Hence, the overall rate for these conditions is described by eqn (4.11):

$$\nu = \frac{V_+ [\text{XO}][\text{Y}]}{K_{m,\text{Y}} [\text{XO}] + K_{m,\text{XO}} [\text{Y}] + [\text{XO}][\text{Y}]} \quad (4.11)$$

with

$$V_+ = \frac{k_2 k_4 [\text{E}]_0}{k_2 + k_4} \quad K_{m,\text{XO}} = \frac{(k_{-1} + k_2) k_4}{k_1 (k_2 + k_4)} \quad K_{m,\text{Y}} = \frac{k_2 (k_{-3} + k_4)}{(k_2 + k_4) k_3} \quad (4.12)$$

where V_+ is the maximum rate, $K_{m,Y}$ is the Michaelis–Menten constant with respect to [Y], $K_{m,XO}$ is the Michaelis–Menten constant with respect to [XO]; [XO] and [Y] are the concentration of electron acceptor (oxygen donor) and electron donor (oxygen acceptor), respectively.

Now two arguable cases have to be considered. If the concentration of one of the substrates was in high excess compared to the other substrate, eqn (4.11) would be simplified again to the typical Michaelis–Menten form with respect to the other substrate(s). As an example: [XO] is present in a high excess compared to [Y], then eqn (4.11) takes on the following form.

$$v = \frac{V_+ [XO][Y]}{K_{m,Y} [XO] + [XO][Y]} = \frac{V_+ [Y]}{K_{m,Y} + [Y]} \quad (4.13)$$

$K_{m,Y}$ is the limiting overall Michaelis–Menten constant for Y when [XO] is saturating. Contrarily, $K_{m,XO}$ is the limiting constant for XO when [Y] is in high excess to [XO].

The other notable case occurs if the experiments were planned in a way that one of the substrate concentrations is constant and the other is varied throughout the experiments. This is most likely the case in experimental practice. But even then eqn (4.11) can be reformed to a typical Michaelis–Menten equation, because the substrate concentration becomes a constant itself and so do terms comprising this concentration and another constant; e.g. a Michaelis–Menten constant:

$$\underset{[XO] \rightarrow \text{const}}{v} = \frac{\frac{V_+ [XO]}{K_{m,XO} + [XO]} \cdot [Y]}{\frac{K_{m,Y} [XO]}{K_{m,XO} + [XO]} + [Y]} = \frac{V_+^{\text{app}} \cdot [Y]}{K_m^{\text{app}} + [Y]} \quad (4.14)$$

The apparent parameters V^{app} and K_m^{app} are available by a typical Michaelis–Menten evaluation. Once determined, it is in addition possible to determine the values for K_m and V_+ since the apparent parameters are themselves also of the Michaelis–Menten form depending on [XO]. For a detailed description of how to perform such analyses, see the respective publication.²⁰

To summarize, “even if a reaction actually has two [...] substrates it can be treated as a single-substrate reaction if only one substrate is varied at time”.²⁰ However, one has to be aware of the fact that the determined values are just apparent ones and that they are not uniform to the parameters derived from eqn (4.1). For the challenging task of comparing different enzymes or model catalysts the parameters V^{app} and K_m^{app} are very convenient given that the same substrate conditions are employed or that at least the same ratio of substrates is used. In conclusion the answer to the question asked in this section’s title is most likely that it’s just a “*Status quo ante*”.

About the validity of the assumed catalytic sequence in Scheme 4.3 it has to be emphasized that in some cases this mechanism has been confirmed

for real enzymes, *e.g.* purified respiratory nitrate reductase from *E. coli* with quinols as electron donor.⁴⁹ Another example was found by Buc *et al.* for the TMAO-reductase also extracted from *E. coli* with benzyl viologen as second substrate. The confirmed rate equation equals eqn (4.12) except that [Y] (= benzyl viologen) has been accounted for using its square concentration.⁵⁰ The reason is that the one-electron donor benzyl viologen is used, while from stoichiometry it follows that two electrons are required to reduce Me_3NO to Me_3N or NO_3^- to NO_2^- .⁵¹

4.3 Kinetic Aspects of Oxygen Transfer Reactions – Enzymes *vs.* Models

4.3.1 Oxygen Transfer Reactions Mediated by Enzymes

Studying the kinetics of enzymes is especially facilitated when the enzyme was isolated from the cell prior to the studies. The advantages are:

- Both substrates can be artificial and their concentrations during the catalytic cycle can be controlled without taking any transport phenomenon into the cell or other distribution limits into account;
- The concentration of the enzyme can be determined more precisely;
- Different solvents apart from the cytosol can be chosen.

The experimental setup for the enzymatic kinetic observation is detailed in the literature. Generally two methodologies are applied: in case of DMSO- and TMAO-reductase it proved beneficial to trail the change in concentration of dimethylsulfide (DMS) or trimethylamine (TMA) *via* the increase of the corresponding signal in the proton NMR (2.11 ppm for DMS; 2.88 ppm for TMA).⁵² This method is most reliable for reaction velocities within the NMR time scale and especially for large enzyme substrate ratios. In case of very fast reactions a more suitable method had been developed by employing artificial substrates which are spectroscopically active in the UV-vis range. These can be for instance reduced forms of benzyl- or methyl viologens, cytochrome *c*, ubiquinol and others.^{53–56} The biggest advantages of this method are that the substrate concentration change is obtained with minimal time intervals and a very good data-to-noise ratio even from the very beginning of the reaction (*e.g.* with a stopped-flow apparatus). It has to be mentioned at this point that due to the maximum measured absorbance should not exceed a value of 2, the total involved substrate concentration is limited by the extinction coefficient in the Bouguer–Lambert–Beer's law. As an example the extinction coefficient at 500 nm for benzyl-viologen was determined as $7800 \text{ L mol}^{-1} \text{ cm}^{-1}$. It follows that with a layer thickness of 0.1 cm the maximum concentration unfortunately is limited to $0.0025 \text{ mol L}^{-1}$!

In this context, the study by Buc *et al.* shall be specifically mentioned here as they were able to substitute molybdenum by tungsten in the TMAO-reductase of *E. coli*.⁵⁰ After purification, the isolated enzymes (wild type and

W-substituted) were successfully tested against the natural substrate Me_3NO but also against sulfoxides, among others (see Table 4.1). Benzyl viologen was used as the second, reducing substrate. Because viologens are one-electron acceptors, two molecules are needed to re-reduce the active site. Buc *et al.* were able to even prove that the mechanism, shown in Scheme 4.3, is valid for these enzyme–substrate systems. They slightly changed eqn (4.12) to eqn (4.15) taking into account that two molecules of benzyl viologen are needed. Other selected enzymatic kinetic data obtained by one of the methods introduced above are summarized in Table 4.1.

$$v = \frac{V_+ [\text{B} - \text{V}][\text{TMAO}]}{K_{m,\text{TMAO}} [\text{B} - \text{V}] + K_{0.5,\text{B}-\text{V}}^2 [\text{TMAO}] + [\text{B} - \text{V}][\text{TMAO}]} \quad (4.15)$$

Interestingly, the tungsten-substituted TMAO-reductase has an almost two-fold higher catalytic efficiency ($8.53 \times 10^6 \text{ L mol}^{-1} \text{ s}^{-1}$) than the molybdenum one ($3.75 \times 10^6 \text{ L mol}^{-1} \text{ s}^{-1}$), although the k_{cat} value was just half of the value for the molybdenum-containing enzyme ($k_{\text{cat}}^{\text{W}} = 53.6 \text{ s}^{-1}$; $k_{\text{cat}}^{\text{Mo}} = 94.7 \text{ s}^{-1}$). This is obviously caused by its much smaller Michaelis–Menten constant.

In general it is inevitable that rates of enzymes and respective model complexes are markedly different. The enzymatic catalytic activity most often exceeds the reaction rate constants of model complexes summarized in Tables 4.2 and 4.3 by several orders of magnitude. Occasionally, though, comparable values may be observed; for instance Majumdar *et al.* in mimicking nitrate reductase using molybdenum complexes with maleonitrile dithiolate (mnt) as ligand were successful in this respect.⁶⁰ The observed catalytic activity ranges from 10 to $139 \text{ L mol}^{-1} \text{ s}^{-1}$. The observed K_m values (1.4 to $4.3 \times 10^{-4} \text{ mol L}^{-1}$) were, however, surprisingly close to the natural archetype (Table 4.1). For enzymes a quite general substrate reactivity trend can be derived from the available data with $\text{Me}_3\text{NO} > \text{NO}_3^- \approx \text{SO}_3^{2-} > (\text{CH}_2)_4\text{SO} > \text{DMSO}$. This trend has also been observed for model complexes as will be discussed in the next part in more detail.

4.3.2 Studying Half-Reactions of Model Complexes

Molybdenum and tungsten complexes as models for oxygen atom transfer enzymes have been deployed in the full catalytic cycle from Scheme 4.3 predominantly in the early days of this field of research.⁶¹ A selection of the respective determined Michaelis–Menten parameters were expertly reviewed by Holm *et al.*¹⁶ Since in some cases both forms of model complexes (M^{IV} and M^{VI} mimicking the fully reduced or fully oxidized active sites, respectively) are isolable and available in a sufficient amount, the isolated half-reactions are much more often investigated than the whole catalytic cycle. This means that either the reduced form of the enzyme model is oxidized by an oxygen donor substrate like TMAO or the oxidized form is reduced by an oxygen acceptor substrate like triphenylphosphine (Ph_3P). The observed kinetic behaviour is in some cases described to be of a saturation type. An observation which

Table 4.1 Michaelis–Menten parameters K_m and k_{cat} determined for isolated enzymes for transforming different substrates. The value $K_{m,1}$ corresponds to the natural substrate (e.g. Me_3NO , Me_2SO) while $K_{m,2}$ refers to the Michaelis–Menten constant for the second substrate (see also eqn (4.11)). The quotient of $k_{cat}/K_{m,1}$ represents the catalytic specificity.^{a,b}

Isoenzyme	Reductant/ oxidant	Substrate	k_{cat}/s^{-1}	$K_{m,1}/\text{mol L}^{-1}$	$K_{m,2}/\text{mol}^{-1}$	$k_{cat}/K_{m,1}/\text{L mol}^{-1}\text{s}^{-1}$	Ref.
Nitrate reductase <i>E. coli</i> $\text{NO}_3^- + 2\text{H}^+ + 2\text{e}^- \rightleftharpoons \text{NO}_2^- + \text{H}_2\text{O}$	M-V	NO_3^-	455	4.2×10^{-4}	1.82×10^{-4}	1.08×10^6	49
	Ubiquinol		7.2	1.9×10^{-6}	7.77×10^{-5}	3.6×10^6	
	B-V		0.26	2.43×10^{-4}	5.9×10^{-5}	1.07×10^3	51
	M-V		0.118	5.71×10^{-4}	5.51×10^{-4}	2.07×10^2	
DMSO reductase <i>Rhodobacter capsulatus</i>	M-V	Me_2SO	42.9	9.7×10^{-6}		4.4×10^6	52
		Me_3NO	134.5	193.8×10^{-6}		0.69×10^{-6}	
<i>Rhodobacter sphaeroides</i>		Me_2SO	50	7×10^{-6}		7.1×10^6	57
		Me_3NO	2300	6.8×10^{-2}		3.4×10^4	
$\text{Me}_2\text{SO} + 2\text{H}^+ + 2\text{e}^- \rightleftharpoons \text{Me}_2\text{S} + \text{H}_2\text{O}$							
TMAO reductase <i>E. coli</i> $\text{Me}_3\text{NO} + 2\text{H}^+ + 2\text{e}^- \rightleftharpoons \text{Me}_3\text{N} + \text{H}_2\text{O}$	B-V	Me_3NO	Wild type	150.5	7×10^{-5}	2.15×10^6	50
			Mo-mutant	94.7	2.52×10^{-5}	3.75×10^6	
			W-mutant	53.6	6.28×10^{-6}	8.53×10^6	
			Me_2SO	40.16	9.74×10^{-4}	5.01×10^4	
Sulfite oxidase <i>Chicken liver</i> $\text{SO}_3^{2-} + \text{H}_2\text{O} \rightleftharpoons \text{SO}_4^{2-} + 2\text{H}^+ + 2\text{e}^-$	Cyto- chrome c	SO_3^{2-}	W-mutant	26.77	2.78×10^{-5}	2.74×10^4	
			$(\text{CH}_2)_4\text{SO}$	55.95	2.52×10^{-5}	2.01×10^6	
				16.6 (pH = 6)	1.02×10^{-5} (pH = 6)	2.2×10^{-6} (pH = 6)	1.63×10^6
				95.0 (pH = 8)	1.64×10^{-5} (pH = 8)	2.2×10^{-6} (pH = 8)	5.78×10^6
Arsenite oxidase <i>Variovorax</i> sp. $\text{H}_2\text{AsO}_3^- + \text{H}_2\text{O} \rightleftharpoons \text{HAsO}_4^{2-} + 3\text{H}^+ + 2\text{e}^-$	Cells	AsO_3^{3-}		96 (pH = 9.5)	1.08×10^{-4} (pH = 9.5)	5.5×10^{-6} (pH = 9.5)	0.92×10^6
					1.23×10^{-7} ^(c)	1.7×10^{-5} (pH = 9.5)	
						1.7×10^{-5} (pH = 9.5)	58
Selenate reductase <i>Enterobacter cloacae</i> $\text{SeO}_4^{2-} + 2\text{H}^+ + 2\text{e}^- \rightleftharpoons \text{SeO}_3^{2-} + \text{H}_2\text{O}$	B-V	SeO_4^{2-}			$V_{sat} = 0.2$ ^(d)	6.25×10^{-3}	59

^aM-V = methyl viologen.

^bB-V = benzyl viologen.

^c= mM $\text{AsO}_3^{3-}\text{ min}^{-1}\text{ cell}^{-1}$.

^d $\mu\text{mol SeO}_4^{2-}\text{ min}^{-1}\text{ mg}^{-1}$ (solubilized membranes).

Table 4.2 Selected second-order rate constants for different molybdenum-containing model–substrate pairs (standard conditions: CH₃CN and 298.15 K).^{a,b,c,d,e,f}

	[MoO _{x+1} (S ₂ CNEt ₂) ₂]	MoO _{x+1} (^t BuL-NS) ₂	[MoO _{x+1} (mnt) ₂] ²⁻	[MoO _{x+1} (bdt) ₂] ²⁻	[Mo(OPh) O _x (mdt) ₂] ⁻	[Mo(OR) O _x (mdt) ₂] ⁻
Substrate oxidation <i>x</i> = 1	HSO ₃ ⁻ (MeO) ₃ P Et ₃ P (EtO) ₂ MeP PPhEt ₂ PPh ₂ Et (MeO) ₂ PhP Ph ₃ P	0.53 ^(e) [86] 0.43 ^(e) [86] 0.23 ^(e) [86] 1.18 ^(e) [80]	5.6 × 10 ⁻³ ^(c) [114]	87 × 10 ⁻² ^(a,b) [41] 2.5 × 10 ⁻² ^(c) [113] 10.9 × 10 ⁻² [40] 110 × 10 ⁻² ^(c) [113] 7.84 × 10 ⁻² [40] 6.14 × 10 ⁻² [40] 0.45 ^(c) [113] 5.59 × 10 ⁻² [40]	[MoO _{x+1} (bdt) ₂] ²⁻ 0.5 × 10 ⁻⁵ [96] 2.6 × 10 ⁻³ (Ph ₃ Si-bdt) ^(c,d) [67] 2.0 × 10 ⁻³ (Ph ₃ Si-tdt) ^(c,d) [67] 5.7 × 10 ⁻³ ^(c,d) [67] 3.6 × 10 ⁻³ (tdt) ^(c,d) [67]	[Mo(OPh) O _x (mdt) ₂] ⁻ 2.0 × 10 ² [115]
Substrate reduction <i>x</i> = 0	Me ₃ NO	1.1 ^[79]	1.16 × 10 ⁻⁴ [67]			
Ph ₃ AsO		5.6 × 10 ⁻² ^(c) [114]			2.8 × 10 ⁻² [75]	R = <i>p</i> -C ₆ H ₄ Br 3.7 × 10 ⁻² [75]
(PhCH ₂) ₃ NO (CH ₂) ₄ SO		1.44 × 10 ⁻³ ^(c) [114]			0.16 × 10 ² [115]	R = <i>p</i> -C ₆ H ₄ OMe 2.4 × 10 ⁻² [75]
DMSO	1.6 × 10 ⁻⁴ [86]	0.101 × 10 ⁻³ ^(c) [114]			1.5 × 10 ⁻⁴ [110]	R = C ₆ F ₅ 0.52 × 10 ⁻² [115]
Ph ₂ SO		0.314 × 10 ⁻³ ^(c) [114]				R = SC ₆ H ₂ ⁱ Pr ₃ 0.14 × 10 ⁻² [112]
					1.3 × 10 ⁻⁶ [110]	

(continued)

Table 4.2 (*continued*)

	$[\text{MoO}_{x+1}(\text{S}_2\text{CNET}_2)_2]$	$\text{MoO}_{x+1}(^t\text{BuL-NS})_2$	$[\text{MoO}_{x+1}(\text{mnt})_2]^{2-}$	$[\text{MoO}_{x+1}(\text{bdt})_2]^{2-}$	$[\text{Mo(OPh)}_{\text{O}_x(\text{mdt})_2}]^-$	$[\text{Mo(OR)}_{\text{O}_x(\text{mdt})_2}]^-$
SeO_4^{2-}					7.2×10^{-4} [112]	$R = \text{SC}_6\text{H}_2^{\text{i}}\text{Pr}_3$ 0.32×10^{-2} [112]
Ph_2SeO^-		$2.16^{(c)}$ [114]				
NO_3^-			$V_{\text{sat}} = 4.2 \times 10^{-3}$ s^{-1}	$K_m = 4.3 \times 10^{-4}$ mol L^{-1} [f] [116]		
Ph_3AsS					29×10^{-2} [75]	$R = p\text{-C}_6\text{H}_4\text{Br}$ 52×10^{-2} [75]
Ph_3SbS					5.5×10^{-2} [75]	$R = p\text{-C}_6\text{H}_4\text{OMe}$ 26×10^{-2} [75]
						$R = p\text{-C}_6\text{H}_4\text{Me}$ 25×10^{-2} [75]

^{a)}Saturation type [s^{-1}].^{b)} H_2O : DMF.^{c)}DMF.^{d)}300 K.^{e)}1,2-C₂H₄Cl₂.^{f)}Full catalytic cycle with PPh₃ as reductant; employed complex: $[\text{Mo(SPh)(mnt)}_2]^-$.

Table 4.3 Selected second-order rate constants for different tungsten-containing model–substrate pairs (standard conditions: CH_3CN and 298.15 K).

		$[\text{WO}_{x+1}(\text{mnt})_2]^{2-}$	$\text{WO}_{x+1}(\text{bdt})_2^{2-}$	$[\text{W}(\text{OPh})\text{O}_x(\text{mdt})_2]^-$	$[\text{W}(\text{OR})\text{O}_x(\text{mdt})_2]^-$
Substrate oxidation $x = 1$	$(\text{MeO})_3\text{P}$	9.7×10^{-6} ^a [113]			
	Et_3P				
	$(\text{EtO})_2\text{MeP}$	3.4×10^{-3} ^a [113]			
	$(\text{MeO})_2\text{PhP}$	0.45×10^{-3} ^a [113]			
	Ph_3P	0.45×10^{-3} ^a [113]	1.0×10^{-5} ^a [96]		
Substrate reduction $x = 0$	AsO_2^-				
	Me_3NO		5.0×10^{-3} ^a [96]		$R = \text{iPr } 0.93$ [108]
	Ph_3AsO			3.2 [108]	$R = p\text{-C}_6\text{H}_4\text{CN } 25.2$ [75]
	PyNO				$R = p\text{-C}_6\text{H}_4\text{Br } 6.8$ [75]
	$(\text{CH}_2)_4\text{SO}$				$R = p\text{-C}_6\text{H}_4\text{OMe } 1.9$ [75]
					$R = p\text{-C}_6\text{H}_4\text{Me } 1.8$ [75]
					$R = \text{Me } 2.0$ [112]
					$R = p\text{-C}_6\text{H}_4\text{CN } 35 \times 10^{-3}$ [108]
					$R = p\text{-C}_6\text{H}_4\text{Br } 4.2 \times 10^{-3}$ [108]
	DMSO				$R = p\text{-C}_6\text{H}_4\text{OMe } 0.58 \times 10^{-3}$ [108]
	SeO_4^{2-}				$R = p\text{-C}_6\text{H}_4\text{Me } 0.62 \times 10^{-3}$ [108]
	NO_3^-				$R = p\text{-C}_6\text{H}_4\text{NH}_2 \sim 0.38 \times 10^{-3}$ [108]
	Ph_3AsS				$R = \text{iPr } \sim 0.004 \times 10^{-3}$ [108]
					$R = \text{OMe } 0.085 \times 10^{-3}$ [112]
	Ph_3SbS				$R = \text{SC}_6\text{H}_2\text{iPr}_3 \sim 0.35 \times 10^{-3}$ [112]

^a)DMF.

will be discussed later in detail. More often it follows simple pseudo first-order kinetics even at very high catalyst to substrate ratios.^{4,62,63} Plots of the observed first-order rate constants depending on the substrate concentration should give linear graphs. Thus the oxygen transfer reactions observed can be expressed by a second-order rate law (eqn (4.16)).

$$v = \frac{d[P]}{dt} = k_i \cdot [M^{IV+2n}O_{1+n}(dt)_2] \cdot [XO_{1-n}] \quad n=0,1 \quad (4.16)$$

(M = Mo, W; dt = bidentate ligand, e.g. dithiolene)

The fact that sometimes a type of saturation kinetics and sometimes pseudo first-order kinetics were observed indicates that the reaction involves two steps: (1) formation of the catalyst–substrate complex and (2) dissociation of the product from the intermediate complex with the associated formation of either the now oxidized or reduced complex form (Scheme 4.4). Actually, “The reaction between a reduced molybdenum centre and an oxygen-donating substrate has been proposed to proceed *via* a transition state where the substrate oxygen atom binds directly to the molybdenum atom”.^{64–66} It has to be considered that the initial condition $[S]_0 \gg [E]_0$ together with the circumstance that the enzyme will not be recycled but consumed are both responsible for the deviating behaviour.

The important rate equations for this system are:

$$\frac{d[ES]}{dt} = k_1 \cdot [E^i] \cdot [S] - k_{-1} \cdot [ES] - k_2 \cdot [ES] \quad (4.17)$$

$$\frac{d[P]}{dt} = \frac{d[E^{ii}]}{dt} = k_2 \cdot [ES] \quad (4.18)$$

The reaction sequence depicted in Scheme 4.4 fits both observations (second-order and saturation-type kinetics) as is evident from the following. From a kinetic viewpoint this sequence is a simple consecutive reaction with a reversible first step: once the enzyme is either reduced or oxidized and the product is released the enzyme is in a different form. Due to the absence of the second substrate it cannot re-launch into the catalytic cycle. In other words: this is not a catalytic reaction and the enzyme responds as a normal reactant!

Three possible scenarios can be derived from the reaction sequence in Scheme 4.4:

1. The consecutive reaction can be treated as a first-order reaction when $k_1[S]$ is larger than k_2 . Hence, after a short transient phase every $[E^i]$ is converted into $[ES]$ (Figure 4.3, bottom). Then step 2 becomes the rate-determining step and consequently even at very high substrate concentrations the measured first-order rate constant will be the same in



Scheme 4.4 Irreversible half-reaction.

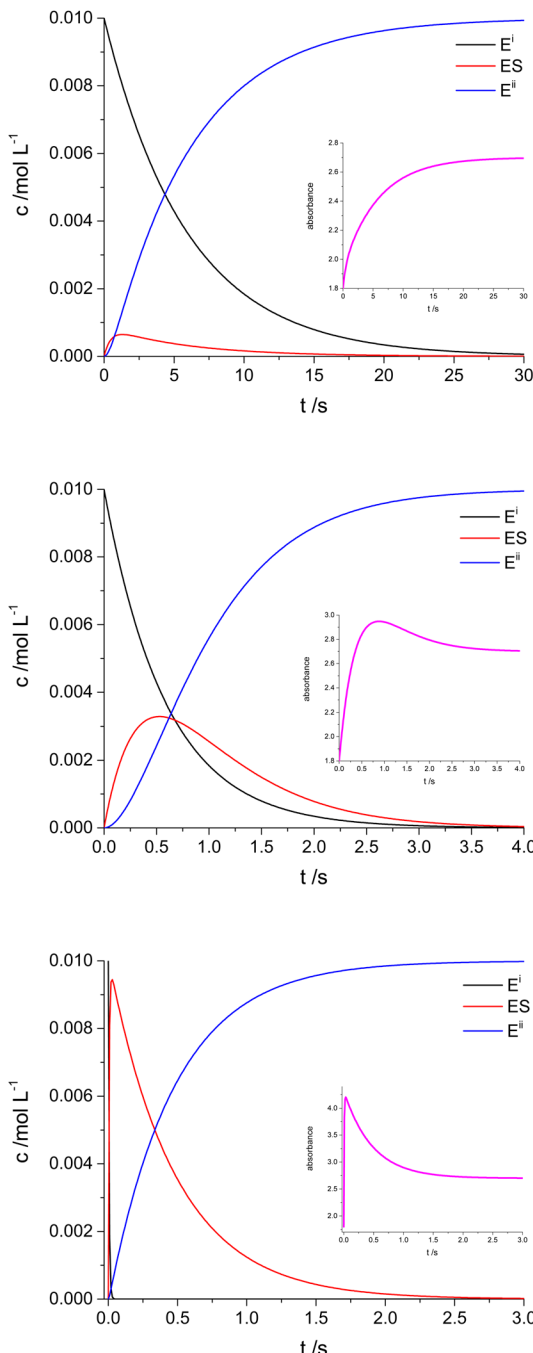


Figure 4.3 Concentration–time graphs for all three scenarios described (see also Scheme 4.4). From top to bottom [S] was raised from 10-fold to 100-fold to 10 000-fold excess compared to $[E]_0$, $[E]_0 = 0.01 \text{ mol L}^{-1}$; $k_1 = 0.017 \text{ L mol}^{-1} \text{ s}^{-1}$; $k_{-1} = 0.01 \text{ s}^{-1}$; $k_2 = 2.1 \text{ s}^{-1}$. In the inset a simulated absorption time curve was calculated from the corresponding concentrations with extinction coefficients $\varepsilon_{\lambda,E^i} = 180 \text{ L mol}^{-1} \text{ cm}^{-1}$; $\varepsilon_{\lambda,\text{ES}} = 430 \text{ L mol}^{-1} \text{ cm}^{-1}$; $\varepsilon_{\lambda,E^{\text{ii}}} = 270 \text{ L mol}^{-1} \text{ cm}^{-1}$.

any case and with no dependence on the substrate concentration at all. Instead, the reaction rate just depends on k_2 and the amount of [ES] available as can be gathered from eqn (4.18). The parameter k_2 equals the observed rate constant for the simple Michaelis–Menten case at high substrate concentrations (first boundary case).

2. When k_2 is larger than $k_1[S]$ again a first-order reaction is observed which now corresponds to the first step as the rate-limiting one. The intermediate concentration [ES] is very low and remains almost constant over a wide range of the reaction (Figure 4.3, top). Due to the nature of a second-order reaction with high excess of one reactant the observed rate is pseudo first-order in $[E^i]$ and depends on the concentration of the excess reactant. A plot of the pseudo first-order rate constant against the substrate concentration gives a straight line and from the slope the underlying second-order rate constant can be determined. As mentioned above, this is the case in many observed oxygen atom transfer reactions. Remember, if a linear dependence on the reaction rate constant $[S]$ is observed then the rate constant determined must correspond to the first step in Scheme 4.4 and also in Scheme 4.2.

If the concentration of the substrate was raised to a much higher level, then the rate of [ES] production would also increase. This would take place until the rate of the first step is again higher than that of the second one or equals it at least. Oku *et al.* actually observed exactly this behaviour with the Ph_3Si -substituted bdt-ligand while the unsubstituted ligand shows the behaviour depicted in scenario 1.⁶⁷ This leads us to scenario 3.

3. Sometimes in literature a kind of saturation kinetics is described after plotting the observed rate constant depending on the substrate concentration utilized. Examples for this behaviour with non-dithiole complex can be found in several publications^{68–72} and it is also described for bis(dithiole) molybdenum complexes.^{41,60,73} If we refer to the reaction sequence in Scheme 4.4, however, it becomes obvious what actually was observed there. We start with the assumption that k_1 is smaller than k_2 ; in the beginning at moderate substrate excesses only the first step can be observed as described in scenario 2. An increase in the substrate concentration now forces the first reaction step to become faster. As this step is the only one that depends on the substrate concentration, the rate for the second step cannot increase. If the level of $k_1[S]$ reached k_2 the reaction could no longer be treated as a first-order reaction (Figure 4.3, middle; evidence for non-first-order behaviour can be found in the inset) until of course the substrate concentration is so high that $k_1[S]$ is larger than k_2 . The latter corresponds to the remarks for scenario 1. A plot of the observed rate constants depending on the appropriate substrate concentration now leads to a curve which looks like a saturation curve with its maximum at k_2 .

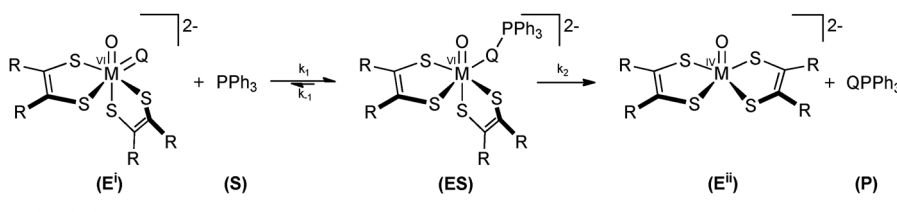
As a current example for the behaviour outlined above Sugimoto *et al.* described the transfer of sulfur and selenium atoms to triphenylphosphine derivatives.^{73,74} The proposed reaction sequence adapted from the original one is depicted in Scheme 4.5.

In the case of tungsten as central metal with a maximum 100-fold excess of the substrate a linear dependence of k_{obs} on $[\text{PPh}_3]$ was observed. Together with the information that the reaction has large negative activation entropies (in case of the sulfur transfer to $[\text{P}(p\text{-Cl-Ph})_3]$ $\Delta H^\ddagger = 25.5 \text{ kJ mol}^{-1}$ and $\Delta S^\ddagger = -138 \text{ kJ mol}^{-1}$) this confirms the proposed reaction sequence. The observed first-order kinetics then correspond to the first step of the consecutive reaction with a faster second step. A different behaviour was observed by the authors when molybdenum was employed as central metal. Contrary to the tungsten analogue all reactions exhibited a type of saturation kinetics when different concentrations of $[\text{PPh}_3]$ up to 150-fold excess were utilized. As explained above, due to the increase of the substrate the observed reaction is now shifted from the left side of the sequence with an intermediate phase in which $k_1[\text{PPh}_3]$ equals k_2 , to the right side as rate-determining step. It follows that in contrast to the tungsten complex the pre-equilibrium is more shifted to the right at the same enzyme–substrate ratio. Consequently, transferred to the catalytic cycle (one substrate is treated as constant), a smaller Michaelis–Menten constant should be observed, which means that the molybdenum-bearing model is working closer to its maximum rate than the analogous tungsten complex.

For explaining the behaviour of the observed rate constant the authors provide a functional dependency (eqn (4.19)).⁷³

$$v = \frac{k_2 \cdot [\text{PPh}_3]}{\left(\frac{k_{-1}}{k_1} + k_2 \right) + [\text{PPh}_3]} \cdot [\text{E}]_0 = k_{\text{obs}} \cdot [\text{E}]_0 \quad (4.19)$$

Thus, the observed rate constant depends on the substrate concentration and on the three fundamental rate constants. It is obviously of the same form as the Briggs–Haldane treatment for a one-substrate enzyme reaction (steady-state treatment, see also eqn (4.2b)). A detailed derivation utilized by Das *et al.* can be found in the supporting information of ref. 41. Unfortunately this function can only lead to approximated values, which is mainly caused by



$Q = \text{S, Se}; M = \text{Mo, W}$

Scheme 4.5 Half-reaction for the transfer of sulfur or selenium to PPh_3 adapted from Sugimoto *et al.*^{73,74}

two arguable assumptions: firstly, the total catalyst/enzyme concentration during the course of the reaction consists only of $[E^i]$ and $[ES]$ and secondly, the sum of $[E^i]$ and $[ES]$ remains constant. This is not true as aforementioned because the starting complex is consumed. Nevertheless, in a case when saturation type kinetics are observed and it is impossible to change reaction conditions in a way that the second step becomes rate limiting (possibly for solubility reasons) this assumption still gives sufficient values for k_2 . However, such an assumption is not valid in a case when $k_1[S]$ equals k_2 . The concentration of $[ES]$ is now not negligible anymore and it behaves like a normal reactant. Consequently, neither the steady state assumption nor the Bodenstein principle can be applied and the observed absorbance-time data cannot be equivalent to a first-order reaction (inset from Figure 4.3, middle).

An additional aspect in studying the half-reactions arises when a reaction is not treated as pseudo first order reaction. This is the case when the substrate is in approximately the same concentration as the metal complex. Caradonna *et al.* for instance studied the required treatment for such a case.⁶⁹ Due to the accumulation of the product in the course of the reaction, the back reaction is not negligible anymore. To the best of our knowledge, analyses of the back reaction have never been mentioned in the literature with respect to oxygen atom transfer reactions of model complexes and this is due to several reasons.^{63,75} Either the reaction rate is too small compared to the forward reaction so that experimental difficulties in determining the reaction rate constant emerged. Or, as was emphasized by Enemark *et al.*:⁶³ "No bis(dithiolene) molybdenum or tungsten complex was observed to reduce Ph_3PO ".^{§§}

For a future scope two proper methods for the analysis of the back reaction can be recommended. The first and easiest way is to treat the back reaction in the same way as discussed above for the normal substrate. The second possible method includes the determination of both constants (k_1 and k_{-1}) directly from the reversible second-order reaction. The wanted values to be determined can be obtained by nonlinear regression analysis of the corresponding integrated rate law.^{76–78}

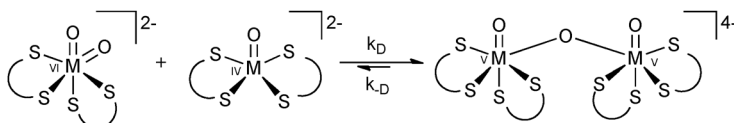
4.3.3 Selected Historical Steps in Functional Model Development

The first generation of model compounds that were able to catalyse oxygen atom transfer reactions utilize the redox couple $\text{Mo}^{\text{IV}}\text{O}/\text{Mo}^{\text{VI}}\text{O}_2$ with no coordination to a ligand that would be mimicking the coordination sphere inside the enzyme. Instead co-ligands in many examples were carbamate ($\text{S}_2\text{CNET}_2^-$), thiokanthato ($\text{S}_2\text{CS}^{\text{i}}\text{Pr}^-$) or xanthogenate ($\text{S}_2\text{CO}^{\text{i}}\text{Pr}^-$) derivatives.^{16,67,79,80} While oxygen atom transfer catalysis was observed with these metal-ligand combinations,

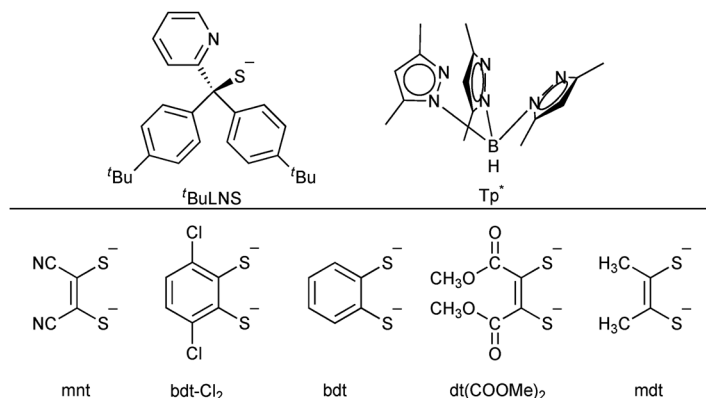
^{§§}The established facts that firstly Ph_3PO is not able to oxidize either tungsten or molybdenum complexes, and secondly that this reaction represents the back reaction of the oxidation of Ph_3P concomitantly, make this system very suitable for a comfortable kinetic analysis according to eqn (4.10) and (4.11).

a massive problem arises from an unwanted dimerization in the course of the catalytic process. This dimerization occurs when both species, $\text{Mo}^{\text{IV}}\text{O}$ and $\text{Mo}^{\text{VI}}\text{O}_2$, are simultaneously present in solution. Subsequently, a comproportionation takes place to oxidation state v together with a dimerization of two molybdate derivatives yielding $\text{O}=\text{Mo}^{\text{V}}-\text{O}-\text{Mo}^{\text{V}}=\text{O}$ species^{16,42,81,82} (see also Scheme 4.6). The formation of the dimer is a reversible reaction, which has also been examined as a single reaction for some derivatives of the ligands mentioned above.^{16,83,84} Because of this reversibility, it represents a resting state within the oxo-transfer cycle. The dimerization of an early tungsten model complex was also observed⁸⁵ but it has not been found in later model generations. In an outstanding publication the Holm group describes a kinetic treatment for the concurrent determination of the wanted reaction rate constant for the substrate oxidation step and the dissociation constant of the unwanted dimer.⁸⁶ This is of major importance because it allows determining the values directly from the obtained absorbance-time data in the UV-vis region.

In order to avoid the unwanted dimerization, steric constraints were incorporated into the used ligands. This hinders the metal centres to approach each other, so either the equilibrium is shifted to the side of the monomeric molybdenum species or the dimerization completely prevented. One of the first bulky sulfur-containing ligands that was able to successfully promote oxygen atom transfer catalysis of its molybdenum complex was developed by Berg and Holm (Scheme 4.7; ${}^{\prime}\text{BuLNS}$ = bis(4-*tert*-butylphenyl)-2-pyridylmethanethiolate).^{61,87}



Scheme 4.6 Reversible formation of a μ -oxo- Mo^{V} dimer from a Mo^{IV} and a Mo^{VI} complex.



Scheme 4.7 Sample ligands most successfully utilized for molybdenum- or tungsten-mediated oxygen atom transfer reactions.

Even though this promising ligand did still lead to dimer formation in non-polar solvents, it prevented molybdenum forming dimers in polar solvents like methanol and acetonitrile. Oxo-transfer reactions were successfully investigated in these solvents for a wide range of reducing or oxidizing substrates like Et_3P , N-, Se- and S-oxides, Ph_2SeO and Ph_3AsO .⁸⁸ Some other tridentate ligands that minimize comproportionation were developed and/or used by Holm and coworkers.^{63,88,89} Among other systems the very famous Tp^* -ligand hydrotris(3,5-dimethyl-1-pyrazolyl)borate had been utilized. With complexes bearing this ligand plus bidentate sulfur containing ligands (e.g. S_2PMe_2^- , S_2PEt_2^- , S_2PPh_2^-) the Enemark group observed a comproportionation of the two molybdenum species only in toluene and not in any other solvent investigated.⁹⁰ On the contrary, the addition of two equivalents of the Tp^* -ligand to a toluene solution containing a dimerization adduct $\text{Mo}_2\text{O}_3[\text{S}_2\text{P}(\text{OEt}_2)]_4$ leads to the disproportionation products $\text{Mo}^{\text{IV}}(\text{O})\text{Tp}^*\{\text{S}_2\text{P}(\text{OEt}_2)\}$ and $\text{Mo}^{\text{VI}}(\text{O})_2\text{Tp}^*\{\text{S}_2\text{P}(\text{OEt}_2)\}$.⁹¹ Both complexes applied for either substrate reduction with DMSO or substrate oxidation with Ph_3P under pseudo-first-order conditions are leading to complete reactions with clear isosbestic points in the UV-vis spectra obtained.⁹¹ Plots of the pseudo first-order rate constant in dependence on the substrate concentration were linear and thus corresponding to the first step of the consecutive reaction. Both complexes were also employed for a truly catalytic cycle resulting in an oxygen atom transfer reaction from DMSO to Ph_3P .^{61,92,93} It was shown that the combination of bulky ligands with first-generation sulfur ligands leads to molybdenum complexes that are able to serve as a functional model for oxo-transferases. However, these models are also quite distinct from the original active site regarding structure and geometry. Most importantly, they do not bear the coordinating and non-innocent dithiolene moiety of the natural MPT.

Thus, for a second generation of model complexes, sulfur-containing ligands bearing the dithiolene moiety were introduced into the respective model chemistry. The first easily accessible and stable ene-dithiolate used in this respect was the mnt-ligand (1,2-dicyanoethylenedithiolate^{††}) developed by Bähr and Schleitzer in 1957 (Scheme 4.7).^{94,95} Probably due to the strong electron-withdrawing effect of the nitrile-groups oxo-molybdenum complexes bearing this small ligand do not dimerize.⁴¹ Instead, molybdenum as well as tungsten complexes with this ligand proved to be very stable even in water containing solvents. In principle the mnt-ligand is the only one known that allows the redox couple $\text{Mo}^{\text{IV}}\text{O}/\text{Mo}^{\text{VI}}\text{O}_2$ to smoothly and functionally model oxygen atom transfer enzymes; in addition it includes the dithiolene moiety and, hence, represents a structural model including the first and second coordination spheres. As this ligand has been known for a long time, a huge library of respective oxygen atom transfer reactions exists (see Tables 4.2 and 4.3). Beside the standard protocol of oxidizing phosphine derivatives, complexes with this ligand also proved to be good mediating catalysts with exceptional substrates like hydrogensulfite and nitrate.

^{††}The original abbreviation comes from maleonitrile dithiolene.

The comproportionation in general and especially for bis(dithiolene) complexes is a parallel reaction in competition to the investigated oxygen atom transfer reaction but it does not depend on the substrate concentration. Thus, a great excess of the substrate accelerates the catalytic reaction and the dimerization might become negligible.^{79,96} In some cases, when not even this kinetic trick does the job, the dithiolene ligands themselves can be modified, as has been demonstrated by Oku *et al.* by adding a bulky Ph₃Si-group to the well-known ligand benzene dithiolene (bdt)^{97,98} and toluene dithiolene (tdt) (see Scheme 4.7).⁶⁷ To avoid dimerization of complexes with other dithiolene ligands, especially those bearing an aliphatic backbone, bulky co-ligands are still used. In particular Basu and Burgmayer developed ligands and complexes with dithiolenes very close to the natural molybdopterin.^{5,99,100} Catalytic reactions with such structurally very advanced models have not been investigated yet but will certainly be very interesting in particular in comparison with the “simpler” model complexes.

The complexes of the second generation of model compounds still utilize the redox couple [M^{IV}O]/[M^{VI}O₂] (M = Mo, W), which is strictly, except for arsenite oxidase, not an enzyme-analogous system. “The most significant difference between arsenite oxidase and the other proteins is the absence of any covalent linkage between protein and the molybdenum atom.”¹⁰¹ Consequently a third generation of model compounds was needed, in which the redox couple [M^{IV}]/[M^{VI}O] (M = Mo, W) is employed. These complexes generally consist of two dithiolene ligands and one additional co-ligand and they are usually synthesized from the zero-valent M(CO)₃(MeCN)₃ precursor with a nickel^{IV}bisdithiolene compound to yield M^{IV}(CO)₂(dt)₂ complexes (dt = dithiolene). The two remaining carbonyls can be substituted easily by any anionic compound, *e.g.* phenolate, thiolate or selenolate derivatives.^{102–109} For both metals (Mo and W) the combination of two 1,2-dimethyl-1,2-dithiolate ligands (mdt; see Scheme 4.7) together with a phenolate co-ligand became very famous as a suitably stable yet reactive analogue of the reduced DMSOR site (in the case of molybdenum). This species undergoes clean, but slow, oxygen atom transfer with *N*-oxides and *S*-oxides.^{4,63,107,110,111} Even with extraordinary substrates like selenate, Ph₃AsS and Ph₃SbS OAT reactions occur with moderate rate constants. Disappointingly, the molybdenum system undergoes a very fast autoredox follow-up reaction, the occurrence of which is consistent with the observed formation of [Mo^VO(mdt)₂][–] and phenol.⁷⁵ From a kinetic point of view this follow-up reaction doesn't matter because it is too fast compared to the oxygen atom transfer and can, hence, be neglected for the determination of the first rate constant for the OAT to the substrate. When appropriate sulfide containing substrates, *e.g.* Ph₃AsS, are employed the system reduces the substrate and is oxidized as expected *via* the coordination of a sulfido ligand (instead of the oxo ligand as in OAT). In a subsequent reaction again phenol is released yielding a μ-S bridged dimer

^{102–109}In earlier experiments this type of complex had been obtained by silylation of second-generation Mo^{IV} – bdt complexes.^{102–105}

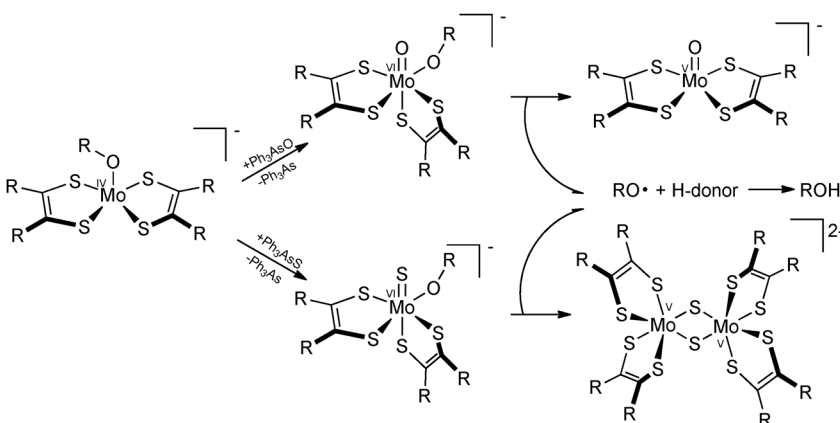
in contrast to the oxo species observed previously (Scheme 4.8). The corresponding tungsten system, however, is far more active in substrate reduction and does not exhibit the follow-up reactions observed with the molybdenum analogue. The two tungsten^{VI} species $[W^{VI}(OPh)O(mdt)_2]^-$ and $[W^{VI}(OPh)S(mdt)_2]^-$ were even prepared independently.^{75,112}

These complexes and their reduced forms are highly sensitive to water giving $W^{IV}O$ or $W^{VI}O_2$ complexes. The rates of such hydrolyses of $[W^{VI}(OPh)(mdt)_2]^-$ and $[W^{VI}(O^{\prime}Pr)(mdt)_2]^-$ were determined by Sung *et al.*¹⁰⁸ Hydrolysis of the first complex followed the saturation type kinetics aforementioned and therefore the application of eqn (4.19) led to values of $7.8 \times 10^{-4} \text{ s}^{-1}$ for k_2 and 4.5 mol L^{-1} for the quotient in the denominator ($K = (k_{-1} + k_2)/k_1$). Interestingly, the hydrolysis reaction with heavy water was determined to be almost one-third slower than with normal water ($k_2 = 2.5 \times 10^{-4} \text{ s}^{-1}$; $K = 8.4 \text{ mol L}^{-1}$).

Tables 4.1 and 4.2 summarize selected rate constants with dependence on the catalyst and the substrates. To keep the tables manageable we restricted the data to standard conditions. That means all data refer to acetonitrile as solvent and room temperature if not indicated otherwise.

Considering the literature available kinetic data summarized in Tables 4.2 and 4.3 the following conclusions can be drawn:

1. *Reactivity ratios* – In every comparable case published the rate constant for substrate reduction is significantly higher for the tungsten complex: $k_W \gg k_{Mo}$. For substrate oxidation the opposite is true: $k_W \ll k_{Mo}$. Thus, under the same conditions (parity of structure and ligation) oxo/sulfido transfer from substrate to metal ($M^{IV} \rightarrow M^{VI}O$) is faster with tungsten and the transfer from metal to substrate ($M^{VI}O \rightarrow M^{IV}$) is faster with



Scheme 4.8 Follow-up reactions of $[Mo(OR)(mdt)_2]^-$ after oxidation by either Ph_3AsO or Ph_3AsS . Adapted with permission from J.-J. Wang, O. P. Kryatova, E. V. Rybak-Akimova, R. H. Holm, *Inorg. Chem.*, 2004, **43**, 8092–8101. Copyright 2004 American Chemical Society.

molybdenum.⁷⁵ Consequently, Wang *et al.* were able to prove that an oxygen atom transfer takes place from $[\text{MoO}_2(\text{bdt})_2]^{2-}$ to $[\text{WO}(\text{bdt})]^{2-}$ and to $[\text{W}(\text{OPh})(\text{mdt})_2]^-$.⁷⁵

2. *Substrate reactivity trends* – The faster sulfido transfer to the metal in comparison to the oxo-transfer is obvious and appears to be general. Within the oxygen atom transfer series a substrate trend from Me_3NO to PH_3PO can be derived in accordance with work by the Holm group.^{4,63,75,98,107,108,112} Especially the difference between *N*-oxides (fast) and *S*-oxides (slow) is clearly evident. Holm and coworkers established the following reactivity trend:



but pointed out at the same time that “identifying a [...] trend is much easier than explaining it”. Efforts to explain the observed trends are starting with the dissociation energies of the substrates¹⁰⁸ but also proton affinities and solution basicity constants are taken into account. As the dissociation energies decrease from Ph_3PO to Me_3NO it would be expected that the respective reaction rate constants increase for the substrates' reduction. This is obviously not the case. Hence, the substrate X–O bond weakening cannot be the dominating feature of the transition state, while the available experimental thermodynamic pK_a -values fit the series above.^{63,108}

3. *Ligand effects (electron donating versus electron withdrawing ligands)* – Ligands containing strongly electron withdrawing functional groups like the nitriles in *mnt* or aromatic molecules like *bdt* weaken the metal dithiolene–sulfur bond, which on the other hand promotes strengthening of the metal oxo bond. While this electronic tuning stabilizes the monomeric species it also decreases the catalytic activity compared to electron-donating ligands. Normally, ligands bearing aliphatic backbones belong to the opposite type, which rather pushes electron density towards the metal centre (*e.g.* *mdt*, $\text{S}_2\text{CNET}_2^-$, $\text{S}_2\text{CPET}_2^-$). Their substituents/backbones provide more electron density for the coordinating sulfur atoms and by that decrease the Lewis acidity of molybdenum. It was shown previously by IR spectroscopy that the Mo=O bond is weakened by an aliphatic character of the dithiolene ligand.^{97,118,119}

Notably, the determined second-order rate constants summarized in Tables 4.2 and 4.3 can be used to simulate a simple catalytic cycle with two substrates, which will be exemplified in detail in the next section.

4.3.4 Half-Reaction Kinetics Applied to a Two-Substrate Catalytic Cycle – A Simulation

Laidler's investigations into the transition state and the quasi steady-state approximation refer not only to the simple Michaelis–Menten case but also to two-substrate systems.³³ In principle a similar type of transition state

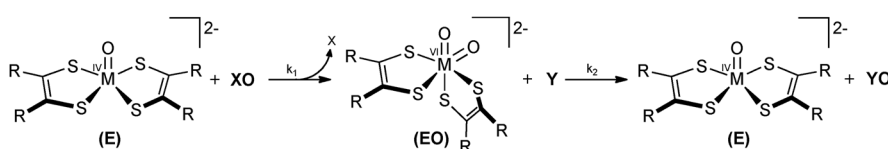
analysis to the simple one-substrate case can be applied. For this system the reaction sequence in Scheme 4.2 is rearranged in a way that after the pre-equilibrium an intermediate catalyst is obtained which then reacts with the second substrate to release the catalyst and the final product. In this sequence a second pre-equilibrium is not established and thus no ternary complex is formed (Scheme 4.9).

The depicted reaction sequence equals the ping-pong mechanism due to the release of actually two products (X and YO). For the dissimilatory nitrate reductase from *E. coli* using ubiquinol as electron donor the ping-pong mechanism was validated in a natural system.⁴⁹ Additional support for the validity of the sequence comes from Majumdar *et al.*, who also proposed this type of mechanism for a synthetic catalytic cycle with $[\text{Mo}^{\text{IV}}(\text{SR})(\text{mnt})_2]^-$ ($\text{R} = \text{C}_2\text{H}_5$; CH_2Ph ; Ph) as catalyst and NO_3^- and PPh_3 as substrates.⁶⁰ A sample concentration–time diagram, which was obtained by the numerical solution of the corresponding system of differential equations for the reaction sequence in Scheme 4.9, is presented in Figure 4.4. For the initial values entered into the simulation we decided to use $0.0559 \text{ L mol}^{-1} \text{ s}^{-1}$ for k_1 and $0.028 \text{ L mol}^{-1} \text{ s}^{-1}$ for k_2 with a total catalyst concentration of 0.01 mol L^{-1} and an excess of both substrates. To be as close to experimental values as possible the value for k_1 was taken from Lorber *et al.* ($[\text{MoO}_2(\text{mnt})_2]^{2-} + \text{PPh}_3$) while k_2 was taken from Wang *et al.* ($[\text{Mo}(\text{OPh})(\text{mdt})_2]^- + \text{Ph}_3\text{AsO}$). Reaction enthalpies ($\text{Ph}_3\text{AsO}/\text{Ph}_3\text{As} > \approx -147 \text{ kJ mol}^{-1}$ and $\text{Ph}_3\text{PO}/\text{Ph}_3\text{P} = -281 \text{ kJ mol}^{-1}$) indicate that the reaction must proceed in the given direction from a thermodynamic point of view.¹⁶

The steady-state equation for $[\text{EO}]$ as the intermediate species is valid in case any of the conditions hold as aforementioned for the simple cases. Again, after a short transition phase, steady-state conditions can be expected to exist over a long period of the reaction. Thus the change in concentration of (EO) is treated as zero (eqn (4.20)).

$$\frac{d[\text{EO}]}{dt} = k_1 ([\text{E}]_0 - [\text{EO}]) ([\text{XO}] - [\text{EO}]) - k_2 [\text{Y}] [\text{ES}] = 0 \quad (4.20)$$

“The steady-state assumption will, however, lead to error in the early stages of reaction, when the concentration of [catalyst–substrate] complex is building up, but if this occurs during the very early stages of the reaction the error will not be considerable over the main course of reaction.”³³ Thus, eqn (4.20) can be integrated when $[\text{XO}]$ and $[\text{Y}]$ are treated as constant. The result is



Scheme 4.9 Ping-pong mechanism composed of two simple half-reactions. It is of special peculiarity that the second step is formal of second order and will reduce to a pseudo first-order at high excess of $[\text{Y}]!$

a kinetic expression for the behaviour of the reaction during the transition state until the maximum concentration of the complex [EO] for the chosen conditions is reached. Given that the two substrates are in great excess of the enzyme the concentration of [EO] in dependence on time is satisfactorily expressed as:

$$[\text{EO}] = \frac{k_1 [\text{XO}]_0}{k_1 [\text{XO}]_0 + k_2 [\text{Y}]_0} \cdot [\text{E}]_0 \cdot \left[1 - e^{-t(k_1 [\text{XO}]_0 + k_2 [\text{Y}]_0)} \right] \quad (4.21)$$

In accordance with Laidler it follows from this expression that for large values of t the exponential term approaches $e^{-\infty}$, which is almost zero. Thus, the remaining term responds to the amount of intermediate [EO] available during the steady-state phase. It becomes apparent that the ratios of substrates together with the ratio of rate constants are responsible for the percentage of [EO] proportional to the total enzyme concentration deployed. Due to the fact that the maximum product rate can only be reached when [EO] equals $[\text{E}]_0$ it can happen that a reaction system with $k_2 \gg k_1$ has a slower overall rate than the opposite case. However, the rate of product formation (or the equal rate of substrate consumption) for this system is now defined as:

$$\frac{d[\text{YO}]}{dt} = k_2 \cdot [\text{Y}] \cdot [\text{EO}] = \frac{k_2 [\text{Y}] \cdot k_1 [\text{XO}] \cdot [\text{E}]_0}{k_1 [\text{XO}] + k_2 [\text{Y}]} \quad (4.22)$$

If one substrate was in great excess compared to the other and to the enzyme concentration, the corresponding term could be treated as being constant. Thus, the typical Michaelis–Menten type equation results in both cases. See eqn (4.23), left, for the case when [XO] is in excess and the right equation for an excess concentration of [Y].

$$\frac{d[\text{YO}]}{dt} = \frac{\overbrace{k_1 [\text{XO}] [\text{E}]_0 \cdot [\text{Y}]}^{V_{\text{sat}}} \cdot [\text{Y}]}{\underbrace{k_1 [\text{XO}] + [\text{Y}]}_{K_m}} \quad \frac{d[\text{YO}]}{dt} = \frac{\overbrace{k_2 [\text{Y}] [\text{E}]_0 \cdot [\text{XO}]}^{V_{\text{sat}}} \cdot [\text{XO}]}{\underbrace{k_2 [\text{Y}] + [\text{XO}]}_{K_m}} \quad (4.23)$$

Both scenarios are exemplified in Figure 4.4; red for an excess of [XO]; blue for an excess of [Y]. Both dotted concentration–time graphs were calculated by applying the corresponding system of differential equations. The continuous lines were obtained by analysing the time-dependent product formation using eqn (4.9) (with $[P] = [\text{S}]_0 - [\text{S}]_t$) and (4.10). These values match extraordinarily well to those calculated from k_1 , k_2 , [XO], [Y] and $[\text{E}]_0$ with eqn (4.23). Given $[\text{XO}] = 10 \text{ mol L}^{-1}$ for example then V_{sat} would be $0.0059 \text{ mol L}^{-1} \text{ s}^{-1}$ and $K_m = 19.1688 \text{ mol L}^{-1}$. Hence, the steady-state treatment for the ping-pong mechanism in Scheme 4.9 is validated.

Thus, the analytical solution of the Michaelis–Menten equation (eqn (4.9) and (4.10)) together with one of the cases in eqn (4.23) presents a possibility to even kinetically evaluate coupled half-reactions accurately. Since the

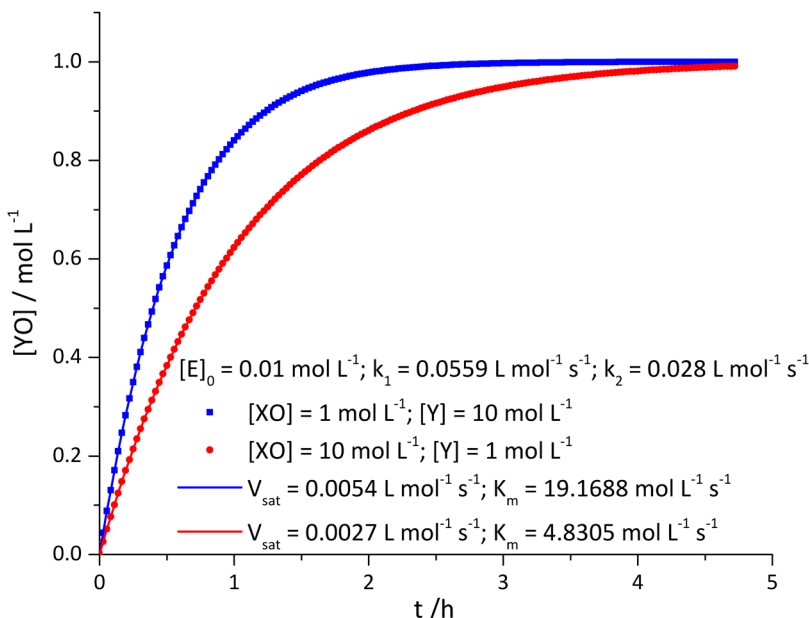


Figure 4.4 Formation of product $[YO]$ depending on time by a simple ping-pong mechanism composed of two half-reactions with $k_1 = 0.0559 \text{ L mol}^{-1} \text{ s}^{-1}$ and $k_2 = 0.028 \text{ L mol}^{-1} \text{ s}^{-1}$. The dotted values were calculated numerically from the differential equations, while the solid line curve was fitted by applying eqn (4.23) together with eqn (4.10) and (4.11).

observation of the half-reactions in the best case gave experimentally accessible second-order rate constants the expected product formation or substrate consumption can now be calculated from two half-reaction rate constants.

4.4 Dedication and Acknowledgements

It is a privilege especially for us as “newbies” in the field of molybdenum and tungsten enzymes to be co-authors of this book alongside so many great scientists and personalities. For the opportunity to contribute to this monograph we would really like to thank Profs Carola Schulzke, Martin L. Kirk and Russ Hille. Carola, our mentor, actually introduced us to this wonderful field of science.

It is also a pleasure to dedicate this chapter to Profs Richard H. Holm, John H. Enemark and C. David Garner. Their contributions to the kinetics of the enzymes and models discussed are of enormous importance considering the following quotation from Halpern: “Kinetic measurements are essential for the elucidation of any catalytic mechanism since catalysis, by definition and significance, is purely a kinetic phenomenon.”¹²⁰ Although enzymes are the natural powerful originals of our artificial catalysts they are still catalysts and consequently the kinetic observation must

play a major role in understanding enzymes. Kinetic observations require meticulousness, engagement and perseverance. All these characteristics are united in the persons of Profs Holm and Enemark. Together with the fundamental success in the synthesis of MPT-derivatives by Prof. Garner these three shaped our modern understanding of molybdenum and tungsten enzymes.

References

1. G. Schwarz, R. R. Mendel and M. W. Ribbe, *Nature*, 2009, **460**, 839.
2. J. B. Howard and D. C. Rees, *Chem. Rev.*, 1996, **96**, 2965.
3. J. M. Tunney, J. McMaster and C. D. Garner, in *Comprehensive Coordination Chemistry II*, ed. J. A. McCleverty, T. J. Meyer, L. Que Junior and W. B. Tolman, 2004, vol. 8, p. 460.
4. R. H. Holm, E. I. Solomon, A. Majumdar and A. Tenderholt, *Coord. Chem. Rev.*, 2011, **255**, 993.
5. P. Basu and S. J. N. Burgmayer, *Coord. Chem. Rev.*, 2011, **255**, 1016.
6. R. Hille, *Arch. Biochem. Biophys.*, 2005, **433**, 107.
7. C. Feng, G. Tollin and J. H. Enemark, *Biochim. Biophys. Acta*, 2007, **1774**, 527.
8. R. A. Rothery, G. J. Workun and J. H. Weiner, *Biochim. Biophys. Acta*, 2008, **1778**, 1897.
9. R. Hille, *Chem. Rev.*, 1996, **96**, 2757.
10. M. J. Romao, M. Archer, I. Moura, J. J. G. Moura, J. LeGall, R. Engh, M. Schneider, P. Hof and R. Huber, *Science*, 1995, **270**, 1170.
11. L. E. Bevers, P.-L. Hagedoorn and W. R. Hagen, *Coord. Chem. Rev.*, 2009, **253**, 269.
12. B. Rosner and B. Schink, *J. Bacteriol.*, 1995, **177**, 5767.
13. R. H. Holm, *Coord. Chem. Rev.*, 1990, **100**, 183.
14. J. A. Ibers and R. H. Holm, *Science*, 1980, **209**, 223.
15. L. Michaelis and M. L. Menten, *Biochem. Z.*, 1913, **49**, 333.
16. R. H. Holm, *Chem. Rev.*, 1987, **87**, 1401.
17. H. Bisswanger, *Enzymkinetik*, VCH Verlagsgesellschaft mbH, Weinheim, 1994.
18. R. A. Copeland, *Enzymes- A Practical Introduction To Structure, Mechanism, and Data Analysis*, VCH Publishers, Inc., New York, 1996.
19. A. Cornish-Bowden, *Principles of Enzyme Kinetics*, Butterworth & Co. Ltd., London, Weinheim, 1976.
20. A. Cornish-Bowden, *Fundamentals of Enzyme Kinetics*, 4th edn, Wiley-Blackwell, 2012.
21. H. J. Fromm, *Initial Rate Enzyme Kinetics*, Springer, Berlin, 1975.
22. A. G. Marongoni, *Enzyme Kinetics – A Modern Approach*, Wiley-Interscience, New York, 2003.
23. I. J. Segel, *Enzyme Kinetics*, Wiley & Sons, New York, 1975.
24. G. E. Briggs and J. B. S. Haldane, *Biochem. J.*, 1925, **19**, 338.
25. D. D. Van Slyke and G. E. Cullen, *J. Biol. Chem.*, 1914, **19**, 141.

26. H.-J. Drexler, A. Preetz, T. Schmidt and D. Heller, in *Handbook of Homogeneous Hydrogenations*, ed. J. G. de Vries and C. J. Elsevier, Wiley-VCH Verlag GmbH & Co. KGaA, Weinheim, Germany, 2007, vol. 1, p. 257.
27. R. Eisenthal, M. J. Danson and D. W. Hough, *Trends Biotechnol.*, 2007, **25**, 247.
28. H. Lineweaver and D. Burk, *J. Am. Chem. Soc.*, 1934, **56**, 658.
29. G. S. Eadie, *J. Biol. Chem.*, 1942, **199**, 85.
30. B. H. J. Hofstee, *J. Biol. Chem.*, 1952, **199**, 357.
31. B. H. J. Hofstee, *Nature*, 1959, **184**, 1296.
32. C. S. Hanes, *Biochem. J.*, 1932, **26**, 1406.
33. K. J. Laidler, *Can. J. Chem.*, 1955, **33**, 1614.
34. S. Schnell and C. Mendoza, *J. Theor. Biol.*, 1997, **187**, 207.
35. B. W. Williams, *J. Chem. Educ.*, 2010, **87**, 647.
36. J. E. Dennis, D. M. Gay and R. E. Welsch, *Commun. ACM*, 1981, **7**, 369.
37. F. N. Fritsch, R. E. Shafer and W. P. Crowley, *Commun. ACM*, 1973, **16**, 123.
38. A. Barry, S. J. Barry and P. Culligan-Hensley, *ACM. Trans. Math. Softw.*, 1995, **21**, 172.
39. M. Goličnik, *J. Enzyme Inhib. Med. Chem.*, 2013, **28**, 879.
40. C. Lorber, M. R. Plutino, L. I. Elding and E. Nordlander, *J. Chem. Soc., Dalton Trans.*, 1997, 3997.
41. S. K. Das, P. K. Chaudhury, D. Biswas and S. Sarkar, *J. Am. Chem. Soc.*, 1994, **116**, 9061.
42. R. H. Holm, *Coord. Chem. Rev.*, 1990, **100**, 183.
43. R. H. Holm, P. Kennepohl and E. I. Solomon, *Chem. Rev.*, 1996, **96**, 2239.
44. A. Majumdar and S. Sarkar, *Coord. Chem. Rev.*, 2011, **255**, 1039.
45. E. L. King and C. Altman, *J. Phys. Chem.*, 1956, **60**, 1375.
46. J. A. Christiansen, *Z. Phys. Chem. Bodenstein Festband*, 1931, 69.
47. J. A. Christiansen, *J. Phys. Chem.*, 1935, **28**, 303.
48. F. G. Helfferich, *Kinetics of Homogeneous Multistep Reactions, Comprehensive Chemical Kinetics*, Elsevier, Amsterdam, 2001.
49. F. F. Morpeth and D. H. Boxer, *Biochemistry*, 1985, **24**, 40.
50. J. Buc, C. L. Santini, R. Giordani, M. Czjzek, L. F. Wu and G. Giordano, *Mol. Microbiol.*, 1999, **32**, 159.
51. J. Buc, C. L. Santini, F. Blasco, R. Giordani, M. L. Cárdenas, M. Chippaux, A. Cornish-Bowden and G. Giordano, *Eur. J. Biochem.*, 1995, **234**, 766.
52. J. P. Ridge, K. F. Aguey-Zinsou, P. V. Bernhardt, I. M. Brereton, G. R. Hanson and A. G. McEwan, *Biochemistry*, 2002, **41**, 15762.
53. B. Adams, A. T. Smith, S. Bailey, A. G. McEwan and R. C. Bray, *Biochemistry*, 1999, **38**, 8501.
54. M. S. Brody and R. Hille, *Biochemistry*, 1999, **38**, 6668.
55. A. Craske and J. Ferguson, *Eur. J. Biochem.*, 1986, **158**, 429.
56. C. Iobbi-Nivol, J. Pommier, J. Simala-Grant, V. Méjean and G. Giordano, *Biochim. Biophys. Acta*, 1996, **1294**, 77.

57. K. E. Johnson and K. V. Rajagopalan, *J. Biol. Chem.*, 2001, **276**, 13178.
58. M. M. Bahar, M. Megharaj and R. Naidu, *J. Hazard. Mater.*, 2013, **262**, 997.
59. C. A. Watts, H. Ridley, K. L. Condie, J. T. Leaver, D. J. Richardson and C. S. Butler, *FEMS Microbiol. Lett.*, 2003, **228**, 273.
60. A. Majumdar, K. Pal and S. Sarkar, *Inorg. Chem.*, 2008, **47**, 3393.
61. J. M. Berg and R. H. Holm, *J. Am. Chem. Soc.*, 1985, **107**, 925.
62. J. H. Enemark and J. A. Cooney, in *Model Complexes for Molybdenum- and Tungsten- Containing Enzymes*, eds. H.-B. Kraatz and N. Metzler-Nolte, Wiley-VCH, Weinheim, 2006, p. 237.
63. J. H. Enemark, J. J. A. Cooney, J.-J. Wang and R. H. Holm, *Chem. Rev.*, 2004, **104**, 1175.
64. A. Thapper, R. J. Deeth and E. Nordlander, *Inorg. Chem.*, 2002, **41**, 6695.
65. H. Schindelin, C. Kisker, J. Hilton, K. V. Rajagopalan and D. C. Rees, *Science*, 1996, **272**, 1615.
66. S. D. Garton, J. Hilton, H. Oku, B. R. Crouse, K. V. Rajagopalan and M. K. Johnson, *J. Am. Chem. Soc.*, 1997, **119**, 12906.
67. H. Oku, N. Ueyama, M. Kondo and A. Nakamura, *Inorg. Chem.*, 1994, **33**, 209.
68. J. M. Berg and R. H. Holm, *J. Am. Chem. Soc.*, 1985, **107**, 917.
69. J. P. Caradonna, P. R. Reddy and R. H. Holm, *J. Am. Chem. Soc.*, 1988, **110**, 2139.
70. J. A. Craig and R. H. Holm, *J. Am. Chem. Soc.*, 1989, **111**, 2111.
71. S. Bhattacharjee and R. Bhattacharyya, *J. Chem. Soc., Dalton Trans.*, 1993, 1151.
72. D. M. Baird, C. Aburri, L. S. Barron and S. A. Rodriguez, *Inorg. Chim. Acta*, 1995, **237**, 117.
73. H. Sugimoto, S. Tatemoto, K. Toyota, K. Ashikari, M. Kubo, T. Ogura and S. Itoh, *Chem. Commun.*, 2013, **49**, 4358.
74. H. Sugimoto, K. Hatakeyama, K. Toyota, S. Tatemoto, M. Kubo, T. Ogura and S. Itoh, *Dalton Trans.*, 2013, **42**, 3059.
75. J.-J. Wang, O. P. Kryatova, E. V. Rybak-Akimova and R. H. Holm, *Inorg. Chem.*, 2004, **43**, 8092.
76. K. A. Connors, *Chemical Kinetics. The Study of Reaction Rates in Solution*, VCH Verlagsgesellschaft mbH, Weinheim, 1990.
77. C. Fischer, R. Thede, H.-J. Drexler, A. König, W. Baumann and D. Heller, *Chem.-Eur. J.*, 2012, **18**, 11920.
78. J. Polster, *Reaktionskinetische Auswertung Spektroskopischer Messdaten*, Vieweg, Braunschweig/Wiesbaden, 1995.
79. R. Durant, C. D. Garner, M. R. Hyde and F. E. Mabbs, *J. Chem. Soc., Dalton Trans.*, 1977, 955.
80. H. H. Huang, W. Huang, H. X. Yang, P. L. Gao and D. G. Han, *Polyhedron*, 1997, **16**, 2163.
81. J. H. Enemark and C. G. Young, in *Advances in inorganic chemistry*, Elsevier Academic Press, Amsterdam, 1994, vol. 40, p. 1.

82. J. A. Craig, E. W. Harlan, B. S. Snyder, M. A. Whitener and R. H. Holm, *Inorg. Chem.*, 1989, **28**, 2082.
83. T. Matsuda, K. Tanaka and T. Tanaka, *Inorg. Chem.*, 1979, **18**, 454.
84. S. Miyake, K. Tanaka and T. Tanaka, *J. Chem. Soc., Dalton Trans.*, 1981, 292.
85. S. Yu and R. H. Holm, *Inorg. Chem.*, 1989, **28**, 4385.
86. M. S. Reynolds, J. M. Berg and R. H. Holm, *Inorg. Chem.*, 1984, **23**, 3057.
87. P. D. Smith, A. J. Millar, C. G. Young, A. Ghosh and P. Basu, *J. Am. Chem. Soc.*, 2000, **122**, 9298.
88. B. E. Schultz, S. F. Gheller, M. C. Muetterties, M. J. Scott and R. H. Holm, *J. Am. Chem. Soc.*, 1993, **115**, 2714.
89. S. F. Gheller, B. E. Schultz, M. J. Scott and R. H. Holm, *J. Am. Chem. Soc.*, 1992, **114**, 6934.
90. S. A. Roberts, C. G. Young, C. A. Kipke, W. E. J. Cleland, K. Yamanouchi, M. D. Carducci and J. H. Enemark, *Inorg. Chem.*, 1990, **29**, 3650.
91. S. A. Roberts, C. G. Young, W. E. Cleland, J. R. B. Ortega and J. E. Enemark, *Inorg. Chem.*, 1988, **27**, 3044.
92. R. H. Holm and J. M. Berg, *Acc. Chem. Res.*, 1986, **19**, 363.
93. E. W. Harlan, J. M. Berg and R. H. Holm, *J. Am. Chem. Soc.*, 1986, **108**, 6992.
94. G. Bähr and G. Schleitzer, *Chem. Ber.*, 1955, **88**, 1771.
95. G. Bähr and G. Schleitzer, *Chem. Ber.*, 1957, **90**, 438.
96. N. Ueyama, H. Oku and A. Nakamura, *J. Am. Chem. Soc.*, 1992, **114**, 7310.
97. H. Sugimoto, M. Harihara, M. Shiro, K. Sugimoto, K. Tanaka, H. Miyake and H. Tsukube, *Inorg. Chem.*, 2005, **44**, 6386.
98. N. Ueyama, H. Oku, M. Kondo, T. Okamura, N. Yoshinaga and A. Nakamura, *Inorg. Chem.*, 1996, **35**, 643.
99. B. R. Williams, D. Gisewhite, A. Kalinsky, A. Esmail and S. J. N. Burgmayer, *Inorg. Chem.*, 2015, **54**, 8214.
100. B. R. Williams, Y. Fu, G. P. A. Yap and S. J. N. Burgmayer, *J. Am. Chem. Soc.*, 2012, **134**, 19584.
101. P. J. Ellis, T. Conrads, R. Hille and P. Kuhn, *Structure*, 2001, **9**, 125.
102. C. Lorber, J. P. Donahue, C. A. Goddard, E. Nordlander and R. H. Holm, *J. Am. Chem. Soc.*, 1998, **120**, 8102.
103. K. B. Musgrave, J. P. Donahue, C. Lorber, R. H. Holm, B. Hedman and K. O. Hodgson, *J. Am. Chem. Soc.*, 1999, **121**, 10297.
104. J. P. Donahue, C. R. Goldsmith, U. Nadiminti and R. H. Holm, *J. Am. Chem. Soc.*, 1998, **120**, 12869.
105. J. P. Donahue, C. Lorber, E. Nordlander and R. H. Holm, *J. Am. Chem. Soc.*, 1998, **120**, 3259.
106. B. S. Lim, P. Donahue and R. H. Holm, *Inorg. Chem.*, 2000, **39**, 263.
107. B. S. Lim and R. H. Holm, *J. Am. Chem. Soc.*, 2001, **123**, 1920.
108. K. M. Sung and R. H. Holm, *J. Am. Chem. Soc.*, 2001, **123**, 1931.
109. D. V. Fomitchev, B. S. Lim and R. H. Holm, *Inorg. Chem.*, 2001, **40**, 645.

110. B. S. Lim, K. M. Sung and R. H. Holm, *J. Am. Chem. Soc.*, 2000, **122**, 7410.
111. K.-M. Sung and R. H. Holm, *J. Am. Chem. Soc.*, 2002, **124**, 4312.
112. J. J. Wang, C. Tessier and R. H. Holm, *Inorg. Chem.*, 2006, **45**, 2979.
113. G. C. Tucci, J. P. Donahue and R. H. Holm, *Inorg. Chem.*, 1998, **37**, 1602.
114. B. E. Schultz and R. H. Holm, *Inorg. Chem.*, 1993, **32**, 4244.
115. B. S. Lim and R. H. Holm, *J. Am. Chem. Soc.*, 2001, **123**, 1920.
116. A. Majumdar, K. Pal and S. Sarkar, *J. Am. Chem. Soc.*, 2006, **128**, 4196.
117. J. J. Jiang and R. H. Holm, *Inorg. Chem.*, 2005, **44**, 1068.
118. H. Sugimoto and K. Sugimoto, *Inorg. Chem. Commun.*, 2008, **11**, 77.
119. H. Sugimoto and H. Tsukube, *Chem. Soc. Rev.*, 2008, **37**, 2609.
120. J. Halpern, *Science*, 1982, **217**, 401.

CHAPTER 5

Synthetic Models of the Nitrogenase Clusters

SONNY C. LEE^a

^aDepartment of Chemistry, University of Waterloo, Waterloo, ON, N2G 4Z6,
Canada

*E-mail: sclee@uwaterloo.ca

5.1 Introduction

The nitrogenase enzymes^{1,2} are the sole mediators of biological nitrogen fixation, the microbial reduction of dinitrogen to ammonia. The enzymatic conversion entails the intervention of a set of biometalloclusters with distinctive, often unique, properties. The enzyme system is complex and particularly resistant to biochemical and biophysical analysis at the molecular level, and the clusters themselves have very limited synthetic precedent in form and reactivity. As a result, a comprehensive chemical understanding of the nitrogenase clusters remains elusive despite decades of study.

One approach to achieving molecular insight into nitrogenase chemistry involves the study of small molecule analogues that reflect or probe aspects of the biochemical system.^{3,4} This strategy includes, for example, functional mimetic chemistry aimed at dinitrogen activation and inspired by nitrogenase function.⁵ The molecular details of the biological process, however, are largely undefined at present (Section 5.2.3), and chemical nitrogen fixation is notoriously difficult to realize under laboratory conditions. Current synthetic

approaches enabling this reactivity bear limited resemblance to the biological system, and the relation of these functional mimics to the enzyme chemistry is unclear.

Structurally targeted models,^{6,7} in contrast, rely on more extensive, better-defined data, permitting the construction of species that more closely align with the known biological chemistry. This represents a stricter synthetic analogue approach to the study of the nitrogenase metallocenters. Because of the many unsolved chemical problems associated with these clusters, nitrogenase synthetic models are not the classical corroborative analogues that characterize biological sites through rigorous coincidence of synthetic-native properties. Rather, these models are speculative analogues that, first and foremost, extend fundamental inorganic chemistry, while simultaneously delineating chemical possibilities for the native system and laying essential foundations for the eventual creation of corroborative analogues.⁴

The structural approach to nitrogenase analogue chemistry has been extensively reviewed.^{6–10} The goal of this account is to survey the present status of these structurally inspired efforts, emphasizing representative and currently relevant examples. Particular focus is directed to the principal contributions of these efforts in the development of tactics and insights for the systematic synthesis of cluster targets.

5.2 The Nitrogenase Metalloclusters: A Synthetic Perspective

The conventional nitrogenase enzyme system^{1,2} consists of two components, the iron (Fe)-protein and the molybdenum-iron (MoFe)-protein. The Fe-protein is an electron carrier that serves, with ATP hydrolysis, as the functionally obligate reductant for the MoFe-protein where substrate chemistry occurs.

Three different metal-containing moieties, all metalloclusters, are required for activity, the F-cluster in the Fe-protein and the P-cluster and iron-molybdenum (FeMo)-cofactor (also known as the M-cluster) in the MoFe-protein. All three clusters are classified as weak-field iron-sulfur (Fe-S) clusters;⁶ the weak-field descriptor is usually implicit and assumed for Fe-S centers unless otherwise noted. Fe-S clusters are marked by tetrahedral, high-spin iron centers organized into cluster frameworks *via* bridging sulfide core ligands. The oxidation states of individual iron centers in Fe-S systems occur in the classical ferrous-to-ferric range, with the ready accessibility of the $\text{Fe}^{+2}/\text{Fe}^{+3}$ redox couples in these environments allowing potential access to multiple cluster redox states. Electronically, these clusters are generally treated as magnetically interacting aggregates of individual high-spin iron centers without invocation of metal-metal bonding. Key, synthetically significant molecular features of the individual nitrogenase clusters are summarized below, with known structures, derived principally from macromolecular crystallography, illustrated in Figure 5.1.

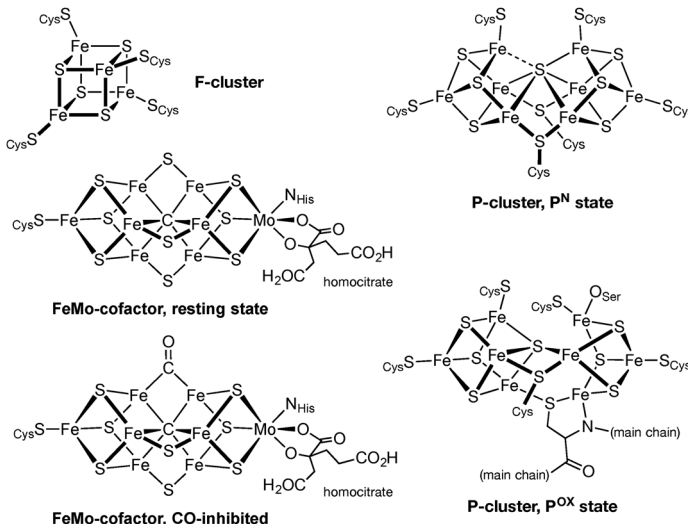


Figure 5.1 The clusters of nitrogenase. The cluster core frameworks are emphasized, and only structurally characterized states are shown; overall cluster charges are not indicated.

5.2.1 The F-Cluster

The F-cluster is an Fe_4S_4 cubane-type cluster with cysteinate terminal ligation.^{11–15} The cubane geometry is the archetypal Fe-S cluster motif,^{7,16} with extensive biological and synthetic representation. While the F-cluster might therefore seem prosaic by synthetic standards, it nonetheless presents a highly distinctive chemical feature in the form of an accessible all-ferrous $[\text{Fe}_4\text{S}_4]^0$ core.^{15,17} This superreduced core redox state was unknown in stable form prior to its observation in *A. vinelandii* Fe protein and, subsequently, has only been observed elsewhere in biology in an *A. fermentans* dehydratase¹⁸ and, very recently, in a precursor cluster to the P-cluster in the MoFe-protein;¹⁹ in the last case, the $[\text{Fe}_4\text{S}_4]^0$ cluster has been suggested as an intermediate in P-cluster biosynthesis. For the F-cluster, the all-ferrous state appears to have no proven physiological role at present, although it may reflect protein environment factors relevant to electron transfer requirements for biological nitrogen fixation.

5.2.2 The P-Cluster

The P-cluster is an intermediary electron transfer center of a structure type found only in nitrogenase. The P-cluster can exist in several oxidation states, of which only the normal, all-ferrous P^{N} state and the doubly oxidized P^{Ox} (also known as P^{2+}) form have been structurally characterized.^{20–22} In the P^{N} state, the P-cluster core can be viewed as two Fe_4S_4 cubanes bridged at a shared μ_6 -sulfide vertex; the resulting octanuclear Fe_8S_7 framework can thus be described as a vertex-fused double cubane (VFDC) structure. Two

μ_2 -cysteinate ligands also bridge the cubane subunits to provide additional core interconnections, yielding an idealized C_{2v} -symmetric core, and terminal cysteinates satisfy the remaining open coordination sites. The P^{OX}-cluster adopts an asymmetric framework derived from the P^N form, with added serinate and protein backbone-derived N-amidate ligation leading to a more open Fe₄S₃ cuboidal subunit and diminished μ_4 -connectivity at the central sulfide bridge.

5.2.3 The FeMo-Cofactor

The FeMo-cofactor cluster is also unique to nitrogenase. The cofactor is known in a number of redox and chemical forms; of these, the resting (also known variously as as-isolated, dithionite-isolated or E₀) state is the best characterized and, until quite recently (*vide infra*), the only form with direct structural visualization.^{22,23} Like the P^N-cluster, resting state FeMo-cofactor can also be deconstructed as a VFDC structure. Unlike the P-cluster, the shared vertex appears to be a trigonal prismatic μ_6 -carbide ligand, and the cubane subunits themselves are differentiated by metal composition as homometallic Fe₄S₃C and heterometallic MoFe₃S₃C fragments. Three μ_2 -sulfide bridges further integrate the two subunits to give a compact, C_{3v} -symmetric MoFe₇S₉C core. All metal sites possess regular, ostensibly saturated coordination geometries, tetrahedral at iron and octahedral at molybdenum. Because of the highly interconnected core framework, terminal ligation occurs only at the end metal positions in the form of cysteinate at iron and histidine imidazole and homocitrate alkoxide-carboxylate at molybdenum. The charge state (z) of and formal oxidation state distribution within the [MoFe₇S₉C]^z cofactor core are uncertain. Assignments derived from a range of spectroscopic and computational analyses suggest z = 3-, 1- or 1+, with molybdenum in either the Mo⁺⁴ or, more recently, Mo⁺³ oxidation state and iron centers distributed across standard Fe⁺² and Fe⁺³ states.²⁴ The significance of the heterometal and the core heteroligand in nitrogenase chemistry is unknown.

All evidence implicates the FeMo-cofactor as the site of substrate reactivity, although direct observation of dinitrogen chemistry at this cluster remains absent to this day.^{25,26} Indeed, poised or active state cofactor structures are unavailable, molecular-level descriptions of substrate- or inhibitor-bound forms are limited, and the substrate binding site or sites are not known with certainty. The only exception is a very recent macromolecular study of the MoFe-protein crystallized under CO-inhibited turnover conditions.²⁷ Structural analysis showed the inhibited cofactor to be identical to the resting state cluster, but with one central μ_2 -sulfide replaced by a μ_2 -CO ligand. Surprisingly, this ligand substitution appears to reverse in the absence of CO; to account for this observation, it has been suggested that the displaced sulfide migrates reversibly, perhaps in the form of hydrosulfide, to a remote, positively charged pocket within the MoFe-protein. How the structure of the CO-inhibited cofactor relates to substrate binding behavior is unclear at present, but the revelation of this new cluster form will certainly inspire fresh approaches in structural modeling.

The FeMo-cofactor can be removed from the MoFe-protein using specific organic solvents (typically, *N*-methylformamide) and re-incorporated into apoprotein with restoration of activity.^{28,29} This implies that the cluster is stable independent of the protein environment. The stability extends to the core structure, which, by spectroscopic criteria, remains largely unchanged upon extraction. The study of the cofactor in solution extracts, without interference from the P-cluster, has yielded valuable, specific physicochemical data, although the cofactor itself has not been isolated in pure form from these solutions, and a small-molecule structural analysis of the cluster remains notably absent. For many years, only limited chemical reactivity was observed for the dissociated cofactor,^{30a} and dinitrogen reduction chemistry continues to require the full ATP-dependent, two-protein enzyme system. Recent studies, however, have revealed that the extracted FeMo-cofactor and related clusters can reduce certain substrates (CO, CN⁻, CO₂) to low molecular weight hydrocarbons (and NH₃ and CO in the case of CN⁻ and CO₂, respectively) using simple divalent lanthanoid reductants.^{30b-d}

Alternative nitrogenases also exist that lack molybdenum and instead contain either vanadium or no heterometal at all.³¹⁻³³ These nitrogenases are generally less active, less selective and less understood than the Mo-containing nitrogenases. Biophysical and biochemical evidence, including, in particular, cofactor isolation and re-incorporation experiments using MoFe-apoprotein, indicate that the iron–vanadium-cofactor is isostructural with the well-studied FeMo-cofactor.

5.3 Synthetic Considerations

The chemical synthesis of Fe–S clusters entails several important considerations.⁶ The tetrahedral iron sites in weak-field Fe–S systems are high-spin, redox-active and lower-coordinate, and interact weakly with each other when organized as clustered arrays. General metal-centered synthetic challenges in these systems therefore include high exchange lability, potential redox and electrophilic instability, and non-selective multi-site reactivity. The native ligand environments about iron consist predominantly of dianionic sulfide core donors and monodentate terminal cysteine thiolate ligands, the latter usually limited to a single ligand per metal site. Thus, the use of chelate ligand designs to control metal chemistry is usually inapplicable at single iron sites and difficult to implement for the cluster as a whole, particularly when biologically relevant charge states and metal environments are desired. Sulfide and thiolate ligands are also redox-active themselves, further complicating the reaction chemistry with iron. Experimentally, these properties lead to species that are unstable with respect to dioxygen, water and standard chromatographic adsorbents; cluster paramagnetism provides characteristic NMR spectra, but crystallographic analysis is usually required for structural elucidation.

These intrinsic constraints must then be applied to the construction of specific metallocluster targets, a generally formidable problem in pure

inorganic synthesis. The following three broadly defined approaches^{6,7} allow an organized classification of weak-field cluster syntheses:

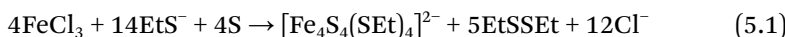
- (i) *Cluster self-assembly* is the spontaneous formation of a cluster from the combination of simple, separate metal, core ligand and terminal ligand precursors. This method is the oldest, most extensively applied approach to the construction of weak-field Fe–S clusters. Self-assembly is the least rational synthetic method in that the starting materials and the final cluster product are typically related only by basic composition and reaction stoichiometry. Nevertheless, this reaction class has proven quite effective, yielding, through variation and optimization of precursors, stoichiometry and reaction conditions, a remarkably diverse set of Fe–S clusters.
- (ii) A more directed approach to cluster synthesis is *fragment condensation*, which relies on the reaction of preorganized components to yield a product of usually higher metal nuclearity. Traditionally, at least one of the components is a cluster itself, and there is a structural or compositional relationship between the reactants and the product cluster, thus allowing a rational basis for cluster construction. In ideal cases, the reactants are identifiable “fragments” of the final product, although this is by no means a requirement. The reverse process, *cluster fragmentation*, is also a viable means of synthesis, although in practice the increase of cluster nuclearity is the more common objective.
- (iii) *Core rearrangement*, the transformation of a pre-existing cluster into another cluster of identical metal nuclearity but different core geometry, is the third general approach to cluster assembly. Like fragment condensation, core rearrangement relies on similarities in, at minimum, composition and, ideally, structure, in this case, between the starting cluster and the desired target. Although the existence of a suitable rearrangement pathway is not predictable *a priori*, the high degree of preorganization evident in the relationship between the starting and end clusters makes the search for such a process rational. Core rearrangements can be induced by a number of factors, *e.g.* changes in ligand set or redox state.

Note finally that these classifications are primarily conceptual and descriptive rather than mechanistic. Although the preorganization evident in fragment condensation and core rearrangement approaches necessarily assumes, for the purposes of synthetic planning, the principle of least motion during cluster assembly, the actual mechanistic pathway is almost always unknown and unpredictable. Likewise, self-assembly reactions must proceed through stepwise sequences that resolve mechanistically as fragment condensations or core rearrangements for some steps. Direct experimental evidence for cluster assembly mechanism is presented in Section 5.6.

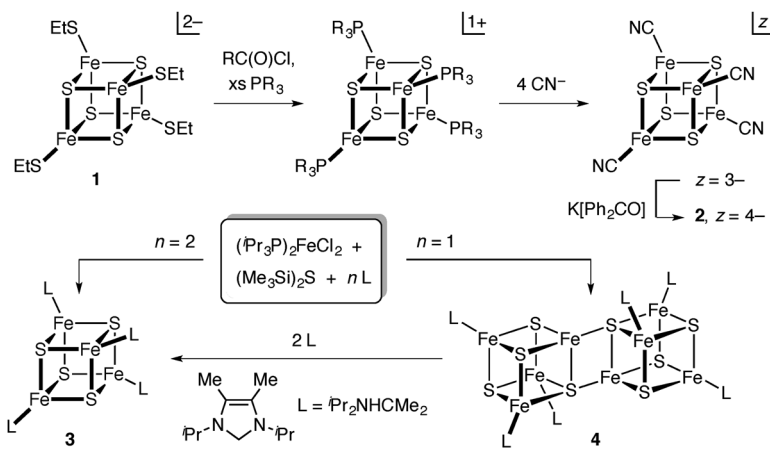
5.4 F-Cluster Analogues: The All-Ferrous State

The superreduced all-ferrous $[\text{Fe}_4\text{S}_4]^0$ state of the F-cluster was presaged by the electrochemical observation of $[\text{Fe}_4\text{S}_4(\text{SR})_4]^{4-}$ species at the beginning of Fe_4S_4 synthetic analogue chemistry.^{34–36} Isolation of this core state in a form stable enough for study proved elusive for many years due to significant oxidative and chemical instabilities observed across a range of terminal ligand environments.

The first stable synthetic weak-field $[\text{Fe}_4\text{S}_4]^0$ cluster was achieved by the Zhou laboratory *via* the upper route in Scheme 5.1.^{37,38} The complete synthesis originates from the well-known $[\text{Fe}_4\text{S}_4]^{2+}$ cubane core, readily obtained as thiolate-ligated **1** by various self-assembly reactions,¹⁶ one common example³⁹ of which is indicated in balanced form as eqn (5.1). Successive ligand substitution reactions coupled with ligand-based (phosphine) and exogenous (benzophenone ketyl) reductants resulted in the isolation of the all-ferrous core as the cyanide-ligated cluster **2**, with the core oxidation state identified in the solid state by single crystal diffractometry and Mössbauer spectroscopy. Access to the superreduced state hinges on the presence of the electron-withdrawing cyanide ligands, which shifts the $z = 4/-3-$ couple ($E_{1/2} = -1.42 \text{ V vs. SCE, MeCN}$) by *ca.* +300 mV relative to the potential of the benzene-thiolate-ligated core. Despite this stabilization, **2** is still quite sensitive to oxidation and requires excess reductant to exist in solution.



Subsequently, a solution-stable superreduced core was obtained using hindered *N*-heterocyclic carbene (NHC) ligation.⁴⁰ The all-ferrous NHC-ligated cubane **3** forms directly by self-assembly (Scheme 5.1). Cluster formation is stoichiometrically controlled, with a 2:1 NHC:Fe ratio leading to the isolated cubane and a 1:1 ratio giving rise to an octanuclear edge-bridged double cubane (EBDC) **4**. The EBDC structure type plays a significant role in recent



Scheme 5.1 Synthetic pathways to all-ferrous $[\text{Fe}_4\text{S}_4]^0$ cubanes.

nitrogenase-related synthetic chemistry and is discussed in detail in Section 5.5.2.2. In an example of a cluster fragmentation reaction, EBDC **4** converts to the single cubane **3** upon treatment with additional NHC ligand.

Although a direct electrochemical comparison of neutral **3** and tetraanionic **2** cannot be made due to solubility differences, the NHC ligand set enables an uncharged cluster that can be manipulated in low-polarity, low-reactivity solvents. These characteristics all aid in the stabilization of the final all-ferrous state. Detailed Mössbauer and EPR analyses of **3** revealed a 3:1 iron site differentiation, with spin antiparallel alignment between the unique site and the other three equivalent, spin parallel sites to give a net $S = 4$ ground state.⁴¹ This electronic structure is shared with the super-reduced F-cluster, suggesting it to be an intrinsic property of the $[\text{Fe}_4\text{S}_4]^0$ core; in this aspect, **3** is a credible corroborative analogue of the all-ferrous state of the F cluster despite the difference in terminal ligation.

5.5 Modeling the Nitrogenase Superclusters

The unique octanuclear clusters of nitrogenase are imposing synthetic targets, and complete chemical models remain out of reach despite long, dedicated study. The P-cluster and the FeMo-cofactor both possess unprecedented structures of high nuclearity and complex connectivity, attributes that have led to their description as “superclusters”. The FeMo-cofactor is distinguished further by its heterometallic and heteroligated core. These conspicuous features challenge and exceed current synthetic methods.

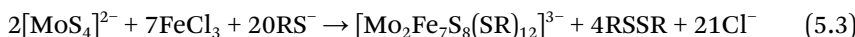
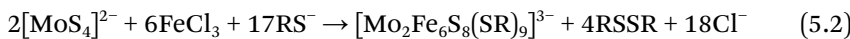
The following sections present the state of contemporary model chemistry for the nitrogenase superclusters using these prominent, distinguishing structural characteristics as investigative themes. The sections are also ordered according to historical development to reflect the evolution of synthetic analogue efforts.

5.5.1 Heterometallic Cores

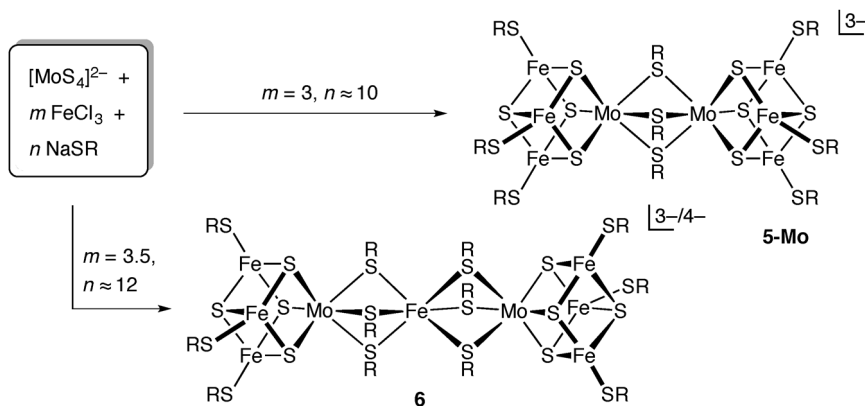
The presence of molybdenum in the FeMo-cofactor²⁸ provides an obvious physicochemical feature differentiating the cofactor from the other metal components in nitrogenase. This compositional distinction, in conjunction with the demonstration of cluster stability in protein-free isolates and the association of this cluster with substrate chemistry, has made the FeMo-cofactor the subject of longest and greatest attention in synthetic nitrogenase chemistry.

Molybdenum extended X-ray absorption fine structure (EXAFS) studies yielded the first structural insight into a metallocenter of nitrogenase.^{42,43} The results of these initial analyses delivered compositional and metrical data on the molybdenum environment and led to the identification of the FeMo-cofactor as a Mo–Fe–S cluster. One proposal for an EXAFS-consistent local molybdenum environment was a MoFe_3S_4 cubane model derived from the established Fe_4S_4 structure.⁴² Independent synthetic efforts from Holm and Garner quickly yielded species possessing this motif in the form

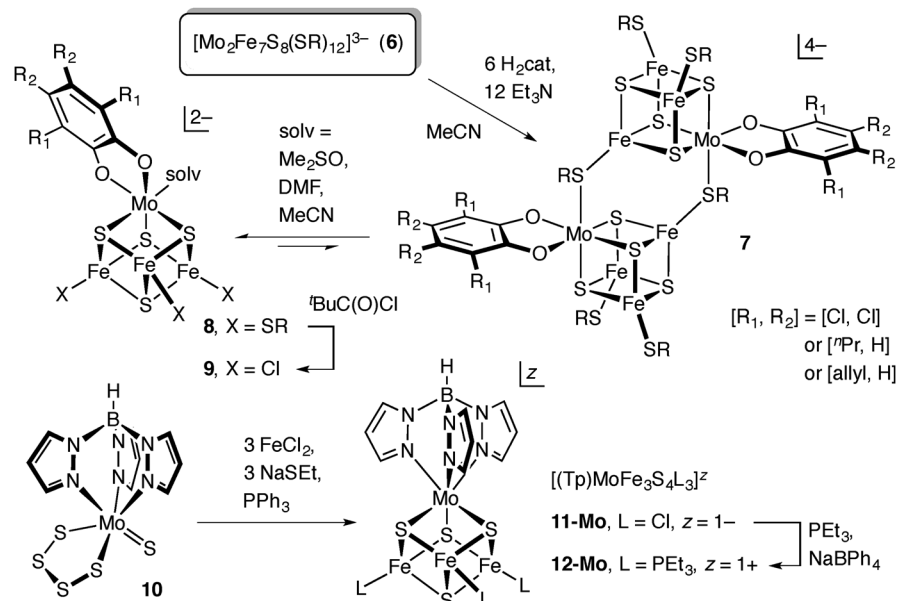
of Mo-bridged double cubane clusters, two examples of which, **5-Mo** and **6**, are indicated in Scheme 5.2; other bridging-ligand combinations are also known.^{44–49} These syntheses proceed in good yields by balanced reactions (eqn (5.2) and (5.3)) similar to those employed in the self-assembly of the Fe_4S_4 core. Given that the tetrathiomolybdate ($[\text{MoS}_4]^{2-}$) reactant is a preorganized source of both molybdenum and core sulfide, these reactions could be considered a form of fragment condensation despite the absence of cluster-containing precursors; experimental support for this view is presented in Section 5.6.



The clusters formed in Scheme 5.2 comprise MoFe_3S_4 cubane subunits interconnected by ligand or ligand/iron bridges at the octahedral molybdenum sites. The net Mo-bridged double cubane structures, however, complicated the study of the fundamental MoFe_3S_4 motif and precluded potential reactivity at molybdenum. Moreover, contemporaneous EPR and ENDOR investigations^{50,51} would conclude correctly that the cofactor cluster contains only one molybdenum, eventually mandating single molybdenum compositions in relevant models of the native heterometallic environment. Cluster fragmentation of the double cubanes to discrete single cubanes was sought and accomplished in the Holm laboratory, initially through the application of moderately hindered catecholate chelates to disrupt the central bridging iron site of **6** (Scheme 5.3, upper route, and eqn (5.4)); under appropriate conditions, the resultant bridged dicubane **7** readily dissociates to give isolated cubane **8**.^{52–57} Recent access to single MoFe_3S_4 cubanes has relied on more efficient, direct syntheses from simple mononuclear reactants including the facially chelated molybdenum-sulfur precursor **10** (Scheme 5.3).⁵⁸ Facial capping prevents intercubane bridging at molybdenum and leads to the C_{3v} -symmetric single cubane

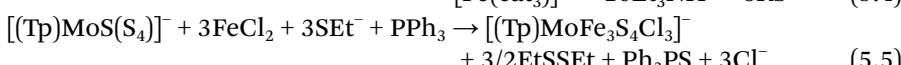
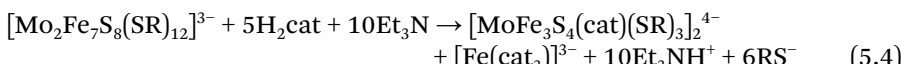


Scheme 5.2 Assembly of molybdenum-bridged double cubanes.

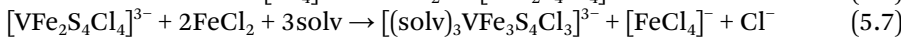
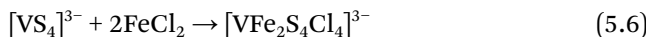


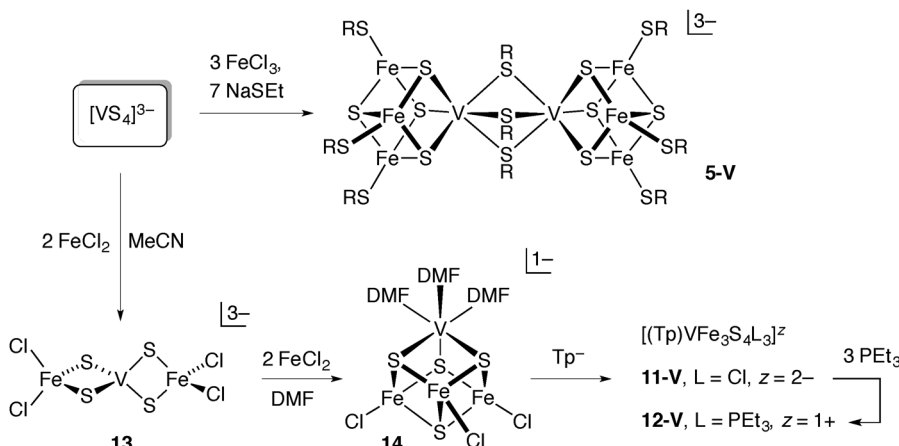
Scheme 5.3 Routes to $M\text{Fe}_3\text{S}_4$ single cubanes.

11-Mo (eqn (5.5)); the advantages of this environment are discussed further in Section 5.5.2.2.



The synthesis of $\text{Mo}\text{Fe}_3\text{S}_4$ cubanes from $[\text{MoS}_4]^{2-}$ led to the successful application of other tetrathiometalates, $[\text{MS}_4]^z$, in the preparation of heterometallic $M\text{Fe}_3\text{S}_4$ cubanes with $M = V, \text{Nb}, \text{W}$ and Re .^{59,60} The vanadium case is of particular interest with respect to the FeV-cofactor of vanadium-containing nitrogenase. In contrast to the 4d and 5d heterometal cubanes, the $V\text{Fe}_3\text{S}_4$ cubane motif is accessible from the tetrathiometalate precursor not only by bridged double cubane formation (5-V),⁶⁰ but also directly as the single cubane **14** via synthesis in a thiolate-free reaction system (Scheme 5.4).⁶¹⁻⁶³ A lower FeCl_2 stoichiometry allows isolation of the linear trinuclear cluster **13** in MeCN, which can then be converted to cubane **14** upon treatment with additional FeCl_2 in DMF. Based on this behavior, a stepwise reaction sequence (eqn (5.6) and (5.7)) can be proposed starting from the fragment condensation of $[\text{VS}_4]^{3-}$ with iron to give **13**, followed by a second fragment condensation of **13** with additional iron, leading ultimately, after reduction and implicit core rearrangement, to the cubane product **14**.





Scheme 5.4 Synthesis of VFe_3S_4 cubanes.

The MFe_3S_4 cubanes derived from these syntheses have been extensively studied and their chemistry reviewed in depth.^{6,7,59,64} The most biologically significant aspect of these clusters lies in their structure: by original XAS^{32,44,45,63} and later crystallographic⁶ criteria, the local MFe_3S_3 ($\text{M} = \text{Mo}$, V) environments of the synthetic clusters showed substantial, quantitative structural agreement with the corresponding sections of the relevant cofactors. A visual and metrical comparison is given in Section 5.5.3.2. This cluster type remains the best synthetic representation of the heterometallic sub-units of the nitrogenase cofactors to this day.

Overall, the clusters are well described as heterometal-substituted derivatives of Fe_4S_4 cubanes, showing similar isotropically shifted ^1H NMR spectra, equivalent structures that diverge significantly only about the heterometal and identical ligand substitution chemistry at iron.⁶ The $\text{M} = \text{Mo}$ and V cubanes are typically obtained initially as isoelectronic $[\text{MFe}_3\text{S}_4]^z$ cores with $z = 3+$ for Mo and $2+$ for V; in these states, ^{57}Fe Mössbauer isomer shift correlations suggest mean iron oxidation states of +2.67 and +2.33 for the two cores, respectively, leading to a formal assignment of +3 for the heterometal oxidation state in both cases.⁴⁹ The molybdenum in resting state FeMo-cofactor has traditionally been viewed with a +4 oxidation state based on early XAS and ENDOR studies; recent XAS and computational studies, however, suggest a +3 assignment, like that in the synthetic cubanes, as a better description.^{65,66} A detailed history and discussion of FeMo-cofactor and synthetic MoFe_3S_4 cubane electronic structure is presented in a recent review.²⁴ Like the all-iron cubanes, oxidized and reduced states are accessible in MFe_3S_4 cores, with Mössbauer data indicating that the redox activity is largely confined to the iron components of the heterometallic clusters.⁴⁹ The redox potentials of isostructural $[(\text{Tp})\text{MFe}_3\text{S}_4\text{L}_3]^z$ clusters (e.g., **11-M**^{58,67}) reveal that $\text{M} = \text{Mo}$ cubanes are more readily oxidized relative to $\text{M} = \text{V}$ species ($E_{\text{Mo}}^{z/z+1} - E_{\text{V}}^{z/z+1} \approx -200$ to -500 mV, $z = 3-$ and $2-$, MeCN).⁶⁸

In solution, the heterometallic clusters display some specific reactivity but no evidence of dinitrogen activation. Reduced bridged double cubanes

$[\text{Mo}_2\text{Fe}_6\text{S}_8(\text{SPH})_9]^z$ ($z = 4-, 5-$) slowly evolve dihydrogen in the presence of appropriate proton donors, as does the reduced $[\text{Fe}_4\text{S}_4(\text{SPH})_4]^{3-}$ cubane in lower yield,⁶⁹ and this behavior has been made photocatalytic in cluster-immobilized frameworks;^{70a} similar electrocatalytic dihydrogen evolution has been observed in FeMo-cofactor extracts as well.^{30,71} Interestingly, the photochemical activity of the cluster-immobilized frameworks has recently been extended to the reduction of dinitrogen to ammonia, although molecular details are unavailable at present.^{70b} In single cubanes, the heterometal centers were originally characterized by simple ligand substitution chemistry, and this reactivity has been applied to create terminal ligand environments that more closely mimic that of the native cluster.^{72,73} Coucouvanis and coworkers expanded this chemistry to include catalytic transformations, using cobaltacene reductant and lutidinium proton donor, of certain non-native nitrogenase substrates, *e.g.* N_2H_4 to NH_3 , C_2H_2 to C_2H_4 and *cis*-MeN=NMe to MeNH₂;^{74–79} substrate-heterometal binding appears necessary for activity, as limited to no activity was observed for $[\text{Fe}_4\text{S}_4\text{Cl}_4]^{2-}$ or for clusters where the heterometal site was terminated by non-labile ligands.

Subsequent discoveries of other biological M–Fe–S centers, *viz.* non-native heterometal incorporation in protein-bound, iron-voided cuboidal Fe_3S_4 clusters⁸⁰ and the $\text{NiFe}_3\text{S}_{(4,5)}$ cluster in Ni-containing carbon monoxide dehydrogenase,^{81–83} further expanded the significance and reach of synthetic MFe_3S_4 cluster chemistry to include M = Co, Ni, Cu, Ag and Tl.^{59,84,85} For these late metals, tetrathiometalate precursors are inaccessible, and the syntheses of these heterometallic cubanes entailed the development of new fragment condensation routes. Other, non-cubane M–Fe–S clusters have also been synthesized; a few relevant examples are noted in later sections, and more extensive compilations are available elsewhere.^{6,8}

5.5.2 Topological Analogues

Although completely faithful synthetic representations of the nitrogenase superclusters remain unrealized, significant progress has been made in constructing, in part or in whole, analogues to the native frameworks. These structural analogues are not accurate in all specifics but instead emphasize generalized or select correspondences to key aspects of composition, connectivity and geometry. Such models have been termed topological analogues,⁶ where topology refers, in the non-specialist sense, to interrelationships between constituent parts. These studies develop inorganic synthetic methods and elucidate basic cluster properties, and their progress and changing goals mirror the evolution and maturation of structural insight into the nitrogenase clusters.

5.5.2.1 Higher Nuclearities and Sulfur-Voided Cubanes

In replicating the MFe_3S_3 environment of the heterometallic cofactors, the MFe_3S_4 cubanes represent an early and accurate achievement in topological modeling. Analytical and XAS data in the pre-crystallographic era, however, showed the FeMo-cofactor to be a much larger cluster with a proposed composition settling in the $\text{MoFe}_{6-8}\text{S}_{7-9}$ range.²⁹ Thus, the MFe_3S_4 cubanes could,

at best, only reflect part of the biological cluster. With this in mind, broad attempts were made to synthesize higher nuclearity analogues, but, in retrospect, the larger clusters prepared in this time period were unrelated to the nitrogenase superclusters for the most part.⁶ These synthetic studies nevertheless expanded Fe–S chemistry and laid important groundwork for further work, and the resulting compounds may yet have utility in the future. For example, sulfide-bridged double cubanes (Figure 5.2), prepared by coupling of single cubane precursors *via* terminal ligand substitution, possess the generic M₈S₉ metal-sulfide composition of the FeMo-cofactor and have attracted attention as potential entry points for the synthesis of cofactor analogues as a result.^{73,86,87}

The full visualization of the nitrogenase superclusters was ultimately obtained through diffractometry of the MoFe protein. The very first crystallographic models of both superclusters were inaccurate in certain critical aspects due to low data resolution (2.7–1.6 Å) and apparent P-cluster redox state heterogeneity.^{20,21,88–90} The most prominent and persistent discrepancy was the absence of the interstitial, monoatomic μ₆-ligand at the center of the FeMo-cofactor, resulting in a void region surrounded by six three-coordinate iron centers with modest inward pyramidalization. This unique environment attracted significant synthetic attention, resulting in a focus on sulfur-voided MFe₃S₃ (M = Mo, Fe) cubane fragments as subunits of the FeMo cofactor, as well as an increased interest in low-coordinate iron environments.

The sulfur-voided Fe₄S₃ cubane core has been known in strong-field form in the self-assembled C_{3v}-symmetric anion⁹¹ of Roussin's black salt, Na[Fe₄S₃(NO)₇], first prepared in the mid-19th century, as well as in modern phosphine-ligated derivatives.^{92,93} Coucovanis and coworkers were able to extend this class to heterometallic MFe₃S₃ cores by carbonylation-induced core fragmentation of the EBDC 15 (Scheme 5.5).^{94–96} Cluster 15 is prepared by fragment condensation *via* simultaneous ligand substitution and phosphine-induced reduction of the heterometal monocubane 9;⁹⁷ the properties of the EBDC cluster type are discussed in the next section. Carbonylation of 15 yields several related, chromatographically separable MFe₃S₃ products that vary depending on the other ligands present; cluster 16 is a representative example. The CO-ligated sulfur-voided cubanes obtained broadly reflect the connectivity of the MFe₃S₃ portion of the cofactor, although the distinctly non-native ligand environments at iron and the strong field nature of these clusters make direct comparisons with the biological system difficult.

Cluster 17-M, synthesized by self-assembly (Scheme 5.5), is another example of a non-cubane, weak-field M–Fe–S core (M = Mo, V).^{98,99} Interest in

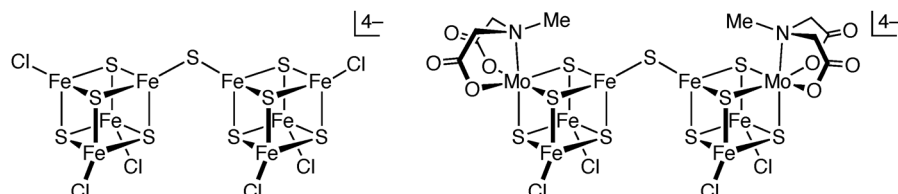
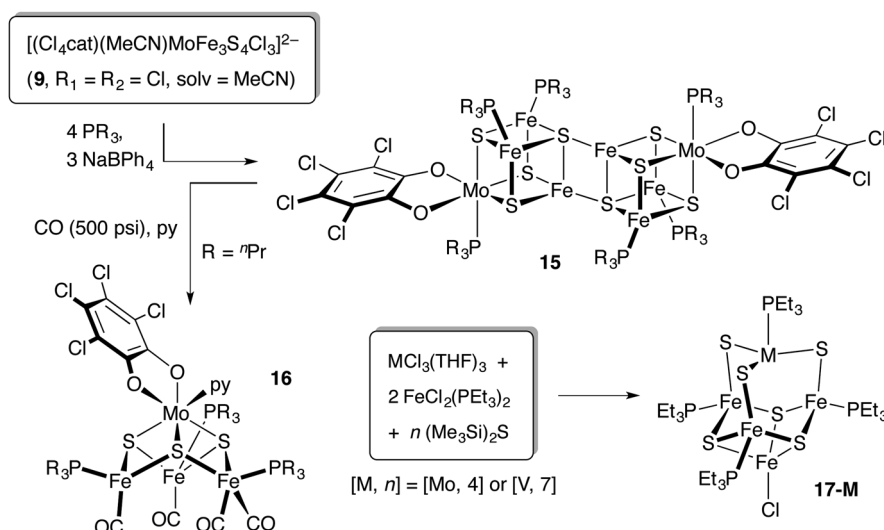


Figure 5.2 Representative sulfide-bridged double cubane clusters.

the system was raised not by the heterometal, but by the remaining Fe_4S_6 portion of the cluster. This 10-atom fragment of **17-M** can be related to the $\text{Fe}_4\text{S}_3(\mu_2\text{-S})_3$ section of the interstitially vacant FeMo-cofactor. Similarities include a highly commensurate, sulfur-voided cubane framework connected to $\mu_2\text{-S}$ bridges, the occurrence of expanded, non-rhombo M Fe_2S_3 faces, and unusual flattened trigonal pyramidal metal geometries at the phosphine-ligated positions that, upon notional exclusion of phosphine ligands, resemble the corresponding putative 3-coordinate iron centers in the cofactor.

In the end, the central void in the FeMo-cofactor proved artifactual. Nevertheless, the timely synthesis of strong-field M Fe_3S_3 and weak-field Fe_4S_3 -containing cores is a testament to expanding capabilities in inorganic synthesis and the ability of nitrogenase to inspire basic inorganic chemistry. Sulfur-voided cubane clusters may yet play a role in synthetic analogue chemistry: the Fe_4S_3 motif occurs as a subunit in the P^{OX}-cluster^{20,21} and constitutes the essential framework of a new tetranuclear cluster type recently identified in dioxygen-tolerant [NiFe]-hydrogenases (Figure 5.3).^{100,101}



Scheme 5.5 Preparation of clusters containing the MFe_3S_3 sulfur-voided cubane moiety ($\text{M} = \text{Mo, Fe}$).

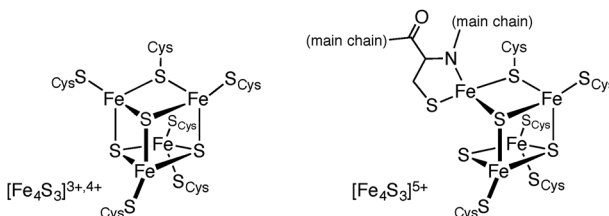


Figure 5.3 Fe_4S_3 clusters in dioxygen-tolerant NiFe-hydrogenases, showing reduced (left) and oxidized (right) structures.

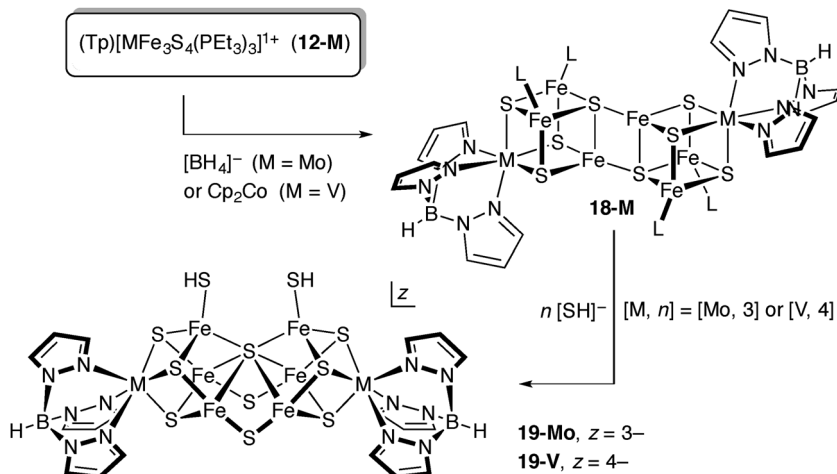
5.5.2.2 All-Sulfide P^N-Type Cores

Prior to the macromolecular structures of the MoFe protein, the P-cluster was largely thought to be an unusual paired set of Fe₄S₄ cubanes; with little specific data available, this cluster was unaddressed synthetically. Following the crystallographic revelation of its unique octanuclear structure, the P-cluster emerged as a synthetic target.

The first topological analogues of the P^N framework were prepared from EBDC clusters. The EBDC structure type was originally discovered by Coucouvanis and coworkers in the form of cluster **15**, and a number of examples, both all-iron [Fe₄S₄]₂ (*e.g.* **4**)^{40,102,103} and heterometallic [MFe₃S₄]₂, (M = Mo, V, W; *e.g.* **15**)^{68,97,104–114} are now known. The EBDC structure consists of two cubane subunits bonded along cluster edges to form a central Fe₂S₂ rhomb with inverted tetrahedral μ₄-S bridges. Despite the unusual geometry at the μ₄-sulfide, the intercubane interaction seems stronger than the intracubane bonds as Fe–S distances for the former are decidedly shorter by 0.08–0.19 Å. EBDC clusters are associated with cubane subunit oxidation states that are reduced relative to the typical, as-isolated states of single cubane clusters. They form, either by self-assembly or by fragment condensation of cubanes, as neutral clusters and usually possess neutral terminal ligation at iron on initial synthesis. The reduced oxidation states presumably increase core sulfide basicity in the cubanes, thereby favoring additional, intercubane bridging, while the neutral net charge reduces destabilizing electrostatic repulsions. In recent years, EDBC clusters have been prominent in nitrogenase model chemistry, as illustrated earlier in Sections 5.4 and 5.5.1.

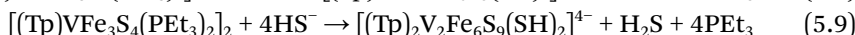
The EBDC motif is an attractive starting point for the creation of nitrogenase-related high nuclearity species, offering a preorganized M₈S₈ precursor of identical nuclearity, close sulfide content and partially congruent topology relative to the nitrogenase superclusters. The addition of a single sulfur to an EBDC core could be envisioned to induce rearrangement to the original core-voided FeMo-cofactor structure; likewise, loss of one sulfur from the EBDC motif might trigger transformation to the P^N framework. Sulfur addition reactions were explored by Holm and coworkers using hydrosulfide and cluster **15**; these reactions led not to a cofactor-type topology but to complex, high-nuclearity clusters containing recognizable P^N-like substructures.^{115,116}

From these initial results, a discrete all-sulfide P^N-type cluster was achieved using the EBDC cluster type **18-M**, itself prepared by reduction of monocubane **12-M** (Scheme 5.6).^{107–109} The C_{3v}-symmetric heterometal-capped monocubanes such as **12-M** are advantageous precursors. The facially capping ancillary ligand provides a stable, unreactive terminal coordination environment at the heterometal. This prevents bridge formation at that site, thereby allowing the direct synthesis of single cubanes (Section 5.5.1). The elimination of heterometal reactivity is of further value if subsequent, iron-specific reactivity is needed. Finally, a trigonally symmetric facial chelate maximizes symmetry, which simplifies stereochemical outcomes in reaction products.



Scheme 5.6 Formation of all-sulfide P^N -type clusters *via* edge-bridged double cubanes.

Treatment of **18-M** with hydrosulfide forms the targeted P^N topological analogue **19-M** in good-to-high yields (*ca.* 50% for $\text{M} = \text{V}$, >80% for $\text{M} = \text{Mo}$).^{107–109} The isolated vanadium-containing product is redox-precise relative to its EBDC precursor, whereas the molybdenum cluster is oxidized by one electron; oxidation appears to arise adventitiously due to the very low $E^{4-/3-}$ redox potential (-1.8 V vs. SCE, MeCN) for **19-M**, behavior consistent with the heterometal-dependent redox correlations noted in Section 5.5.1 for isostructural $[(\text{Tp})\text{MFe}_3\text{S}_4\text{L}_3]^z$ cubanes.⁶⁸ ^{57}Fe Mössbauer analysis confirms predominantly ferrous formulations, giving oxidation state assignments of $(\text{V}^{+3})_2(\text{Fe}^{+2})_6$ for **19-V** and $(\text{Mo}^{+3})_2(\text{Fe}^{+2})_5\text{Fe}^{3+}$ for **19-Mo**. Note that the simple reaction conditions and resulting core rearrangement reflected in balanced eqn (5.8) and (5.9) subsume a degree of mechanistic complexity that conceptually includes terminal ligand substitution by hydrosulfide, incorporation of core sulfide and reorganization of core bridge connectivity; experimental mechanistic insights into this transformation are presented in Section 5.6. The preparation of the analogous all-iron species from a corresponding homometallic EBDC cluster has not been reported.



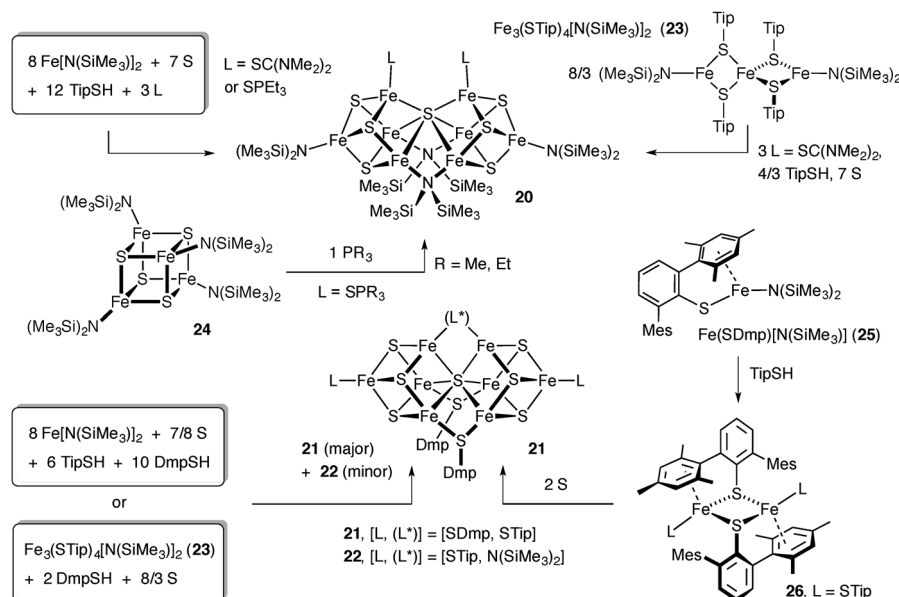
The all-sulfide P^N -type cores replicate the overall structure of the P^N framework, albeit with μ_2 -sulfide and molybdenum in place of the μ_2 -thiolate and end iron atoms in the biological cluster.^{107–109} The unusual and characteristic distorted trigonal prismatic μ_6 -sulfide ligand is reproduced faithfully, although the bend at the common vertex is more pronounced in the synthetic systems as measured by exterior, non-rhomb $\text{Fe}-(\mu_6-\text{S})-\text{Fe}$ angles

(ca. 141° for **19-Mo** and **19-V** vs. 158° for the P^N-cluster). In cluster derivatives differing by terminal and μ₂ ligand substitution,^{110–112,117,118} this exterior angle varies somewhat, indicating a degree of intrinsic flexibility at the junction between the fused cubane subunits. As a whole, the metrical divergences between the synthetic and native frameworks are relatively modest despite the mismatch in μ₂-bridges and end metals. The isotropically shifted NMR spectra of the synthetic clusters exhibit C_{2v}-symmetric signal patterns consistent with retention of the solid-state structure in solution.

5.5.2.3 Neutral Octanuclear Clusters

Tatsumi, Ohki and coworkers have established a distinct synthetic approach that has yielded a number of intriguing Fe-S clusters including full-framework, all-iron analogues of both nitrogenase superclusters.^{119,120} Their method employs cluster assembly under non-polar conditions: reactions are conducted in non-polar solvents (typically, toluene) using discrete, soluble metal precursors, and anionic ligands are introduced (in cases where ligand redox state is constant) *via* protolysis rather than salt-metathesis. In addition, terminal, or potentially terminal, ligands present during cluster formation are sterically encumbered to varying degrees, with thiolate ligands in particular possessing moderate-to-exceptional hindrance. Non-polar and low-polarity conditions have precedent in earlier Fe-S chemistry, for example in the creation of phosphine-ligated^{98,99,121–123} or subsite-differentiated thiourea¹²⁴ or isonitrile-ligated¹²⁵ clusters; likewise, non-polar, protolytic transformations play a major role in the Fe-S-analogous iron-imide (Fe-NR) chemistry described in Section 5.5.3.2. The inventive combination and exploration of these reaction conditions and ligand sets, however, has revealed an unexpected and significant new synthetic manifold.

The reactions in Scheme 5.7 afford topological analogues of both the P^N-cluster and the FeMo-cofactor.^{126–129} The products **20**–**22** contain the VFDC motif common to both nitrogenase superclusters, with μ₆-sulfide as the vertex in the synthetic species. Two^{126,128,129} or three^{127,130} monoanionic ligands, *viz.* hindered thiolates, bis(trimethylsilyl)amide and/or triphenylmethoxide (Section 5.5.3.1), provide additional intercubane bridges to attain the proper nitrogenase supercluster connectivities. The clusters possess neutral and/or monoanionic terminal ligand complements that give net charge neutrality, leading to formal oxidation state distributions of (Fe⁺²)₆(Fe⁺³)₂ for the P^N analogue **20**^{126,128} and (Fe⁺²)₅(Fe⁺³)₃ for the cofactor analogues **21** and **22**.¹²⁷ Interestingly, the P^N-like clusters possess a core redox state that corresponds to that of the structurally distinct P^{OX} cluster. Cluster-type **20** and isoelectronic ligand-substituted derivatives exhibit quasi-reversible one- and two-electron reduction processes by cyclic voltammetry, the latter leading to the actual all-ferrous core oxidation state of the P^N-cluster; these reduced forms, however, have not as yet been characterized. These observations have led to speculation that the P^N structure is the physiologically active form of the P-cluster, and that the characterized P^{OX}-cluster is not a functionally-relevant state.¹²⁸



Scheme 5.7 Pathways to neutral octanuclear clusters with P^{N} - and FeMo-cofactor-like topologies. Dmp = 2,6-dimesitylphenyl; Tip = 2,4,6-triisopropylphenyl.

Like the all-sulfide P^{N} -type topological analogues, the core frameworks of these neutral all-iron clusters differ from the native clusters in key features: (i) for central μ_2 -bridges, amide substitutes for thiolate in the P^{N} model and monoanions for sulfide in the FeMo-cofactor analogues; and (ii) in the cofactor analogues, μ_6 -sulfide replaces μ_6 -carbide and iron supplants molybdenum, although the latter substitution may actually be appropriate for the cofactor of the iron-only nitrogenase. Of the two analogue types, the core of the P^{N} analogue **20** replicates the native cluster quite closely, notwithstanding differences in oxidation state and μ_2 -bridge. The $\text{Fe}-(\mu_2\text{-bridge})$ distance in **20** (2.06 Å),¹²⁸ however, is much shorter than those of either the all-sulfide P^{N} -type clusters **19 M** (2.23 Å)^{107–109} or the P^{N} -cluster (2.40 Å),^{20,21} and the exterior $\text{Fe}-(\mu_6\text{-S})-\text{Fe}$ angle (*ca.* 144°) is closer to those in **19-M** than to the equivalent angle in the native cluster. Ideally, replacement of the bridging amide ligand by thiolate would furnish an exact structural analogue of the target core, but substitution chemistry at bridging positions has not been reported in this cluster or in the FeMo-cofactor analogues; terminal ligands, however, can be replaced, and closer alignment with the P^{N} -cluster has been reached through thiolate and thiolate-analogue coordination at these positions.¹²⁸ The cofactor models, in contrast, are more distant topological analogues, with major distortions due to the dissimilar interstitial ligand. As expected, metal-interstitial bond distances are much longer ($\gtrsim 0.3$ Å) for sulfide relative to carbide. Bending distortions at the μ_6 -sulfide also occur, with non-triangle-edge $\text{Fe}\cdots\text{Fe}$ distances of the central Fe_6 trigonal prism varying substantially by 0.7–0.9 Å compared to <0.05 Å for the symmetric trigonal prism in the cofactor.

The syntheses of these neutral clusters employ a range of self-assembly and fragment condensation reactions. Mechanistically, these are complex reaction systems, and it is unclear how the specific synthesis conditions favor the formation of higher nuclearity frameworks. Balanced cluster formation equations are not offered, and reaction stoichiometries appear to be empirically determined. Solution ^1H NMR data for these compounds are also unreported; for highly hindered thiolates, it has been observed elsewhere that even simple complexes of this ligand type exhibit complicated, potentially dynamic NMR spectra.¹³¹ Thiolate steric bulk appears essential for the cofactor analogues, but its role is unknown; obvious, generic possibilities include the solubilization of inorganic cores, and the stabilization of reactive intermediates and product geometries.

Despite these uncertainties, mechanistically relevant observations can be discerned. The Fe_8S_7 VFDC core motif common to all of the synthetic clusters suggests a shared cluster assembly pathway. Given the VFDC framework, it is tempting to consider a fragment condensation mechanism in which the key step in octanuclear core assembly is a simple fusion of two discrete cubane clusters. This idea has support in the formation of the P^{N} -type cluster from the reaction¹²⁹ of the amide-ligated Fe_4S_4 cubane **24**^{132,133} and simple trialkylphosphines (Scheme 5.7). An abstract mechanistic sequence for this reaction has been proposed consisting of (i) sulfur-atom transfer from **24** to phosphine giving phosphine sulfide and a reduced, sulfur-voided Fe_4S_3 core, followed by (ii) condensation of the Fe_4S_3 fragment with another, intact cubane **24** to form the VFDC structure. Redox-coupled phosphine–sulfur reactivity is chemically reasonable, and the proposed sequence is rational based on the structural correlations. The mechanistic significance of the cubane-based fragment condensation system, however, is tempered by its modest product yield (30%) compared to simple self-assembly (70%). The end VFDC product requires the loss of half of the amide ligands present in the starting cubane cluster as well as intervening redox chemistry, and the phosphine reaction conditions provide no simple means of achieving this; these complications may explain the difference in yields. Finally, it can be noted that the core structures of the two analogue types differ only in the μ_2 -bridging about the interstitial region, and that the occurrence of two or three μ_2 -bridges appears dependent on the identity of the bridging ligand. This relationship might originate from geometric and/or steric constraints. Exact causes notwithstanding, $(\text{Me}_3\text{Si})_2\text{N}^-$ ligation alone seems capable of spanning just two μ_2 -positions, with concomitant distortion at the $\mu_6\text{-S}$ vertex leaving the third span too wide for amide-bridging. The reaction systems appear to control cluster product selectivity through this compositional-structural relationship. The one-electron difference in redox state between the two core types presumably reflects the preservation of cluster neutrality under non-polar conditions.

5.5.3 Heteroligated Cores

The interstitial monoatomic heteroligand at the center of the FeMo-cofactor core was initially detected in a high-resolution (1.16 Å) crystallographic analysis of the MoFe-protein in 2002,²² a decade after the original,

lower-resolution structures first revealed the overall supercluster structures. This analysis was unable to identify the atom with certainty, although bond distances and resolution-dependent electron-density profiles indicated a 2p element consistent with carbon, nitrogen or oxygen. For nearly a decade afterwards, this result constituted the totality of experimental evidence for the core heteroligand. Very recently (2011–2012), incisive experiments involving high-resolution macromolecular X-ray analysis,³ electron spin echo envelope modulation (ESEEM)³ and X-ray emission (XES)¹³⁴ spectroscopies and biochemical radiolabeling^{135,136} have all produced data pointing to the astonishing assignment of carbide as the heteroligand.

The revelation of the interstitial light atom in the cofactor has focused specific synthetic attention to the construction of core-heteroligated Fe–Q–S clusters. The presence of heteroligand Q increases the complexity of core composition, connectivity and chemistry, compounding the intrinsic challenges associated with synthetic Fe–S chemistry (Section 5.3). The very different physicochemical properties of anionic 2p donors relative to sulfide present new problems in the introduction and maintenance of both ligand types in the same cluster. These differences increase with increasing charge for isoelectronic ligands and increasing donor basicity at parity of ligand charge, in both cases ordering as O < N < C. Thus, carbide ligation poses the most difficult synthetic scenario.

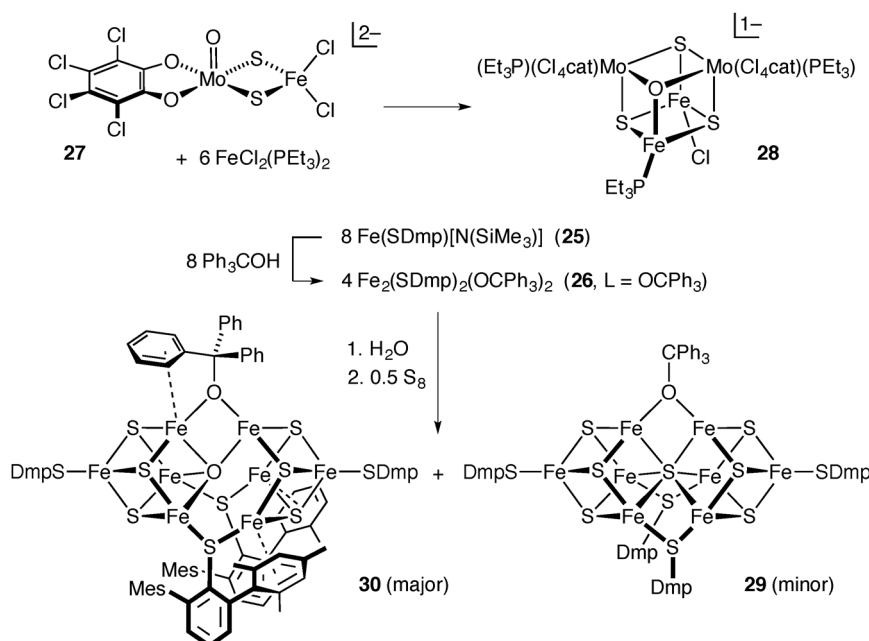
To date, iron-bound carbide occurs in molecular form only in strong-field carbonyl clusters,¹³⁷ via CO reduction, and in porphyrin and porphyrin-like dimers,¹³⁸ by reduction of tri- or tetrahalomethanes. In the biosynthesis of the FeMo-cofactor, carbide appears to come from the methyl group of *S*-adenosylmethionine, although the process by which it is converted to interstitial carbide remains unresolved.¹³⁵ Available routes for carbide incorporation are therefore quite limited, and substantial synthetic development is probably necessary before Fe–C–S clusters can be realized. Alternative heteroligated Fe–Q–S cores, however, have been achieved. These efforts constitute necessary first steps toward the systematic construction of cofactor-relevant heteroligated cores.

The following sections focus on rational (or rationalizable) syntheses of weak-field Fe–Q–S clusters, where Q is a 2p donor bridging three or more metal centers. These criteria select the most challenging and cofactor-relevant synthetic exemplars at present. All other Fe–Q–S clusters fall into one of two remaining broad classes.⁷ First are cases where Q is a heavy element donor, current examples of which are confined strictly to Q = Se. In these systems, selenium behaves as a congener of sulfur; weak-field Fe–S–Se clusters are long known, but selective syntheses are more recent developments derived from mechanistic studies (Section 5.6). The second class comprises clusters with μ_2 -heteroligands, either monoanions of various types, chalcogenide dianions (oxide or, in overlap with the first class, selenide), or imide dianion. This class has the widest representation in Fe–Q–S chemistry and can be further divided into two sub-classes: (i) clusters with μ_2 -Q tightly integrated within compact core frameworks, e.g. clusters 20–22 in Section 5.5.2.3, where Q-bridging is most often an incidental aspect of the overall cluster

synthesis; and (ii) systems with μ_2 -Q introduced specifically to displace terminal ligands and couple pre-existing cluster precursors, resulting in loosely connected aggregates with chemically distinct cluster substructures. The μ_2 -amide and -imide bridged dinuclear Fe-Q-S synthetic intermediates in Section 5.5.3.2 belong to the first sub-class and were constructed deliberately to access heteroligated core environments.

5.5.3.1 Oxide–Sulfide Cores

The first oxide-containing Fe–S cluster, **28**, was obtained in the form of a heterometallic $[\text{Mo}_2\text{Fe}_2\text{OS}_3]$ cubane core from the reaction of the Mo-containing dinuclear cluster **27** with mononuclear iron precursors (Scheme 5.8).¹⁰⁵ The core oxide ligand appears to originate from the terminal Mo=O group in the dinuclear precursor. Limited information is available for this reaction system. Based on the composition and structure of the product, cubane formation in this system might be viewed, in simplified mechanism, as a fragment condensation of two dinuclear **27**, with loss of one oxo ligand *via* atom transfer to phosphine and retention of the other oxo donor as a bridging core ligand; additional ligand substitution and further reduction is necessary, likely involving the iron components of the reaction system. The discovery of **28** predated the first observation of the core heteroligand in the FeMo-cofactor.



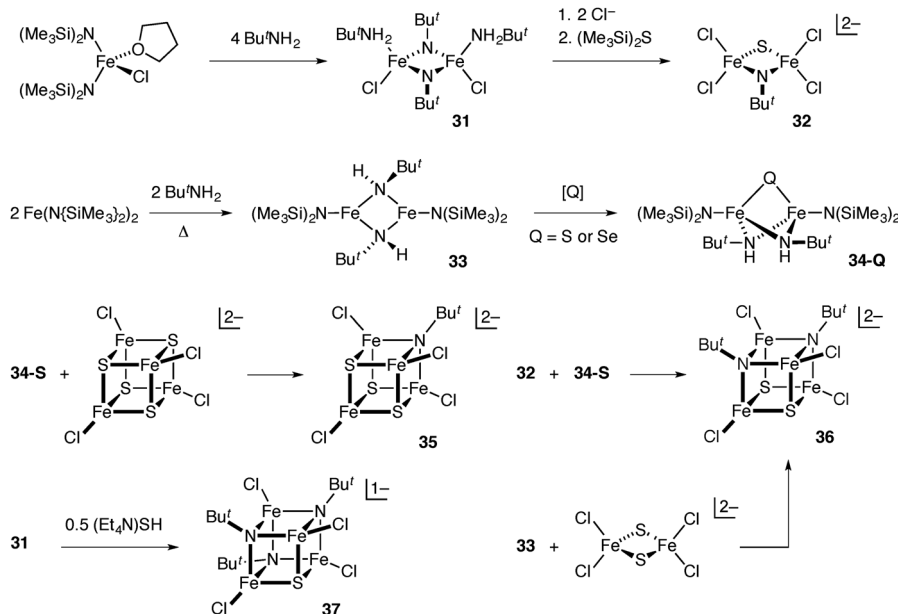
Scheme 5.8 Synthesis of clusters containing iron–oxide–sulfide cores.

In a more recent study, oxide was specifically incorporated into an octanuclear Fe–S framework by Tatsumi and coworkers.¹³⁰ This synthesis (Scheme 5.8), based on the neutral cluster assembly systems of Section 5.5.2.3, involves the reaction of the diferroso alkoxide thiolate precursor **26** ($L = OCPh_3$) with water and elemental sulfur. The two octanuclear products **29** and **30** were co-purified by HPLC and isolated as a mixture in low yield. Single crystals of **30** contain variable amounts of **29** as a minor substitutional impurity and also show orientational disorder in the core framework of **30**; both disorders likely arise from the uniform and symmetrical cluster-encapsulating exteriors afforded by the sterically encumbered ligand set. Cluster **29** is an alkoxide-bridged isoelectronic derivative of the cofactor topological analogues **21** and **22** discussed previously. Cluster **30** is a further isoelectronic derivative of **29**, in which an oxide ligand, apparently derived from water, occurs in place of the μ_6 -sulfide in **29**. The consequent changes in interstitial environment, *e.g.* the reduced ionic radius of oxide, lead to significant structural distortions. An asymmetric framework results, consisting of an Fe_4OS_3 cubane subunit bridged through a single external bond at the trigonal pyramidal μ_4 -oxide to an Fe_4S_3 cuboidal fragment; pendant arene groups on the hindered ligands provide additional, weak interactions that satisfy coordination sites left vacant on the central irons due to the distortion. Although interest in **30** has been framed in the context of the FeMo-cofactor, the cluster can also be viewed as a topological relative of the P^{OX} structure, sharing a core connectivity that differs only in an $Fe_2(\mu_4\text{-O})(\mu_2\text{-OR})$ rhomb substituting for $Fe_2(\mu_4\text{-S})(\mu_2\text{-SCys})$ and a central $\mu_2\text{-SR}$ bridge that is absent in the native cluster.

5.5.3.2 Imide–Sulfide Cores

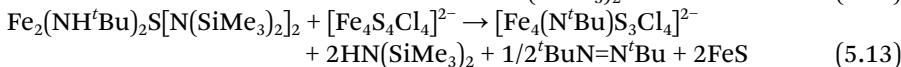
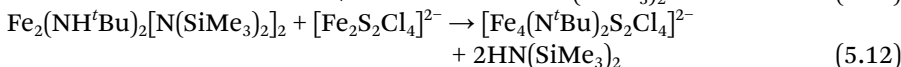
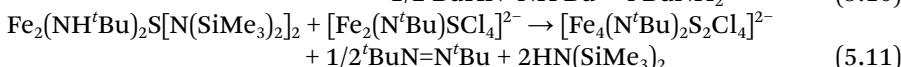
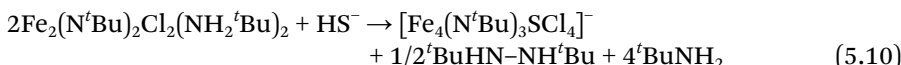
Weak-field iron–imide–sulfide (Fe–NR–S) clusters have been achieved in the author's laboratory. Interest in this general cluster type was inspired not only by the 2p core heteroligand in the FeMo-cofactor but also by speculative molecular mechanisms of cofactor action. A number of mechanistic proposals have invoked the interaction of dinitrogen with the central iron centers in the cofactor and the intermediacy of various iron–nitrogen bonded moieties including core-bound nitrogenous ligands.¹³⁹ These proposals provided the original impetus for our studies of weak-field clusters containing iron and nitrogen anion (N-anion) cores,^{6,140–142} and the resultant chemistry laid the foundation for the directed synthesis of mixed Fe–NR–S species.

The synthetic manifold in Scheme 5.9 summarizes the preparation of mixed-core $[Fe_4(N^tBu)_nS_{4-n}Cl_4]^z$ cubane clusters ($n = 1\text{--}3:35\text{--}37$).^{143,144} The homoleptic $[n, z] = [0, 2\text{--}3\text{--}]$ and $[4, 0/1\text{--}]$ parent species are established, fundamental clusters in Fe–S and Fe–NR chemistry, and the mixed-core derivatives complete the congeneric set. The individual core-heteroligated clusters were synthesized *via* specific, composition-selective routes, with pure products isolated in moderate-to-good yields. The final cubane assembly reactions are all formal fragment condensations that employ a range of di- and



Scheme 5.9 Construction of $[\text{Fe}_4(\text{N}^t\text{Bu})_n\text{S}_{4-n}]^z$ iron-imide-sulfide cubanes ($n = 1–3$).

tetranuclear precursors including simpler, N-anion-sulfide intermediates, *viz.* the dinuclear amide- and imide-sulfide clusters 34-Q and 32. Notional balanced eqn ((5.10)–(5.13)) can be formulated for these condensations, but supporting observation and quantitation of proposed co-products has been hindered by the nature of the weak-field cluster assembly chemistry; these issues, as well as the experimental study of cluster assembly mechanism in these systems, are discussed in the next section.

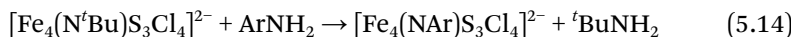


Previous studies^{6,140–142} have demonstrated that the physical properties of Fe-NR clusters generally parallel those of their Fe-S analogues, subject to predictable variations based on recognized differences in ligand characteristics. The mixed-core clusters combine aspects of these limiting homoleptic compositions.¹⁴⁴ Thus, Fe-NR and Fe-NR-S systems remain weak-field in nature and display electronic, structural and redox properties similar to analogous Fe-S clusters. Structurally, Fe-Q distances are shorter, Q–Fe–Q

angles sharper and Fe–Q–Fe angles wider for Q = NR *vs.* S, leading to near right-angle vertices for μ_3 -NR ligands in both homoleptic and heteroleptic cubane frameworks. The strongly donating imide ligands stabilize oxidized core states, leading to progressive linear decreases in potential for equivalent redox couples (-435 mV for $z = 1/-2-$, -385 mV for $z = 2/-3-$, MeCN) for each increment in n . The influence of imide ligation on the electronic structure of these clusters has been probed by XAS spectroscopy and computational analysis; the results reveal a relatively modest effect on core sulfide and terminal chloride bonding in the cubane systems.¹⁴⁵

Chemical differences between imide and sulfide ligand types, however, are substantive and dictate synthetic tactics. In ionic form, N-anions are considerably more basic than sulfur anions (*e.g.* in DMSO:¹⁴⁶ PhNH₂, $pK_a = 30.6$; PhSH, 10.3) and, when coordinated to weak-field iron, the former remain more reactive than the latter. Furthermore, redox transformations coupled to weak-field iron are much more accessible with sulfur than nitrogen. As a result, imide ligation is introduced in Scheme 5.9 by protolysis rather than the salt-metathesis or redox routes typical in Fe–S chemistry. Protolysis requires iron precursors with reactive ligands as latent bases; the relative instability of these complexes forces the incorporation of imide (or equivalent N-anions) early in the synthetic sequence.

Once formed, Fe–NR–S cubane cores are reasonably stable and can be handled under conditions typical in Fe–S chemistry (*e.g.* polar aprotic solvents, anaerobic conditions). Individual clusters show no compositional disproportionation under ambient conditions, and mixtures of species with different core compositions do not react to form new cores.¹⁴⁴ Terminal chloride ligands can be substituted by salt metathesis; for NMR-active ligands, this gives rise to isotropically shifted spectral signatures consistent with the core symmetries observed crystallographically. The μ_3 -N^tBu core ligand can be selectively replaced *via* transamination by arylamines with retention of the core framework (eqn (5.14)); this behavior has been observed in Fe–NR systems, but equivalent reactivity has not been reported in Fe–S chemistry.¹⁴⁷



Of the species generated, cubane **35** has special significance: the 8-atom Fe₄NS₃ core of **35** offers a structural representation of the Fe₄CS₃ subunit of the FeMo-cofactor, with minor deviations similar to those of synthetic heterometal cubanes compared to the MFe₃S₃ fragment of the cofactor (Section 5.2.2).¹⁴⁴ The two synthetic systems are superimposed against the FeMo-cofactor in Figure 5.4, with corresponding relevant distances provided in Table 5.1. Although μ_3 -imide is not μ_6 -carbide, the N-anion ligand is a strongly basic, light atom donor with a formal dianionic charge state commensurate with that of carbide tetraanion divided equally between the two cuboidal halves of the cofactor. This, in conjunction with the presence of terminal monoanions at positions occupied by sulfide in the cofactor, adds electronic correspondence to the structural view of **35** as a topological analogue of the Fe₄CS₃ cubane subunit of the FeMo-cofactor.

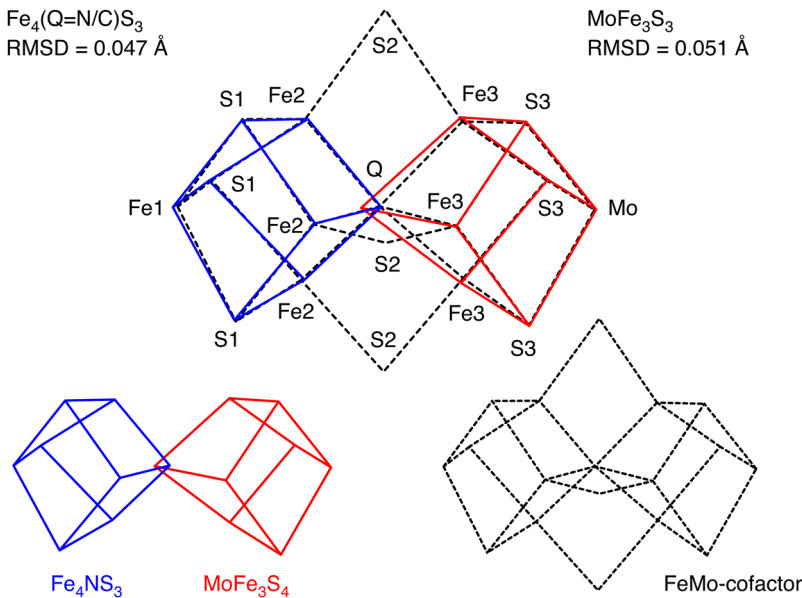


Figure 5.4 Least-squares superpositions (top) of the Fe_4NS_3 core (blue solid lines) of $[\text{Fe}_4(\text{N}^t\text{Bu})_3\text{S}_3\text{Cl}_4]^{2-}$ (35)¹⁴⁴ and the MoFe_3S_3 fragment (red solid lines) of $[(\text{THF})(\text{al}_2\text{cat})\text{MoFe}_3\text{S}_4\text{Cl}_3]^{2-}$ (9, solv = THF, R_1 = allyl, R_2 = H)⁵⁵ against the corresponding Fe_4CS_3 and MoFe_3S_3 portions of the FeMo-cofactor (black dashed lines) in *A. vinelandii* MoFe-protein (1.16 Å resolution²²). Root-mean-square deviations for the fitted fragments are indicated. For reference, the relevant cubane cores of 35 and 9 are shown separately at lower left and the FeMo-cofactor (black dashed lines) at lower right using the same color and line designations per the superposition diagram. Note that the entire MoFe_3S_4 cubane core of 9 is depicted, although only the shared MoFe_3S_3 fragment is fit.

Table 5.1 Comparison^a of selected mean distances (Å) in synthetic clusters 35¹⁴⁴ and 9 (solv = THF, R_1 = allyl, R_2 = H)⁵⁵ against corresponding values in the FeMo-cofactor.²²

	35/FeMo-cofactor	9/FeMo-cofactor	
$\text{Fe}_2\text{-N/C}$	1.953(9)/1.98(5)	Mo-S ₃	2.361(16)/2.345(15)
$\text{Fe}_1\text{-S}_1$	2.292(11)/2.276(14)	Fe ₃ -S ₃	2.277(15)/2.234(18)
$\text{Fe}_2\text{-S}_1$	2.305(6)/2.27(2)	Mo···Fe ₃	2.773(16)/2.69(2)
$\text{Fe}_1\text{-Fe}_2$	2.770(10)/2.665(9)	Fe ₃ ···Fe ₃	2.725(6)/2.614(18)
$\text{Fe}_2\text{-Fe}_2$	2.655(3)/2.654(12)		

^aSee Figure 5.4 for the atom labeling scheme. The metrics are averaged to C_{3v} symmetry for all clusters; for the FeMo-cofactor, all four independent cofactor clusters in the crystal structure are averaged. Listed uncertainties are standard deviations from the mean.

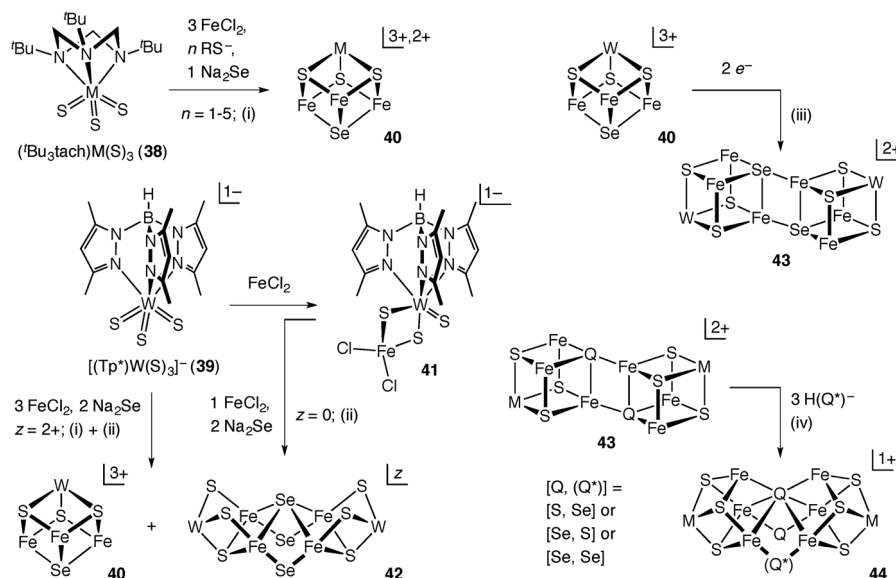
5.6 Cluster Assembly Mechanisms: Chalcogen-Labeled Cores

Mechanistic study of Fe–S cluster assembly is a difficult endeavor. Weak-field cluster formation reactions are multi-step processes marked by exchange lability and low reaction barriers. Cluster assembly systems are often heterogeneous,

iron-containing species are paramagnetic and non-negligible quantities of chemical reaction mass can remain unidentified at the end of reaction. Precise *in situ* monitoring and detection of minor species or intermediates are therefore problematic, as is the complete accounting of reaction products needed to verify hypothetical stoichiometries. Thus, in discussions of cluster syntheses, mechanistic conjectures are inferred largely from perceived compositional and structural relationships between reactants and assigned products.

Recent studies have sought direct evidence of molecular mechanism through the stereochemical disposition of chalcogen labels. Selenium is used as a sulfur-analogue to track the fate of chalcogen-containing components. Although physicochemical differences exist between the two chalcogens – most prominently in atomic radii, but also in other properties such as redox potentials, acid-base behavior and bond strengths – the known parallels between Fe–Se and Fe–S cluster chemistry suggest that selenium is a viable surrogate for sulfur.^{148,149} The physical differences between the chalcogens can be leveraged to permit the facile detection of chalcogen substitution by electron density in crystallographic analyses and by perturbation of isotropically shifted resonances in NMR spectroscopy.

Chalcogen incorporation was monitored in the syntheses in Scheme 5.10;^{113,117,150} compound labels **40**–**44** in this scheme refer to general cluster core configurations without specific reference to terminal ligands. All reactions involved heterometallic clusters prepared from the facially chelated mononuclear molybdenum or tungsten trisulfide species **38**¹⁵⁰ and **39**,¹¹³ and from the previously described MoFe_3S_4 cubane **12-Mo**,¹¹⁷ site-specific



Scheme 5.10 Chalcogen-labeled cluster syntheses ($\text{M} = \text{Mo}, \text{W}$). Roman numerals refer to reaction types indicated in the text. For clarity, only general cluster core frameworks are depicted. Terminal ligands (not shown): **40**, $M-^t\text{Bu}_3\text{tach}$ and $\text{Fe}-(\text{Cl} \text{ or } \text{SR})$ (upper left reaction only); all other clusters, $\text{W}-\text{Tp}^*$, $\text{Mo}-\text{Tp}$, $\text{Fe}-\text{Cl}$ (**40**, **42**), $\text{Fe}-\text{PET}_3$ (**43**), $\text{Fe}-(\text{Q}^*)\text{H}$ (**44**).

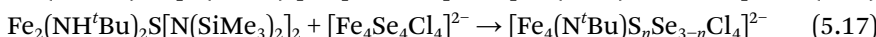
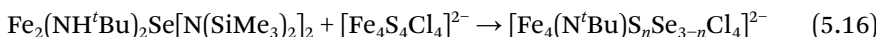
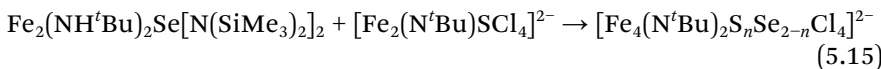
chalcogen incorporation was analyzed by single-crystal diffractometry. Four general cluster assembly systems were investigated:

- (i) *MFe₃S₃Se cubanes (40) from mononuclear MS₃ precursors (38 and 39) and selenium sources.* All systems yielded the MFe₃S₃Se cubane core **40** exclusively, with selenium incorporated specifically at the cubane vertex opposite the heavy metal. The MS₃ moiety appears to remain intact during cluster assembly, serving as one corner of the product cubane. These observations support the view of the MS₃ group as a preorganized “fragment” that templates the condensation of the final cluster structure; this notion is further bolstered by the observation of iron adducts (*e.g.* **41**) and incomplete cubane structures assembled around the MS₃ motif in these systems.^{113,150}
- (ii) *Double cuboidal W₂Fe₆S₆Q₃ cores (42) from a WS₃ precursor (39) and selenide.* As in (i), the WS₃ moiety appears in the final cluster, suggesting a similar role as a discrete preorganized component in cluster assembly.
- (iii) *EBDC cores (43) from MFe₃S₃Se cubanes (40).* The cubane subunits in the EBDC **43** show the same S₃Se arrangement as the single cubane reactant **40**; this observation is consistent with the direct fragment condensation of intact cubane cores to form the EBDC structure. Intercubane bridging occurs at selenium vertices, leading to a distal transoid arrangement of the tungsten centers. This stereochemical outcome might be dictated by the minimization of steric repulsions arising from the facially capped heterometal; all known [MFe₃Q₄]₂ EBDC cores share this heterometal stereochemistry.
- (iv) *P^V-type cores (44) from EBDC cores (43) and hydrochalcoide.* The core transformation is induced by reaction with external hydrochalcoide. Use of all-sulfide and Se-labeled EBDC cores allows assignment of the exogenous chalcogen to a μ_2 bridge position in **44** and the two formerly edge-bridging μ_4 -chalcogens in **43** to μ_2 and μ_6 sites in **44**. In a separate experiment (not shown in Scheme 5.10), hydroselenide was not observed to introduce selenide into the core of all-sulfide **44**, suggesting that exogenous chalcogen incorporation occurs during formation of the product framework.¹¹³ As in the other reactions, local WQ₃ environments persist in the products. From these observations, core rearrangement appears to be an accurate mechanistic description for this reaction, and the principle of least motion holds in terms of final chalcogen positions.

Although the preceding selenium-tracking experiments only reveal the fates of select reactant atoms in cluster assembly, the results nevertheless offer evidence that, in the cases analyzed, the conceptual and descriptive reaction classifications of fragment condensation and core rearrangement have actual, underlying mechanistic bases. Also significant is the consistent behavior of the heterometal environment: the heavy metal-ligand connections are apparently never severed in these cluster assembly

reactions, an outcome explicable based on the higher ligand bond strengths in 4d and 5d metals and the substitutional inertness of these metals relative to high-spin iron. This behavior likely extends to $[MS_4]^z$ precursors as well (see eqn (5.6) and (5.7)) for evidence of templating at M = V), although in these cases a heterometal-chalcogen bond must ultimately be broken to form MFe_3S_4 cubane structures, and it is interesting to speculate whether molybdenum plays a similar stabilizing role in the FeMo-cofactor. Note finally that the observation of heterometal environment stability is based mainly on tungsten-containing systems due to the unavailability of the Mo-analogue of 39; however, identical outcomes were observed in those cases where equivalent molybdenum and tungsten species were studied, and it seems reasonable to assume that the tungsten-exclusive findings will also apply to congeneric molybdenum systems.

The site-selective selenium incorporation manifested in the heterometallic cluster syntheses contrasts with the results of selenium-tracking experiments in Fe–NR–S cubane chemistry.¹⁴⁴ As noted in Section 5.5.3.2, these core-heteroligated species are obtained selectively *via* specific reaction routes that can be described in most cases as stoichiometrically simple fragment condensations of two reactants in equimolar ratio. Selenium-tracking was conducted for the assembly of diimide-disulfide cubane 36 and imide-trisulfide cubane 35 *via* reactions (5.15)–(5.17), with products identified and quantitated by ^1H NMR spectroscopy. In reactions (5.15) and (5.16), the full range of sulfide–selenide compositions was observed, while the all-selenide cluster was the main product in reaction (5.17). A mechanistic interpretation of these outcomes is not apparent. Unlike the examples shown in Scheme 5.10, these systems contain no heterometal, and the precursor fragments involved in the assembly reactions are compositionally and structurally more distant from the end products. The former suggests that exchange lability may complicate tracking experiments or fundamentally alter cluster assembly pathways, while the latter implies that the operative mechanisms are almost certain to be more complex than those in Scheme 5.10.



The selective incorporation of selenium into the central μ_2 -S positions of the FeMo-cofactor was very recently reported.¹⁵¹ Selenium substitution was accomplished through the use of $[\text{SeCN}]^-$ as a non-native nitrogenase substrate under turnover conditions, and the chalcogen label was tracked by macromolecular crystallographic analysis. Selenium was found initially only at the specific μ_2 -S position corresponding to the substitution site observed in the CO-inhibited cofactor structure,²⁷ upon further catalytic turnover

using acetylene substrate, the selenium label was found to redistribute to the other μ_2 -S positions. While these results do not directly address the subject of cluster assembly mechanism, they nevertheless demonstrate the use of chalcogen labels to identify reactive sections of an Fe-S core, which, in this case, may have implications for nitrogenase catalysis mechanisms.

5.7 Status and Prospects

At this juncture, the metalloclusters of nitrogenase persist as remarkable and challenging targets for inorganic synthesis. Significant progress has been made. Corroborative synthetic analogues exist for the all-ferrous state of the F-cluster and the local Mo-Fe-S environment of the FeMo-cofactor; efforts to model the latter have led to general, systematic methods for selective heterometal incorporation in Fe-S systems. Topological analogues now reproduce the overall framework connectivity of both nitrogenase superclusters; the convergence to VFDC structures in unrelated systems suggests that this octanuclear core framework, unsuspected in Fe-S chemistry prior to their revelation in the biological clusters, is actually a readily attainable and general motif. Finally, the discovery of the interstitial light atom ligand in the FeMo-cofactor has prompted the synthesis of analogous heteroligated Fe-S cores; while this area is still at an early stage of development, it is clear that the addition of another cluster core component will, like the earlier introduction of heterometals, greatly expand the range of Fe-S chemistry.

All of this progress has depended on the successful synthesis of specific cluster targets. The directed construction of nitrogenase-relevant clusters remains simultaneously an empirical and rational endeavor. An intrinsic degree of unpredictability is expected given the nature of weak-field cluster chemistry. However, recent results show that the crude conceptions of cluster assembly reactions used in synthetic planning are indeed mechanistically accurate in some cases. The development of deeper insight into cluster formation chemistry will enhance synthetic analysis and capabilities. These chemical investigations will also complement the considerable, ongoing progress being made in the biochemical description of Fe-S^{152,153} and nitrogenase¹⁵⁴ cluster biosynthesis.

The examples in this chapter represent only a fraction of the extensive synthetic chemistry inspired by the nitrogenase clusters, but they clearly illustrate contributions, deliberate and serendipitous, obtained from speculative synthetic analogue study. Nitrogenase has long served as an inspiration for creative studies in fundamental inorganic chemistry, and it will certainly continue in this role for the foreseeable future.

Abbreviations

al₂cat	3,6-Diallylcatecholate(2-)
^tBu₃tach	1,3,5-Tri- <i>tert</i> -butyl-1,3,5-triazacyclohexane
Cl₄cat	Tetrachlorocatecholate(2-)

Cp	Cyclopentadienide(1−)
DMF	Dimethylformamide
DmpS	2,6-Dimesitylbenzenethiolate(1−)
EBDC	Edge-bridged double cubane
ENDOR	Electron nuclear double resonance
ESEEM	Electron spin echo envelope modulation
EXAFS	Extended X-ray absorption fine structure
HPLC	High-performance liquid chromatography
MeCN	Acetonitrile
NHC	N-heterocyclic carbene
iPr₂NHCMe₂	1,3-Diisopropyl-4,5-dimethylimidazol-2-ylidene
NR	Imide
Q	Cluster core ligand
RMSD	Root-mean-square deviation
SCE	Saturated calomel electrode
THF	Tetrahydrofuran
TipS	2,4,6-Triisopropylbenzenethiolate(1−)
Tp	Tris(pyrazolyl)hydroborate(1−)
Tp*	Tris(3,5-dimethylpyrazolyl)hydroborate(1−)
VFDC	Vertex-fused double cubane
XAS	X-ray absorption spectroscopy
XES	X-ray emission spectroscopy

Acknowledgements

It is a genuine pleasure to dedicate this chapter to Richard H. Holm, whose preeminent contributions to inorganic and bioinorganic chemistry are well-known and, for the specific area of nitrogenase cluster analogue studies, prominent throughout this present account. It is the author's distinct privilege to have had continuing opportunities to learn from and work with Dick Holm over the years. Recent research on metal cluster chemistry in the author's laboratory has been supported by the National Science and Engineering Research Council.

References

1. B. K. Burgess and D. J. Lowe, *Chem. Rev.*, 1996, **96**, 2983.
2. J. B. Howard and D. C. Rees, *Chem. Rev.*, 1996, **96**, 2965.
3. J. A. Ibers and R. H. Holm, *Science*, 1980, **209**, 223.
4. S. C. Lee and R. H. Holm, *Proc. Natl. Acad. Sci. U. S. A.*, 2003, **100**, 3595.
5. (a) I. Čorić and P. L. Holland, *J. Am. Chem. Soc.*, 2016, **138**, 7200; (b) K. C. MacLeod and P. L. Holland, *Nat. Chem.*, 2013, **5**, 559.
6. S. C. Lee and R. H. Holm, *Chem. Rev.*, 2004, **104**, 1135.
7. S. C. Lee, W. Lo and R. H. Holm, *Chem. Rev.*, 2014, **114**, 3579.
8. S. M. Malinak and D. Coucouvanis, *Prog. Inorg. Chem.*, 2001, **49**, 592.
9. P. A. Eldredge and B. A. Averill, *J. Cluster Sci.*, 1990, **1**, 269.

10. Y. Ohki and K. Tatsumi, *Z. Anorg. Allg. Chem.*, 2013, **639**, 1340.
11. M. M. Georgiadis, H. Komiya, P. Chakrabarti, D. Woo, J. J. Kornuc and D. C. Rees, *Science*, 1992, **257**, 1653.
12. J. L. Schlessman, D. Woo, L. Joshua-Tor, J. B. Howard and D. C. Rees, *J. Mol. Biol.*, 1998, **280**, 669.
13. S. B. Jang, L. C. Seefeldt and J. W. Peters, *Biochemistry*, 2000, **39**, 641.
14. S. B. Jang, L. C. Seefeldt and J. W. Peters, *Biochemistry*, 2000, **39**, 14745.
15. P. Strop, P. M. Takahara, H.-J. Chiu, H. C. Angove, B. K. Burgess and D. C. Rees, *Biochemistry*, 2001, **40**, 651.
16. P. V. Rao and R. H. Holm, *Chem. Rev.*, 2004, **104**, 527.
17. S. J. Yoo, H. C. Angove, B. K. Burgess, M. P. Hendrich and E. Münck, *J. Am. Chem. Soc.*, 1999, **121**, 2534.
18. M. Hans, W. Buckel and E. Bill, *JBIC, J. Biol. Inorg. Chem.*, 2008, **13**, 563.
19. K. Rupnik, C. C. Lee, J. A. Wiig, Y. Hu, M. W. Ribbe and B. J. Hales, *Biochemistry*, 2014, **53**, 1108.
20. J. W. Peters, M. H. Stowell, S. M. Soltis, M. G. Finnegan, M. K. Johnson and D. C. Rees, *Biochemistry*, 1997, **36**, 1181.
21. S. M. Mayer, D. M. Lawson, C. A. Gormal, S. M. Roe and B. E. Smith, *J. Mol. Biol.*, 1999, **292**, 871.
22. O. Einsle, F. A. Tezcan, S. L. A. Andrade, B. Schmid, M. Yoshida, J. B. Howard and D. C. Rees, *Science*, 2002, **297**, 1696.
23. T. Spatzal, M. Aksoyoglu, L. Zhang, S. L. A. Andrade, E. Schleicher, S. Weber, D. C. Rees and O. Einsle, *Science*, 2011, **334**, 940.
24. R. Bjornsson, F. Neese, R. R. Schrock, O. Einsle and S. DeBeer, *JBIC, J. Biol. Inorg. Chem.*, 2015, **20**, 447.
25. B. M. Hoffman, D. R. Dean and L. C. Seefeldt, *Acc. Chem. Res.*, 2009, **42**, 609.
26. B. M. Hoffman, D. Lukyanov, Z.-Y. Yang, D. R. Dean and L. C. Seefeldt, *Chem. Rev.*, 2014, **114**, 4041.
27. T. Spatzal, K. A. Perez, O. Einsle, J. B. Howard and D. C. Rees, *Science*, 2014, **345**, 1620.
28. V. K. Shah and W. J. Brill, *Proc. Natl. Acad. Sci. U. S. A.*, 1977, **74**, 3249.
29. B. K. Burgess, *Chem. Rev.*, 1990, **90**, 1377.
30. (a) B. E. Smith, M. C. Durrant, S. A. Fairhurst, C. A. Gormal, K. L. C. Grönberg, R. A. Henderson, S. K. Ibrahim, T. Le Gall and C. J. Pickett, *Coord. Chem. Rev.*, 1999, **185–186**, 669; (b) C. C. Lee, Y. Hu and M. W. Ribbe, *Angew. Chem. Int. Ed.*, 2012, **51**, 1947; (c) C. C. Lee, Y. Hu and M. W. Ribbe, *Angew. Chem. Int. Ed.*, 2015, **54**, 1219; (d) C. C. Lee, Y. Hu and M. W. Ribbe, *mBio*, 2015, **6**, e00307–15.
31. R. R. Eady, *Chem. Rev.*, 1996, **96**, 3013.
32. R. R. Eady, *Coord. Chem. Rev.*, 2003, **237**, 23.
33. Y. Hu, C. C. Lee and M. W. Ribbe, *Dalton Trans.*, 2012, **41**, 1118.
34. B. V. DePamphilis, B. A. Averill, T. Herskovitz, L. Que and R. H. Holm, *J. Am. Chem. Soc.*, 1974, **96**, 4159.
35. J. Cambray, R. W. Lane, A. G. Wedd, R. W. Johnson and R. H. Holm, *Inorg. Chem.*, 1977, **16**, 2565.

36. C. Zhou, J. W. Raebiger, B. M. Segal and R. H. Holm, *Inorg. Chim. Acta*, 2000, **300–302**, 892.
37. T. A. Scott and H.-C. Zhou, *Angew. Chem., Int. Ed.*, 2004, **43**, 5628.
38. T. A. Scott, C. P. Berlinguette, R. H. Holm and H.-C. Zhou, *Proc. Natl. Acad. Sci. U. S. A.*, 2005, **102**, 9741.
39. G. Christou and C. D. Garner, *J. Chem. Soc., Dalton Trans.*, 1979, 1093.
40. L. Deng and R. H. Holm, *J. Am. Chem. Soc.*, 2008, **130**, 9878.
41. M. Chakrabarti, L. Deng, R. H. Holm, E. Münck and E. L. Bominaar, *Inorg. Chem.*, 2009, **48**, 2735.
42. S. P. Cramer, W. O. Gillum, K. O. Hodgson and L. E. Mortenson, *J. Am. Chem. Soc.*, 1978, **100**, 3398.
43. S. P. Cramer, W. O. Gillum, K. O. Hodgson, L. E. Mortenson, E. I. Stiefel, J. R. Chisnell, W. J. Brill and V. K. Shah, *J. Am. Chem. Soc.*, 1978, **100**, 3814.
44. T. E. Wolff, J. M. Berg, C. Warrick, K. O. Hodgson, R. H. Holm and R. B. Frankel, *J. Am. Chem. Soc.*, 1978, **100**, 4630.
45. T. E. Wolff, J. M. Berg, K. O. Hodgson, R. B. Frankel and R. H. Holm, *J. Am. Chem. Soc.*, 1979, **101**, 4140.
46. T. E. Wolff, J. M. Berg, P. P. Power, K. O. Hodgson and R. H. Holm, *Inorg. Chem.*, 1980, **19**, 430.
47. T. E. Wolff, P. P. Power, R. B. Frankel and R. H. Holm, *J. Am. Chem. Soc.*, 1980, **102**, 4694.
48. G. Christou and C. D. Garner, *J. Chem. Soc., Dalton Trans.*, 1980, 2354.
49. G. Christou, P. K. Mascharak, W. H. Armstrong, G. C. Papaefthymiou, R. B. Frankel and R. H. Holm, *J. Am. Chem. Soc.*, 1982, **104**, 2820.
50. J. Rawlings, V. K. Shah, J. R. Chisnell, W. J. Brill, R. Zimmerman, E. Münck and W. H. Orme-Johnson, *J. Biol. Chem.*, 1978, **253**, 1001.
51. B. M. Hoffman, J. E. Roberts and W. H. Orme-Johnson, *J. Am. Chem. Soc.*, 1982, **104**, 860.
52. W. H. Armstrong and R. H. Holm, *J. Am. Chem. Soc.*, 1981, **103**, 6246.
53. W. H. Armstrong, P. K. Mascharak and R. H. Holm, *J. Am. Chem. Soc.*, 1982, **104**, 4373.
54. P. K. Mascharak, W. H. Armstrong, Y. Mizobe and R. H. Holm, *J. Am. Chem. Soc.*, 1983, **105**, 475.
55. R. E. Palermo and R. H. Holm, *J. Am. Chem. Soc.*, 1983, **105**, 4310.
56. R. E. Palermo, R. Singh, J. K. Bashkin and R. H. Holm, *J. Am. Chem. Soc.*, 1984, **106**, 2600.
57. J. Huang, C. Goh and R. H. Holm, *Inorg. Chem.*, 1997, **36**, 356.
58. D. V. Fomitchev, C. C. McLauchlan and R. H. Holm, *Inorg. Chem.*, 2002, **41**, 958.
59. R. H. Holm, *Adv. Inorg. Chem.*, 1992, **38**, 1.
60. W. Cen, S. C. Lee, J. Li, F. M. MacDonnell and R. H. Holm, *J. Am. Chem. Soc.*, 1993, **115**, 9515.
61. J. A. Kovacs and R. H. Holm, *J. Am. Chem. Soc.*, 1986, **108**, 340.
62. J. A. Kovacs and R. H. Holm, *Inorg. Chem.*, 1987, **26**, 702.
63. J. A. Kovacs and R. H. Holm, *Inorg. Chem.*, 1987, **26**, 711.

64. R. H. Holm and E. D. Simhon, *Molybdenum Enzymes*, Wiley, New York, 1985, ch. 1.
65. R. Bjornsson, F. A. Lima, T. Spatzal, T. Weyhermüller, P. Glatzel, E. Bill, O. Einsle, F. Neese and S. DeBeer, *Chem. Sci.*, 2014, **5**, 3096.
66. R. Bjornsson, M. U. Delgado-Jaime, F. A. Lima, D. Sippel, J. Schlesier, T. Weyhermüller, O. Einsle, F. Neese and S. DeBeer, *Z. Anorg. Allg. Chem.*, 2015, **641**, 65.
67. S. M. Malinak, K. D. Demadis and D. Coucouvanis, *J. Am. Chem. Soc.*, 1995, **117**, 3126.
68. T. A. Scott and R. H. Holm, *Inorg. Chem.*, 2008, **47**, 3426.
69. T. Yamamura, G. Christou and R. H. Holm, *Inorg. Chem.*, 1983, **22**, 939.
70. (a) B. D. Yuhas, A. L. Smeigh, A. P. Douvalis, M. R. Wasielewski and M. G. Kanatzidis, *J. Am. Chem. Soc.*, 2012, **134**, 10353; (b) A. Banerjee, B. D. Yuhas, E. A. Margulies, Y. Zhang, Y. Shim, M. R. Wasielewski and M. G. Kanatzidis, *J. Am. Chem. Soc.*, 2015, **137**, 2030.
71. T. Le Gall, S. K. Ibrahim, C. A. Gormal, B. E. Smith and C. J. Pickett, *Chem. Commun.*, 1999, 773.
72. K. D. Demadis and D. Coucouvanis, *Inorg. Chem.*, 1995, **34**, 436.
73. J. Huang, S. Mukerjee, B. M. Segal, H. Akashi, J. Zhou and R. H. Holm, *J. Am. Chem. Soc.*, 1997, **119**, 8662.
74. D. Coucouvanis, P. E. Mosier, K. D. Demadis, S. Patton, S. M. Malinak, C. G. Kim and M. A. Tyson, *J. Am. Chem. Soc.*, 1993, **115**, 12193.
75. L. J. Laughlin and D. Coucouvanis, *J. Am. Chem. Soc.*, 1995, **117**, 3118.
76. S. M. Malinak, K. D. Demadis and D. Coucouvanis, *J. Am. Chem. Soc.*, 1995, **117**, 3126.
77. D. Coucouvanis, K. D. Demadis, S. M. Malinak, P. E. Mosier, M. A. Tyson and L. J. Laughlin, *J. Mol. Catal. A: Chem.*, 1996, **107**, 123.
78. K. D. Demadis, S. M. Malinak and D. Coucouvanis, *Inorg. Chem.*, 1996, **35**, 4038.
79. S. M. Malinak, A. M. Simeonov, P. E. Mosier, C. E. McKenna and D. Coucouvanis, *J. Am. Chem. Soc.*, 1997, **119**, 1662.
80. M. K. Johnson, R. E. Duderstadt and E. C. Duin, *Adv. Inorg. Chem.*, 1999, **47**, 1.
81. H. Dobbek, V. Svetlitchnyi, L. Gremer, R. Huber and O. Meyer, *Science*, 2001, **293**, 1281.
82. C. L. Drennan, J. Heo, M. D. Sintchak, E. Schreiter and P. W. Ludden, *Proc. Natl. Acad. Sci. U. S. A.*, 2001, **98**, 11973.
83. H. Dobbek, V. Svetlitchnyi, J. Liss and O. Meyer, *J. Am. Chem. Soc.*, 2004, **126**, 5382.
84. J. Zhou, M. J. Scott, Z. Hu, G. Peng, E. Münck and R. H. Holm, *J. Am. Chem. Soc.*, 1992, **114**, 10843.
85. J. Zhou, J. W. Raebiger, C. A. Crawford and R. H. Holm, *J. Am. Chem. Soc.*, 1997, **119**, 6242.
86. P. R. Challen, S. M. Koo, W. R. Dunham and D. Coucouvanis, *J. Am. Chem. Soc.*, 1990, **112**, 2455.
87. J. Huang and R. H. Holm, *Inorg. Chem.*, 1998, **37**, 2247.
88. J. Kim and D. C. Rees, *Nature*, 1992, **360**, 553.

89. J. Kim and D. C. Rees, *Science*, 1992, **257**, 1667.
90. M. K. Chan, J. Kim and D. C. Rees, *Science*, 1993, **260**, 792.
91. C. T. W. Chu and L. F. Dahl, *Inorg. Chem.*, 1977, **16**, 3245.
92. M. J. Scott and R. H. Holm, *Angew. Chem., Int. Ed. Engl.*, 1993, **32**, 564.
93. C. Goh and R. H. Holm, *Inorg. Chim. Acta*, 1998, **270**, 46.
94. M. A. Tyson and D. Coucouvanis, *Inorg. Chem.*, 1997, **36**, 3808.
95. J. Han, K. Beck, N. Ockwig and D. Coucouvanis, *J. Am. Chem. Soc.*, 1999, **121**, 10448.
96. D. Coucouvanis, J. Han and N. Moon, *J. Am. Chem. Soc.*, 2002, **124**, 216.
97. K. D. Demadis, C. F. Campana and D. Coucouvanis, *J. Am. Chem. Soc.*, 1995, **117**, 7832.
98. E. Nordlander, S. C. Lee, W. Cen, Z. Y. Wu, C. R. Natoli, A. Di Cicco, A. Filippioni, B. Hedman, K. O. Hodgson and R. H. Holm, *J. Am. Chem. Soc.*, 1993, **115**, 5549.
99. W. Cen, F. M. MacDonnell, M. J. Scott and R. H. Holm, *Inorg. Chem.*, 1994, **33**, 5809.
100. J. Fritsch, P. Scheerer, S. Frielingsdorf, S. Kroschinsky, B. Friedrich, O. Lenz and C. M. T. Spahn, *Nature*, 2011, **479**, 249.
101. Y. Shomura, K.-S. Yoon, H. Nishihara and Y. Higuchi, *Nature*, 2011, **479**, 253.
102. C. Goh, B. M. Segal, J. Huang, J. R. Long and R. H. Holm, *J. Am. Chem. Soc.*, 1996, **118**, 11844.
103. H.-C. Zhou and R. H. Holm, *Inorg. Chem.*, 2003, **42**, 11.
104. F. Osterloh, B. M. Segal, C. Achim and R. H. Holm, *Inorg. Chem.*, 2000, **39**, 980.
105. J. Han, M. Koutmos, S. Al-Ahmad and D. Coucouvanis, *Inorg. Chem.*, 2001, **40**, 5985.
106. C. Hauser, E. Bill and R. H. Holm, *Inorg. Chem.*, 2002, **41**, 1615.
107. Y. Zhang, J.-L. Zuo, H.-C. Zhou and R. H. Holm, *J. Am. Chem. Soc.*, 2002, **124**, 14292.
108. Y. Zhang and R. H. Holm, *J. Am. Chem. Soc.*, 2003, **125**, 3910.
109. J.-L. Zuo, H.-C. Zhou and R. H. Holm, *Inorg. Chem.*, 2003, **42**, 4624.
110. Y. Zhang and R. H. Holm, *Inorg. Chem.*, 2004, **43**, 674.
111. C. P. Berlinguette, T. Miyaji, Y. Zhang and R. H. Holm, *Inorg. Chem.*, 2006, **45**, 1997.
112. R. P. Pesavento, C. P. Berlinguette and R. H. Holm, *Inorg. Chem.*, 2007, **46**, 510.
113. B. Zheng, X.-D. Chen, S.-L. Zheng and R. H. Holm, *J. Am. Chem. Soc.*, 2012, **134**, 6479.
114. N. Taniyama, Y. Ohki and K. Tatsumi, *Inorg. Chem.*, 2014, **53**, 5438.
115. F. Osterloh, Y. Sanakis, R. J. Staples, E. Müncck and R. H. Holm, *Angew. Chem., Int. Ed.*, 1999, **38**, 2066.
116. F. Osterloh, C. Achim and R. H. Holm, *Inorg. Chem.*, 2001, **40**, 224.
117. C. P. Berlinguette and R. H. Holm, *J. Am. Chem. Soc.*, 2006, **128**, 11993.
118. M. L. Hlavinka, T. Miyaji, R. J. Staples and R. H. Holm, *Inorg. Chem.*, 2007, **46**, 9192.
119. Y. Ohki and K. Tatsumi, *Z. Anorg. Allg. Chem.*, 2013, **639**, 1340.

120. Y. Ohki, *Bull. Chem. Soc. Jpn.*, 2014, **87**, 1.
121. I. Noda, B. S. Snyder and R. H. Holm, *Inorg. Chem.*, 1986, **25**, 3851.
122. B. S. Snyder and R. H. Holm, *Inorg. Chem.*, 1988, **27**, 2339.
123. M. S. Reynolds and R. H. Holm, *Inorg. Chem.*, 1988, **27**, 4494.
124. U. Bierbach, W. Saak, D. Haase and S. Pohl, *Z. Naturforsch.*, 1991, **46b**, 1629.
125. C. Goh, A. Nivorozhkin, S. J. Yoo, E. L. Bominaar, E. Münck and R. H. Holm, *Inorg. Chem.*, 1998, **37**, 2926.
126. Y. Ohki, Y. Sunada, M. Honda, M. Katada and K. Tatsumi, *J. Am. Chem. Soc.*, 2003, **125**, 4052.
127. Y. Ohki, Y. Ikagawa and K. Tatsumi, *J. Am. Chem. Soc.*, 2007, **129**, 10457.
128. Y. Ohki, M. Imada, A. Murata, Y. Sunada, S. Ohta, M. Honda, T. Sasamori, N. Tokitoh, M. Katada and K. Tatsumi, *J. Am. Chem. Soc.*, 2009, **131**, 13168.
129. Y. Ohki, K. Tanifuji, N. Yamada, R. E. Cramer and K. Tatsumi, *Chem.-AsianJ.*, 2012, **7**, 2222.
130. S. Ohta, Y. Ohki, T. Hashimoto, R. E. Cramer and K. Tatsumi, *Inorg. Chem.*, 2012, **51**, 11217.
131. M. J. Zdilla, A. K. Verma and S. C. Lee, *Inorg. Chem.*, 2008, **47**, 11382.
132. Y. Ohki, Y. Sunada and K. Tatsumi, *Chem. Lett.*, 2005, **34**, 172.
133. C. R. Sharp, J. S. Duncan and S. C. Lee, *Inorg. Chem.*, 2010, **49**, 6697.
134. K. M. Lancaster, M. Roemelt, P. Ettenhuber, Y. Hu, M. W. Ribbe, F. Neese, U. Bergmann and S. DeBeer, *Science*, 2011, **334**, 974.
135. J. A. Wiig, Y. Hu, C. C. Lee and M. W. Ribbe, *Science*, 2012, **337**, 1672.
136. J. A. Wiig, C. C. Lee, Y. Hu and M. W. Ribbe, *J. Am. Chem. Soc.*, 2013, **135**, 4982.
137. Some examples: (a) E. H. Braye, L. F. Dahl, W. Hubel and D. L. Wampler, *J. Am. Chem. Soc.*, 1962, **84**, 4633; (b) M. R. Churchill, J. Wormald, J. Knight and M. J. Mays, *J. Am. Chem. Soc.*, 1971, **93**, 3073; (c) E. M. Holt, K. H. Whitmire and D. F. Shriver, *J. Organomet. Chem.*, 1981, **20**, 3119.
138. Some examples: (a) D. Mansuy, J.-P. Lecomte, J.-C. Chottard and J.-F. Bartoli, *Inorg. Chem.*, 1981, **20**, 3119; (b) G. Rossi, V. L. Goedken and C. Ercolani, *J. Chem. Soc., Chem. Commun.*, 1988, 46; (c) L. Galich, A. Kienast, H. Huckstadt and H. Homborg, *Z. Anorg. Allg. Chem.*, 1998, **624**, 1235.
139. J. W. Peters and R. K. Szilagyi, *Curr. Opin. Chem. Biol.*, 2006, **10**, 101.
140. J. S. Duncan, T. M. Nazif, A. K. Verma and S. C. Lee, *Inorg. Chem.*, 2003, **42**, 1211.
141. J. S. Duncan, M. J. Zdilla and S. C. Lee, *Inorg. Chem.*, 2007, **46**, 1071.
142. M. J. Zdilla, A. K. Verma and S. C. Lee, *Inorg. Chem.*, 2011, **50**, 1551.
143. X.-D. Chen, J. S. Duncan, A. K. Verma and S. C. Lee, *J. Am. Chem. Soc.*, 2010, **123**, 15884.
144. X.-D. Chen, W. Zhang, J. S. Duncan and S. C. Lee, *Inorg. Chem.*, 2012, **51**, 12891.
145. C. J. Pollock, L. L. Tan, W. Zhang, K. M. Lancaster, S. C. Lee and S. DeBeer, *Inorg. Chem.*, 2014, **53**, 2591.

146. F. G. Bordwell, *Acc. Chem. Res.*, 1988, **21**, 456.
147. L. L. Tan, B. Nayyar, M. K. Devgan and S. C. Lee, unpublished work.
148. S. B. Yu, G. C. Papaefthymiou and R. H. Holm, *Inorg. Chem.*, 1991, **30**, 3476.
149. L. L. Tan, R. H. Holm and S. C. Lee, *Polyhedron*, 2013, **58**, 206.
150. A. Majumdar and R. H. Holm, *Inorg. Chem.*, 2011, **50**, 11242.
151. T. Spatzal, K. A. Perez, J. B. Howard and D. C. Rees, *eLife*, 2015, DOI: 10.7554/eLife.11620.
152. R. Lill, *Nature*, 2009, **460**, 831.
153. E. M. Shephard, E. S. Boyd, J. B. Broderick and J. W. Peters, *Curr. Opin. Chem. Biol.*, 2011, **15**, 319.
154. M. W. Ribbe, Y. Hu, K. O. Hodgson and B. Hedman, *Chem. Rev.*, 2014, **114**, 4063.

CHAPTER 6

Synthesis of Mono- and Bisdithiolene Molybdenum and Tungsten Model Compounds

HIDEKI SUGIMOTO^{†a}

^aDepartment of Material and Life Science, Graduate School of Engineering, Osaka University, 2-1 Yamadaoka, Suita, Osaka, Japan

*E-mail: sugimoto@mls.eng.osaka-u.ac.jp

6.1 Introduction

Molybdenum (Mo) and tungsten (W) are unique 4d (Mo) and 5d (W) transition elements found in biological systems. Mo is the most abundant transition metal in sea water and is present as $[Mo^{VI}O_4]^{2-}$ with a high concentration of 1×10^{-2} mg L⁻¹. This means that entire biological ecosystems cover their Mo demand ultimately from the sea. Both Mo and W vary from +4 (d²) to +6 (d⁰) oxidation states in the biological reaction cycles. Because 3d transition metals in biological systems adopt oxidation states from +1 to +5,¹ Mo and W ions are in comparison harder than the 3d transition metal ions in biological reactions with respect to the HSAB rule (hard acid, hard base; soft acid, soft base). Due to their higher charge, the ionic radii are close to those of the 3d metal ions; 0.79–0.73 Å for Mo(IV)–Mo(VI); 0.80–0.74 Å for W(IV)–W(VI); and 0.91–0.67 Å for the 3d transition metal ions despite the atomic radii of

[†]This chapter is personally dedicated to Dr R. H. Holm, Dr D. Garner and Dr J. H. Enemark.

Synthesis of Mono- and Bisdithiolene Molybdenum and Tungsten Model Compounds 167

Mo (1.40 Å) and W (1.41 Å) being significantly larger than those of the latter (1.35–1.25 Å).²

Mo- and W-containing enzymes participate in a wide range of reactions in carbon, sulfur and nitrogen metabolism. As a result, Mo or W enzymes are present in all forms of life from ancient archaea to human beings.^{1,3,4,5} Until now, more than 50 Mo enzymes have been reported. With respect to W enzymes, about a dozen examples have been characterized, most of which are found in hyperthermophilic archaea growing at ~100 °C.⁴ The majority of Mo and W enzymes are oxotransferases and/or hydroxylases, which catalyze the forward reaction of the following net oxygen atom exchange or the backward reaction, coupled to proton and electron transfer between substrate E (or R-H)/EO (or R-OH) and an Fe-S cluster, heme or flavin.



This type of reaction involves proton-coupled electron transfer (PCET) and utilizes water as an ultimate source or sink of oxygen. PCETs are reactions in which there is a change in both electron and proton content between reactants and products, resulting in the net transfer of formally H⁰, and which allow the build-up of multiple redox components.⁶ As a result, this reaction type is a cornerstone of many important biological energy conversion processes such as dihydrogen oxidation in hydrogenase, dinitrogen fixation in nitrogenase, dioxygen reduction in cytochrome *c* oxidase and dioxygen evolution in Photosystem II.¹

All Mo centers at the active sites are coordinated with one or two metal-binding pyranopterin dithiolene (MPT) ligands with an ene-1,2-dithiolate moiety.^{3,4} The Mo enzymes that bear a Mo center coordinated by two MPT ligands were classified into the dimethylsulfoxide reductase (DMSOR) family. The Mo enzymes having only one MPT ligand were classified into two groups. One is the sulfite oxidase family, the members of which have Mo centers possessing one additional amino acid residue, and the other is the xanthine oxidase family with Mo centers not coordinated by an amino acid residue. On the other hand, all of the known W centers of the W enzymes are coordinated by two MPTs. A schematic representation of the families is shown in Figure 6.1. Such MPT ligation is unique in the Mo and W oxidoreductase enzymes and has not been found in any other metal bearing enzyme. When dithiolene ligands coordinate to a transition metal, the metal complex can display interesting redox, valence tautomeric and geometric chemistry arising out of the “redox active property” of dithiolenes as indicated in Figure 6.2.⁷ Consequently, there is an open question regarding the exact role of MPT during catalytic turnovers of the Mo and W enzyme reaction centers. Because most of the Mo and W enzymes include neighboring Fe-S clusters, hemes and/or flavins, which have strongly absorbing chromophores, observation of the electronic transitions of the Mo or W reaction centers is difficult. Additionally, such sulfur-rich coordination environments of the reaction centers often result in unfavorable structural changes of the reaction centers to the catalytically inactive ones by air oxidation or hydrolytic reactions. Therefore,

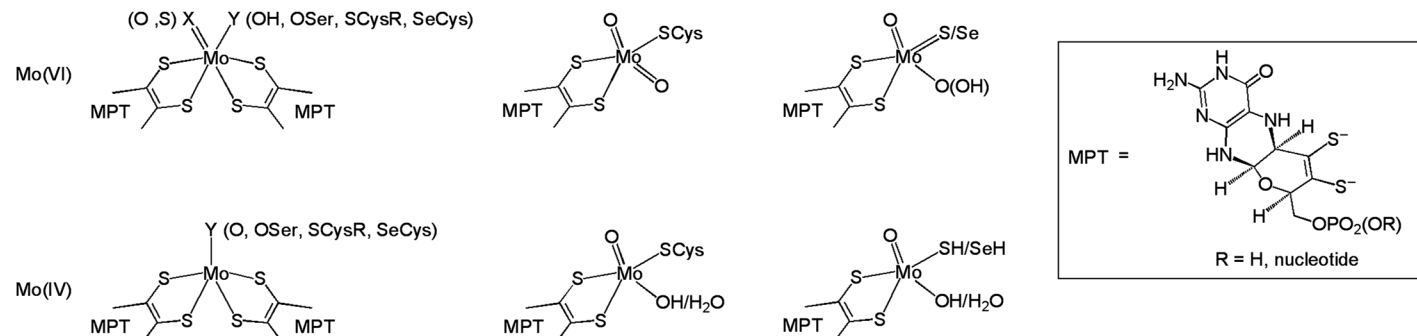


Figure 6.1 Schematic active site structures of DMSO reductase (left), sulfite oxidase (middle) and xanthine oxidase (right) families, and the structure of pyranopterindithiolate (MPT).

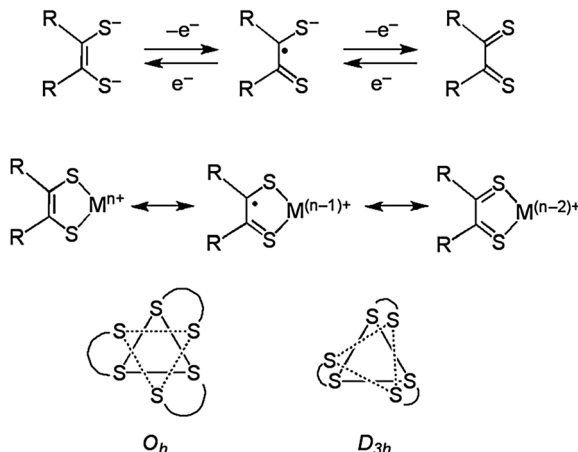


Figure 6.2 Non-innocence of dithiolenes and its consequences: redox (top), valence tautomerism (middle) and geometry (bottom). Reproduced from ref. 36 with permission from The Royal Society of Chemistry.

model compounds of the Mo and W enzyme reaction centers can help in understanding the coordination structure-electronic structure-function relationship of the enzymes' reaction centers.

Until 1996, additional ligands besides MPT at the metal centers of the Mo and W enzymes had been believed to be oxo ligands because of the frequent occurrence of $M^{IV}O$ and $M^{VI}O_2$ units ($M = Mo$ and W) in synthetic and natural Mo and W compounds.^{2,3,4} However, progress of X-ray crystallographic, EXAFS and XAS analytical techniques have provided the evidence for a variety of amino acid residues coordinating to the Mo and W centers of the enzymes as monodentate or bidentate ligands. Since the discovery of the "true" active site structures, much synthetic effort has gone into modeling these unusual Mo and W coordination structures. This chapter describes the advances made with mono(ene-1,2-dithiolate) and bis(ene-dithiolate) Mo and W models. Although aromatic dithiolates such as benzene-1,2-dithiolate (bdt) in a strict sense are "not true ene-1,2-dithiolates", bdt had been frequently employed as an easily accessible ligand in the early stages of the respective model studies. Therefore, some of the model compounds with aromatic dithiolates are also included in this chapter.

6.2 Model Compounds for the DMSOR Family

As mentioned above, enzymes of the DMSOR family are distinguished from other molybdenum enzymes by the presence of a bis(MPT)Mo center. Based on the type of the additional ligands, the family can be further subdivided (see below). Generally, model compounds for the Mo(iv) oxidation level of the enzyme reaction centers can be synthesized by several procedures but model complexes for the Mo(vi) level are difficult to be accessed.

6.2.1 The Mo^{VI}O₂ and Mo^{IV}O Couple

The Mo^{VI}O₂/Mo^{IV}O center is included in only one Mo enzyme, arsenite oxidase (AO), in which no amino acid residue coordinates to the Mo center. AO is an oxygen atom transfer enzyme and promotes a net oxygen atom exchange between the arsenite substrate and water.^{3,5,8} The Mo^{VI}O₂ center is reduced to the corresponding Mo^{IV}O one by the reaction with arsenite.⁸ The resultant Mo^{IV}O center is re-oxidized to the Mo^{VI}O₂ structure, incorporating one water oxygen atom *via* PCET. In the resonance Raman measurements, the oxidized arsenite oxidase exhibited two $\nu(\text{C}=\text{C})$ vibrational modes at 1525 and 1598 cm⁻¹, indicating that the two MPT ligands are inequivalent in their electronic structure.⁸

The first model compound of the molybdenum(IV) state of AO was prepared using an aromatic dithiolene ligand, benzene-1,2-dithiol (H₂bdt). In 1986, [Mo^{IV}O(bdt)₂]²⁻ was synthesized as a Et₄N⁺ salt by the reaction of K₄[Mo^{IV}O₂(CN)₄] with two equivalents H₂bdt and the product's crystal structure was determined.⁹ The 4,5-dimethoxy derivative was also prepared by following this synthetic procedure.¹⁰ The Mo(IV) center has a distorted square-pyramidal geometry. Since then, more than 30 examples of bis(dithiolene)Mo^{IV}O compounds have been synthesized. The ligand structures for crystallographically characterized complexes are shown in Figure 6.3.

The first bis(dithiolene)Mo^{IV}O complex having an aliphatic dithiolene ligand is (Et₄N)₂[Mo^{IV}O(S₂C₂(COOMe)₂)₂], which was synthesized by addition of the alkyne to (Et₄N)₂[Mo^{IV}O(S₄)₂].¹¹ Other examples of aliphatic dithiolene ligands employed for Mo^{IV}O complex syntheses are S₂C₂(CN)₂,¹² S₂C₂H₂,¹³ S₂C₂Ph₂,¹⁴ and S₂C₂Me₂¹⁵ as symmetrical dithiolenes and 2-sdt, 2-pedt and 4-pedt as unsymmetric dithiolenes.¹⁶ Based on the Mo^{IV}=O stretches in IR measurements and Mo^{IV}=O bond distances, it is apparent that as the electron-donation ability of the dithiolene substituent increases, the Mo^{IV}=O bond weakens in the order R = Me > H > Ph > COOMe > CN. The electron-donating abilities of the substituents are also reflected in the redox potentials for the Mo(IV)/Mo(V) and Mo(V)/Mo(VI) series. In the 2-pedt and 4-pedt Mo^{IV}O

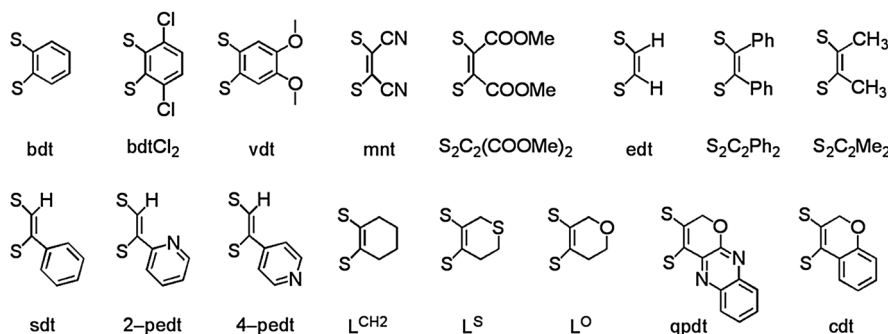


Figure 6.3 Chemical ligand structures of crystallographically characterized bis(dithiolene)Mo^{IV}O complexes.

complexes, the C–S bonds at the C2 position of the dithiolene ligands can have double-bond character whereas the C–C bonds can exhibit single-bond character as a result of the resonance and inductive effects induced by the attached pyridine.¹⁶ More recently, fused pyrano-ring dithiolene ligands were attached to the Mo^{IV}O center yielding typical square-pyramidal molybdenum(IV) centers.^{17,18,19} The effects of the heteroatom of the pyrano-ring on the spectroscopic properties were also studied replacing the oxygen atom of the ring by an S atom or a CH₂ group.¹⁶ Furthermore, Mo^{IV}O complexes coordinated by two structurally different dithiolene ligands were prepared as Et₄N⁺ salts by the following consecutive reactions:



The bdtCl₂ derivative (3,6-dichloro-benzene-1,2-dithiolate) was also prepared by a manner similar to the bdt complex.²⁰ Since AO is an oxidase enzyme, bis(dithiolene)Mo^{VI}O₂ complexes would serve as models for the oxidizing active site. However, in contrast to the stability of the Mo^{IV}O complexes, the corresponding bis(dithiolene)Mo^{VI}O₂ complexes have been hypothesized to be unstable and still remain difficult to prepare and isolate. To date, only five bis(dithiolene)Mo^{VI}O₂ complexes have been isolated and characterized by X-ray crystallography. (Et₄N)₂[Mo^{VI}O(bdt)₂] was employed as starting material for the preparation of the first Mo^{VI}O₂ complex. The oxidation with Me₃NO gave the corresponding Mo^{VI}O₂ complex (Et₄N)₂[Mo^{VI}O(bdt)₂].²¹ Later, the 3,6-dichloro substituted derivative (Et₄N)₂[Mo^{VI}O₂(bdtCl₂)₂], was also reported,²² but the complex was synthesized differently by ligand exchange of chloride of Mo^{VI}O₂Cl₂ with 2 equiv. of bdtCl₂²⁻.²² The first Mo^{VI}O₂ complex including an aliphatic dithiolene ligand is (Bu₄N)₂[Mo^{VI}O₂(mnt)₂], which was prepared from MoO₄²⁻ and 2 equivalents of Na₂mnt in the presence of Bu₄NBr.²³ The second example of an aliphatic dithiolene Mo^{VI}O₂ complex is one bearing S₂C₂(COOMe)₂ ligands. The complex was prepared by a manner similar to that for the Mo^{VI}O₂-bdt complex.²⁰ The Mo^{VI}O₂ form of the mixed dithiolene complex (Et₄N)₂[Mo^{VI}O₂(S₂C₂(COOMe)₂)(bdtCl₂)], was also crystallized and characterized crystallographically.²⁰ The crystal structural analyses of the bdt, bdtCl₂, mnt and S₂C₂(COOMe)₂ compounds as well as of the mixed ligand complexes reveal that all the Mo^{VI} centers possess an intermediate structure, *i.e.* mixed octahedral and trigonal prismatic geometries. Thus, two sulfur atoms of one dithiolene ligand of such Mo^{VI}O₂ complexes are inequivalent. Various temperature ¹H NMR spectral measurements for (Et₄N)₂[Mo^{VI}O₂(S₂C₂(COOMe)₂)₂] in (CD₃)₂CO reveal that the molybdenum(vi) center exhibits an isomerization between Δ and Λ forms above -80 °C as shown in Figure 6.4 and the conversion rate becomes slower than the ¹H NMR time scale below -85 °C; ΔG[‡] for the isomerization process has been calculated to be 42 kJ mol⁻¹.²⁰ The Mo^{VI}O₂ complexes discussed above are coordinated by dithiolenes with electron-withdrawing substituents. Unwanted

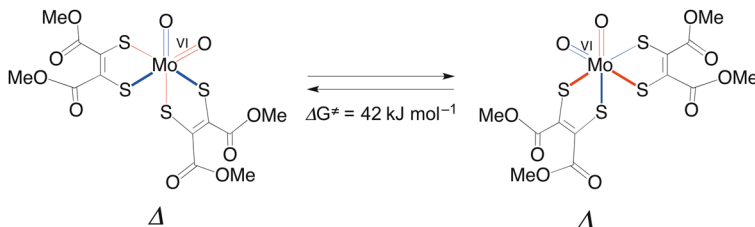


Figure 6.4 Isomerization between two structures of a bis(dithiolene) $\text{Mo}^{\text{VI}}\text{O}_2$ complex.

intramolecular redox reactions between the highly oxidized molybdenum(vi) center and the coordinated dithiolenes may be prevented by these substituents. Considering the chemical structure of the active sites of Mo enzymes, the MPT includes an electron-donating aliphatic substituent attached to the dithioline moiety. In this context, di-oxo molybdenum(vi) complexes with dithiolenes bearing electron-donating groups were specifically targeted for preparation. A $\text{Mo}^{\text{VI}}\text{O}_2$ complex comprising a fused pyrano-ring dithioline ligand can be prepared from the corresponding $\text{Mo}^{\text{IV}}\text{O}$ complex and Me_3NO and was spectroscopically characterized, but the $\text{Mo}^{\text{VI}}\text{O}_2$ complex could not be isolated.¹⁷

The bis(dithiolene) $\text{Mo}^{\text{IV}}\text{O}/\text{Mo}^{\text{VI}}\text{O}_2$ model complexes were used to evaluate the $\text{Mo}=\text{O}$ bond character of arsenite oxidase. Regarding the synthetic bis(dithiolene) $\text{Mo}^{\text{IV}}\text{O}$ complexes which were characterized by X-ray structural analysis, the $\text{Mo}^{\text{IV}}=\text{O}$ bond lengths are in a range of 1.67 to 1.72 Å and are comparable with that of the molybdenum(iv) state of AO (1.7 Å, derived from EXAFS experiments).^{8,9–19,24} As the molybdenum(vi) state of single crystals of AO is reduced to the molybdenum(iv) oxidation level by X-ray irradiation, a crystallographic comparison of the metrical parameters of molybdenum(vi) model complexes with the active site of AO cannot be made. Here, the $\text{Mo}^{\text{VI}}=\text{O}$ and $\text{C}=\text{C}$ bond nature of the model complexes is compared spectroscopically with that of the molybdenum(vi) center of AO. The synthetic bis(dithiolene) $\text{Mo}^{\text{VI}}\text{O}_2$ models exhibit $\nu(\text{Mo}^{\text{VI}}=\text{O})_{\text{sym}}$ stretching values at higher wavenumbers (885 – 847 cm⁻¹) when compared with the $\text{Mo}^{\text{VI}}\text{O}_2$ form of AO (822 cm⁻¹),^{8,20–23} suggesting the presence of different perturbations around the molybdenum(vi) coordination sphere of AO influencing the $\text{Mo}^{\text{VI}}=\text{O}$ bonds. Hydrogen bonds between oxo ligands of the AO $\text{Mo}^{\text{VI}}\text{O}_2$ center and the peptide backbone may weaken these bonds. Indeed, in the crystal structure of $(\text{Ph}_4\text{P})_2[\text{Mo}^{\text{IV}}\text{O}(\text{sdt})_2] \cdot \text{C}_2\text{H}_5\text{OH}$, a hydrogen bonding interaction between the oxo ligand and an ethanol molecule gives rise to a lower lying $\nu(\text{Mo}^{\text{IV}}=\text{O})$ stretching excitation (879 cm⁻¹) compared to $(\text{Ph}_4\text{P})_2[\text{Mo}^{\text{IV}}\text{O}(2\text{-pedt})_2]$ (902 cm⁻¹) and $(\text{Ph}_4\text{P})_2[\text{Mo}^{\text{IV}}\text{O}(4\text{-pedt})_2]$ (900 cm⁻¹) compounds with strictly terminal oxo ligands.¹⁵ $(\text{Et}_4\text{N})_2[\text{Mo}^{\text{VI}}\text{O}_2(\text{S}_2\text{C}_2(\text{COOMe})_2)_2]$ shows two $\nu(\text{C}=\text{C})$ stretches at 1494 and 1510 cm⁻¹ in the resonance Raman spectrum using 458 nm excitation. The experimental vibrational frequencies are in reasonable agreement with the DFT calculated frequencies of these modes

(1510 and 1538 cm⁻¹).²⁰ The presence of such inequivalent dithiolene ligands (with respect to the electronic structure) was also established for AO in its Mo^{VI}O₂ state as noted above.⁸

The catalytic cycle in AO enzymes involves OAT as a forward reaction and PCET for the regeneration of the active site. The OAT reactivity toward AsO₂⁻ was investigated using the models (Et₄N)₂[Mo^{VI}O₂(S₂C₂(COOMe)₂)₂] and (Et₄N)₂[Mo^{VI}O₂(S₂C₂(COOMe)₂)(bdtCl₂)] in CH₃CN-H₂O.²⁰ The OAT reaction yielded the bis(dithiolene)₂Mo^{IV}O complexes and the product AsO₃⁻ mimicking the natural transformation catalyzed by AO. The oxygen atom transfer was analyzed kinetically as a second-order reaction, $v = k[\text{MoO}_2][\text{AsO}_2]$. The rate constant values for the two investigated OAT model catalysts are almost identical, 2.7×10^{-2} M⁻¹ s⁻¹. This is consistent with the observation of very similar LMCT transitions for the two complexes as well as similar Mo^{VI}=O bond strengths inferred from the O_{oxo}-Mo-O_{oxo} stretching wavenumbers (873 cm⁻¹ vs. 869 cm⁻¹). (Et₄N)₂[Mo^{VI}O₂(S₂C₂(COOMe)₂)₂] exhibits Mo-(S_{dt})₄ and O_{oxo}-Mo-O_{oxo} metal-ligand stretching modes as well as ligand-based ene-1,2-dithiolate C-S and C=C stretches in the resonance Raman spectrum. The crystallographic, computational and spectroscopic results for the Mo^{VI}O₂ complex indicate the presence of considerable π -delocalization between the Mo^{VI}O₂ and S₂C₂(COOMe)₂ moieties. This was interpreted to result in a greater Mo^{VI}-S covalency in the complex.

As a model reaction mimicking the regeneration path from the reduced Mo^{IV}O center to the Mo^{VI}O₂ center in the AO catalytic cycle, the PCET reactivity of the bis(dithiolene)₂Mo^{IV}O complex with bdtCl₂ ligands was investigated.²⁵ The Mo^{IV}O complex (Bu₄N)₂[Mo^{IV}O(bdtCl₂)₂]⁺ is oxidized to the corresponding Mo^{VI}O₂ complex with 2 equiv. of K₃[Fe(CN)₆] at pH > 9 in an aqueous medium. When the reaction was carried out in labeled water, H₂¹⁸O, the ¹⁸O oxygen atom was incorporated into the complex and ended up as one of the two oxo ligands of the resultant Mo^{VI}O₂ complex.²⁵ In acetonitrile, the Mo^{VI}O₂ complex is also formed from the Mo^{IV}O complex by an electrochemical oxidation at 0.20 V vs. SCE in the presence of 2 equiv. of Et₄NOH, where the oxidation potential for the Mo^{IV}O/Mo^VO couple is 0.04 V. The reaction scheme for the PCET reaction is illustrated in Figure 6.5. The PCET reaction for the conversion process of a bis(dithiolene)₂Mo^{IV}O complex to the corresponding Mo^{VI}O₂ complex was further detailed by utilizing the S₂C₂(COOMe)₂ and bdt complexes.²⁶ Both complexes were converted to the oxidized Mo^{VI}O₂ complexes by PCET processes. Formation of the S₂C₂(COOMe)₂ ligand bearing Mo^{VI}O₂ complex by electrochemical oxidation of the corresponding Mo^{IV}O complex in aqueous medium is observable in alkaline solutions above pH 11 within the cyclic voltammetry (CV) time scale at 100 mVs⁻¹ as shown in Figure 6.6. At lower pH solution, the CV exhibits a reversible redox couple (Figure 6.6, solid line) based on the Mo^{IV}O/Mo^VO one-electron transfer process that corresponds to the equilibrium of Figure 6.5. As the solution pH increases, the redox wave becomes irreversible due to the subsequent chemical reaction involving PCET reaction to give the Mo^{VI}O₂ form. Contrary to this, CV measurements of the bdt complex under the same

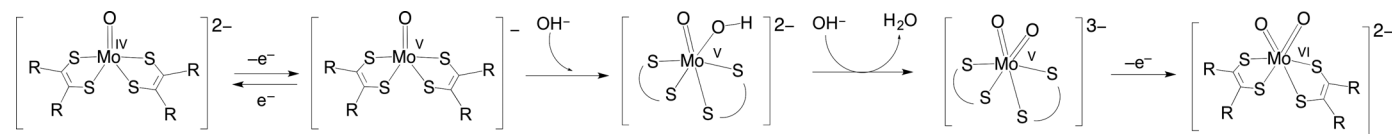


Figure 6.5 Formation mechanism of bis(dithiolene)Mo^{VI}O₂ complexes from bis(dithiolene)Mo^{IV}O precursors by proton-coupled electron transfer reactions in H₂O.

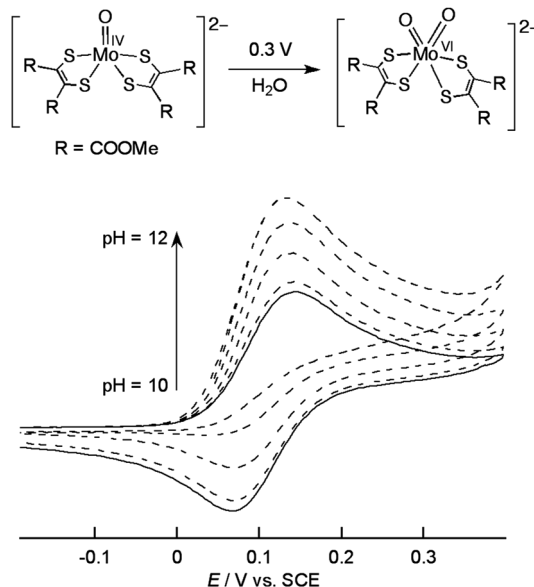


Figure 6.6 The pH-dependent changes in the cyclic voltammogram representing structural changes of the bis(dithiolene)Mo^{IV}O complex to the bis(dithiolene)Mo^{VI}O₂ complex. Dithiolene = S₂C₂(COOMe)₂. Solid line: reversible Mo^{IV}O/Mo^{VI}O redox couple, dashed lines: irreversible redox process following subsequent PCET reaction.

conditions do not provide any evidence for the generation of a Mo^{VI}O₂ complex. Notably, when the scan rates of the CV are set to slower than 20 mVs⁻¹, the formation of the Mo^{VI}O₂ complex can be monitored within the CV time scale. This shows that the structural change accompanying the oxidation of the Mo^{IV}O complex with S₂C₂(COOMe)₂ to its Mo^{VI}O₂ form is faster than that of the bdt complex. By kinetically studying the PCET reactions, different rate determining steps were found for the two complexes. For the S₂C₂(COOMe)₂ complex it is the reaction of the Mo^VO(OH) center with a base (OH⁻) on the deprotonation path yielding the Mo^{VI}O₂ center, whereas for the bdt complex it is the addition of OH⁻ to the Mo^VO center on the coordination path giving the Mo^VO(OH) center. The Mo^{IV}O complexes with S₂C₂(COOMe)₂ and bdt exhibit Mo(IV)/Mo(V) redox processes at -0.03 V and -0.19 V vs. SCE, respectively, in a mixed solvent of H₂O/CH₃CN = 1 : 1. Comparing the redox potentials for this transformation in aqueous solution clearly indicates that the S₂C₂(COOMe)₂ ligand has a weaker electron donating ability than bdt. Thus, the Mo^VO center of the S₂C₂(COOMe)₂ complex serves as a stronger Lewis acid for binding the incoming OH⁻ than that of the analogous bdt complex. In the case of a strong Lewis acidic reaction center, the successive deprotonation of the Mo^VO(OH) center by the second OH⁻ ion occurs quickly and, subsequently, the following electron transfer process from the resultant Mo^{VI}O₂ center to an oxidant yielding the Mo^{VI}O₂ moiety becomes the rate-determining step.

In the case of the molybdenum complexes with bdt, on the other hand, the square pyramidal Mo^{VI}O structure is strongly stabilized by the bdt ligand with better electron donation and the coordination of the incoming OH⁻ ion to the less acidic Mo^{VI}O center is relatively slow and constitutes, consequently, the rate-determining step.

6.2.2 The Mo^{VI}O and Mo^{IV} Couple

Most of the molybdenum enzymes of the DMSOR family utilize a redox couple consisting of mono-oxo molybdenum(vi) and des-oxo molybdenum(iv) centers for the oxygen atom transfer reactions.^{3,5} DMSOR, TMAOR (trimethyl amine N-oxide reductase), NIR (nitrate reductase), SeR (selenate reductase), EBDH (ethylbenzene dehydrogenase) and TH (pyrogallol-phloroglucinol transhydroxylase) feature such centers. Detailed descriptions of the different subtypes are given in other chapters of this book. DMSOR is the best characterized enzyme and even the crystal structures of its two oxidation levels at both ends of the catalytic reaction were determined.²⁷ The oxidized molybdenum(vi) center of DMSOR adopts an intermediate geometry between trigonal prismatic and octahedral, where the sixth position is occupied by one oxygen donor atom of a serinate (Ser) residue of the peptide. The reduced molybdenum(iv) state has a square pyramidal structure with two MPT and one apical Ser. The geometry of the molybdenum(vi) center renders the two MPT ligands inequivalent regarding electronic structure, which is supported by the appearance of the two distinct $\nu(C=C)$ stretching bands at 1576 and 1526 cm⁻¹ in the resonance Raman spectrum.²⁸ With respect to the molybdenum(iv) structure, the two MPT ligands are equivalent in their electronic structure and characterized by only one $\nu(C=C)$ vibration band at 1568 cm⁻¹.²⁸ The molybdenum-(VI) and -(IV) centers of TMAOR have the same coordination environments as those of DMSOR.^{5,29} The molybdenum centers of the NIRs feature different protein-based ligands compared to DMSOR.^{3,30} Two NIRs from *Desulfovibrio desulfuricans* and from *Escherichia coli* include a square-pyramidal molybdenum(iv) center coordinated by one sulfur donor atom of cysteinate (Cys) and a trigonal-prismatic molybdenum(iv) center bound to two oxygen donor atoms of an aspartate residue (Asp), respectively.⁵ The molybdenum(iv) centers of DMSOR, TMAOR and NIRs abstract one oxygen atom from their respective substrate ((CH₃)₂SO, (CH₃)₃NO or NO₃⁻). The oxo ligand of the resulting Mo^{VI}O center is converted to one water molecule by two PCET reactions and the original Mo^{IV} center is regenerated. The EBDH enzyme possesses a molybdenum center of which the coordination sphere is similar to that of NIR from *Escherichia coli*, *i.e.* Mo^{VI}O(MPT)₂(Asp) and Mo^{IV}(MPT)₂(Asp) active site compositions.³¹ The oxygen atom is inserted into a C-H bond of ethylbenzene and the resulting molybdenum(iv) center is re-oxidized by PCET using one water molecule as an oxygen source. The molybdenum center of TH is coordinated by two MPTs and one Ser in the reduced state similar to that of DMSOR. Selenate reductase (SeR) mediates the reduction of SeO₄²⁻ to SeO₃²⁻ in a similar fashion as DMSOR, TMAOR and

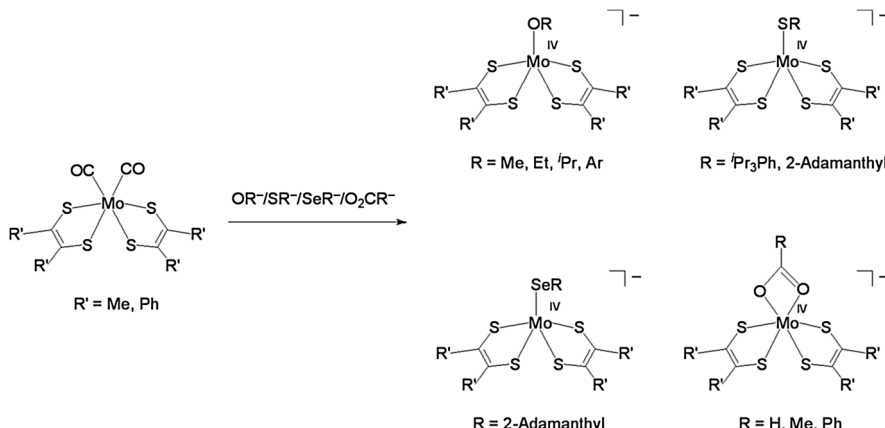


Figure 6.7 Synthesis and chemical structures of model complexes for the active sites of DMSO reductase family enzymes.

NIRs.³² Although the active site structure of SeR has not yet been identified precisely, a combination of the $\text{Mo}^{\text{VI}}\text{O}(\text{OH})(\text{MPT})_2$ and $\text{Mo}^{\text{IV}}(\text{OH})(\text{MPT})_2$ centers was proposed to be involved in the catalytic cycle.³³

The discovery of the des-oxo molybdenum(IV) centers in molybdenum enzymes has rendered the respective molybdenum-based biochemistry and coordination chemistry a hot topic in the field. As mentioned above, a square pyramidal des-oxo bis(dithiolene) Mo^{IV} structure is very rare in synthetic molybdenum compounds. Because the frequently employed molybdenum(IV) precursors such as $[\text{Mo}^{\text{IV}}\text{O}_2(\text{CN})_4]^{2-}$, $[\text{Mo}^{\text{IV}}\text{O}(\text{SC}_6\text{H}_5)_4]^{2-}$ and $[\text{Mo}^{\text{IV}}\text{OCl}(\text{CH}_3\text{CN})_4]^+$ already contain at least one oxo ligand, molybdenum(IV) compounds without oxo ligands have been and still are very difficult to prepare.³⁴⁻³⁹ The synthetic problems were overcome by the development of two preparative methods.⁴⁰⁻⁴³ One of the two routes involves silylation of $[\text{Mo}^{\text{IV}}\text{O}(\text{dithiolene})_2]^{2-}$ (dithiolene = bdt and edt) and the second comprises the substitution of the two carbonyl groups of $[\text{Mo}(\text{CO})_2(\text{S}_2\text{C}_2\text{R}_2)]$ ($\text{R} = \text{Me}$ and Ph) with an alcoholate, thiolate or carboxylate anion. By these two methods, a variety of $[\text{Mo}^{\text{IV}}(\text{OR/SR//O}_2\text{CR})(\text{dithiolene})_2]^-$ complexes were synthesized as illustrated in Figure 6.7 and characterized crystallographically.^{13,40-42} The respective molybdenum(IV) centers adopt a square-pyramidal geometry for the $\text{Mo}^{\text{IV}}(\text{OR/SR})$ complexes and show trigonal prismatic stereochemistry for the $\text{Mo}^{\text{IV}}(\text{O},\text{CR}-\kappa\text{O},\text{O})$ complexes. The carboxylate ligand chelates the molybdenum(IV) center in an almost symmetrical fashion *via* its two oxygen atoms. Unfortunately with respect to modeling, an asymmetric η^2 -carboxylate binding fashion revealed by the distinct Mo-O bond distances of 1.9 and 2.4 Å was observed in the NIR from *Escherichia coli*.³⁰ The unsymmetrical chelate mode found in this NIR may be due to interactions with amino acid residues surrounding the molybdenum(IV) center. The synthesis of $[\text{Mo}^{\text{IV}}(\text{OH})(\text{dithiolene})_2]^-$ complexes as models of the SeR reaction center has proven to be challenging since a reaction of an OH^- anion with $[\text{Mo}(\text{CO})_2(\text{dithiolene})_2]$ results in formation of 0.5 equivalents

of the oxo complex, $[\text{Mo}^{\text{IV}}\text{O}(\text{dithiolene})_2]^{2-}$. Therefore, the methoxo derivative (Et_4N^+) $[\text{Mo}^{\text{IV}}(\text{OMe})(\text{S}_2\text{C}_2\text{Me}_2)_2]$, was synthesized by using OMe^- instead of OH^- .⁴³ In the complex, the $\text{Mo}^{\text{IV}}(\text{OMe})$ center possesses a square-pyramidal geometry and the $\text{Mo}-\text{O}$ distance is $1.862(3)$ Å. The significantly shorter $\text{Mo}^{\text{IV}}-\text{oxygen}$ bond length compared to that estimated for SeR (2.22 Å by EXAFS analysis) suggests that possibly a monodentate ligand other than OH^- coordinates to the molybdenum(IV) center. With respect to modeling the one oxo ligand attached to molybdenum(VI) in the oxidized form of the molybdenum enzymes, bis($\text{S}_2\text{C}_2\text{Me}_2$)- $\text{Mo}^{\text{VI}}\text{O}(\text{OR})$, $-\text{Mo}^{\text{VI}}\text{O}(\text{SR})$ and $-\text{Mo}^{\text{VI}}\text{O}(\text{O}_2\text{CR}-\text{kO})$ compounds or the $\text{S}_2\text{C}_2\text{Ph}_2$ derivatives thereof have not yet been characterized. When the des-oxo molybdenum(IV) model complexes are treated with enzymatic substrates such as R_2SO , $\text{R}'_3\text{NO}$ or NO_3^- , an internal auto-redox reaction of the generated mono-oxo molybdenum(VI) complexes quickly proceeds to yield the square-pyramidal mono-oxo molybdenum(V) complexes, dissociating the OR^- , SR^- or RCOO^- ligand, respectively, from the metal center.

The first $\text{Mo}^{\text{VI}}\text{O}(\text{OR})(\text{dithiolene})_2$ complex was synthesized by using an aromatic dithiolene, bdt.⁴⁰ The complex (Et_4N^+) $[\text{Mo}^{\text{VI}}\text{O}(\text{OSi}^t\text{BuPh}_2)(\text{bdt})_2]$ was prepared by silylating the corresponding $\text{Mo}^{\text{VI}}\text{O}_2$ complex. The X-ray crystallographic analysis shows a $\text{Mo}=\text{O}$ bond length of $1.715(2)$ Å and a $\text{Mo}-\text{OSi}$ bond length of $1.932(2)$ Å.⁴⁰ As explained above, attempts to obtain the molybdenum(VI) complex from the molybdenum(IV) complex by oxygen atom transfer from DMSO , Me_3NO or NO_3^- in a manner similar to the molybdenum enzymes have been unsuccessful. Later, the $\text{S}_2\text{C}_2(\text{COOMe})_2$ ligand was employed as an ene-1,2-dithiolate ligand in the synthesis of a mono-oxo molybdenum(VI) complex. Contrary to the bdt system, the mono-oxo molybdenum(VI) complex, (Et_4N^+) $[\text{Mo}^{\text{VI}}\text{O}(\text{OSi}^t\text{Pr}_3)(\text{S}_2\text{C}_2\text{COOMe})_2]$, is prepared by oxygen atom abstraction from R_3NO of its resulting des-oxo molybdenum(IV) precursor (Figure 6.8) and the obtained complex is stable enough for isolation.⁴⁴ The $\nu(\text{Mo}=\text{O})$ stretch is observed at 880 cm^{-1} in the IR spectrum. X-ray crystal structural analysis of the complex reveals that the molybdenum(VI) center exhibits a distorted octahedral structure with a S1-S2-S3-S4 dihedral angle of 108° , which gives rise to a key difference between the two $\text{S}_2\text{C}_2(\text{COO})_2$ ligands, Part A and Part B as denoted in Figure 6.8. The solution electronic absorption spectrum of the molybdenum(VI) complex is remarkably similar to that of the molybdenum(VI) state of DMSOR displaying two low-energy bands at $13\,533 \text{ cm}^{-1}$ ($\epsilon = 1350 \text{ M}^{-1} \text{ cm}^{-1}$) and $17\,549 \text{ cm}^{-1}$ ($\epsilon = 2800 \text{ M}^{-1} \text{ cm}^{-1}$).⁴⁵ The resonance Raman spectrum

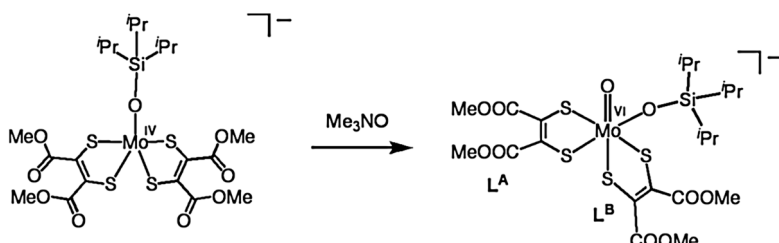


Figure 6.8 Synthesis and crystallographically determined structure of the $\text{Mo}^{\text{VI}}\text{O}$ complex coordinated by two inequivalent ene-1,2-dithiolate ligands.

(rR) shows two dithiolene C=C stretches at 1554 and 1489 cm⁻¹, reflecting the marked inequivalence of the two S₂C₂(COOMe)₂ ligands with respect to their interactions with the molybdenum(vi) center, and the ν (C=C) stretching values are also in good agreement with the enzyme data.²⁸ In contrast, a single C=C stretch is observed at 1550 cm⁻¹ for the des-oxo molybdenum(iv) model complex, reflecting the two equivalent dithiolene ligands in the square-pyramidal geometry.⁴⁴ Theoretical chemical calculations strongly support the *cis* S(p_z) orbital associated with dithiolene (B) (Figure 6.8) acting as an acceptor in the low-energy LMCT transitions and Band 1 is assigned as a HOMO → LUMO transition displaying considerable dithiolene (A) → Mo(d_{xy}) CT character. With respect to Band 2, this involves a dithiolene (A + B) → Mo(d_{xy}) CT transition with dominant HOMO-1 → LUMO character. Their respective EDDMs are shown in Figure 6.9. This model study suggests that the d_{xy} redox orbital in the molybdenum(vi) state of DMSOR possesses a strong π-type bonding interaction with a single S_{dithiolene} donor, and this is thought to provide a covalent pathway for electron transfer regeneration of the molybdenum(iv) state of DMSOR.

Another procedure to access mono-oxo molybdenum(vi) complexes was established as shown in Figure 6.10. By reacting a five-coordinate bis(dithiolene)mono-oxo molybdenum(vi) complex with carboxylate anions at low

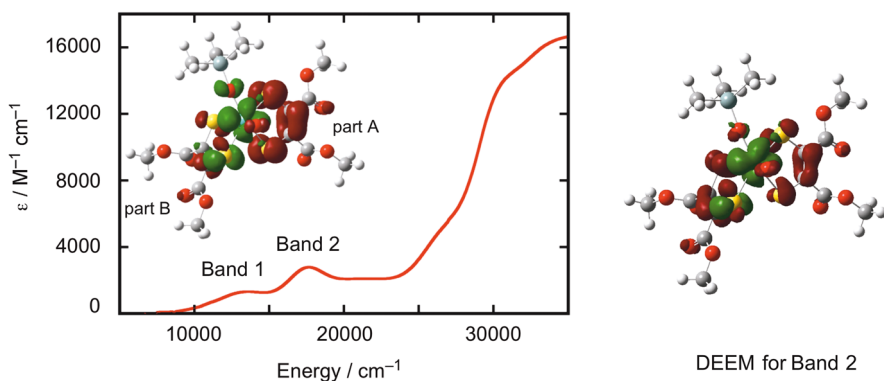


Figure 6.9 Electronic spectrum of $[\text{Et}_4\text{N}]^+[\text{Mo}^{\text{VI}}\text{O}(\text{OSi}_i\text{Pr}_3)(\text{S}_2\text{C}_2\text{COOMe})_2]^-$ and the two EDDMs: (inset) EDDM for Band 1, right for Band 2. Copyright ref. 44.

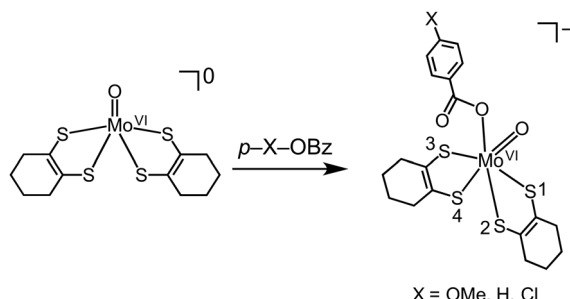


Figure 6.10 Synthesis and chemical structure of the model complex for EBDH.

temperature, model complexes of the molybdenum(vi) state of EBDH were synthesized.⁴⁶ The complexes undergo an internal redox reaction to yield square-pyramidal oxo molybdenum(v) complexes at room temperature. The structure of $[\text{Mo}^{\text{VI}}\text{O}(\text{OBz})(\text{S}_2\text{C}_6\text{H}_8)_2]^-$ was optimized by DFT calculations and shown to exhibit a slightly larger S1–S2–S3–S4 dihedral angle of 126° than the 108° experimental dihedral angle for $[\text{Mo}^{\text{VI}}\text{O}(\text{OSi}^{\text{i}}\text{Pr}_3)(\text{S}_2\text{C}_2(\text{COOMe})_2)]^-$ as discussed above. This suggests that an ene-1,2-dithiolate ligand with electron-donating substituents can stabilize a trigonal prismatic molybdenum(vi) structure, while one having electron-withdrawing groups can stabilize an octahedral molybdenum(vi) center. The presence of the electron-donating groups on the ene-1,2-dithiolate causes red shifts of the absorption bands at $13\,533$ and $17\,549\text{ cm}^{-1}$ of $[\text{Mo}^{\text{VI}}\text{O}(\text{OSi}^{\text{i}}\text{Pr}_3)(\text{S}_2\text{C}_2(\text{COOMe})_2)]^-$ to $12\,500$ and $16\,700\text{ cm}^{-1}$ in the visible region.

Four examples of oxygen atom transfer reactions from enzymatic substrates with $(\text{Et}_4\text{N})[\text{Mo}^{\text{IV}}(\text{OR/SR/O}_2\text{CCR})(\text{S}_2\text{C}_2\text{Me}_2)_2]$ complexes are schematically illustrated in Figure 6.11. Unfortunately, most of the oxygen atom transfer reactions are complicated by the formation of $[\text{Mo}^{\text{V}}\text{O}(\text{S}_2\text{C}_2\text{Me}_2)_2]^-$, following an intramolecular redox reaction of the presumably generated mono-oxo-molybdenum(vi) complexes. The oxygen atom transfer reactions obey second-order kinetics and follow an associative mechanism. In the $\text{Mo}^{\text{IV}}(\text{OR})$ system, introduction of electron-withdrawing groups to the axial ligands increases the value of the second-order rate constant, k_2 ($\text{M}^{-1}\text{ s}^{-1}$),

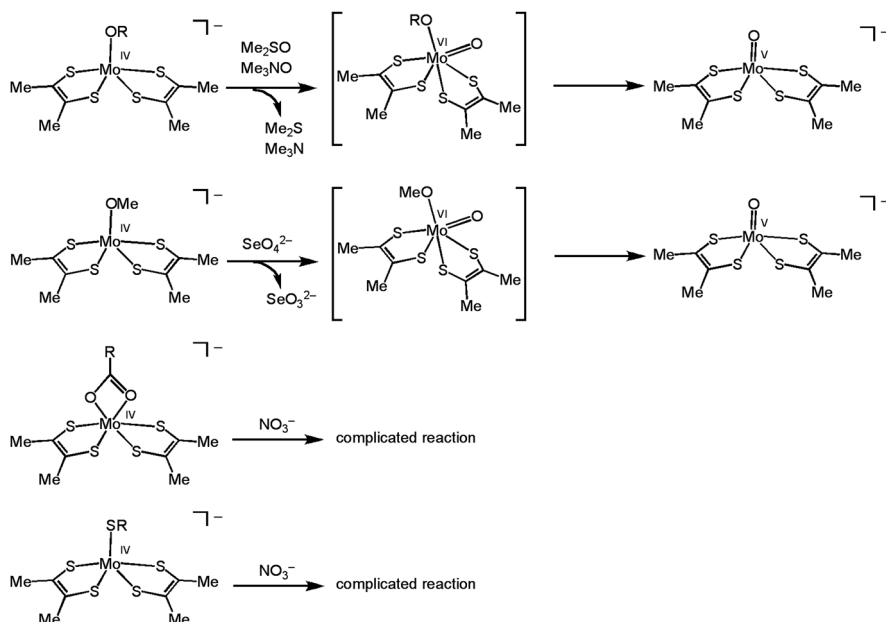


Figure 6.11 Reactivity of molybdenum(iv) state model complexes in oxygen atom abstraction from the substrates.

whereas larger (bulkier) axial ligands result in slower reactions.¹³ On the other hand, when $(Et_4N)[Mo^{IV}(SR)(S_2C_2Me_2)_2]$ ($R = Me$ and Ph) compounds and their O_2CCR derivatives are treated with NO_3^- modeling the reactivity of NIR, the reactions give complicated mixtures.⁴⁷ As found in the DMSOR and TMAOR model systems, a model reaction for SeR using $(Et_4N)[Mo^{IV}(OMe)(S_2C_2Me_2)_2]$ and SeO_4^{2-} yields SeO_3^{2-} following second-order kinetics, but the $Mo^{VI}O(OMe)$ species generated has not been observed.⁴⁸ Detailed mechanisms for oxygen atom transfer reactions by bis(dithiolene)molybdenum(IV) complexes are described in Chapters 3 and 4 of this book.

6.2.3 $Mo^{VI}S(Se\text{-}R)$ and $Mo^{IV}S$ Couple

Crystal structure analyses of molybdenum-dependent FDH revealed the existence of seleno-cysteinate ($Se\text{-}Cys$) coordination to the molybdenum center. In the molybdenum(VI) oxidation state of the enzyme, one terminal sulfide group occupies the sixth position to complete a trigonal prismatic $Mo^{VI}S(Se\text{-}Cys)(MPT)_2$ geometry. The reduced enzyme has a square-pyramidal $Mo^{IV}(Se\text{-}Cys)(MPT)_2$ center.⁴⁹ Another reduced molybdenum(IV) form has a square pyramidal $Mo^{IV}S(MPT)_2$ structure, where seleno-cysteine has vanished from the first coordination sphere.⁵⁰ As the $Mo^{VI}S(Se\text{-}Cys)$ structure was reported to be an inactive form, the detailed reaction mechanism for the formate oxidation remains unclear. Because formate is a good hydride donor itself, it is suggested that formate oxidation begins with it replacing the $Se\text{-}Cys$ ligand of $Mo^{VI}S(Se\text{-}Cys)(MPT)_2$. A subsequent intramolecular hydride transfer from the formate ligand to the sulfido group in the $Mo^{VI}S(HCOO)$ species gives carbon dioxide and a square-pyramidal $Mo^{IV}(SH)$ center. Deprotonation of the $Mo^{IV}(SH)$ center may then yield the original $Mo^{VI}S(MPT)_2$ structure.

$Mo^{VI}S(SeR)(dithiolene)_2$ complexes as molybdenum(VI) state models have not yet been synthesized. As molybdenum(IV) state models, a series of square pyramidal $Mo^{IV}S(dithiolene)_2$ complexes using $S_2C_6H_8$, $S_2C_2Ph_2$ and $S_2C_2(COOMe)_2$ ligands were reported.^{51,52} The respective structures are illustrated in Figure 6.12. X-ray structural data indicate that the Mo=S bond lengths decrease according to the order $S_2C_6H_8 > S_2C_2Ph_2 > S_2C_2(COOMe)_2$,

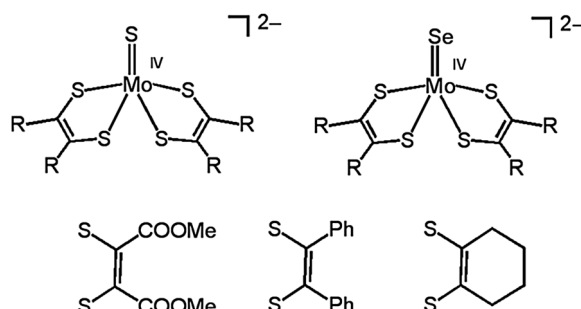


Figure 6.12 Molybdenum(IV) state model complexes for FDH.

reflecting the relative electron-donating and -withdrawing nature of the substituents on the dithiolene ligands. Dithiolene ligand effects on the nature of the Mo=S bonds have been probed by electrochemical investigations. It was shown that the redox potential for the Mo(v)/Mo(IV) couple is shifted to more positive values as the ligand changes from $S_2C_6H_8$ to $S_2C_2Ph_2$ to $S_2C_2(COOMe)_2$. Electrochemical, spectroscopic and bonding calculations are consistent with a redox orbital that is dominantly $Mo(d_{x^2-y^2})$ in character and possesses no contribution from the terminal sulfido donor. In addition to the $Mo^{IV}=S$ complexes, the selenide derivatives, $[Mo^{IV}Se(\text{dithiolene})_2]^{2-}$, were synthesized.⁵³ This series enables a systematic study of the effects of the terminal chalcogenide ligand on the geometric and electronic structure, when including the known $Mo^{IV}O$ complexes with identical dithiolene ligands (Figure 6.12). The origin of the spectral shifts in the $[Mo^{IV}E(\text{dithiolene})]^{2-}$ ($E = O, S, Se$) series can be explained by (1) the much stronger ligand field exerted by the terminal oxo ligand, which leads to much higher energy ligand field bands for the MoO series, and (2) the nature of the LUMO+1 wave function, which possesses increased E character and low-energy CT transitions as the apical chalcogenide electronegativity decreases.⁵³

6.3 Model Compounds for the Sulfite Oxidase Family

The molybdenum(vi) oxidation state of sulfite oxidase contains a square-pyramidal $Mo^{VI}O_2$ center with one MPT and one thiolate of cysteine, $Mo^{VI}O_2(S\cdot Cys)(MPT)$. One oxo ligand situated at the equatorial plane is replaced by OH^- or H_2O in the molybdenum(iv) state, $Mo^{IV}O(OH/H_2O)(S\cdot Cys)(MPT)$.⁵⁴ Aside from sulfite oxidases the assimilatory nitrate reductase belongs to this family. In the catalytic cycle of sulfite oxidation, one oxygen atom of the $Mo^{VI}O_2$ center is transferred to the substrate yielding the $Mo^{IV}O(OH/H_2O)$ center together with the product. The resultant molybdenum(iv) center returns to the original molybdenum(vi) state by two PCETs incorporating one water-derived oxygen atom.

It had been very difficult to synthesize mono(dithiolene)molybdenum(vi) complexes without any further chelating ligand in addition to one dithiolene. $[Mo^{VI}O_2(2,4,6-iPr_3-C_6H_2SH)(bdt)]^-$ is the first molybdenum(vi) state model for sulfite oxidase and still remains the sole compound of this type.⁵⁴ The complex was prepared by the stepwise replacement of monodentate ligands of $Mo^{VI}O_2(OSiPh_3)_2$ with one bdt^{2-} and one thiolate as shown in Figure 6.13. The molybdenum(vi) center has a square-pyramidal geometry with the Mo atom displaced by 0.74 Å from the 3S + O equatorial plane. A paramagnetic molybdenum(v) model is also available as $[Mo^VCl(2,4,6-iPr_3-C_6H_2SH)(bdt)]^-$ (Figure 6.13).⁵⁵ Unfortunately, similar molybdenum(vi) model complexes with true (non-aromatic) ene-1,2-dithiolate ligands and molybdenum(iv) model complexes still remain challenging targets.

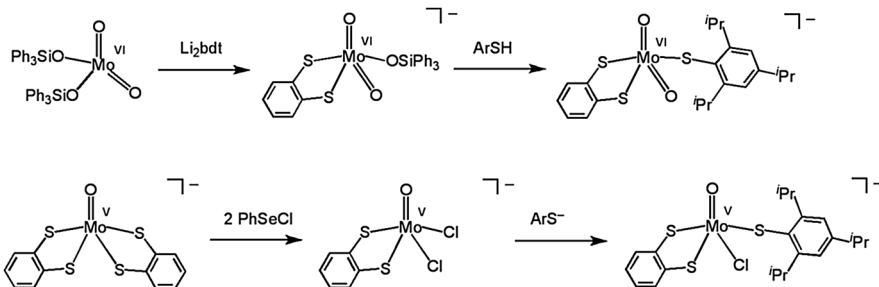


Figure 6.13 Synthesis and chemical structures of molybdenum(VI) and (V) state model complexes for sulfite oxidase.

6.4 Model Compounds for the Xanthine Oxidase Family

A five-coordinate $\text{Mo}^{\text{VI}}\text{O}(\text{S})$ reaction center coordinated by one MPT and one hydroxo or oxo group, $\text{Mo}^{\text{VI}}\text{O}(\text{S})(\text{OH})(\text{MPT})$, comprises the active site in the oxidized xanthine oxidoreductase, aldehyde oxidoreductase and quinolone 2-oxidoreductase enzymes.^{5,56,57} In the respective catalytic cycles, the $\text{Mo}^{\text{VI}}\text{O}(\text{S})$ center is the active oxidant and assumed to be reduced to the corresponding $\text{Mo}^{\text{IV}}\text{O}(\text{SH})$ species following hydride transfer from the substrate to the sulfido ligand. One hydroxide ion, OH^- , derived from water binds the resulting carbocation to give the hydroxylated product. This mechanism is supported by the fact that the oxo ligands of the $\text{Mo}^{\text{VI}}\text{O}(\text{S})$ and $\text{Mo}^{\text{IV}}\text{O}(\text{SH})$ centers were not replaced by ^{18}O atoms in the presence of H_2^{18}O during catalysis. Nicotinate dehydrogenase is a selenium-dependent enzyme of which the molybdenum site structure is very similar to that of xanthine oxidoreductase except that a terminal selenide group occupies the place of the sulfide ligand of xanthine oxidoreductase, $\text{Mo}^{\text{VI}}\text{O}(\text{Se})(\text{OH})(\text{MPT})$.⁵⁸ In this family, replacement of the sulfide or selenide group with an oxo group renders the enzymes inactive.

No really accurate model complex for enzymes of this family has been prepared yet. This is probably due to the fact that five- and six-coordinate $\text{Mo}^{\text{VI}}\text{O}(\text{S}/\text{Se})$ complexes are prone to yield $\text{Mo}^{\text{V}}\text{O}(\text{S}/\text{Se}-\text{S}/\text{Se})\text{Mo}^{\text{V}}\text{O}$ or $\text{Mo}^{\text{IV}}\text{O} + \text{S}/\text{Se}$ species *via* intramolecular redox reactions. However, a couple of bis(dithiolene)molybdenum(VI) complexes, $[\text{Mo}^{\text{VI}}\text{O}(\text{S})(\text{S}_2\text{C}_2(\text{COOMe}))_2]^{2-}$ and $[\text{Mo}^{\text{VI}}\text{O}(\text{Se})(\text{S}_2\text{C}_2(\text{COOMe}))_2]^{2-}$, have been reported.⁵⁹ These complexes are prepared by reacting $[\text{Mo}^{\text{VI}}\text{O}(\text{OSi}^t\text{BuPh}_2)(\text{S}_2\text{C}_2(\text{COOMe}))_2]^-$ with the corresponding SH^- or SeH^- anion of a Et_4N^+ salt at low temperature. At room temperature, the oxo-sulfide- and oxo-selenide-molybdenum(VI) complexes undergo an intramolecular redox reaction, resulting in formation of the $\text{Mo}^{\text{IV}}\text{O}$ complex and elemental sulfur or selenium. In combination with the dioxo-molybdenum(VI) derivative (see Section 6.2.1), the three complexes complete a series of isostructural $\text{Mo}^{\text{VI}}\text{O}(E)$ complexes ($E = \text{O}, \text{S}$ and Se) allowing the systematic investigation of the dimensions of the molybdenum(VI) centers, their electronic structures and their atom transfer reactivity.

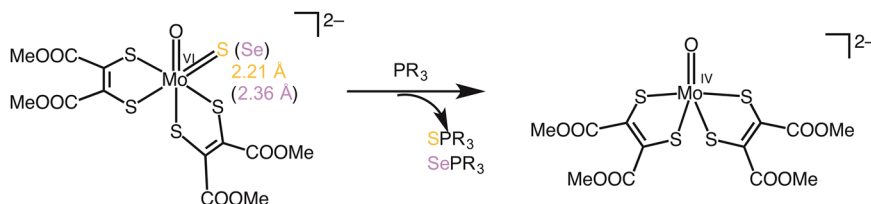


Figure 6.14 Active site models for xanthine oxidase and nicotinic acid dehydrogenase and their atom transfer reactivity.

(Figure 6.14). The structures of the $\text{Mo}^{\text{VI}}\text{O}(\text{S})$ and $\text{Mo}^{\text{VI}}\text{O}(\text{Se})$ complexes were optimized by DFT calculations at the (U)B3LYP level of theory. The two molybdenum(vi) centers can be described as distorted octahedrons as in the case of the dioxo molybdenum(vi) complex. The theoretical $\text{Mo}=\text{S}$ bond length of 2.21 Å is slightly longer than those of the five-coordinate $\text{Mo}^{\text{VI}}\text{O}(\text{S})$ centers of xanthine oxidoreductase (2.13 Å)⁵⁵ and quinolone 2-oxidoreductase (2.13 Å),⁵⁸ probably due to the difference of the coordination numbers or because theoretical methods generally tend to overestimate metal to sulfur bonds. The optimized $\text{Mo}=\text{Se}$ distance of 2.36 Å is also slightly longer than that of the five-coordinate $\text{Mo}^{\text{VI}}\text{O}(\text{Se})$ center of NDH (2.29 Å).⁵⁸ The $\nu(\text{C}=\text{C})$ frequencies of the $\text{Mo}^{\text{VI}}\text{O}(\text{Se})$ complex in resonance Raman measurements are close to those of the $\text{Mo}^{\text{VI}}\text{O}(\text{S})$ and $\text{Mo}^{\text{VI}}\text{O}_2$ complexes, suggesting that the $\nu(\text{C}=\text{C})$ stretches are not sensitive to exchanging the terminal oxide, sulfide and selenide ligands. The bond dissociation energy (kcal mol⁻¹) of the $\text{Mo}^{\text{VI}}=\text{E}$ bonds decreases as the E atom goes from O (88 kcal mol⁻¹) to S (47) and to Se (35). The negative net charge of the chalcogen atom E decreases in the order of $\text{E} = \text{O} (-1.07) < \text{E} = \text{S} (-0.85) < \text{E} = \text{Se} (-0.69)$, reflecting the chalcogens' electronegativity. The absorption band in the UV-vis at ~485 ($\text{E} = \text{S}$) and ~490 nm ($\text{E} = \text{Se}$) with molar extinction coefficients larger than $3500 \text{ M}^{-1} \text{ cm}^{-1}$ is absent in the $\text{Mo}^{\text{VI}}\text{O}_2$ complex, suggesting that the band involves some contributions of S or Se → Mo(vi) charge transfer. The $\text{Mo}^{\text{VI}}\text{O}(\text{S})$ and $\text{Mo}^{\text{VI}}\text{O}(\text{Se})$ complexes exhibit selective sulfur or selenium atom transfer to tertiary phosphines yielding phosphine sulfide or selenide and the $\text{Mo}^{\text{IV}}\text{O}$ complex. The pseudo-first-order rate constants, k_{obs} (s⁻¹), for the S and Se atom transfer exhibit saturation behavior as the substrate concentration increases as shown in Figure 6.15 (a)–(c). Comparison of the k_b values for the atom transfer to PPh_3 at -80°C ($\sim 10^{-6} \text{ s}^{-1}$ for $\text{E} = \text{S}$ vs. $2.4 \times 10^{-2} \text{ s}^{-1}$ for $\text{E} = \text{Se}$) indicates that the selenium atom transfer is significantly faster than the sulfur atom transfer by *ca.* four orders of magnitude. In contrast, oxygen atom transfer from the $\text{Mo}^{\text{VI}}\text{O}_2$ complex to Ph_3P does not proceed at room temperature. Based on the DFT calculations, the significantly enhanced atom transfer reactivity for $\text{E} = \text{S}$ and Se when compared with that for $\text{E} = \text{O}$ can be explained from the LUMO's character, where the LUMO orbitals of the two complexes have 34.42% and 35.33% contribution of the sulfido and selenido ligands, respectively. The LUMO of the $\text{Mo}^{\text{VI}}\text{O}_2$ complex, on the other hand, involves only 9.74% oxo ligand character.

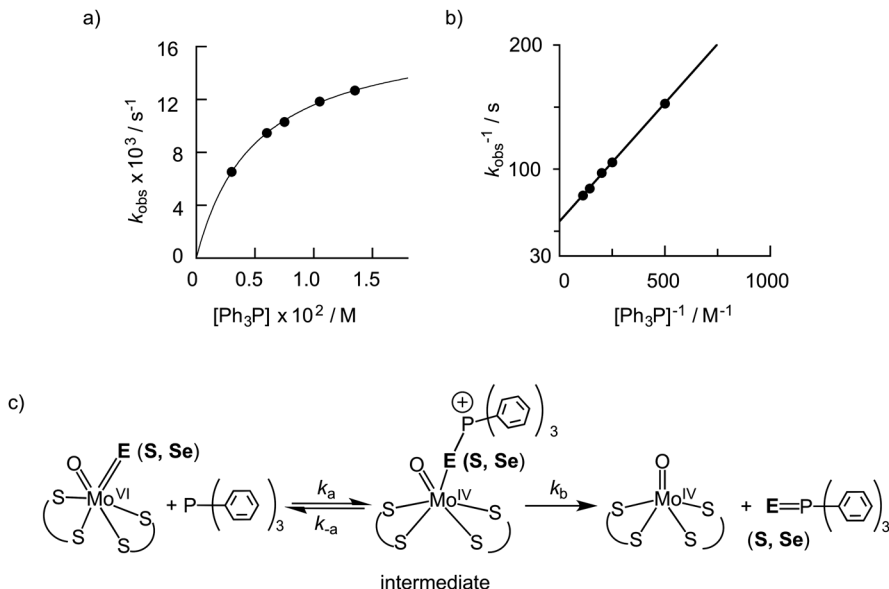


Figure 6.15 Atom transfer reactivity of bis(dithiolene)Mo^{VI}O(S/Se) complexes to triphenylphosphine. Reproduced from ref. 59 with permission from the Royal Society of Chemistry.

6.5 W-substituted Model Compounds for the DMSOR and Xanthine Oxidase Families

As mentioned above, most of the bis- and mono-(dithiolene)molybdenum(vi) complexes are too unstable for isolation and characterization. Instead, the tungsten(vi) ion has often been used for preparation of complexes isostructural with the molybdenum(vi) species. By this strategy, the molybdenum(vi) oxidation state of DMSO reductase, nitrate reductase from *Desulfovibrio desulfuricans*, ethylbenzene dehydrogenase and nitrate reductase from *Escherichia coli*, and selenate reductase have been modeled by $[\text{W}^{\text{VI}}\text{O}(\text{OPh})(\text{S}_2\text{C}_2\text{Me}_2)_2]^-$,⁶⁰ $[\text{W}^{\text{VI}}\text{O}(\text{SC}_6\text{H}_{2,4,6}\text{iPr}_3)(\text{S}_2\text{C}_2\text{Me}_2)_2]^-$,⁶¹ $[\text{W}^{\text{VI}}\text{O}(\text{C}_6\text{H}_5\text{COO})(\text{S}_2\text{C}_2\text{Me}_2)_2]^-$,⁶¹ and $[\text{W}^{\text{VI}}\text{O}(\text{OMe})(\text{S}_2\text{C}_2\text{Me}_2)_2]^-$,⁶² respectively. The respective chemical structures are shown in Figure 6.16. These tungsten(vi) complexes were prepared by oxygen atom transfer from Ph_3AsO or Me_3NO to the corresponding des-oxo tungsten(iv) complexes. All of the crystal structures were determined and each showed a tungsten(vi) center having a distorted octahedral geometry. As tungsten-substituted models for the xanthine oxidase family, two five-coordinate mono(dithiolene)W^{VI}O(S) compounds were synthesized.⁶³ $[\text{W}^{\text{VI}}\text{O}_3(\text{bdt})_3]^{2-}$ was exposed to H_2S in CH_3CN to yield $[\text{W}^{\text{VI}}\text{O}_2(\text{S})(\text{bdt})]^{2-}$ and the treatment of $[\text{W}^{\text{VI}}\text{O}_2(\text{OSi}\text{iPr}_3)(\text{bdt})]^{2-}$ with 2 equiv. of iPr_3SiSH gives $(\text{Et}_4\text{N})[\text{W}^{\text{VI}}\text{O}(\text{S})(\text{OSi}\text{iPr}_3)(\text{bdt})]$. These two W^{VI}O(S) centers adopt distorted square-pyramidal geometries with apical oxo and basal sulfide ligation. The former complex serves as a low-pH molybdenum(vi) state model whereas the latter

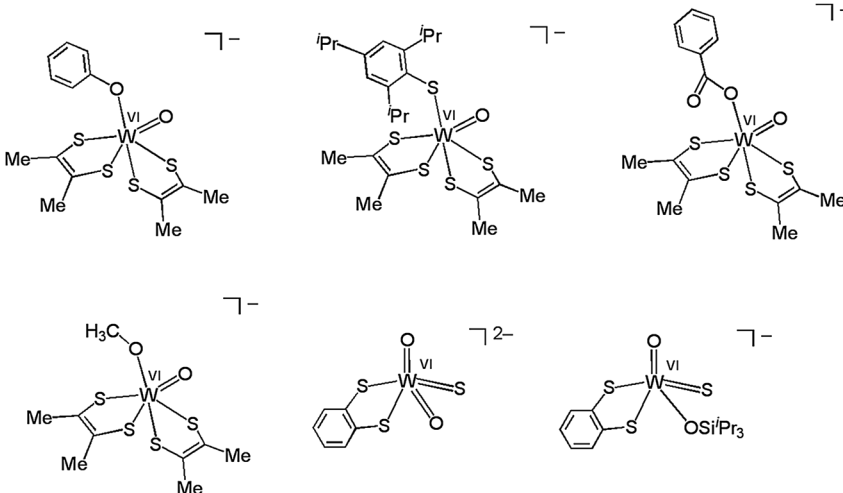


Figure 6.16 Tungsten-substituted model complexes for the DMSOR and xanthine oxidase families.

one stands as a high-pH model. So far, no mono(dithiolene) $\text{W}^{\text{VI}}\text{O}(\text{Se})$ compounds have been prepared.

6.6 Model Compounds for Tungsten-Dependent Enzymes

Known tungsten-containing enzymes comprise the three families of aldehyde ferredoxin oxidoreductase (AOR),⁶⁴ formate dehydrogenase (FDH) and *N*-formylmethanofuran dehydrogenase (FMDH)⁶⁵ and acetylene hydratase (AH),⁶⁶ and all of the enzymes have a bis(MPT)tungsten active site. Since tungsten enzymes are quite air sensitive, structural characterization has been carried out only for the tungsten(vi) oxidation state.

6.6.1 The $\text{W}^{\text{VI}}\text{O}(\text{S})$ Center

The $\text{W}^{\text{VI}}\text{O}(\text{S})(\text{MPT})_2$ active oxidizes aldehyde to carboxylic acid, involving hydride transfer from the aldehyde to the terminal sulfide ligand followed by OH^- binding to the formyl group.⁶⁴ Some model complexes were reported although their crystallographic characterization could not be carried out so far.⁶⁷ The complexes $[\text{W}^{\text{VI}}\text{O}(\text{S})(\text{dithiolene})_2]^{2-}$ (dithiolene = $\text{S}_2\text{C}_2\text{Ph}_2$ and bdt) are generated by the reaction of the corresponding square-pyramidal $[\text{W}^{\text{V}}\text{O}(\text{dithiolene})_2]^-$ compounds with an equimolar amount of Et_4NSH . As shown in Figure 6.17, the $\text{W}^{\text{V}}\text{O}$ compound acts as both a reaction substrate and an oxidant whereas the SH^- works as both a ligand and a base. The $\text{W}^{\text{V}}\text{O}$ species reacts with SH^- to produce the corresponding $\text{W}^{\text{V}}\text{O}(\text{SH})$ species (intermediate A). Another SH^- (base) abstracts the proton of the SH group

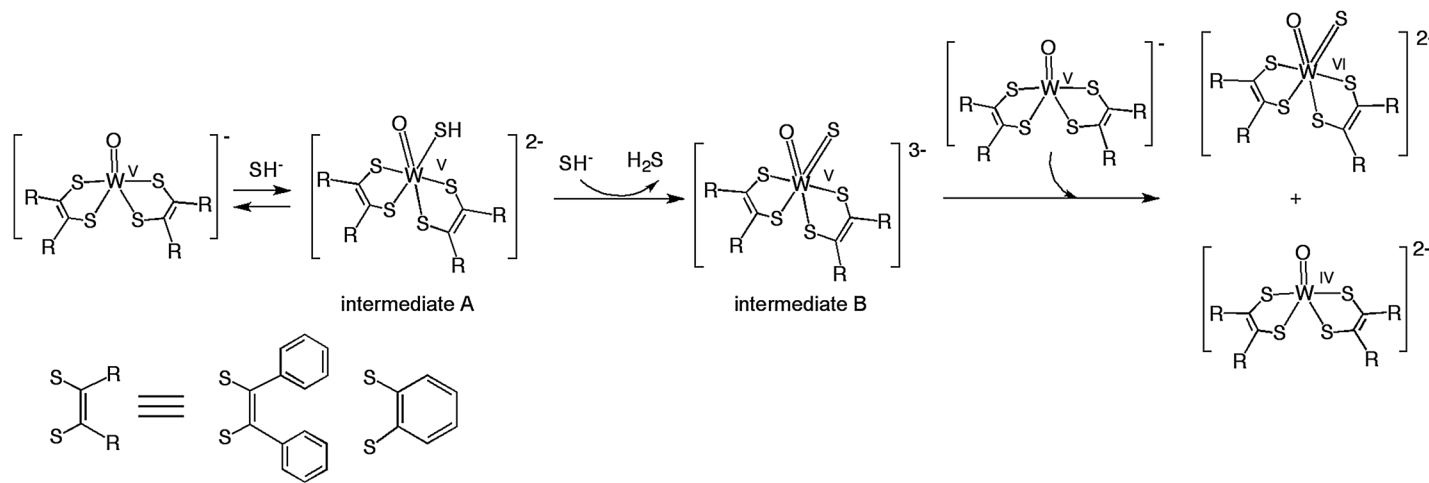


Figure 6.17 Synthesis and chemical structure of the $\text{W}^{\text{VI}}\text{O}(\text{S})$ model complex for the AOR active site.

of A, yielding the $\text{W}^{\text{V}}\text{O}(\text{S})$ species (intermediate B). Then, the redox reaction between B and remaining $\text{W}^{\text{V}}\text{O}$ species (oxidant) quickly occurs generating the $\text{W}^{\text{VI}}\text{O}(\text{S})$ compound together with the square-pyramidal $\text{W}^{\text{IV}}\text{O}$ compound. The $\text{W}^{\text{VI}}\text{O}(\text{S})$ complex is hydrolyzed to the $\text{W}^{\text{VI}}\text{O}_2$ derivative in the presence of a small amount of water, reflecting the relative stability of $\text{W}^{\text{VI}}=\text{S}$ and $\text{W}^{\text{VI}}=\text{O}$ bonds. A similar hydrolytic reaction is thought to be involved in the enzymatic inactivation process. An alternative route for accessing $\text{W}^{\text{VI}}\text{O}(\text{S})(\text{dithiolene})_2$ complexes is based on the substitution of the $\text{OSi}^{\prime}\text{BuPh}_2$ ligand of $[\text{W}^{\text{VI}}\text{O}(\text{OSi}^{\prime}\text{BuPh}_2)(\text{S}_2\text{C}_2(\text{COOMe})_2)_2]^-$ by sulfide with one equiv. of SH^- (Et_4N salt).⁶⁸ The respective 3D structure was optimized by DFT calculations. The model complex exhibits some similarities to the tungsten center of the AOR family of tungsten enzymes regarding structure and reactivity. The $\text{W}^{\text{VI}}\text{O}(\text{S})$ complex has a $\text{W}=\text{S}$ bond distance of 2.23 Å according to DFT calculations, which is close to the experimental distance between the tungsten and ambiguously assigned monodentate sulfur atoms of the active AOR.⁶⁴ The observation of two distinct signals in the rR spectrum (1509 and 1477 cm⁻¹), hence, two inequivalent $\text{S}_2\text{C}_2(\text{COOMe})_2$ ligands, also mimics the appearance of the two $\nu(\text{C}=\text{C})$ stretches found for AOR (1595 and 1576 cm⁻¹).⁶⁹ The selective sulfur atom transfer from the $\text{W}^{\text{VI}}\text{O}(\text{S})$ centers to triphenylphosphines indicates that the sulfide group works as a good electrophile. The sulfide significantly contributes to the LUMO accounting for 34.5% of the orbital's character. In contrast, the orbital has only 0.3% contribution from the oxo ligand. In the AOR family, the dioxo-tungsten(vi) center comprises an inactive form. This is supported and well explained by this model study, which shows the negligibly small contributions of the two oxo ligands to the LUMO of the dioxo derivative, $[\text{W}^{\text{VI}}\text{O}_2(\text{S}_2\text{C}_2(\text{COOMe})_2)]^{2-}$ ($1.41\% \times 2$).

6.6.2 The $\text{W}^{\text{VI}}\text{S}(\text{Se-R})$ Center

Tungsten-dependent FDH bears a trigonal prismatic $\text{W}^{\text{VI}}\text{S}(\text{Se-Cys})(\text{MPT})_2$ center. Its structure is isostructural with the molybdenum(vi) center of molybdenum-dependent FDH.⁶⁵ FMDH is assumed to have a similar active site structure to FDH. By the reaction of the square-pyramidal $[\text{W}^{\text{IV}}(-\text{SeAd})(\text{S}_2\text{C}_2\text{Me}_2)_2]^-$ complex with Ph_3SbS , the model complex $[\text{W}^{\text{VI}}\text{S}(\text{SeAd})(\text{S}_2\text{C}_2\text{Me}_2)_2]^-$ (SeAd = 1-adamantylselenate) was synthesized (Figure 6.18).

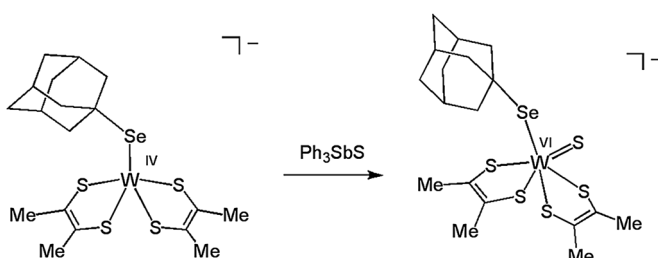


Figure 6.18 Tungsten(vi) model for the tungsten-dependent FDH.

Its crystal structure and reactivity with formate, however, have not yet been reported, emphasizing the considerable difficulties involving the respective model chemistry.

6.6.3 The W^{VI}(CO/CN)(SR) Center

Benzoyl-coenzyme A reductases (BCRs) catalyze a benzene ring reduction to a cyclic diene, where the transformation proceeds at a W^{IV}(CO)(S•Cys)(MPT)₂ or W^{IV}(CN)(S•Cys)(MPT)₂ center, although some uncertainty regarding the two-atomic ligand remains.⁷⁰ Comprising an organometallic type of active site structure, this motif is unique among the molybdenum and tungsten enzymes as is its reactivity. Prior to this report, the Holm group had already synthesized such type of complexes with [W^{IV}(CO)(SAr)(S₂C₂Me₂)₂]⁻ and [W^{IV}(CO)(SAd)(S₂C₂Me₂)₂]⁻.^{71,72} The respective chemical structures are depicted in Figure 6.19. The crystal structural determination shows that the stereochemistry of the tungsten centers is best described as a distorted trigonal prism. The C–O distances (1.12–1.15 Å) are close to the diatomic distance (1.19 Å) found for the active site.

6.6.4 The Unidentified W Center

The enzyme WOR4 plays a role in S⁰ reduction utilizing dihydrogen. Unfortunately, the precise active site structure is still unclear.⁷¹ Three different [W^{IV}O(dithiolene)₂]²⁻ complexes (dithiolene = mnt, bdtCl₂ and bdt) were treated with S⁰ and converted to [W^{VI}O(S₂)(dithiolene)₂]²⁻ at room temperature.^{73,74,75} The pentagonal-bipyramidal geometries of the tungsten(vi) centers were determined by X-ray structural analysis. Among the three respective W^{VI}O(S₂) complexes, the one with bdt reacts with dihydrogen retrieving the W^{IV}O complex and evolving H₂S.⁷⁵ The other two complexes are not changed by the presence of dihydrogen. As shown in Figure 6.20, based on DFT studies and labeling experiments using ³⁴S, a W^{VI}O(η^1 -S₂) intermediate exhibiting a monodentate S₂²⁻ coordination and a triplet ground state has been proposed to be the active oxidant of dihydrogen. In [W^{VI}O(S₂)(bdt)₂]²⁻, the weakened W^{VI}–S bonds in the strained WS₂ ring facilitate the dissociation of one of the W^{VI}–S₂ bonds due to the stronger *trans* influence of bdt compared to bdtCl₂ and mnt.

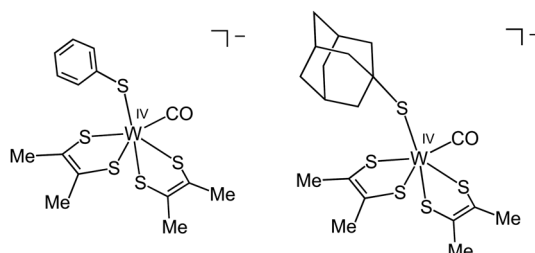


Figure 6.19 Active site models for benzoyl-coenzyme A reductase.

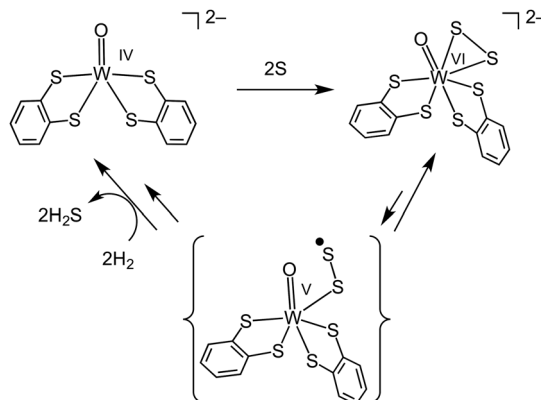


Figure 6.20 Sulfurization and de-sulfurization of the tungsten bdt model complex for WOR4.

6.7 Conclusion

In summary, the model chemistry using dithiolene ligands for the molybdenum and tungsten enzyme active sites is well advanced. In particular molybdenum dithiolene complexes are available in impressive numbers and varieties. At the same time the most challenging tasks still await to be mastered and ever more refined synthetic methods will be required. In addition, as the recent case of the BCRs shows, there might be some more unusual active sites out there waiting to be discovered. Model chemists working in this field will surely be well occupied for some time to come.

References

1. R. H. Holm, P. Kennepohl and E. I. Solomon, *Chem. Rev.*, 1996, **96**, 2239.
2. D. F. Shriver and P. W. Atkins, *Inorganic Chemistry*, 3rd edn, Oxford University Press, New York, 1999.
3. R. Hille, *Chem. Rev.*, 1996, **96**, 2757.
4. M. K. Johnson, D. C. Rees and M. W. W. Adams, *Chem. Rev.*, 1996, **96**, 2817.
5. R. Hille, J. Hall and P. Basu, *Chem. Rev.*, 2014, **114**, 3963.
6. M. H. V. Huynh and T. J. Meyer, *Chem. Rev.*, 2007, **107**, 5004.
7. E. Stiefel, *Prog. Inorg. Chem.*, 2004, 52.
8. T. Conrads, C. Hemann, G. N. George, I. J. Pickering, R. C. Prince and R. Hille, *J. Am. Chem. Soc.*, 2002, **124**, 11276.
9. S. Boyde, S. R. Ellis, C. D. Garner and W. Clegg, *J. Chem. Soc., Chem. Commun.*, 1986, 1541.
10. A. Döring, C. Fischer and C. Schulzke, *Z. Anorg. Allg. Chem.*, 2013, **639**, 1552.
11. D. Coucouvanis, A. Hadjikyriacou, A. Toupadakis, S. M. Koo, O. Ileperuma, M. Draganjac and A. Salifoglou, *Inorg. Chem.*, 1991, **30**, 754.

Synthesis of Mono- and Bisdithiolene Molybdenum and Tungsten Model Compounds 191

12. S. K. Das, P. K. Chaudhury, D. Biswas and S. Sarkar, *J. Am. Chem. Soc.*, 1994, **116**, 9061.
13. J. P. Donahue, C. R. Goldsmith, U. Nadiminti and R. H. Holm, *J. Am. Chem. Soc.*, 1998, **120**, 12869.
14. B. S. Lim and R. H. Holm, *J. Am. Chem. Soc.*, 2001, **123**, 1920.
15. B. S. Lim, J. P. Donahue and R. H. Holm, *Inorg. Chem.*, 2000, **39**, 263.
16. E. S. Davies, R. L. Beddoes, D. Collison, A. Dinsmore, A. Docrat, J. A. Joule, C. R. Wilson and C. D. Garner, *J. Chem. Soc., Dalton Trans.*, 1997, 3985.
17. H. Sugimoto, M. Harihara, M. Shiro, K. Sugimoto, K. Tanaka, H. Miyake and H. Tsukube, *Inorg. Chem.*, 2005, **44**, 6386.
18. P. P. Samuel, S. Horn, A. Doring, K. G. V. Havelius, S. Reschke, S. Leimkuhler, M. Haumann and C. Schulzke, *Eur. J. Inorg. Chem.*, 2011, 4387.
19. J.-P. Porcher, T. Fogeron, M. Gomez-Mingot, E. Derat, L.-M. Chamoreau, Y. Li and M. Fontecave, *Angew. Chem., Int. Ed.*, 2015, **54**, 14090.
20. H. Sugimoto, S. Tatemoto, K. Suyama, H. Miyake, S. Itoh, C. Dong, J. Yang and M. L. Kirk, *Inorg. Chem.*, 2009, **48**, 10581.
21. N. Yoshinaga, N. Ueyama, T. Okamura and A. Nakamura, *Chem. Lett.*, 1990, 1655.
22. H. Sugimoto, M. Tarumizu, K. Tanaka, H. Miyake and H. Tsukube, *Dalton Trans.*, 2005, 3558.
23. S. K. Das, P. K. Chaudhury, D. Biswas and S. Sarkar, *J. Am. Chem. Soc.*, 1994, **116**, 9061.
24. P. J. Ellis, T. Conrads, R. Hille and P. Kuhn, *Structure*, 2001, **9**, 125.
25. H. Sugimoto, M. Tarumizu, H. Miyake and H. Tsukube, *Eur. J. Inorg. Chem.*, 2006, 4494.
26. H. Sugimoto, H. Tano, H. Miyake and S. Itoh, *Dalton Trans.*, 2011, **40**, 2358.
27. H. Schindelin, C. Kisker, J. Hilton, K. V. Rajagopalan and D. C. Rees, *Science*, 1996, **272**, 1615.
28. S. D. Garton, J. Hilton, H. Oku, B. R. Crouse, K. V. Rajagopalan and M. K. Johnson, *J. Am. Chem. Soc.*, 1997, **119**, 12906.
29. C. Mirjam, D. S. Jean-Philippe, P. Janine, G. Gerard, M. Vincent and H. Richard, *J. Mol. Biol.*, 1998, **284**, 435.
30. M. Jormakka, D. Richardson, B. Byrne and S. Iwata, *Structure*, 2004, **12**, 95.
31. D. P. Kloer, C. Hagel, J. Heider and G. E. Schulz, *Structure*, 2006, **14**, 1377.
32. A. Messerschmidt, H. Niessen, D. Abt, O. Einsle, B. Schink and P. M. H. Kroneck, *Proc. Natl. Acad. Sci. U. S. A.*, 2004, **101**, 11571.
33. M. J. Maher, J. Santini, I. J. Pickering, R. C. Prince, J. M. Macy and G. N. George, *Inorg. Chem.*, 2004, **43**, 402.
34. J. H. Enemark, J. J. A. Cooney, J.-J. Wang and R. H. Holm, *Chem. Rev.*, 2004, **104**, 1175.
35. J. McMaster, J. M. Tunney and C. D. Garner, *Prog. Inorg. Chem.*, 2004, **52**, 539.
36. H. Sugimoto and H. Tsukube, *Chem. Soc. Rev.*, 2008, **37**, 2609.

37. R. H. Holm, E. I. Solompn, A. Majumdar and A. Tenderholt, *Coord. Chem. Rev.*, 2011, **255**, 993.
38. C. Schulzke, *Eur. J. Inorg. Chem.*, 2011, 1189.
39. A. Majumdar, *Dalton Trans.*, 2014, **43**, 8990.
40. J. P. Donahue, C. R. Goldsmith, U. Nadiminti and R. H. Holm, *J. Am. Chem. Soc.*, 1998, **120**, 12869.
41. B. S. Lim, J. P. Donahue and R. H. Holm, *Inorg. Chem.*, 2000, **39**, 263.
42. J.-J. Wang, C. Tessier and R. H. Holm, *Inorg. Chem.*, 2006, **45**, 2979.
43. J.-J. Wang, C. Tessier and R. H. Holm, *Inorg. Chem.*, 2006, **45**, 2979.
44. H. Sugimoto, S. Tatemoto, K. Suyama, H. Miyake, R. P. Mtei, S. Itoh and M. L. Kirk, *Inorg. Chem.*, 2010, **49**, 5368.
45. N. Cobb, T. Conrads and R. Hille, *J. Biol. Chem.*, 2005, **280**, 11007.
46. H. Sugimoto, M. Sato, L. J. Giles, K. Asano, T. Suzuki, M. L. Kirk and S. Itoh, *Dalton Trans.*, 2013, **42**, 15927.
47. J. Jiang and R. H. Holm, *Inorg. Chem.*, 2005, **44**, 1068.
48. J. Jiang and R. H. Holm, *Inorg. Chem.*, 2004, **43**, 1302.
49. J. C. Boyington, V. N. Gladyshev, S. V. Khangulov, T. C. Stadtman and P. D. Sun, *Science*, 1997, **275**, 1305.
50. H. C. A. Raaijmakers and M. J. Romao, *J. Biol. Inorg. Chem.*, 2006, **11**, 1261.
51. H. Sugimoto, T. Sakurai, H. Miyake, K. Tanaka and H. Tsukube, *Inorg. Chem.*, 2005, **44**, 6927.
52. H. Sugimoto, H. Tano, K. Suyama, T. Kobayashi, H. Miyake, S. Itoh and M. L. Kirk, *Dalton Trans.*, 2011, **40**, 1119.
53. H. Tano, R. Tajima, H. Miyake, S. Itoh and H. Sugimoto, *Inorg. Chem.*, 2008, **47**, 7465.
54. C. Kisker, H. Schindelin, A. Pacheco, W. A. Wehbi, R. M. Gaarrett, K. V. Rajagopalan, J. H. Enemark and D. C. Rees, *Cell*, 1997, **91**, 973.
55. B. S. Lim, M. W. Willer, M. Miao and R. H. Holm, *J. Am. Chem. Soc.*, 2001, **123**, 8343.
56. K. Okamoto, K. Matsumoto, R. Hille, B. T. Eger, E. F. Pai and T. Nishino, *Proc. Natl. Acad. Sci. U. S. A.*, 2004, **101**, 7931.
57. I. Bonin, B. M. Martins, V. Purvanov, S. Fetzner, R. Huber and H. Dobbek, *Structure*, 2004, **12**, 1425.
58. N. Wagener, A. J. Pierik, A. Ibdah, R. Hille and H. Dobbek, *Proc. Natl. Acad. Sci. U. S. A.*, 2009, **106**, 11055.
59. H. Sugimoto, S. Tatemoto, K. Toyota, K. Ashikari, M. Kubo, T. Ogura and S. Itoh, *Chem. Commun.*, 2013, **49**, 4358.
60. B. S. Lim, K.-M. Sung and R. H. Holm, *J. Am. Chem. Soc.*, 2001, **122**, 7410.
61. J. Jiang and R. H. Holm, *Inorg. Chem.*, 2004, **43**, 1302.
62. J.-J. Wang, C. Tessier and R. H. Holm, *Inorg. Chem.*, 2006, **45**.
63. S. Groysman, J.-J. Wang, R. Tagore, S. C. Lee and R. H. Holm, *J. Am. Chem. Soc.*, 2008, **130**, 12794.
64. M. K. Chan, S. Mukund, A. Kletzin, M. W. W. Adams and D. C. Rees, *Science*, 1995, **267**, 1463.

65. H. Raaijmakers, S. Macieira, J. M. Dias, S. Teixeira, S. Bursakov, R. Huber, J. J. G. Moura, I. Moura and M. J. Romao, *Structure*, 2002, **10**, 1261.
66. G. B. Seiffert, G. M. Ullmann, A. Messerschmidt, B. Schink, P. M. H. Kroenck and O. Einsle, *Proc. Natl. Acad. Sci. U. S. A.*, 2007, **104**, 3073.
67. H. Sugimoto, H. Tano, R. Tajima, H. Miyake, H. Tsukube, H. Ohi and S. Itoh, *Inorg. Chem.*, 2007, **46**, 8460.
68. H. Sugimoto, K. Hatakeyama, K. Toyota, S. Tatemoto, M. Kubo, T. Ogura and S. Itoh, *Dalton Trans.*, 2013, **42**, 3059.
69. M. K. Johnson, *Prog. Inorg. Chem.*, 2004, **52**, 491.
70. T. Weiner, S. G. Huwiler, J. W. Kung, S. Weidenweber, P. Hellwig, H.-J. Stark, T. Biskup, S. Weber, J. J. H. Cotelesage, G. N. George, U. Ermler and M. Boll, *Nat. Chem. Biol.*, 2015, **11**, 815.
71. K.-M. Sung and R. H. Holm, *Inorg. Chem.*, 2000, **39**, 1275.
72. R. Roy and M. W. W. Adams, *J. Bacteriol.*, 2002, **184**, 6952.
73. J. Yadav, S. K. Das and S. Sarkar, *J. Am. Chem. Soc.*, 1997, **119**, 4315.
74. H. Sugimoto, R. Tajima, T. Sakurai, H. Ohi, H. Miyake, S. Itoh and H. Tsukube, *Angew. Chem., Int. Ed.*, 2006, **45**, 3520.
75. H. Sugimoto, H. Tano, K. Toyota, R. Tajima, H. Miyake, I. Takahashi, S. Hirota and S. Itoh, *J. Am. Chem. Soc.*, 2010, **132**, 8.

CHAPTER 7

Models for the Xanthine Oxidase Family of Enzymes

CHARLES G. YOUNG^a

^aDepartment of Chemistry and Physics, La Trobe Institute for Molecular Science, La Trobe University, Melbourne, Victoria 3086, Australia

*E-mail: Charles.Young@latrobe.edu.au

7.1 Introduction

Pterindithiolene–molybdenum enzymes constitute a large and important class of biomolecules that catalyze two-electron redox reactions, typically involving net oxygen atom transfer (OAT) to or from small organic molecules and oxyanions with water being the source or sink of oxygen atoms.^{1–12} These enzymes are widely distributed in microorganisms, plants and animals and play key roles in cellular metabolism, catabolism and respiration^{1–12} and Earth's biogeochemical cycles, weather patterns and albedo.^{13,14} Hille¹ has classified the enzymes into three families named after the archetypal Mo enzymes xanthine oxidase (XnO), sulfite oxidase (SO) and dimethyl sulfoxide reductase (DMSOR). A full description of these enzymes can be found in many excellent reviews, both general^{1–12} and specifically devoted to the title xanthine oxidase family of enzymes.^{8–12} The modelling of Mo enzymes has also been extensively reviewed^{15–23} but not from the unique perspective proffered in this contribution. Finally, molybdenum^{24–26} and (more particularly) molybdenum–sulfur (Mo/S)^{27–32} coordination chemistry underpins enzyme model studies and reviews in these areas are particularly relevant and illuminating.

RSC Metallobiology Series No. 6

Molybdenum and Tungsten Enzymes: Bioinorganic Chemistry

Edited by Russ Hille, Carola Schulzke, and Martin L. Kirk

© The Royal Society of Chemistry 2017

Published by the Royal Society of Chemistry, www.rsc.org

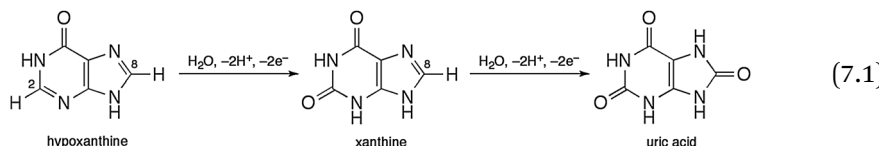
This review focuses on efforts to synthesize small molecule analogues of enzymes from the xanthine oxidase family, also known as molybdenum hydroxylases; the term “molybdenum hydroxylase model” (MoHM) is used to refer to these systems. The semantics relating to what constitutes a valid model and whether particular compounds deserve that status are set aside in favour of a broad and inclusive approach. The fact is, there are no “accurate” models of these enzymes and restrictive definitions would severely limit the scope and potential value of this contribution. The review begins with a brief account of developments in the “biological sphere” and how they have informed model studies over time.^{1–12} The enzyme active sites revealed by these studies, which epitomize “idealized” MoHMs, are then presented. The next section provides background useful to the synthesis of MoHMs, especially oxosulfido-Mo species. Available MoHMs are then discussed. In each case, oxidized active site models are treated first, followed by reduced active site models. The review concludes with a short summary and prospectus for future work in this area.

7.2 Molybdenum Hydroxylases

7.2.1 Overview of the Enzymes

Most enzymes of the xanthine oxidase family catalyze the hydroxylation of C–H bonds in aromatic heterocycles (purines, pyrimidines, pterins), aldehydes and related organic substrates.^{1–10} Xanthine oxidase, the head of the family, is typically isolated from bovine milk and employs dioxygen as its electron acceptor; physiologically, mammalian XnO is active in the dehydrogenase form (XnDH), where NAD⁺ acts as the electron acceptor. The enzymes from other sources, e.g. birds, insects and bacteria, are stable dehydrogenases. These enzymes play important roles in purine catabolism, pro-drug activation, oxidative stress response and microbial protection mechanisms.

In its role in purine catabolism, XnDH catalyzes sequential hydroxylation of the C-2 and C-8 atoms of hypoxanthine, converting it first to xanthine and then to uric acid (eqn (7.1), keto forms shown). In humans, enzyme deficiency is associated with xanthinuria types I and II, the symptoms of which include urinary tract infections, myopathy, arthritis, arthralgia, kidney stones and acute renal failure, while over-activity causes hyperuricemia and the deposition of urate salts in the joints leading to gout.^{33,34}



Mammalian aldehyde oxidases (AOs) catalyze the oxidation of aldehydes to carboxylic acids and play important roles in the metabolism of N-heterocyclic compounds, the reduction of nitro-aromatic compounds and the

biotransformation of many drugs and xenobiotics.^{1–10} The enzymes, typically isolated from rabbit or rat liver, are closely related to bovine XnO, as they feature related active sites and modes of action. Bacterial AOs contain a dinucleotide form of molybdopterin (MPT) and use ferredoxin rather than NAD⁺ or O₂ as oxidizing substrate. The aldehyde:ferredoxin oxidoreductase (AOR) from *Desulfovibrio gigas* is involved in an electron transfer chain that couples aldehyde oxidation to hydrogen production.^{1–10}

Aerobic carbon monoxide dehydrogenase (CODH)^{5–7,11,12} is found in carboxidotrophic bacteria that derive their carbon and energy from the oxidation of CO to CO₂.³⁵ These and related soil organisms are estimated to remove ca. 200 million tonnes of CO from the biosphere, contributing to carbon sequestration and cycling and the removal of toxic CO from the lower atmosphere.³⁶ Less well-known members of the xanthine oxidase family include quinoline-2-oxidoreductase (QOR), nicotinate dehydrogenase (NDH), pyrogallol transhydroxylase and 4-hydroxybenzoyl-CoA reductase.^{1,7}

7.2.2 Key Discoveries Informing Model Studies

Today, there is an abundance of knowledge relating to Mo–MPT enzymes.^{1–12} However, this was not always the case, as the following “potted history” shows. The focus here is on discoveries, mainly concerning XnO/XnDH,³⁷ that have significantly influenced the work of synthetic model chemists; these are summarized in the timeline shown in Figure 7.1.

Xanthine oxidase was identified by Morgan *et al.*³⁸ in 1922 following the enzyme’s initial isolation by Schardinger³⁹ in 1902. However, it was many decades later that Mo was identified as a requirement for XnO activity.^{40,41} This, along with the earlier discovery that Mo was required for nitrogenase

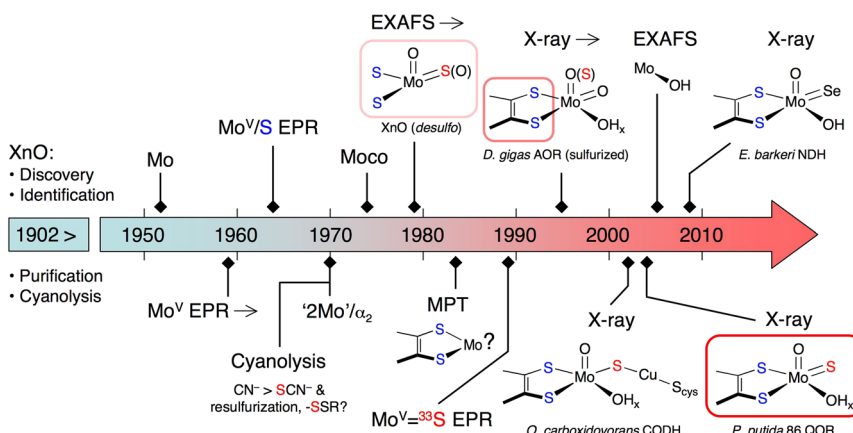


Figure 7.1 Timeline of discoveries informing MoHM studies (getting hotter with time!). Sulfido and dithiolene ligand donor atoms are indicated in red and blue, respectively.

activity,⁴² stimulated research into Mo coordination chemistry.⁴³ Electron paramagnetic resonance (EPR) studies of the d¹ Mo(v) forms of XnO were initiated by Bray in the late 1950s;^{44,45} this technique remains at the vanguard of methods used to probe Mo–MPT enzymes.^{46–48} Early EPR studies by Meriwether *et al.*⁴⁹ strongly implicated sulfur (possibly thiolate) ligation to Mo at the active site of XnO. Determination of the tertiary structure of the enzyme, α_2 with 1 Mo atom per subunit, led to the investigation of dinuclear Mo-thiolate compounds as MoHMs.⁴³ Subsequent studies focused on the synthesis and chemistry of strictly mononuclear model complexes, the Mo centres being well separated in enzymes. In 1970, Massey and Edmondson⁵⁰ reported that cyanolysis of XnO (originally observed by Szent-Györgyi⁵¹ in 1926) produced free thiocyanate and that desulfo-XnO could be reactivated by sulfide. These results indicated the presence of a catalytically essential sulfur atom, thought for many years to be part of a persulfide moiety (–SSR). The existence of an exchangeable Mo-cofactor (Moco) was confirmed by Nason and coworkers in 1974.⁵² The similarity of XnO and mammalian AOs was recognized in the mid 1900s and *D. gigas* AOR was identified in 1987.⁵³

In the late 1970s, the application of Extended X-ray Absorption Fine Structure (EXAFS) spectroscopy^{48,54} to XnO identified the catalytically essential sulfur atom as a terminal sulfido ligand possessing an Mo=S distance of *ca.* 2.15 Å.^{55–58} Attempts to synthesize oxosulfido-Mo complexes began and complexes of this type soon appeared (see Section 7.4.1.1.2). EPR studies of isotopically labelled “very rapid” xanthine oxidase (*vide infra*)⁵⁹ and oxosulfido-Mo(v) model compounds (Section 7.4.1.2.1) supported the presence of a terminal sulfido ligand at Mo. The identity of the two other S-donor ligands identified by EXAFS remained a mystery until 1982, when Rajagopalan and coworkers⁶⁰ proposed the bidentate coordination of MPT in Moco. This sparked investigations into the possible binding modes of MPT as well as the chemical synthesis of MPT and Moco.^{61–64} After 30 years, the total synthesis of MPT and Moco are now close to becoming a reality.^{65–67}

Advances in protein crystallography have been responsible for major insights into the structures of Mo and related W enzymes.^{68,69} Early results⁷⁰ confirmed the essential structure (in two forms) and dithiolenic coordination mode of MPT proposed by Rajagopalan and coworkers.⁶⁰ Crystal structures of *D. gigas* AOR^{71,72} revealed a five-coordinate, square-pyramidal active site but the identification of an apical sulfido ligand⁷² remained contentious.⁷³ Nevertheless, MoHMs of the type [(DT)MoOS(OH)][–] (DT = dithiolene) were now squarely on the drawing board. Recently, Moura and coworkers^{74,75} provided evidence that *D. gigas* AOR is a functional dioxo-Mo(vi) hydroxylase.

Meanwhile, Meyer and Rajagopalan^{76,77} had established that the CODHs from *Oligotropha carboxidovorans* and *Hydrogenophaga pseudoflava* were Mo hydroxylases. The crystal structures of these enzymes eventually revealed a heterobimetallic MoO(μ -S)Cu active site (Figure 7.2(a)) and provided the first, albeit indirect, crystallographic evidence for a basal sulfido ligand

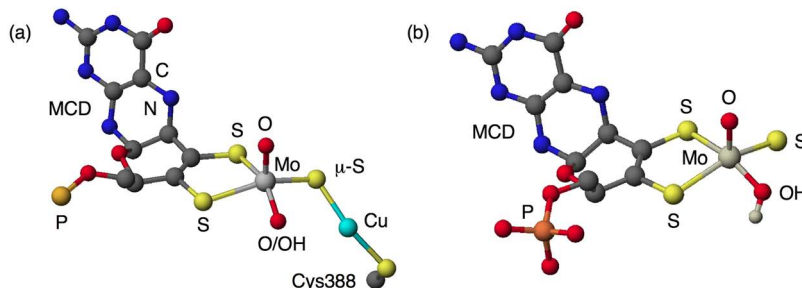


Figure 7.2 (a) Active site of *O. carboxidovorans* CODH. An aqua ligand is weakly bound to the Cu centre but is displaced by CO in the first step of the catalytic cycle. (b) Active site of *P. putida* 86 QOR.

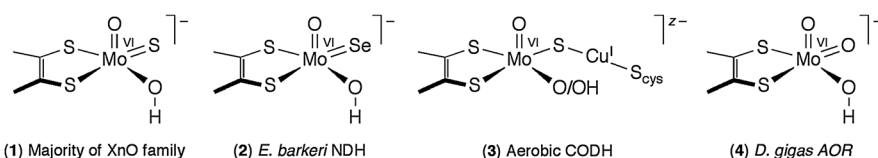
in Mo hydroxylases.^{78,79} EXAFS studies supported the presence of two oxo ligands (apical and basal) at the active site.⁷⁹ CODH is also deactivated by cyanide but can be reactivated by sulfide and Cu(I).^{78–80}

Half a century after the first crystals of XnO were obtained,⁸¹ the crystal structures of bovine XnO and XnDH were reported by Nishino, Pai and coworkers;⁸² however, the position of the sulfido ligand still remained uncertain. Finally, in 2004, the crystal structures of *Pseudomonas putida* 86 QOR (Figure 7.2(b))⁸³ and substrate (FYX-051)-bound bovine XnDH⁸⁴ revealed the presence of basal sulfide-based ligands. Subsequent EXAFS studies of oxidized XnO supported the presence of a hydroxo ligand at physiological pH and its deprotonation to form an Mo–O[−] moiety under basic conditions.⁸⁵ The most common active site structure of the Mo hydroxylases and the prime target of MoHM studies was now precisely defined. In 2009, the crystal structure of *Eubacterium barkeri* NDH, isolated by Holcenberg and Stadtman⁸⁶ in 1969, identified a new type of Mo hydroxylase active site wherein a terminal selenido ligand replaces the sulfido ligand present in other enzymes.⁸⁷

The past two decades have witnessed spectacular progress in our understanding of MPT/Moco^{88,89} and Mo–MPT enzymes.^{1–12} Advances in enzymology, molecular biology, genetics, spectroscopy and protein crystallography have all contributed to progress in defining the genetics, biosynthesis, biochemistry, structures and functions of these important biomolecules. These techniques have been augmented by high-level computational studies^{90–92} and investigations into orbital control of enzyme mechanisms.^{92–94} Model studies, which once served to define the fundamental chemistry of Mo and inform enzyme studies, have become less relevant as these powerful, direct probes for the enzymes have emerged. However, the synthetic challenge of modelling enzyme active sites remains and this continues to drive advances in Mo (and W) coordination chemistry. The synthetic challenge is underscored by the fact that accurate MoHMs are yet to appear.

7.2.3 Active Sites and Model Targets

The biological studies summarized above have fully defined the oxidized active sites of the enzymes and provided “idealized” targets for MoHM studies. These targets are represented in structures (1)–(4), in rough order of prevalence in enzymes. In the enzymes, the dithiolene ligand represents MPT (or a dinucleotide derivative thereof) while in models it represents a synthetic simulant of this unique biological ligand.



(1) Majority of XnO family

(2) *E. barkeri* NDH

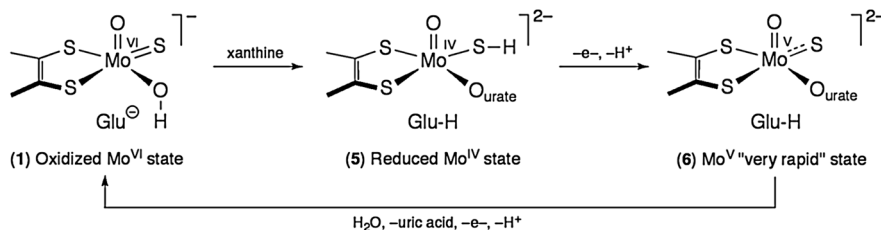
(3) Aerobic CODH

(4) *D. gigas* AOR

The majority of Mo hydroxylases contain the oxosulfido-Mo(vi) active site (1)^{1–10} and this active site (or components thereof) has inspired the bulk of MoHM studies. Accordingly, studies directed at understanding or replicating this active site are the main focus of this review. Substantial background to this area is provided in Section 7.3.2.1 and available models are discussed in Section 7.4.1.1. There are only a handful of models for the oxoselenido-Mo(vi) (2) and MoO(μ -S)Cu (3) active sites; background and models for these active sites are described in Sections 7.3.2.1 and 7.4.1.1 (in combination with oxosulfido MoHMs) and Sections 7.3.2.3 and 7.4.2.2, respectively. To date, the dioxo(hydroxo)-Mo(vi) active site (4) is restricted to *D. gigas* AOR,^{74,75} inactive desulfo Mo hydroxylases^{1–12} and deprotonated MoeA,⁹⁵ an intermediate in Moco biosynthesis. At this point in time it has limited and uncertain relevance to Mo hydroxylases.⁷ Accordingly, models of this site will not be discussed in this review.

As well as oxidized enzyme states, a variety of reduced Mo(iv) and Mo(v) states are accessed during enzyme turnover or inhibition. Typically, Mo(vi) and Mo(iv) states are inter-converted by two-electron substrate transformations and Mo(v) states are generated during the first of the two sequential one-electron transfers required to regenerate the active site.^{1–12} Direct characterization of the diamagnetic, d², Mo(iv) states is limited but the paramagnetic, d¹, Mo(v) states have been extensively probed by EPR, Electron-Nuclear Double Resonance (ENDOR) and Magnetic Circular Dichroism (MCD) spectroscopies.^{96–98}

In the case of xanthine oxidation by XnO/XnDH (Scheme 7.1), oxidized enzyme (1) is reduced to a hydrosulfido-Mo(iv) centre, [(MPT)Mo^{IV}O(SH)(urate)]²⁻ (5), upon substrate oxidation. This is then oxidized by one electron to produce the “very rapid” Mo(v) form, [(MPT)Mo^VOS(urate)]²⁻ (6), named after the very rapid ($t_{1/2} \sim 10$ ms) appearance of the attendant “very rapid” EPR signal.⁴⁶ Displacement of oxidized substrate by hydroxide and further oxidation releases uric acid and regenerates the oxidized enzyme.⁸ Many other Mo(v) states can be generated during the turnover or inhibition of Mo hydroxylases.⁴⁶ Various one-electron reduced Mo^VCu^I forms of CODH have



Scheme 7.1

also been generated and EPR and ENDOR studies show strong coupling to both ^{95,97}Mo ($I = 5/2$, 25%) and ^{63,65}Cu ($I = 3/2$, 100%).^{80,99–101}

The majority of model studies have focused on the synthesis of the oxidized enzyme active sites (or components thereof) but reduced active sites and chemically/catalytically functional systems boasting the inter-conversion of all three accessible enzyme oxidation states are also important targets for model studies. Models of reduced Mo hydroxylases are described in Sections 7.4.1.2 and 7.4.2.2.

7.3 Active Site Components: Synthetic Background

7.3.1 General Challenges

In simple terms, the modelling of the oxosulfido-Mo(vi) active site (1) requires the combination of the two components shown in Figure 7.3; the first is the oxosulfido moiety itself (Figure 7.3(a), red boxes), the second is the mono(dithiolene) moiety (Figure 7.3(b), blue box). Active sites (2)–(4) can be similarly partitioned into related chalcogenide and dithiolenic components. It should be obvious that the modelling of Mo hydroxylase active sites is first and foremost an exercise in Mo/S chemistry, a rich but notoriously difficult area.^{27–32}

There are at least three significant synthetic challenges that must be overcome in generating MoHMs. The first is combining an oxidizing Mo(vi) centre with reducing sulfido and selenido ligands without initiating redox reactions leading to undesirable or intractable (decomposition) products. This requires the judicious choice of co-ligands and careful control of the redox potential of reagents and reaction conditions (especially temperature). The second is preventing dinucleation or polymerization through the formation of bridging oxo or sulfido ligands. This is commonly achieved through the use of sterically bulky co-ligands to prevent the close approach of Mo centres; spatial isolation *via* intercalation¹⁰² or polymer support¹⁰³ has been exploited in the development of oxotransferase models but is yet to be applied in MoHMs. These two challenges are intimately connected, as the reduction of Mo increases the tendency for association – this is especially true of Mo(v) species. In oxosulfido-Mo(vi) chemistry, both phenomena appear to

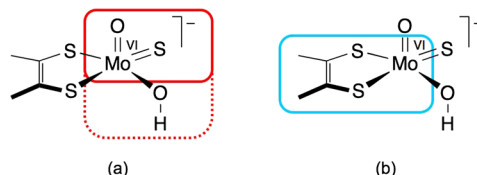


Figure 7.3 The principal components of XnO/XnDH models. (a) The oxosulfido-Mo(vi) moiety (with or without the hydroxo co-ligand). (b) The mono(dithiolene)-Mo(vi) moiety (often including the oxo ligand in known complexes).

be exacerbated by the presence of sulfur-donor co-ligands, including dithiolenes. Indeed, these ligands are often active participants in undesirable redox reactions and are themselves prolific bridging ligands. The third challenge is preventing hydrolysis of the sulfido/selenido ligands and/or dithiolene ligand exchange to produce thermodynamically stable oxo or bis- and tris-dithiolene species. This may require second-coordination-sphere, host-guest or encapsulation strategies that mimic the protective role of the apo-protein in Mo enzymes.

The following section discusses the background, strategies and types of reagents necessary for the generation of the chalcogenide active site components of (1) (Figure 7.3(a)) or their equivalents for (2) and (3). This is followed by consideration of strategies for the generation of mono(dithiolene) components (Figure 7.3(b); Section 7.3.3) and the stabilization, post-synthesis, of MoHMs (Section 7.3.4).

7.3.2 The Chalcogenido Components: Background, Synthetic Approaches and Reagents

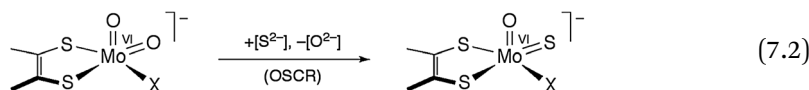
7.3.2.1 Oxosulfido- and Oxoselenido-Mo(VI) Species

Molybdenum has a special affinity for sulfur and the close energy match of the Mo 4d and S 3p orbitals often leads to fascinating but unpredictable chemistry.²⁷⁻³² Molybdenum forms many solid-state sulfides, including the principal ore molybdenite (MoS_2), Mo_2S_3 , Mo_2S_5 , non-stoichiometric sulfides and Chevrel phases. These compounds enjoy increasing use as lubricants, electronic materials and catalysts.¹⁰⁴⁻¹⁰⁸

The molecular chemistry of Mo and S is staggering in its diversity, complexity and frequently counter-intuitive reactions.²⁷⁻³² Accordingly, Mo/S compounds vary widely in their nuclearity and metal oxidation state(s) and often display extensive catenation of sulfur, producing di- and polysulfido ligands that undergo facile inter-conversion, disproportionation and com-proportionation reactions. This behaviour has thwarted many efforts to syn-thesize MoHMs (*vide infra* and Section 7.3.3.1). A sense of the complexity of Mo/S chemistry and metal/sulfur chemistry more generally can be gleaned from specialist reviews in this area.²⁷⁻³²

The majority of sulfido-Mo/W complexes are di- or polynuclear, μ -sulfido or di- μ -sulfido species. Mononuclear complexes are relatively rare and are generally stable only in the presence of redox-inactive (innocent), sterically bulky co-ligands^{24–26} or at low temperatures (a notable aspect of many successful syntheses). Terminal sulfido-Mo complexes can be prepared by a variety of reactions but most involve the conversion of oxo ligands into sulfido ligands, herein referred to as oxo \rightarrow sulfido conversion reactions (OSCRs), or sulfur atom transfer (SAT) reactions (often combined with prior OAT). Terminal sulfido-Mo complexes are characterized by a moderately strong $\nu(\text{Mo=S})$ IR band in the range 505–425 cm^{−1} (depending on the presence or absence of other strong field ligands and oxidation state), strong S_{1s} \rightarrow (Mo_{4d} + S_{3p}) S K preedge transition bands and Mo=S distances around av. 2.154 Å ($\sigma = 0.087$ Å). Comprehensive reviews of sulfido- and selenido-transition metal chemistry are available elsewhere.^{109–111}

7.3.2.1.1 Synthetic Strategy 1: Oxo to Sulfido/Selenido Ligand Conversions. The OSCR is a conceptually simple strategy for the synthesis of oxosulfido-Mo(vi) species, the reaction of a pre-formed [(DT)MoO₂X][−] (e.g. X = OH[−]) complex with a suitable sulfiding reagent (eqn (7.2)) offering the ideal strategy for the synthesis of models for active site (1). A similar approach may be envisioned for the synthesis of oxoselenido-Mo model compounds.



Unfortunately, this approach is fraught with problems arising from the facile reduction of Mo(vi) by available sulfiding agents and subsequent catenation and/or aggregation (usually *via* μ -sulfido bridge formation).^{27–32} Only a few tetrahedral or pseudo-tetrahedral dioxo-Mo(vi) complexes have been converted to stable oxosulfido-Mo(vi) analogues using this method (Section 7.4.1.1). However, some of these complexes, particularly the thiomolybdates, are useful precursors in relevant oxosulfido-Mo(vi) chemistry. Similar difficulties attend oxo \rightarrow selenido conversion reactions.

Oxo \rightarrow sulfido conversion reactions are generally more successful at Mo(v) and Mo(iv) centres, as these are less susceptible to redox and catenation/aggregation reactions. The products of these reactions may serve as models for reduced enzyme states or be amenable to oxidation to form oxosulfido-Mo(vi) species (*vide infra*). However, Holm and coworkers have noted that “the transformation of Mo=O \rightarrow Mo=S for multiply bound terminal ligands does not have a general solution”.¹¹² This statement acknowledges the fact that OSCRs are unpredictable and success (when it comes) may involve considerable trial-and-error. It is hoped that this situation will change as more research is conducted and as new reagents and methodologies emerge.

The most successful reagents available for OSCRs include hydrogen sulfide, hydrosulfides, boron sulfide and hexamethyldisilthiane. Brief accounts of these reagents and their applications are given in the following paragraphs.

Hydrogen selenide and $\text{NEt}_4\text{SeH}^{113}$ are among the few reagents currently used for oxo → selenido conversion reactions.

Hydrogen sulfide, H_2S , is a colourless, poisonous, corrosive, flammable and potentially explosive gas familiar to most people as “rotten egg gas”. Its “discovery” is credited to Carl Wilhelm Scheele in 1777.¹¹⁴ The gas is commercially available and applications range from organosulfur¹¹⁵ and metal-sulfur^{27–32,109–111} chemistry to the production of heavy water (Girdler-Spevack process).

In aqueous solution H_2S is a weak acid, producing hydrosulfide ($\text{p}K_{\text{a}1} = 6.9$) and sulfide ($\text{p}K_{\text{a}2} > 14$). Dissolution of H_2S in ammonia solution produces fuming ammonium hydrosulfide/sulfide solutions that serve as powerful but strongly reducing reagents for converting oxometallates into thiometallates.¹¹⁶ Tetraalkylammonium hydrosulfides, NR_4SH , are prepared by reacting alcoholic solutions of NR_4OH with H_2S gas; these are typically soluble in organic solvents and are convenient, stoichiometrically controllable (weighable) H_2S equivalents.¹¹⁷ Control of stoichiometry is critically important in limiting undesirable outcomes in reactions involving H_2S (or its equivalents). Silylthiols such as Ph_3SiSH and Pr_3^iSiSH have also found application for the same reasons.^{118–120}

The use of H_2S is diminishing due to the influence of overzealous occupational health and safety officers, who naively equate the gas's odour threshold (*ca.* 0.5 ppb) with toxic levels ($\text{LC}_{50} = 800$ ppm). Indeed, the smell (stench) of many sulfur compounds, often but not always associated with hydrolysis to H_2S , deters many officers/workers and stymies work in this area.

Main group sulfides such as boron sulfide, phosphorus sulfide and antimony sulfide are useful reagents for OSCRs. Boron sulfide (B_2S_3) was first reported by Berzelius¹²¹ and can be prepared by the high-temperature reactions of boron with sulfur vapour and boron or metal borides with H_2S .¹²² Crystalline B_2S_3 adopts a polymeric, layered structure containing 4- and 6-membered B_nS_n rings linked by two-coordinate sulfur atoms.¹²³ The current applications of the compound include organic synthesis and battery and solid-state electrolyte production (see patent literature).

Historically, boron sulfide was used to synthesize solid-state sulfides such as MS_2X_2 and MSX_3 ($\text{M} = \text{Mo, W}; \text{X} = \text{Cl}^-, \text{Br}^-$)¹²⁴ but these compounds are of limited value as MoHM precursors. Its early applications in molecular OSCRs include the synthesis of VS(acen) (acen = *N,N'*-ethylenebis(acetylacetonylideneiminato)),¹²⁵ $\text{MOS}(\text{ONC}_5\text{H}_{10})_2$ ($\text{M} = \text{Mo,}^{126} \text{W}^{127}$) (Section 7.4.1.1.2), $\text{Tp}^*\text{MoS}(\text{S}_2\text{CNR}_2)$ (Tp^* = hydrotris(3,5-dimethylpyrazolyl)borate; R = alkyl)¹²⁸ and $\text{Tp}^*\text{MoS}\text{Cl}_2$ ¹²⁹ (Section 7.4.1.1.3) from their oxo analogues. Following reaction, the addition of alcohols converts excess B_2S_3 to soluble trialkyl borates¹³⁰ and in favourable cases precipitates the desired product. Unfortunately, reduction and polysulfide formation complicate reactions directed at dioxo-Mo(vi) complexes. For example, $\text{Tp}^*\text{MoX}(\text{S}_4)$ ($\text{X} = \text{halide, NCS}^-$),¹³¹ $[\text{Tp}^*\text{MoOSX}]^-$ ($\text{X} = \text{halide, S-donor anion}$)^{132,133} and $[\text{Tp}^*\text{MoO}_2]_2(\mu-\text{O})(\mu-\text{S}_2)$ ^{134,135} are observed as the products of attempted OSCRs involving $\text{Tp}^*\text{MoO}_2\text{X}$ and B_2S_3 .

One of the most effective forms of boron sulfide was the powdered, amorphous form once available from Morton Thiokol. However, commercial supplies of this material were discontinued in the wake of the Space Shuttle *Challenger* disaster. Samples prepared in the laboratory¹²² are much less effective and their difficult synthesis and limited reactivity discourages usage.

Phosphorus sulfide and Lawesson's reagent, $[(4\text{-MeOC}_6\text{H}_4)\text{P}(\text{S})]_2(\mu\text{-S})_2$, are important reagents in organic chemistry^{136,137} but they have found limited applications in metal OSCRs. The synthesis of Tp^*WOSCl and $\text{Tp}^*\text{WS}_2\text{Cl}$ from $\text{Tp}^*\text{WO}_2\text{Cl}$ is a notable example of an OSCR effected by phosphorus sulfide (see Section 7.4.1.1.3).^{138–141}

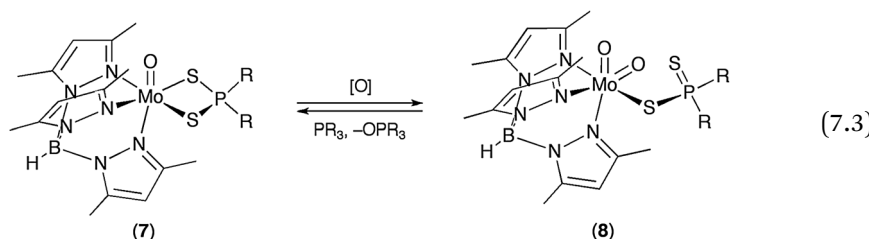
Hexamethyldisilthiane or bis(trimethylsilyl)sulfide, $(\text{Me}_3\text{Si})_2\text{S}$, is a colourless, moisture-sensitive, flammable liquid (b.p. 160 °C) with a strong stench. It was first prepared from trimethylsilyl chloride and silver sulfide by Eaborn in 1950¹⁴² but cheaper, more convenient syntheses facilitated its commercial production. The compound has many applications in organic synthesis, *e.g.* reduction, sulfuration and silylation reactions¹⁴³ and in the production of metal sulfide-based electronic devices, semiconductors, nanoparticles and quantum dots.¹⁴⁴

The use of $(\text{Me}_3\text{Si})_2\text{S}$ in transition metal OSCRs, to produce molecular as well as solid-state sulfides, began in the early 1980s;^{145,146} the first applications in Mo and W chemistry included the conversion of $\text{MoO}_2(\text{ONR}_2)_2$ ($\text{R} = \text{Et}$; $\text{R}_2 = \text{C}_5\text{H}_{10}$) into $\text{MoOS}(\text{ONR}_2)_2$ and $\text{MoS}_2(\text{ONR}_2)_2$ ¹⁴⁷ and $\text{NET}_4^+[\text{WO}_3(\text{CH}_2\text{CMe}_3)]$ into $\text{NET}_4^+[\text{WS}_3(\text{CH}_2\text{CMe}_3)]$.¹⁴⁸ Holm and coworkers also employed $(\text{Me}_3\text{Si})_2\text{S}$ for the sulfidation of early transition metal systems (including Mo).^{149–151} Solid-state metal sulfides are accessible using this reagent and MoOSCl_2 has been prepared (again, this compound appears to have limited value as an MoHM precursor).¹⁵² A significant limitation of hexamethyldisilthiane is its inability to facilitate OSCRs in sterically hindered systems.

7.3.2.1.2 Synthetic Strategy 2: Atom Transfer Methodologies. Bidirectional OAT reactions capable of inter-converting dioxo-Mo(vi) and oxo-Mo(iv) complexes are a notable feature of high-valent Mo chemistry.^{15–26} Oxygen atom acceptors that reduce Mo(vi) to Mo(iv) are restricted to tertiary phosphines but a variety of oxygen atom donors, *e.g.* *N*- and *S*-oxides, peroxides, nitrate and water/dioxygen, are capable of oxidizing Mo(iv) to Mo(vi). Comproportionation to form μ -oxo-Mo(v) dimers is an undesirable aspect in many systems but this can be prevented using sterically bulky co-ligands, electrostatic repulsion or the intercalation or immobilization of complexes on clays and resins.^{15–23}

The first solution-based, comproportionation-free, bidirectional OAT to be reported involved the inter-conversion of $\text{Tp}^*\text{MoO}(\kappa^2\text{-S}_2\text{PR}_2)$ (7; $\text{R} = \text{OME}$, OEt) and $\text{Tp}^*\text{MoO}_2\{\kappa^1\text{-SP}(\text{S})\text{R}_2\}$ (8) (eqn (7.3)).¹⁵³ Similar transformations, involving the $\text{R} = \text{alkyl}$ derivatives, were subsequently reported by Laughlin and Young.¹³³ Indeed, a large number of scorpionate complexes exhibit

similar OAT chemistry and several “holistic” systems emulate many facets of Mo oxotransferase (SO and DMSOR) behaviour.^{17,154,155}



In principle, the reaction of oxo-Mo(IV) complexes with SAT reagents could produce oxosulfido-Mo(VI) species, especially in the presence of innocent, sterically protective co-ligands. Indeed, this strategy has proved indispensable in the development of scorpionate-based MoHMs (Section 7.4.1.1.3). Related conversions, *e.g.* of Mo(II) complexes to sulfido-Mo(IV) species, followed by OAT, may also be useful in the synthesis of oxosulfido-Mo(VI) complexes. Potential sulfur atom donors include elemental sulfur,¹⁵⁶ thiiranes, thiols and phosphine sulfides. However, sulfur's propensity for catenation limits its usefulness in single-atom SAT reactions. To date, thiols and phosphine sulfides have found limited application in such reactions.¹¹¹

Thiiranes (also known as episulfides, thioepoxides or alkene sulfides) were discovered in the early 1900s but their usage was limited until 1934 when Dachlauer and Jackel developed commercially viable syntheses.¹⁵⁷ Thiiranes contain saturated, strained, three-membered C–S–C rings that undergo facile nucleophilic ring opening and SAT.¹⁵⁸ They find many applications in industrial (pharmaceuticals, polymers, pesticides/herbicides) and laboratory-based organic synthesis.^{159–161} Ethylene sulfide (thiirane, b.p. 56 °C), propylene sulfide (methyl thiirane, b.p. 72–75 °C) and cyclohexene sulfide (b.p. 55–58 °C/12 mm Hg) are commonly encountered SAT reagents; they are all colourless, flammable, toxic liquids with a strong stench and a sensitivity towards thermal polymerization/decomposition (store at 2–8 °C).

The use of thiiranes, notably propylene and cyclohexene sulfides, in metal-sulfur chemistry began in the early 1960s in the burgeoning field of cyclopentadienyl (Cp) chemistry. This proved to be a very rich field, a wide variety of (mostly polynuclear) complexes being formed using different (or sometimes the same!) starting materials, reagents and conditions.^{162,163} Work in this area also demonstrated the ease with which some dithiolate and dithiolene ligands exchange and/or add carbon backbones;¹⁶⁴ while this is a remarkable and useful¹⁶⁵ attribute it is yet another potential complication in the synthesis of MoHMs.

Fortunately, not all thiirane-based SAT reactions are as complicated as those observed in Cp chemistry. Some early examples of clean, stoichiometric, ligand- and metal-based SAT include the synthesis of Mo(NS)(S₂CNR₂)₃ (R = alkyl) from MoN(S₂CNR₂)₃,¹⁶⁶ MoS(S₂CNET₂)₂(PhC₂Ph) from Mo(S₂CNET₂)₂(CO)(PhC₂Ph),¹⁶⁷ CpMo(CO)₃(SR) (R = H, Me) from CpMo(CO)₃R¹⁶⁸ and MoO(S₂)(S₂CNR₂)₂ (R = alkyl) from MoO(S₂CNR₂)₂.¹⁶⁹ The excellent review

by Donahue contains many more recent examples of successful SAT reactions.¹¹¹ Propylene sulfide has been a useful reagent for the conversion of oxo-Mo(**IV**) scorpionate complexes to oxosulfido-Mo(**VI**) species as described in Section 7.4.1.1.3.

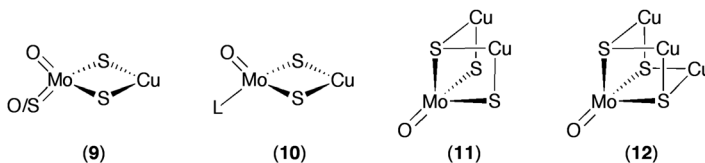
7.3.2.2 Hydrosulfido-Mo Species

Oxo(hydrosulfido)-Mo(v) and -Mo(iv) complexes are sought after as models for reduced Mo hydroxylases but only a few such complexes are currently available. Typically, they are prepared through the reactions of H₂S with suitable Mo complexes or the protonation of sulfido-Mo complexes (Section 7.4.1.2.1). The conversion of hydroxo ligands into hydrosulfido ligands using carbon disulfide is a potentially useful but unexplored method for accessing hydrosulfido-MoHMs.¹⁷⁰ The stability of hydrosulfido complexes depends on reaction conditions and kinetic *versus* thermodynamic factors. Aggregation to form polynuclear sulfido complexes or insoluble metal sulfides can be suppressed by stoichiometric control, the use of sterically bulky co-ligands, control of solution acid-base conditions, electrostatic repulsion, low temperatures and serendipity (advantageous insolubility *etc.*).^{171,172}

Hydrosulfido-Mo complexes typically exhibit a very weak $\nu(\text{S}-\text{H})$ IR band at *ca.* 2600 cm^{-1} , a high-field ^1H NMR resonance ($\delta < 0$) and Mo-SH distances in the range 2.37–2.59 Å. Paramagnetic species, *e.g.* mononuclear Mo(v) complexes, may be expected to show splittings attributable to proton coupling in their EPR spectra; the absence of coupling may indicate the presence of chloro ligands instead of hydrosulfido ligands, which are indistinguishable by, *e.g.*, X-ray crystallography. The properties of hydrosulfido species are influenced by the nature of the co-ligands, oxidation state, geometry (*e.g.* trans influences) and lattice/solution hydrogen-bonding interactions. Comprehensive reviews of hydrosulfido-metal chemistry are available elsewhere.^{171,172}

7.3.2.3 μ -Sulfido Bridged Oxo-Mo-Cu Complexes

Molybdenum and copper form many sulfido-bridged complexes, ranging in size and complexity from simple dinuclear species through incomplete and complete cubanes to large, complex clusters.^{173–179} The initial driver of Mo/Cu/S chemistry was its relevance to Mo-induced Cu-deficiencies in ruminants (Mo–Cu antagonism).^{180–182} The importance of Mo/Cu/S chemistry in medicine^{181–185} and the synthesis of electro-optical devices and metal-organic frameworks^{176–179} now stimulate Mo/Cu/S chemistry. Efforts to model the active site of CODH (3)^{5–7,11,12} and the so-called Orange Protein¹⁸⁶ are additional drivers of research in this area.



Most Mo/Cu/S complexes are derived from tetrathiomolybdate or sulfur-rich Mo species, so relatively few of them contain the terminal oxo-Mo moiety required by CODH models.^{173–179} Virtually all oxo-Mo/Cu/S complexes are restricted to the structural types shown in (9)–(12) (ligands (typically halides, pseudohalides and phosphines), charges and putative Mo–Cu bonding not shown); these are characterized by a di- μ -sulfido bridge, short Mo–S distances (*ca.* 2.2 Å) and the close approach (*ca.* 2.6 Å) of Mo and Cu centres. In contrast, the active site of CODH (3) contains only a *single* μ -sulfido ligand and a large Mo–Cu distance (>3.7 Å). Accordingly, the major challenge in producing CODH models is circumventing the formation of the thermodynamically preferred di- μ -sulfido Mo–Cu linkage that dominates Mo/Cu/S chemistry.

Success in modelling CODH is likely to require the use of sterically encumbered co-ligands, on both Mo and Cu, and a limit (preferably only one!) on the number of the “potential” sulfido ligands in the reactants. These strategies would act to prevent the close approach of the metal centres, encourage the formation of a single μ -sulfido rather than a di- μ -sulfido bridge and protect the product from undesirable, “downstream” reactions. The use of reduced oxosulfido-Mo complexes may also facilitate reactions between Mo and Cu complexes (see Section 7.4.2.2). A variety of sterically hindered thiols¹⁸⁷ and copper-thiolate reagents, including Cu(SAr*)L (SAr*[–] = 2,6-bis(2,4,6-triisopropylphenyl)benzenethiolate; L = leaving group)¹⁸⁸ and [Cu(STrip)(SSiPh₃)][–] (STrip[–] = 1-(thiolato)tryptcene)¹⁸⁹ are of potential utility. Finally, very different reactions can be displayed by the same Mo precursor toward different Cu complexes and a degree of trial-and-error is required for success in this area.

7.3.3 The Mono(dithiolene) Component: Background and Synthetic Approaches

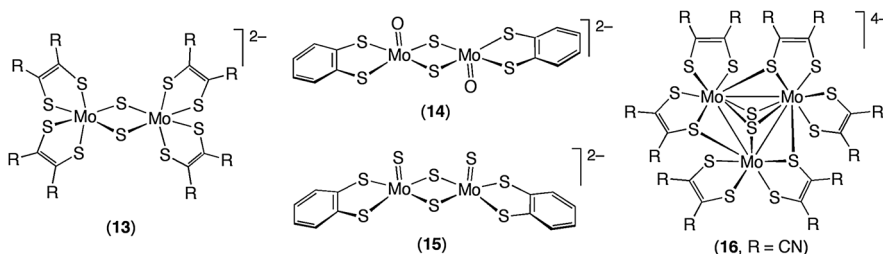
7.3.3.1 Dithiolene Complexes

Metallodithiolene complexes have long been of interest due to their unusual properties, unique geometric and electronic structures, non-innocent behaviour and potential applications.^{190–193} Several of these attributes are no doubt important in the function of Mo–MPT enzymes.^{194,195} Indeed, Rothery *et al.*^{196,197} have argued that the dithiolene ligand(s) are primary determinants of enzyme reactivity and mechanism.

The synthesis of dithiolene complexes has been exhaustively reviewed by Rauchfuss.¹⁹⁸ The most common methods used to prepare Mo enzyme model compounds are the reactions of alkynes with polysulfido-Mo complexes and of protected or free dithiolene ligands with Mo complexes. Dithiolene-Mo complexes fall into two broad classes, those containing arene-1,2-dithiolates (pseudo-dithiolenes) and those containing true dithiolenes; both are accorded equal status here. These synthetic methods and structural types all feature in the excellent, dithiolene-based models now available for enzymes of the SO and DMSOR families^{15–23} and biologically relevant mixed-ligand dithiolene and pterindithiolene complexes;^{61–64} the reader is referred to

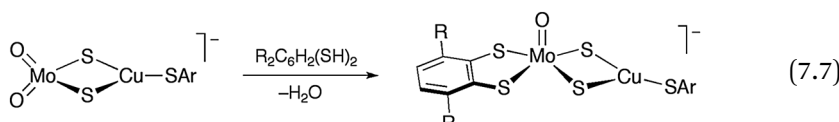
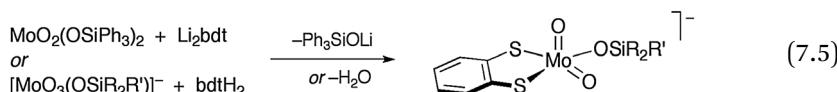
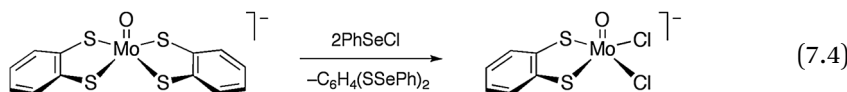
the references cited and other chapters within this monograph for further details. In contrast, the synthesis and stabilization of mono(dithiolene) complexes as MoHMs remains a significant, unmet challenge.

To date, all attempts to prepare mono(dithiolene)-MoHMs have yielded undesirable, thermodynamically favoured, di- or polynuclear-Mo(V/IV) complexes or bis- or tris(dithiolene) species. The aspects of Mo/S redox chemistry that underpin these outcomes have been mentioned above and are reviewed elsewhere.^{27–32} These problems can be circumvented when W (which is harder to reduce) is used in place of Mo but that does not achieve the ultimate aim of producing MoHMs. A few specific examples of thwarted MoHM syntheses illustrate the problem: complexes (**13**) are produced in attempted SAT reactions directed at $(\text{NEt}_4)_2[\text{MoO}(\text{S}_2\text{C}_2\text{R}_2)_2]$ ($\text{R} = \text{CO}_2\text{Me}$)^{31,199} and $\text{NEt}_4[\text{Mo(OAr)}(\text{S}_2\text{C}_2\text{Me}_2)_2]$ ($\text{OAr}^- = p\text{-phenolate derivative}$)²⁰⁰ and upon sulfidation of $\text{Mo}(\text{CO})_2(\text{S}_2\text{C}_2\text{R}_2)_2$ ($\text{R} = \text{Me}$;²⁰¹ $\text{R}_2 = c\text{-C}_4\text{H}_8$ ²⁰²); complex (**14**) forms upon attempted OSCRs involving $\text{NEt}_4[\text{MoO}_3(\text{bdt})]$ ($\text{bdt} = \text{benzene-1,2-dithiolate}$);^{203,204} complex (**15**) is produced upon oxidation of $(\text{NEt}_4)_2[\text{MoS}(\text{S}_4)(\text{bdt})]$;²⁰⁵ addition of methanesulfonic acid to a H_2S saturated solution of $(\text{NEt}_4)_2[\text{MoO}(\text{mnt})_2]$ ($\text{mnt} = \text{S}_2\text{C}_2(\text{CN})_2^{2-}$) produces (**16**);²⁰⁶ and tris(dithiolene) complexes are produced in the reactions of $[\text{MoS}(\text{S}_4)_2]^{2-}$ with dimethyl acetylenedicarboxylate²⁰⁷ and 2-(phenylethynyl) quinoxaline²⁰⁸ as well as in the reaction of MoCl_5 with sterically demanding dithiolenic Diels–Alder adducts.²⁰⁹ The following section summarizes successful strategies for the synthesis of mononuclear mono(dithiolene)-Mo (and -W) complexes.



7.3.3.2 Strategies for the Synthesis of Mono(dithiolene) Complexes

Methods for the conversion of bis(dithiolene) complexes into mono(dithiolene) complexes have been reported by Holm and coworkers. For example, Lim *et al.*²¹⁰ demonstrated the conversion of $\text{NEt}_4[\text{MoO}(\text{DT})_2]$ into $\text{NEt}_4[\text{MoOCl}_2(\text{DT})]$ ($\text{DT} = \text{S}_2\text{C}_2\text{Me}_2^{2-}$, bdt) upon reaction with two equivalents of PhSeCl (eqn (7.4)). The reaction of $(\text{NEt}_4)_2[\text{WO}(\text{S}_2\text{C}_2\text{Me}_2)_2]$ with Ph_3SbS also results in the removal of a dithiolene ligand, with the formation of $(\text{NEt}_4)_2[\text{WOS}_2(\text{S}_2\text{C}_2\text{Me}_2)]$.^{203,204}



Silylation of molybdate to give $\text{MoO}_2(\text{OSiPh}_3)_2$ followed by ligand exchange using Li_2bdt in tetrahydrofuran (eqn (7.5)) produces $\text{NEt}_4[\text{MoO}_2(\text{OSiPh}_3)(\text{bdt})]$.²¹⁰ Related compounds, $\text{NEt}_4[\text{MoO}_2(\text{OSiR}_2\text{R}')(\text{bdt})]$ ($\text{R}_2\text{R}' = \text{Me}, \text{Pr}^i_3, \text{Me}_2\text{Bu}^t, \text{Ph}_2\text{Bu}^t$), can be accessed through the reactions of $\text{NEt}_4[\text{MoO}_3(\text{OSiR}_2\text{R}')]$ and bdtH_2 (eqn (7.5)) or pre-formed $(\text{NEt}_4)_2[\text{MO}_3(\text{bdt})]$ ($\text{M} = \text{Mo, W}$) (*vide infra*) and $\text{R}_2\text{R}'\text{SiCl}$.²¹⁰ Complexes of the type $(\text{NEt}_4)_2[\text{ME}(\text{S}_4)(\text{DT})]$ ($\text{M} = \text{Mo, W}; \text{E} = \text{O, S}$) are also produced when $(\text{NEt}_4)_2[\text{ME}(\text{S}_4)_2]$ are reacted with one equivalent of bdtH_2 or 3,6-dichlorobenzene-1,2-dithiol (Cl_2bdtH_2).²⁰⁵

Reactions that result in the replacement of an oxo ligand by a single dithiolene ligand include those shown in eqn (7.6) and (7.7). Thus, the reactions of $(\text{NEt}_4)_2[\text{MO}_4]$ ($\text{M} = \text{Mo, W}$) with one equivalent of $\text{C}_6\text{H}_4(\text{SSiMe}_3)_2$ in MeCN (at -20°C for Mo) produce $(\text{NEt}_4)_2[\text{MO}_3(\text{bdt})]$.²¹¹ In the case of W, the reactions of $(\text{NEt}_4)_2[\text{WO}_{4-x}\text{S}_x]$ with $\text{C}_6\text{H}_4(\text{SSiMe}_3)_2$ ²⁰⁴ or sulfidation of $(\text{NEt}_4)_2[\text{WO}_3(\text{bdt})]$ using silylthiols²¹¹ provide access to $(\text{NEt}_4)_2[\text{WO}_{3-x}\text{S}_x(\text{bdt})]$ ($x = 0-2$) (Section 7.4.1.1.5). Finally, the reactions of $(\text{NEt}_4)_2[\text{O}_2\text{Mo}(\mu\text{-S}_2)\text{Cu}(\text{SAr})]$ with bdtH_2 or Cl_2bdtH_2 give $(\text{NEt}_4)_2[(\text{DT})\text{MoO}(\mu\text{-S}_2)\text{Cu}(\text{SAr})]$ ($\text{DT} = \text{bdt, Ar} = \text{Ph, } o\text{-Tol (o-tolyl); DT} = \text{Cl}_2\text{bdt, Ar} = \text{Ph}$).²¹² These Mo/Cu complexes serve as models for CODH (Section 7.4.2.2).

7.3.4 Maintaining Mononuclearity Post-Synthesis

The suppression of the thermodynamically favoured “decomposition” of Mo enzyme active sites is achieved by the stabilization and steric protection afforded by the apoprotein. Co-ligand steric protection also plays an important role in stabilizing known MoHMs (Section 7.4). Unfortunately, the synthesis of sterically encumbered dithiolene ligands, an obvious strategy for

the generation of MoHMs, is a huge challenge as substituents are directed away from, as opposed to over, the metal centre. Alternative approaches, *e.g.* employing sterically bulky bis(thiolato) ligands and/or second coordination sphere, host–guest or encapsulation strategies, are likely to be required for the stabilization of sulfur-rich, mononuclear MoHMs. Approaches that address issues of solubility, stability and functionality in aqueous solutions are additionally desirable. The successful adoption of traditional spatial isolation methods, *e.g.* intercalation¹⁰² or polymer support,¹⁰³ always remains a possibility.

Sterically bulky, bis(thiolate) “dithiolene mimics” include mercapto-calix-arenes,^{213,214} cyclodextrin-dithiols^{215,216} and *de novo* designed peptides.^{217,218} A possible binding mode for a dimercaptocalix[4]arene is shown in Figure 7.4(a), the forward projecting R-groups acting to impede close approach of Mo centres (Hg complexes of this type are known²¹⁹). The stabilization of $[\text{Fe}_4\text{S}_4]^{2-}$ complexes containing co-ligand thiolates derived from α - and β -cyclodextrins is another example that could be adapted for MoHM studies.^{215,216} Coordination of Mo to bis(cysteinate) *de novo* designed peptides could also stabilize MoHMs through the steric protection of the peptide chain. Moura and coworkers²²⁰ have realized a related concept in the synthesis of a Mo-substituted rubredoxin (Figure 7.4(b)). The incorporation of several relevant prosthetic groups into *de novo* designed peptides has been demonstrated.²²¹

The use of water-soluble cyclodextrins and related molecules as second coordination sphere ligands in host/guest complexes also has considerable potential.^{222,223} Cyclodextrins such as β -cyclodextrin (**17**) could act as hosts to species such as $[\text{MoO}_2(\text{ER})(\text{bdt})]^-$ ($\text{E} = \text{O}, \text{S}$; R including adamantyl, *e.g.* (**18**)) or $[\text{MoO}_3(\text{bdt})]^{2-}$, through inclusion of the R or bdt (or related) groups, and these could be converted to host guest species such as (**19**)–(**21**), while suppressing redox or di/polymerization reactions. Work in this area has been initiated but

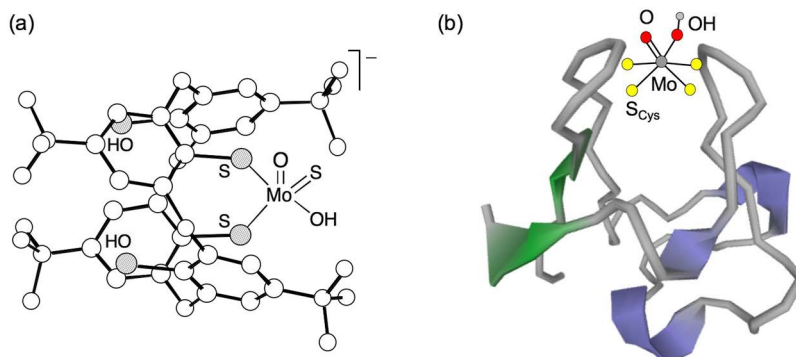
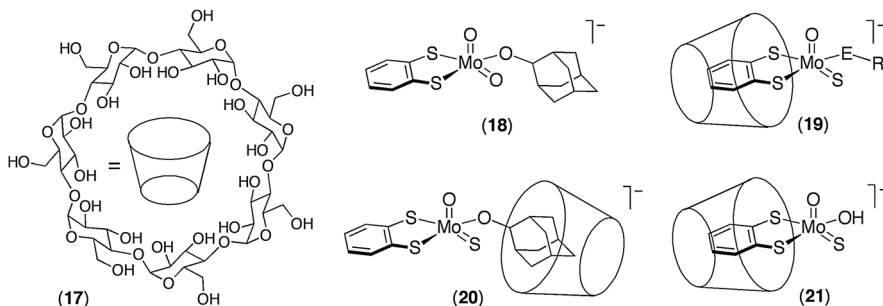


Figure 7.4 (a) A potential MoHM containing a sterically protective dimercaptocalix[4]arene ligand. (b) Cartoon representation of oxo(hydroxo)-Mo moiety coordinated by the four S_{Cys} ligands of aporubredoxin.

positive results are yet to emerge.²²⁴ There is also considerable potential for dendrimers^{225,226} and supramolecular structures, *e.g.* micelles,²²⁷ to stabilize MoHMs.



7.4 Molybdenum Hydroxylase Models

7.4.1 Models of Enzymes Containing Oxo sulfido and Oxo selenido Active Sites

7.4.1.1 Models of Oxidized Enzymes

The vast majority of MoHM studies have targeted active site (**1**) or components thereof. A timeline representing important developments in this area is presented in Figure 7.5 (see Sections 7.3.1–7.3.3 for background).

7.4.1.1.1 Thiomolybdates. Thiomolybdates are included in our discussion not because they are MoHMs *per se* but because they are historically important, being the only mononuclear oxosulfido-Mo(VI) species known for

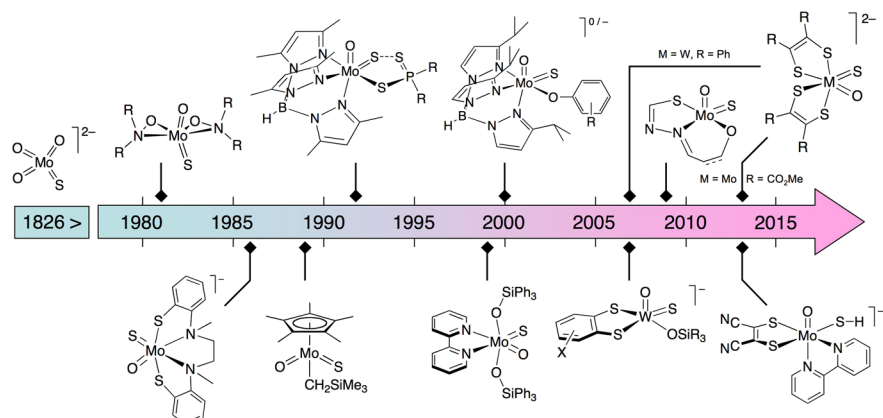
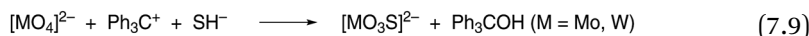
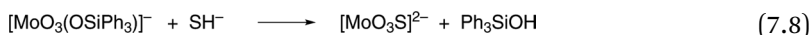


Figure 7.5 Timeline for developments in the synthesis of models for active site (**1**) and its reduced forms (getting warmer (but not yet hot!) with time).

over 150 years following their discovery by Berzelius,²²⁸ and because they are potentially very useful MoHM precursors.

The yellow-red thiomolybdates, $[\text{MoO}_x\text{S}_{4-x}]^{2-}$ ($x = 0-3$), are formed in the reactions of molybdate with H_2S or other sulfiding agents in basic aqueous solutions.^{173,174} The complexes are formed in sequence ($x = 3 \rightarrow 2 \rightarrow 1 \rightarrow 0$), with very specific reaction conditions and cations required for the isolation (often in impure form) of intermediate complexes. The crystal structures of many thiomolybdate salts have been determined, wherein the discrete dianions exhibit distorted tetrahedral or tetrahedral (for $[\text{MoS}_4]^{2-}$) geometries, with $\text{Mo}=\text{O}$ and $\text{Mo}=\text{S}$ distances of *ca.* 1.76 and 2.20 Å, respectively. Authoritative reviews of the synthesis, properties and coordination chemistry of these complexes have been prepared by Müller and coworkers.^{173,174} Other articles cover more recent advances and applications in this area.^{26,106,181}

Intermediate oxothiomolybdates are attractive starting materials for the synthesis of MoHMs and Partyka and Holm²¹¹ have reported convenient syntheses for the most attractive of these, $(\text{NET}_4)_2[\text{MoO}_3\text{S}]$; the syntheses involve initial monosilylation or monotritylation of molybdate followed by treatment with one equivalent of NET_4SH as shown in eqn (7.8) and (7.9) (cation = NET_4^+). The W analogue can be prepared by the reaction in eqn (7.9). Compounds of this type can be silylated to form $\text{MoOS}(\text{OSiPh}_3)_2$, which is amenable to further complexation to form MoHMs (Section 7.4.1.1.4).^{229,230}

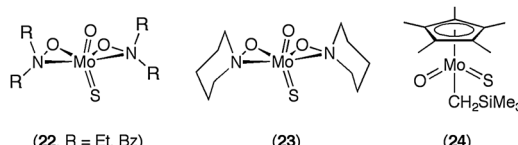


The silyl-molybdate derivative, $\text{NET}_4[\text{MoO}_3(\text{OSiPh}_3)]$, was also found to react with Ph_3SiSH to yield $\text{NET}_4[\text{MoO}_2\text{S}(\text{OSiPh}_3)]$.²¹¹ Later, Wang and Holm¹²⁰ extended this chemistry, preparing $\text{NET}_4[\text{MO}_{3-x}\text{S}_x(\text{OSiR}_2\text{R}')]$ ($\text{M} = \text{Mo}$, $x = 0-3$; $\text{M} = \text{W}$, $x = 3$; $\text{R}_2\text{R}' = \text{Me}_3$, Pr_3^i , Ph_3 , Me_2Bu^t and Ph_2Bu^t) and structurally characterizing representatives of each type of compound (av. $d(\text{Mo}=\text{O})$ 1.70–1.72 Å, av. $d(\text{Mo}=\text{S})$ 2.10–2.15 Å). Finally, NMR and allied studies showed that $(\text{NBu}^n)_2[\text{Mo}_2\text{O}_7]$ reacts with $(\text{Me}_3\text{Si})_2\text{S}$ in MeCN to produce $\text{NBu}^n_4[\text{MoO}_{3-x}\text{S}_x(\text{OSiMe}_3)]$ ($x = 0-3$, in that order).¹⁵⁰ Complexes of this type may prove useful in the synthesis of dithiolenic MoHMs.

A variety of selenomolybdates are also accessible *via* reactions of molybdate and thiomolybdates with H_2Se in aqueous solutions.^{173,174,231} Salts of $[\text{MoOSeS}_2]^{2-}$ ²³² are attractive precursors for models of the *E. barkeri* NDH active site (2).

7.4.1.1.2 Pseudo-Tetrahedral Oxosulfido-Mo(vi) Complexes. The first mono-nuclear, oxosulfido-Mo(vi) complexes containing organic co-ligands were $\text{MoOS}(\text{ONR}_2)_2$ ($\text{R} = \text{Et, Bz}$ (22); $\text{R}_2 = \text{C}_5\text{H}_{10}$ (23)), reported by Wieghardt and coworkers in the early 1980s.^{233,234} The study of these compounds provided key spectroscopic and structural data for oxosulfido-Mo centres and

demonstrated the spectroscopic and electrochemical effects of progressive substitution of oxo by sulfido ligands.



The compounds are prepared by reacting $\text{MoO}_2(\text{ONR}_2)_2$ with $\text{H}_2\text{S}^{233,234}$ ($(\text{Me}_3\text{Si})_2\text{S}^{147}$ or boron sulfide¹²⁶ in dry solvents, with prolonged treatments resulting in the formation of $\text{MoS}_2(\text{ONR}_2)_2$ species. Oxoselenido complexes, $\text{MoOSe}(\text{ONR}_2)_2$ ($\text{R} = \text{Et}; \text{R}_2 = \text{C}_5\text{H}_{10}$), are also accessible *via* the reaction of $\text{MoO}_2(\text{ONR}_2)_2$ with $\text{H}_2\text{Se}^{234}$. The oxosulfido complexes exhibit $\nu_{\text{Mo}=\text{O}}$ and $\nu_{\text{Mo}=\text{S}}$ IR bands at *ca.* 910 and 515 cm^{-1} , respectively.^{126,234} The ^{95}Mo chemical shifts of the full set of compounds vary considerably, with nuclear shielding increasing in the order $\text{Se} < \text{S} < \text{O}^{126,147,235}$. The complexes exhibit pseudo-tetrahedral geometries, the small bite-angle hydroxylamido ligands each occupying “one” coordination site. The $\text{Mo}=\text{O}$ and $\text{Mo}=\text{S}$ distances of (23) are 1.711(4) and 2.101(2) \AA , respectively,¹²⁶ the $\text{Mo}=\text{S}$ distances in the bis-(sulfido) complexes being slightly longer (*ca.* 2.15 \AA).^{234,235} Pseudo-tetrahedral $\text{MoOSe}(\text{ONC}_5\text{H}_{10})_2$ exhibits $\text{Mo}=\text{O}$ and $\text{Mo}=\text{Se}$ distances of 1.719(4) and 2.299(1) \AA , respectively.²³⁶

Substitution of oxo by sulfido ligands leads to more positive reduction potentials, $E(\text{Mo}^{\text{VI}}/\text{Mo}^{\text{V}})$ for $\text{MoXY}(\text{ONC}_5\text{H}_{10})_2$ ($\text{XY} = \text{O}_2, \text{OS}, \text{S}_2$) being $-2.50, -1.94$ and -1.59 V (vs. Fc^+/Fc in DMF), respectively.²³⁷ Cyanolysis of $\text{MoOS}(\text{ONC}_5\text{H}_{10})_2$ produces thiocyanate (65–80%) (cf. cyanolysis of XnO) but is complicated by the production of free $\text{HNC}_5\text{H}_{10}$ and $\text{HONC}_5\text{H}_{10}$ upon reaction.²³⁶

Pseudo-tetrahedral, organometallic oxosulfido-M(vi) ($M = Mo, W$) complexes such as $Cp^*MoOS(CH_2SiMe_3)$ ($Cp^* = \eta^5-C_5Me_5^-$) (24), $\nu_{Mo=O} = 906\text{ cm}^{-1}$, $\nu_{Mo-S} = 495\text{ cm}^{-1}$,²³⁸ $Cp^*WOS(Me)$ ²³⁹ and $Cp^*MoOS(SBu')$ ²⁴⁰ are also known.

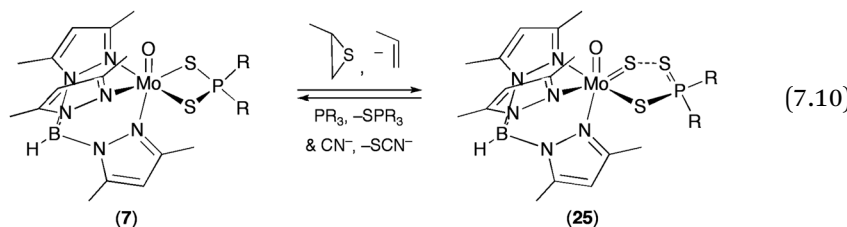
7.4.1.1.3 Oxosulfido-Mo(vi) Scorpionate Complexes. Scorpionate ligands^{241,242} have been central to the development of important MoHMs. Although they may appear to be a poor substitute for the MPT ligand, these strongly chelating, redox-innocent and sterically functional ligands have supported the stabilization of oxosulfido-Mo moieties (Figure 7.3(a)) and facilitated the development of broad MoHMs featuring multiple oxidation states, biologically relevant chemical behaviour and enzyme-like spectroscopic properties. In contrast, there are very few mononuclear, oxosulfido dithiolene-Mo complexes (see Section 7.4.1.1.5) and none bearing just a single dithiolene ligand. The study of scorpionate MoHMs has provided key insights into the synthesis and electronic structures of oxosulfido-Mo complexes and enzyme active sites (*vide infra*).

Work in this area began in the mid-1980s when Enemark and coworkers explored the potential of OSCRs in the synthesis of sulfido-Mo complexes.

These reactions were generally unsuccessful when directed at dioxo-Mo(VI) complexes (Section 7.3.2.1.1) but greater success was achieved in Mo(IV)¹²⁸ and Mo(V)¹²⁹ chemistry. The synthesis of Tp^{*}MoSCl₂ and the spectroscopic and crystallographic characterization of its phenolate and arenedithiolate derivatives provided key spectroscopic and electronic/geometric structural data for mononuclear, terminal sulfido-Mo(V) complexes (Mo=S = highest ligand field).^{129,243–248} The compounds exhibited a strong $\nu_{\text{Mo=S}}$ band at 505–490 cm⁻¹, lower EPR g values than their oxo analogues (the opposite of the trend for singly bonded, O- and S-donor ligands) and S K-preedge features assignable to S_{1s} → (Mo_{4d} + S_{3p}) transitions.

Later, Young and coworkers synthesized Tp^{*}WOSX (X = Cl⁻, OPh⁻, SPH⁻, SePh⁻, (-)-mentholate, S₂PR₂⁻) using OSCRs; the sulfido ligands in these complexes are “unperturbed”, *i.e.* they do not participate in weak bonding interactions with other moieties. The synthesis and study of these complexes predated and informed the synthesis of stable oxosulfido-Mo(VI) scorpiionate complexes (*vide infra*).^{140,141} In particular, and cutting a long story short, examination of the measured and projected reduction potentials of known and target molecules as well as the observed effects of particular co-ligands (especially the instability of redox-active thiolate co-ligands) led to abandonment of OSCRs in favour of atom transfer methodologies, ultimately focused on complexes containing innocent phenolate co-ligands (*vide infra*).

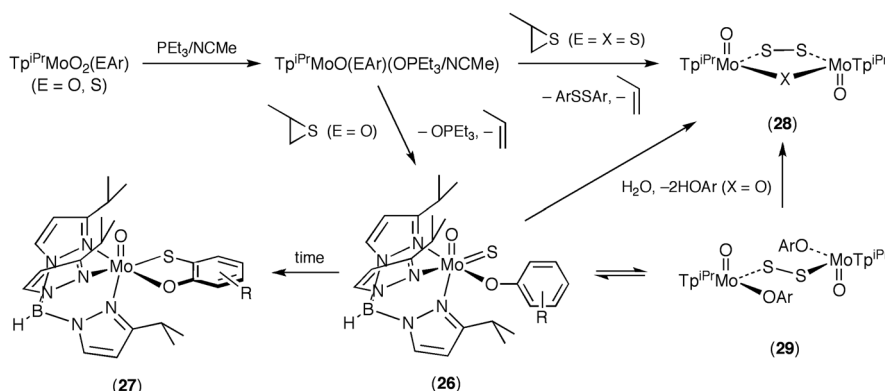
Initial work in this area involved the reaction of (7) (R = Et, Prⁱ, Ph) with propylene sulfide to give Tp^{*}MoOS{ κ^1 -S(S)PR₂} (25; eqn (7.10), forward).^{249,250} The synthesis of these compounds emulates the reaction in eqn (7.3) with one significant difference, *i.e.* the presence of a weak, stabilizing interaction between the “perturbed” sulfido and uncoordinated dithiophosphinate sulfur atoms of (25) absent in (8). The isopropyl and phenyl derivatives exhibit distorted octahedral geometries with average Mo=S and S···S distances of 2.214 and 2.392 Å, respectively, indicative of Mo=S and S···S bond orders of ~2 and ~1/3, respectively. Interestingly, the S···S interaction does not mask the reactivity of the sulfido ligand and the complexes undergo SAT in preference to OAT (eqn (7.10), reverse), including cyanolysis producing thiocyanate and (7) (or (8)) under aerobic conditions. The W(VI) analogues, Tp^{*}WOS(κ^1 -S₂PR₂) (R = OEt, Ph), can be accessed through both OAT and SAT reactions.^{251,252} These and related pyridine-2-dithio- and pyridine-2-thiolato-Mo and -W complexes display interesting internal redox reactions that produce EPR-active M(V) complexes upon both (one-electron) reduction and oxidation. These reactions underscore the often counter-intuitive redox interplay of Mo and S; details of these reactions can be found elsewhere.^{250,251,253}



Increasing the steric bulk of the scorpionate ligand and employing phenolate co-ligands facilitated the synthesis of “unperturbed” oxosulfido-Mo(vi) complexes, $\text{Tp}^{\text{iPr}}\text{MoOS(OAr)}$ (**26**; Tp^{iPr} = hydrotris(3-isopropylpyrazolyl)borate; OAr = phenolate derivative).^{254–256} These complexes are isolated as the kinetic products of the reaction sequence in Scheme 7.2, wherein $\text{Tp}^{\text{iPr}}\text{MoO(OAr)}(\text{OPEt}_3)$, generated in the reaction of $\text{Tp}^{\text{iPr}}\text{MoO}_2(\text{OAr})$ with PEt₃, undergoes a SAT reaction with propylene sulfide in MeCN to form (**26**). Associated reactions are also summarized in Scheme 7.2. Thermodynamic products include oxo-Mo(v) 2-mercaptophenolate derivatives (**27**) (highlighting the reactivity of the sulfido ligand) and $[\text{Tp}^{\text{iPr}}\text{MoO}]_2(\mu\text{-O})(\mu\text{-S}_2)$ (**28**; X = O) in the presence of adventitious water.²⁵⁵ Thiolate derivatives are inaccessible due to redox reactions leading to the elimination of disulfide and the formation of $[\text{Tp}^{\text{iPr}}\text{MoO}]_2(\mu\text{-S})(\mu\text{-S}_2)$ (**28**; X = S).²⁵⁷

Characterization data (IR, molecular mass and S and Mo K-edge X-ray absorption spectroscopy) indicated that the $\text{Tp}^{\text{iPr}}\text{MoOS(OAr)}$ compounds participate in a monomer(**26**)–dimer(**29**) equilibrium, favouring an oxosulfido-Mo(vi) monomer in solution.^{254–256} The compounds isolated depend on the steric bulk of the phenolate co-ligand. For example, the phenolate derivative crystallizes as dimeric $[\text{Tp}^{\text{iPr}}\text{MoOS(OPh)}]_2$, which features Mo(v) centres linked by a bent μ -disulfido bridge with Mo–S and S–S distances of 2.324(1) and 2.095(2) Å, respectively.²⁵⁴ Figure 7.6(a) shows the closely related structure of $[\text{Tp}^{\text{iPr}}\text{MoOS(OC}_6\text{H}_3\text{Bu}^t\text{-3,5})]_2$ ²⁵⁵ and the nature of the redox rearrangements involved in the monomer–dimer equilibrium.

Increasing the steric bulk of the phenolate co-ligand, as in the 2-Bu^s, 2-Bu^t and 4-Ph phenolate derivatives, allows the preparation of complexes that are mononuclear in both the solution and solid states. This was confirmed by IR ($\nu_{\text{Mo=O}} = 910 \text{ cm}^{-1}$, $\nu_{\text{Mo=S}} = 485 \text{ cm}^{-1}$), X-ray absorption spectroscopy and the structural characterization of $\text{Tp}^{\text{iPr}}\text{MoOS(OC}_6\text{H}_4\text{Bu}^s\text{-2)}$ (Figure 7.6(b)), which revealed a mononuclear, distorted octahedral complex with Mo=O and Mo=S distances of 1.692(5) and 2.132(2) Å, respectively.²⁵⁵ The $\text{Tp}^{\text{iPr}}\text{MoOS(OAr)}$ complexes participate in SAT rather than OAT reactions and undergo cyanolysis to generate thiocyanate and oxo-Mo(IV) species (modelling the cyanolysis



Scheme 7.2

of XnO). The complexes also serve as precursors for oxosulfido-Mo(v) complexes (Section 7.4.1.2.1), which in turn can be converted to models for CODH (Section 7.4.2.2).

The electronic structures of these compounds and related Mo(v) species (Section 7.4.1.2.1) have been studied by S K-edge and Mo L-edge X-ray absorption spectroscopy, vibrational spectroscopy and computational chemistry.²⁵⁸ Results indicate the presence of a strongly covalent Mo=S bond, with a large contribution of sulfur to the frontier orbitals, including a *ca.* 35% contribution to the π^* (formally Mo d_{xy}) lowest unoccupied molecular orbital (LUMO). A typical LUMO representation and S K-edge X-ray absorption spectrum are shown in Figure 7.7. The insights provided, combined with studies focused

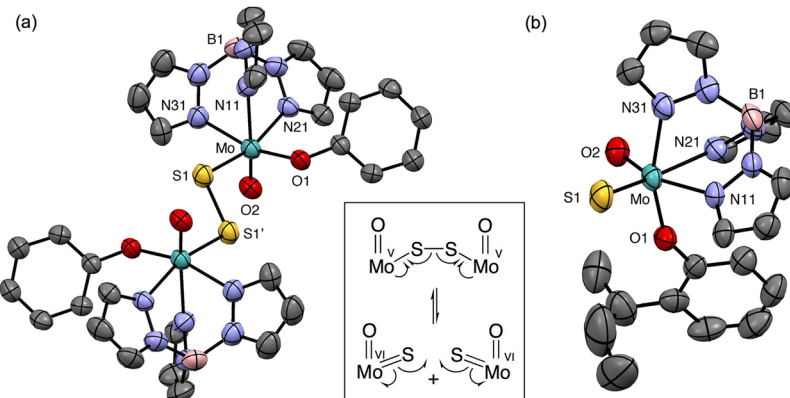


Figure 7.6 ORTEP projections of (a) $[\text{Tp}^{\text{iPr}}\text{MoOS}(\text{OC}_6\text{H}_3\text{Bu}^t\text{-3,5})]_2$ and (b) $\text{Tp}^{\text{iPr}}\text{MoOS}(\text{OC}_6\text{H}_4\text{Bu}^s\text{-2})$ (Pr^{i} and/or Bu^t groups removed for clarity). The boxed inset shows the redox interconversion of oxosulfido-Mo(vi) and μ -disulfido oxo-Mo(v) forms.

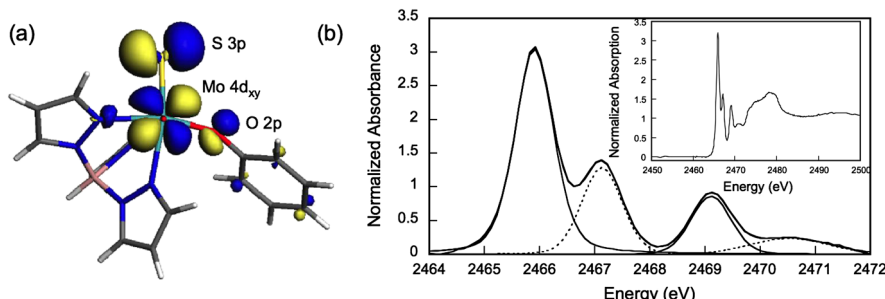
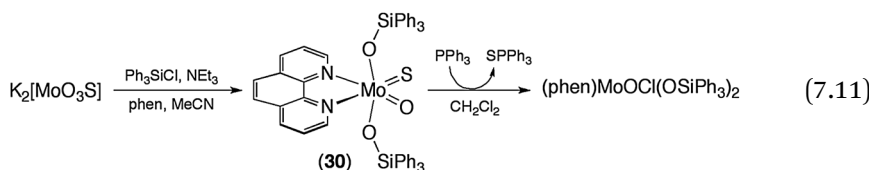


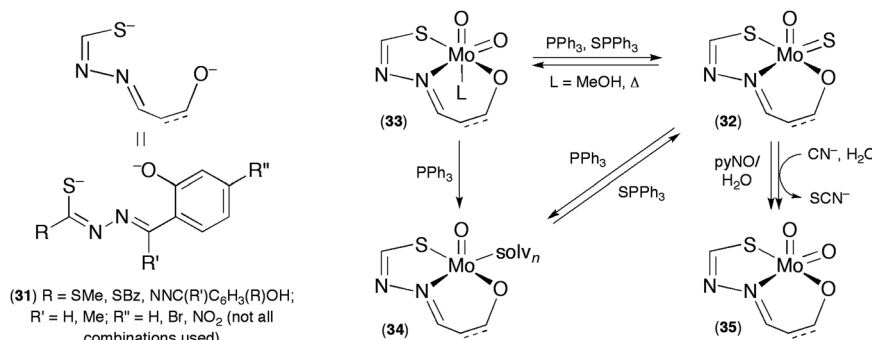
Figure 7.7 (a) The π^* LUMO and major contributing orbitals of computational model $\text{TpMoOS}(\text{Ph})$ (Tp = hydrotrispyrazolylborate; 0.05 au isosurface plot). (b) Resolved S K-preedge X-ray absorption spectrum of $\text{Tp}^{\text{iPr}}\text{MoOS}(\text{Ph})$ showing $\text{S}_{1s} \rightarrow (\text{Mo}_{4d} + \text{S}_{3p})$ transitions, the lowest energy being $\text{S}_{1s} \rightarrow \pi^*(\text{Mo}_{4d_{xy}} + \text{S}_{3p})$. Inset: normalized S K-edge spectrum. Adapted with permission from ref. 258. Copyright (2008) American Chemical Society.

on the enzyme,^{92–94} indicate that the mechanism of XnO is under the orbital control of the MoOS unit, the highly delocalized LUMO acting to polarize the substrate carbon centre for nucleophilic attack by the Mo-activated water and serving as an electronic sink in the two-electron oxidation of substrate. This topic is discussed in detail in recent reviews by Kirk and coworkers.^{92–94}

7.4.1.1.4 Other Oxosulfido-Mo(vi) Hard-Donor Complexes. The first octahedral, oxosulfido-Mo(vi) complexes to contain an “unperturbed” terminal sulfido ligand were MoOS(OSiPh₃)₂L (L = 1,10-phenanthroline (phen) (30), 2,2'-bipyridine (bpy) derivative), reported by Holm and coworkers²²⁹ in 1999 (see Section 7.4.1.1.3 for earlier, “perturbed” complexes). The complexes were synthesized by reacting K₂[MoO₃S], Ph₃SiCl and L in basic (NEt₃) MeCN (eqn (7.11)) and are stabilized by the hard-donor ligand set. They were structurally characterized by X-ray diffraction (with O/S disorder) and EXAFS, giving Mo=O and Mo=S distances of *ca.* 1.71 and 2.18 Å, respectively. The complexes undergo SAT in preference to OAT with PPh₃, followed by chlorine atom abstraction in dichloromethane to produce MoOCl(OSiPh₃)₂L (eqn (7.11)). Analogous W complexes ($\nu_{W=O}$ *ca.* 930 cm⁻¹, $\nu_{W=S}$ 480 cm⁻¹) were later reported.²³⁰



Oxosulfido-Mo(vi) complexes bearing a range of dibasic, tridentate ONS-donor ligands obtained from the condensation of thiocarbodihydrazone/dithiocarbazate and substituted salicylaldehydes/2-hydroxyacetophenone (L-SNO, 31) have also been reported (Scheme 7.3, solv = MeCN unless specified).^{259,260} Complexes of the type MoOS(L-ONS) (32) were obtained by “oxo-removal/sulfido-addition” reactions at MoO₂(L-ONS)(HOMe) (33) using a combination of PPh₃ and SPPh₃ in a ~1:10 mole ratio. The $\nu_{Mo=O}$ (*ca.*

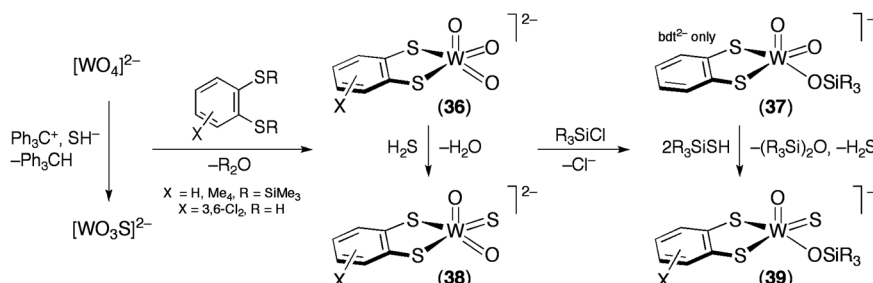


Scheme 7.3

965 cm^{-1})^{259,260} and some $\nu_{\text{Mo-S}}$ (*ca.* 520 cm^{-1})²⁵⁹ IR bands in these compounds are very high, possibly as a result of penta-coordination. Complexes (32) and (33) can be converted to oxo-Mo(IV) species, MoO(L-ONS)(solv) (34), and are inter-converted by a number of processes including cyanolysis to form thiocyanate and $\text{MoO}_2(\text{L-ONS})$ (35) (under oxidizing conditions). None of these complexes has been structurally characterized.

7.4.1.1.5 Dithiolene Complexes. Currently, there are no models combining the oxosulfido-Mo(vi) and mono(dithiolene) components of Mo hydroxylase active site (**1**) (Figure 7.3). However, a model system containing W in place of Mo has been reported by Holm and coworkers (Scheme 7.4, cation = NEt_4^+).^{203,204} Thus, the reactions of $(\text{NEt}_4)_2[\text{WO}_4]$ with benzene-1,2-dithiol derivatives yield $(\text{NEt}_4)_2[\text{WO}_3(\text{DT})]$ (36; DT = bdt, Cl_2bdt , Me_4bdt (3,4,5,6-tetramethylbenzene-1,2-dithiolate)), that are converted to $\text{NEt}_4[\text{WO}_2(\text{OSiR}_3)(\text{bdt})]$ (37; R = Pr^i , Ph) upon reaction with R_3SiCl (Scheme 7.4, upper). In a parallel sequence of reactions, $(\text{NEt}_4)_2[\text{WO}_3\text{S}]$ is converted to $(\text{NEt}_4)_2[\text{WO}_2\text{S}(\text{DT})]$ (38) and $\text{NEt}_4[\text{WOS}(\text{OSiR}_3)(\text{bdt})]$ (39) (Scheme 7.4, lower). The oxo complexes (36) and (37) can be converted to oxosulfido complexes (38) and (39), respectively, through reactions with H_2S or R_3SiSH . The reactions and manipulations are typically performed at low temperatures ($-30\text{ }^\circ\text{C}$) in MeCN or tetrahydrofuran. As noted earlier, attempts to prepare related oxosulfido-Mo(vi) complexes were thwarted by the formation of *anti*- $(\text{NEt}_4)_2[\text{Mo}^{\text{V}}_2\text{O}_2(\mu\text{-S})_2(\text{bdt})_2]$.^{203,204}

X-ray diffraction revealed two geometries for the anion in $(\text{NEt}_4)_2[\text{WO}_2\text{S}(\text{bdt})]$ (Figure 7.8(a)). Both are square pyramidal, with apical oxo and basal oxo, sulfido and dithiolene ligands; the av. W=O and W=S distances are 1.767 and 2.243(3) Å, respectively.^{203,204} A square-pyramidal structure, with an apical oxo ligand and W=O , W=S and W-O distances of 1.753(6), 2.153(6) and 1.902(6) Å, respectively, is also observed for $\text{NEt}_4[\text{WOS}(\text{OSiPr}_3)(\text{bdt})]$ (Figure 7.8(b)). These complexes are W-based structural analogues of the deprotonated and protonated forms, respectively, of active site (**1**); the hydrosulfido analogue could not be accessed. The results of Density Function Theory (DFT) calculations suggest that active site (**1**) adopts an intrinsic coordination geometry rather than a protein induced geometry.^{203,204}



Scheme 7.4

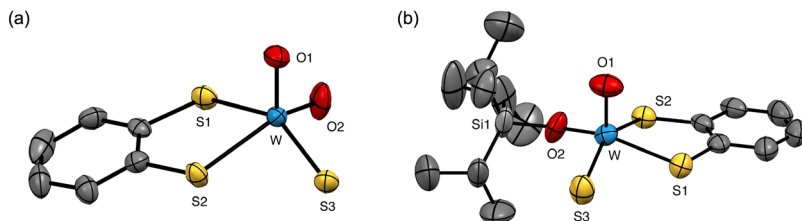
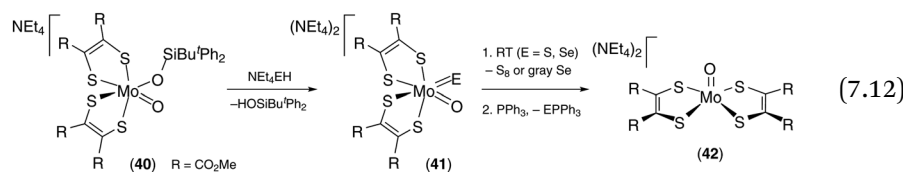


Figure 7.8 ORTEP projections of the anions in (a) $(\text{NEt}_4)_2[\text{WO}_2\text{S}(\text{bdt})]$ and (b) $\text{NEt}_4[\text{WOS}(\text{OSiPr}_3^{\text{i}})(\text{bdt})]$.

Progress towards the synthesis of oxosulfido/selenido-Mo dithiolene complexes has been reported by Sugimoto *et al.*,¹¹³ however, to date, these complexes are restricted to bis(dithiolene) species. Reactions of $\text{NEt}_4[\text{MoO}(\text{OSiBu}^{\text{t}}\text{Ph}_2)(\text{DT})_2]$ (**40**; DT = $\text{S}_2\text{C}_2(\text{CO}_2\text{Me})_2^{2-}$) with NEt_4OH (in MeCN at RT), NEt_4SH (in MeCN at <-20 °C) or NEt_4SeH (in EtCN at <-80 °C) produce isolable $(\text{NEt}_4)_2[\text{MoOE}(\text{DT})_2]$ (**41**) (eqn (7.12)), specifically $(\text{NEt}_4)_2[\text{MoO}_2(\text{DT})_2]$ ($\nu_{\text{MoO}_2} = 869$ and 839 cm $^{-1}$), $(\text{NEt}_4)_2[\text{MoOS}(\text{DT})_2]$ ($\nu_{\text{Mo=O}} = 919$ cm $^{-1}$, $\nu_{\text{Mo=S}} = 442$ cm $^{-1}$) and $(\text{NEt}_4)_2[\text{MoOSe}(\text{DT})_2]$ ($\nu_{\text{Mo=O}} = 917$ cm $^{-1}$, $\nu_{\text{Mo-Se}} = 367$ cm $^{-1}$), respectively; the sulfido and selenido complexes are thermally unstable with respect to $(\text{NEt}_4)_2[\text{MoO}(\text{DT})_2]$ (**42**) and sulfur or grey selenium, respectively. Based on DFT calculations, the sulfido/selenido compounds are proposed to possess distorted *cis*-octahedral structures with Mo=O, Mo=S and Mo=Se distances of 1.72, 2.21 and 2.36 Å, respectively. The compounds react with PPh_3 to produce EPPh_3 , the sulfur and selenium atom transfer reactions following pseudo-first-order, saturation kinetics indicative of the formation of an Mo-EPPh₃ intermediate. The atom transfer rates for these compounds are in the order Se > S > O, correlating with similar trends in Mo=E bond energy, Mo=Se (35 kcal mol $^{-1}$) > Mo=S (47 kcal mol $^{-1}$) > M=O (88 kcal mol $^{-1}$), and the chalcogenide character of the LUMO, Se (35.3%) > S (34.4%) > O (9.7%). Analogous W chemistry has also been reported.^{261,262} The use of low temperatures is a notable feature of all the dithiolene chemistry described in this section.



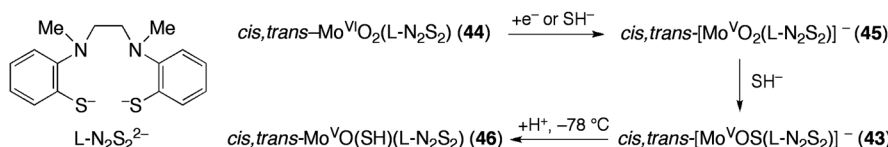
7.4.1.2 Models of Reduced Enzymes

7.4.1.2.1 Oxo sulfido- and Oxo(hydrosulfido)-Mo(v) Compounds. Only a handful of mononuclear, EPR-active oxosulfido- and oxo(hydrosulfido)-Mo(v) complexes are known; fewer still have been isolated and unambiguously characterized (see Figure 7.5). The first of these complexes were prepared by

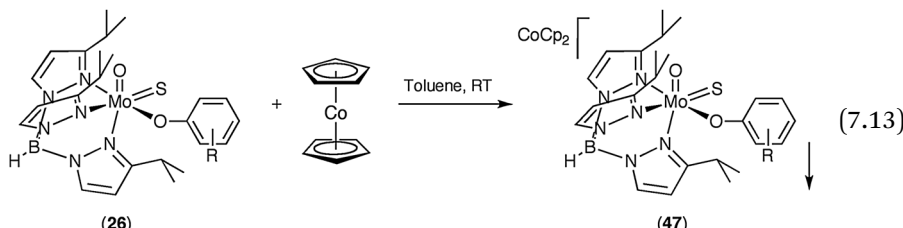
Spence and Wedd and coworkers.^{263–266} The most stable and extensively studied, *cis,trans*-[MoOS(L-N₂S₂)][−] (**43**) (L-N₂S₂H₂ = *N,N'*-dimethyl-*N,N'*-bis(2-mercaptophenyl)ethylenediamine; *cis* and *trans* indicate the disposition of the oxo and thiolate donors, respectively), was synthesized *in situ* upon reaction of *cis,trans*-MoO₂(L-N₂S₂) (**44**) with NBuⁿ₄SH in dry, deoxygenated tetrahydrofuran or MeCN (Scheme 7.5). The first step in the reaction is a rapid, one-electron reduction producing *cis,trans*-[MoO₂(L-N₂S₂)][−] (**45**). This is followed by slow oxo → sulfido exchange leading to the formation of (**43**). The oxo(hydrosulfido)-Mo(v) complex, MoO(SH)(L-N₂S₂) (**46**), was formed upon addition of CF₃CO₂H to (**43**) at −78 °C. Elegant EPR studies of these complexes (*vide infra*) provided key insights into the Mo(v) states and mechanism of XnO.^{263–266} Similar reactions were later employed in the *in situ* preparation of related scorpionate complexes, *e.g.* [Tp^xMoOSX][−] (Tp^x = Tp* and Tp^{iPr}; X = halide, S-donor anion)^{132,133} and [Tp^{*}MoOS(S₂PR₂)][−]^{250,253} but the hydrosulfido complexes could not be accessed in these systems.

The oxosulfido-Mo(v) complex (**43**) is characterized by a broad, solution EPR spectrum with *g* = 1.9435 and a rhombic frozen-glass spectrum with significant anisotropy ($\Delta g = 0.128$).²⁶³ The presence of a terminal sulfido ligand was demonstrated using a compound doubly labelled with ⁹⁸Mo (*I* = 0) and ³³S (*I* = 3/2), which shows a large, anisotropic coupling to ³³S ($a_S = 10.8 \times 10^{-4} \text{ cm}^{-1}$).²⁶⁵ The solution (*g* = 1.9759) and frozen-glass EPR spectrum of (**46**) exhibits coupling to a single proton ($a_H = 10.0 \times 10^{-4} \text{ cm}^{-1}$) that is absent in the deuterated analogue.²⁶³ EPR studies of the ¹⁷O- and ³³S-labelled compounds showed weak coupling to both nuclei ($a_O = 2.2 \times 10^{-4} \text{ cm}^{-1}$ and $a_S = 1.4 \times 10^{-4} \text{ cm}^{-1}$), consistent with a *cis,trans*-MoO(SH)(L-N₂S₂) geometry.^{265,266} The complex undergoes isomerization and/or decomposition above −60 °C to form *trans*-MoO(SH)(L-N₂S₂) (or more probably *cis,cis*-MoO(SH)(L-N₂S₂))²⁶⁷.

In 1989, Singh *et al.*²⁴⁶ claimed to have isolated PPh₄[MoOS(L-N₂S₂)] and *trans*-MoO(SH)(L-N₂S₂) following aqueous work-up of the aforementioned *in situ* reactions. Routine analytical and spectroscopic data supported this claim but X-ray absorption spectra were not consistent with the presence of a terminal sulfido ligand in PPh₄[MoOS(L-N₂S₂)]; indeed, these observations led the authors to propose a sulfido-based radical formulation for this compound. However, it is possible and most likely that the compounds have been incorrectly formulated.^{15,268} Certainly, if “PPh₄[MoOS(L-N₂S₂)]” is an oxosulfido-Mo(v) compound it is distinctly different from other compounds of this type (*vide infra*).



Scheme 7.5



To date, $[\text{CoCp}_2][\text{Tp}^{\text{iPr}}\text{MoOS}(\text{OAr})]$ (47; OAr^- = phenolate derivative), prepared from (26) as the (precipitated) kinetic products of the reaction in eqn (7.13), are the only isolated and unambiguously characterized oxosulfido-Mo(v) compounds to have been reported.^{254,269,270} These compounds exhibit isotropic ($g \sim 1.925$, $a_{\text{Mo}} = 40-45 \times 10^{-4} \text{ cm}^{-1}$) solution and highly anisotropic ($\Delta g = 0.124-0.150$), rhombic, frozen-glass EPR spectra typical of other oxosulfido-Mo(v) compounds (*vide supra*) and S and Mo K-edge X-ray absorption spectra indicative of the presence of a terminal sulfido ligand (Figure 7.9). The reduced intensity of the lowest energy S K-preedge transition, compared to that of Mo(vi) analogues (Figure 7.7(b)), is consistent with a transition to the π^* singly occupied molecular orbital (SOMO). The crystal structure of $[\text{CoCp}_2][\text{Tp}^{\text{iPr}}\text{MoOS}(\text{OC}_6\text{H}_4\text{CO}_2\text{Et}-2)]$ (Figure 7.10) confirmed the ionic formulation and revealed a distorted octahedral Mo anion possessing $\text{Mo}=\text{O}$ and $\text{Mo}=\text{S}$ distances of $1.760(5)$ and $2.219(2)$ Å, respectively.^{269,270} The compound and its Mo(vi) precursor have been studied by advanced spectroscopy,²⁵⁸ revealing a high degree of covalency in the Mo=S unit and supporting the notion of orbital control of mechanisms in Mo hydroxylases.⁹²⁻⁹⁴

The compounds react with cyanide, resulting in removal of the sulfido ligand as thiocyanate. The high reactivity of the sulfido ligand is indicated by its attack on the co-ligand phenyl group to form κ^2-O,S -2-mercaptophenolate complexes (27)²⁷⁰ and the instability of $[\text{CoCp}_2][\text{Tp}^{\text{iPr}}\text{MoOS}(\text{OC}_6\text{H}_4\text{CO}_2\text{Ph}-2)]$

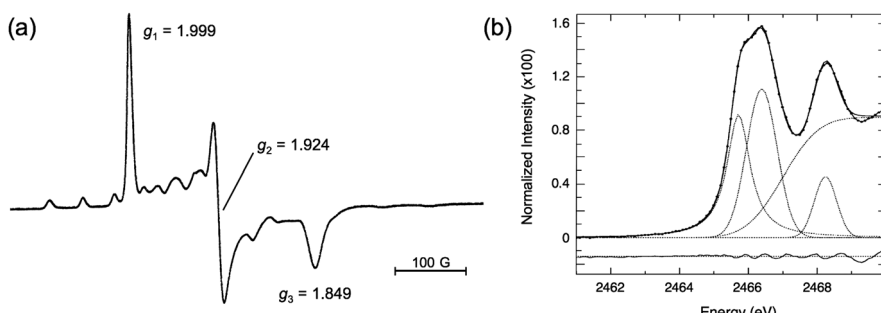


Figure 7.9 (a) Frozen-glass EPR spectrum of $[\text{CoCp}_2][\text{Tp}^{\text{iPr}}\text{MoOS}(\text{OPh})]$ in toluene. (b) Resolved S K-preedge X-ray absorption spectrum of $[\text{CoCp}_2][\text{Tp}^{\text{iPr}}\text{MoOS}(\text{OPh})]$ showing $\text{S}_{1s} \rightarrow (\text{Mo}_{4d} + \text{S}_{3p})$ transitions, the lowest energy being that to the π^* SOMO. Adapted with permission from ref. 270. Copyright (2015) American Chemical Society.

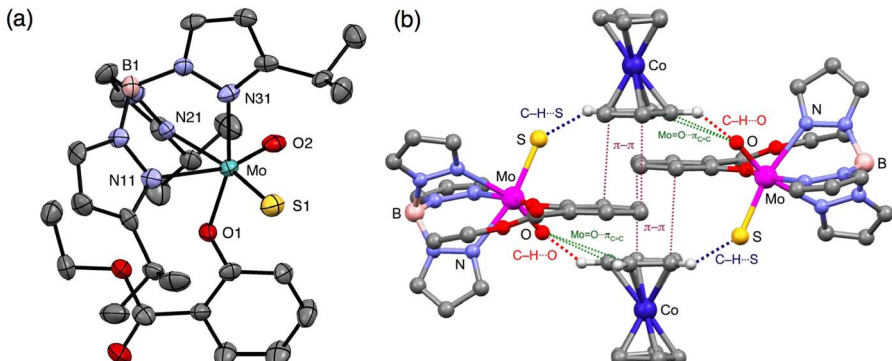


Figure 7.10 Crystal structure of $[\text{CoCp}_2][\text{Tp}^{\text{iPr}}\text{MoOS}(\text{OC}_6\text{H}_4\text{CO}_2\text{Et}-2)]$ showing (a) ORTEP projection of anion and (b) inter-ionic interactions stabilizing and ordering the oxo and sulfido ligands. Part (b) adapted with permission from ref. 270. Copyright (2015) American Chemical Society.

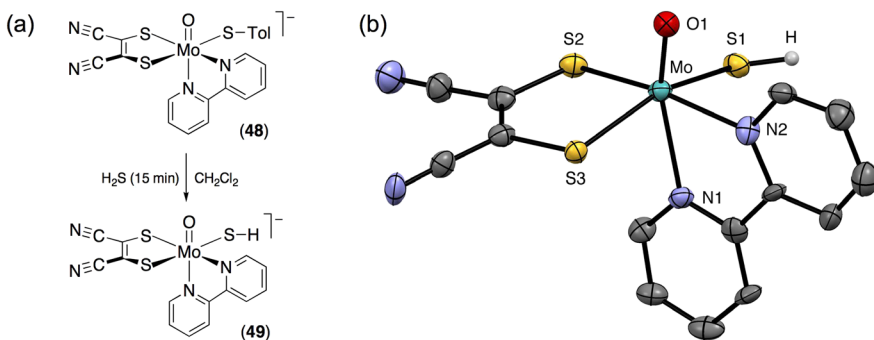


Figure 7.11 (a) Synthetic reaction producing oxo(hydrosulfido)-Mo(IV) compound (49) (complex anions only shown). (b) ORTEP projection of the anion in $\text{NBu}_4^{\text{n}}[\text{MoO}(\text{SH})(\text{mnt})(\text{bpy})]$ (49).

with respect to $[\text{CoCp}_2][\text{Tp}^{\text{iPr}}\text{MoO}\{\kappa^2-\text{O},\text{S}-\text{OC}_6\text{H}_4(\text{CO})\text{S}-2\}]$.²⁶⁹ Complexes (47) serve as precursors for models of CODH (Section 7.4.2.2).

7.4.1.2.2 Oxo(hydrosulfido)-Mo(IV) Complexes. The reactions of $\text{NBu}_4^{\text{n}}[\text{MoO}(\text{STol})(\text{mnt})\text{L}]$ ($\text{L} = \text{bpy}$ (48), phen) with stoichiometrically limited amounts of H_2S in dichloromethane produce oxo(hydrosulfido)-Mo(IV) compounds of the type $\text{NBu}_4^{\text{n}}[\text{MoO}(\text{SH})(\text{mnt})\text{L}]$ (49 for $\text{L} = \text{bpy}$) (Figure 7.11(a)).²⁷¹ The diamagnetic compounds are characterized by $\nu_{\text{Mo}=\text{O}}$ and $\nu_{\text{S}-\text{H}}$ IR bands at ca. 935 and 2587 cm^{-1} , respectively. The crystal structures of both derivatives revealed anions possessing distorted octahedral geometries with *cis*-oxo(hydrosulfido) ligands, equatorial dithiolene ligands and average $\text{Mo}=\text{O}$ and $\text{Mo}-\text{S}$ distances of 1.69 and 2.457 \AA , respectively; the structure of the anion in (49) is shown in Figure 7.11(b). The compounds are oxidized to EPR-active

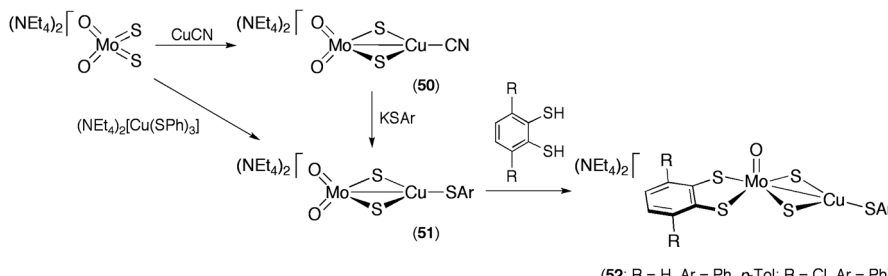
species with $g = 1.976$; these spectra are assigned to hydrosulfido complexes even though proton coupling is not evident. These signals are replaced by broad signals at $g = 1.949$, which are ascribed to hydrolysis to form “desulfo” compounds. The oxo-Mo(IV) compounds are good models for the allopurinol inhibited form of XnO but are unstable in solution, undergoing hydrolysis and oxidation to form, *e.g.* $\text{NBu}_4^+[\text{Mo}_2\text{O}_2(\mu\text{-O})_2(\text{SH})(\text{mnt})(\text{bpy})]$, $\text{Mo}_2\text{O}_2(\mu\text{-O})_2(\text{SH})_2(\text{bpy})_2$ and $\text{Mo}_2\text{O}_2(\mu\text{-O})(\text{SH})_4(\text{bpy})_2$.^{271,272}

7.4.2 Models for the MoO(μ -S)Cu Active Site of CODH

7.4.2.1 Oxo-di- μ -sulfido-Mo^{VI}Cu^I Dithiolene Complexes

Tatsumi and coworkers²¹² have employed the reaction sequence shown in Scheme 7.6 to prepare a range of Mo^{VI}Cu^I dithiolene compounds modelling oxidized CODH (3). The sequence involves the reactions of $(\text{NEt}_4)_2[\text{MoO}_2\text{S}_2]$ with Cu(I) reagents to give dioxo-Mo^{VI}Cu^I compounds, $(\text{NEt}_4)_2[\text{O}_2\text{Mo}(\mu\text{-S})_2\text{CuX}]$ ($X = \text{CN}^-$ (50), SPH^- (51, Ar = Ph)); cyano complex (50) can also be converted to (51) (Ar = Ph, *o*-Tol, *p*-Tol) upon reaction with thiolates. Complexes (51) react with bdtH₂ or Cl₂bdtH₂ (see eqn (7.7)) to yield $(\text{NEt}_4)_2[(\text{DT})\text{MoO}(\mu\text{-S})_2\text{Cu}(\text{SAr})]$ (52; DT = bdt, Cl₂bdt; Ar = Ph, *p*-Tol (related compounds were similarly prepared)). These compounds are significant in containing biologically relevant Mo^{VI}O(dithiolene) and Cu^I(SR) moieties, even though the metal centres are linked by a di- μ -sulfido bridge. Accordingly, they are among the most complete structural analogues of (3). The crystal structure of $(\text{NEt}_4)_2[(\text{bdt})\text{MoO}(\mu\text{-S})_2\text{Cu}(\text{SPH})]$ (among others) revealed a square-pyramidal Mo centre with an apical oxo ligand, an almost planar Mo(μ -S)₂Cu core, a trigonal-planar Cu centre and an Mo–Cu distance of 2.596(1) Å (see Figure 7.12). The complexes are resistant to reactions with Bu^tNC (which reacts with CODH) in refluxing MeCN and are decomposed by CO.

More recently, analogous tungsten complexes, $(\text{NEt}_4)_n[(\text{bdt})\text{WO}(\mu\text{-S})_2\text{CuL}]$ ($L = \text{Pr}_2^+\text{NHCM}_2$, SAr[–], Ar[–], SSiPr₃[–] and SSiPh₃[–]; $n = 1, 2$), have been isolated from the reactions of $(\text{NEt}_4)_2[\text{WOS}_2(\text{bdt})]$ with sterically hindered Cu complexes.²⁷³ Attempts to similarly prepare mono- μ -sulfido complexes from $(\text{NEt}_4)_2[\text{WO}_2\text{S}(\text{bdt})]$ produced only di- μ -sulfido species; this is ascribed to



Scheme 7.6

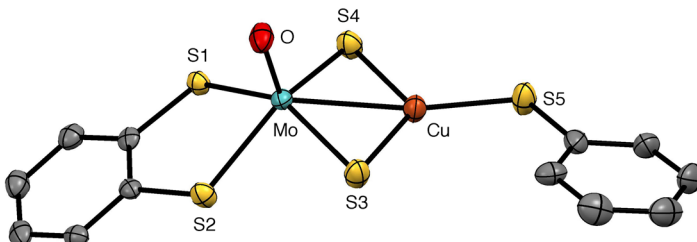
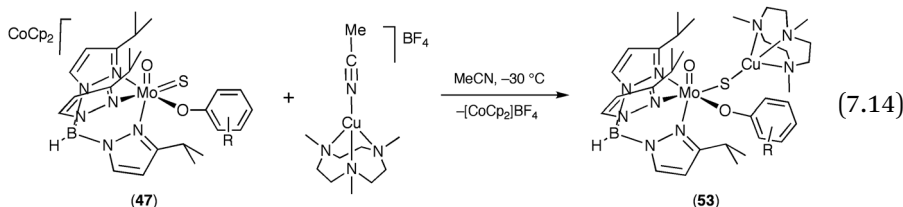


Figure 7.12 ORTEP projection of the anion in $(\text{NEt}_4)_2[(\text{bdt})\text{MoO}(\mu\text{-S})_2\text{Cu}(\text{SPh})]$.

disproportionation reactions producing WO_3 and Cu species.²⁷³ The complexes exhibit square-pyramidal structures closely related to that shown in Figure 7.12 for $[(\text{bdt})\text{MoO}(\mu\text{-S})_2\text{Cu}(\text{SPh})]^{2-}$. Structurally characterized $(\text{NEt}_4)_2[(\text{bdt})\text{WO}(\mu\text{-S})_2\text{Cu}(\text{SC}_6\text{H}_4\text{S}^\cdot)]$ is proposed to contain a monodentate thiyl radical anion coordinated to Cu.²⁷⁴ The linking of MoO(dithiolene) and Cu moieties by a single μ -sulfido bridge remains an unmet synthetic challenge.

7.4.2.2 Oxo- μ -Sulfido- $\text{Mo}^{\text{V}}\text{Cu}^{\text{I}}$ Scorpionate Complexes

To date, $\text{Tp}^{\text{iPr}}\text{MoO}(\text{OC}_6\text{H}_3\text{Bu}^t_{-3,5})(\mu\text{-S})\text{Cu}(\text{Me}_3\text{tcn})$ is the only complex in the literature to feature a single μ -sulfido bridge between Mo and Cu centres.²⁷⁵ It is formed in the reaction of $[\text{CoCp}_2][\text{Tp}^{\text{iPr}}\text{MoOS}(\text{OC}_6\text{H}_3\text{Bu}^t_{-3,5})]$ and $[\text{Cu}(\text{NCMe})(\text{Me}_3\text{tcn})]\text{BF}_4^-$ ($\text{Me}_3\text{tcn} = 1,4,7\text{-trimethyl-1,4,7-triazacyclononane}$) in MeCN at -30°C , followed by solvent removal and trituration in diethyl ether. The method can be extended to the synthesis of other phenolate derivatives, $\text{Tp}^{\text{iPr}}\text{MoO}(\text{OAr})(\mu\text{-S})\text{Cu}(\text{Me}_3\text{tcn})$ (53) according to eqn (7.14).²⁷⁶ Interestingly, the reactions of (26) with Cu^{I} or Cu^{II} complexes do not yield tractable Mo/Cu products, nor do the reactions of (47) with other Cu reactants trialled.²⁷⁰ These observations demonstrate that a range of reactants and conditions, varying Mo and Cu oxidation states and co-ligands as well as temperatures and solvents, need to be explored in the search for compounds of this type.



The complexes adopt the same overall structure, wherein a six-coordinate, distorted octahedral Mo centre is bridged to a four-coordinate, distorted tetrahedral Cu centre *via* a single, bent μ -sulfido ligand. The structure of the $3,5\text{-Bu}^t_2$ derivative shown in Figure 7.13(a) is typical of these species. The Mo=O and Mo–O distances of 1.675–1.700 and 1.974–2.005 Å, respectively,

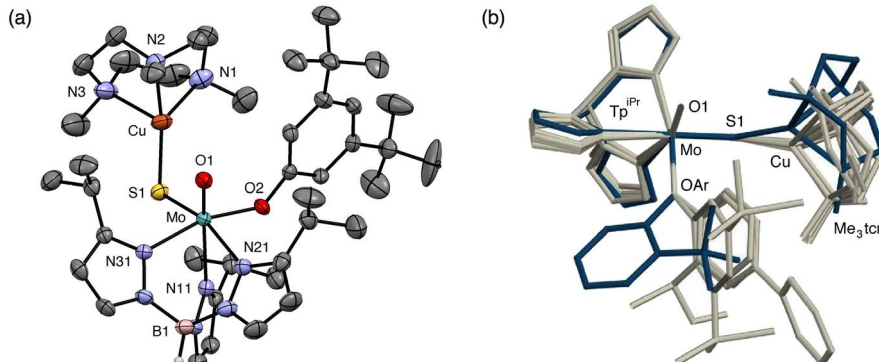


Figure 7.13 (a) ORTEP projection of $\text{Tp}^{\text{iPr}}\text{MoO}(\text{OC}_6\text{H}_3\text{Bu}^t_2-3,5)(\mu\text{-S})\text{Cu}(\text{Me}_3\text{tn})$. (b) Superposition of structures of $\text{Tp}^{\text{iPr}}\text{MoO}(\text{OC}_6\text{H}_4\text{Bu}^t-2)(\mu\text{-S})\text{Cu}(\text{Me}_3\text{tn})$ (blue) and related structurally characterized compounds.

are characteristic of oxo and phenolate ligands but the Mo–S distances (av. 2.28 Å) are similar to those observed for $\text{Mo}(\mu\text{-S})_2\text{Cu}$ species (av. 2.26–2.28 Å).^{173–179,231} The separation between the metal centres is *ca.* 3.8 Å, much longer than observed in $\text{Mo}(\mu\text{-S})_2\text{Cu}$ complexes (*ca.* 2.6 Å)^{173–179} and close to the value observed in protein crystal structures of CODH.^{78,79}

The detailed structures depend on the nature of the phenolate ligand substituents, with the 2-Bu^t derivative adopting a structure very different from other structurally characterized derivatives (Figure 7.13(b)). This unique structure has the phenolate ring nestled into a cleft of the Tp^{iPr} ligand with the *t*-butyl group projecting toward the Cu centre. The Mo–S–Cu angle is only 115.55(9)° and the Mo–Cu distance is a relatively short 3.753(2) Å. In other derivatives, the phenolate ring projects away from the Tp^{iPr} ligand and lies close to the Cu centre. The angles subtended at S range from 118.89(5)° in the bulkier 3,5-Bu^t₂ derivative to 134.22(3)° in the phenolate complex, the Mo–Cu distances ranging from 3.80–4.04 Å. The O=Mo–S–Cu and O–Mo–S–Cu torsion angles of the complexes and CODH differ considerably, being *ca.* 40° (av. for major structural type) *vs.* 122° (CODH) and 60° *vs.* 14°, respectively.

The complexes are paramagnetic and exhibit 4-line solution EPR spectra (Figure 7.14(a)) centred at $g \sim 1.937$ with large hyperfine couplings of *ca.* 41×10^{-4} cm⁻¹ to ^{95,97}Mo. The spectra are consistent with an $\text{Mo}^{\text{V}}\text{Cu}^{\text{I}}$ formulation but with extensive delocalization of the d¹ Mo(v) electron onto the Cu centre, the 4-line spectral pattern arising from coupling to ^{63,65}Cu. Interestingly, the Cu coupling constants appear to be dependent on the geometry of the MoO(μ -S)Cu unit, with most complexes exhibiting α_{Cu} in the range 55–63 $\times 10^{-4}$ cm⁻¹ but the unique 2-Bu^t derivative having $\alpha_{\text{Cu}} = 33.6 \times 10^{-4}$ cm⁻¹. Frozen-glass EPR spectra are interpreted in terms of overlapping 4-line patterns at three different principal g values and with highly variable and geometry-dependent coupling constants to Mo and Cu. The EPR studies of these

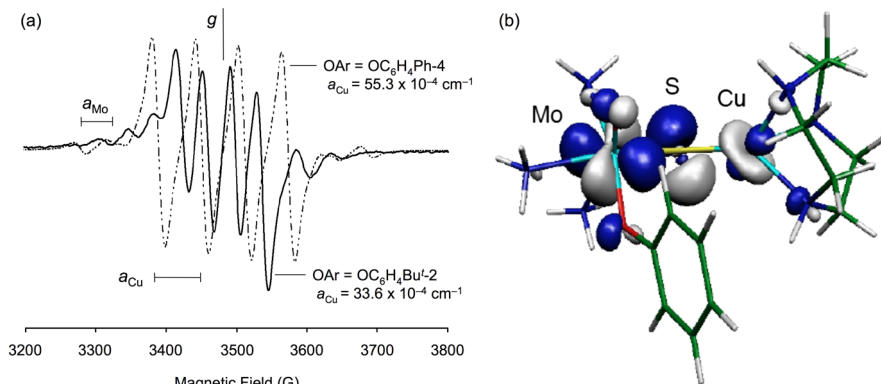


Figure 7.14 (a) Solution EPR spectra of derivatives indicated. (b) SOMO for a computational model of $\text{Tp}^{\text{IPr}}\text{MoO(OAr)}(\mu\text{-S})\text{Cu}(\text{Me}_3\text{tcn})$ (see text). Part (b) adapted with permission from ref. 275. Copyright (2006) American Chemical Society.

compounds strongly support the EPR spectral assignments subsequently made for CODH.^{99,100} The combined spectroscopic and structural studies highlight the sensitivity of electronic coupling to geometry and solution effects in these complexes (and by inference CODH).

The observation of large Cu superhyperfine coupling constants in these complexes and CODH ($a_{\text{Cu}} \sim 60 \times 10^{-4} \text{ cm}^{-1}$) indicates a very high degree of electronic delocalization across the $\text{MoO}(\mu\text{-S})\text{Cu}$ moiety. Indeed, calculations performed on $[(\text{NH}_3)_3\text{MoO(OPh)}(\mu\text{-S})\text{Cu}(\text{tcn})]^+$ ($\text{tcn} = 1,4,7\text{-triazacyclononane}$) show extensive delocalization of the SOMO over the Mo (Mo d_{xy}, 44%) and S (S p, 25%) atoms and onto the Cu site (21%, primarily Cu d_{xz} and d_{z2} with some s character) *via* a pseudo- σ^* Cu-S orbital interaction (Figure 7.14(b)). The implications of orbital structure and electronic delocalization on the properties and function of CODH have been examined by Stein and Kirk.⁹³

Finally, these complexes react with cyanide, leading to successive decupration (forming oxosulfido-Mo(v) species (Section 7.4.1.2.1)) and desulfurization leading to the formation of thiocyanate. Similar cyanolytic deactivation of CODH has been observed.⁷⁸⁻⁸⁰

7.5 Conclusion

This contribution has reviewed the history, relevant background chemistry, synthetic strategies and progress towards the modelling of Mo hydroxylases (the xanthine oxidase family of enzymes). Work to date has achieved the synthesis of important active site components but their combination in “idealized” MoHMs (active site replicates) is complicated by the redox interplay of Mo and S and the thermodynamic instability of mononuclear,

oxosulfido(dithiolene)-Mo(vi) complexes, as well as the current lack of knowledge and synthetic tools to overcome these difficulties. The eventual synthesis of “idealized” MoHMs is likely to require the development and deployment of new reagents and synthetic methodologies, as well as strategies for the stabilization of synthesized target molecules. It is hoped that this review will provide a platform for future work and eventual success in the synthesis of MoHMs.

Dedication and Acknowledgements

It is both a pleasure and a privilege to dedicate this chapter to Profs John H. Enemark, C. David Garner and Richard H. Holm, in recognition of their enormous contributions to the fields of inorganic and bioinorganic chemistry.

I first met Dave at the Fourth International Symposium on Nitrogen Fixation held at ANU (Canberra, Australia), in December 1980, when I was a PhD student with Dr John Broomhead’s group. It was great to meet Dave, as we shared a common philosophy – that Mo enzymes provided the perfect excuse to do good Mo coordination chemistry!

In 1984, I became a postdoc in John’s group in Tucson. John was a fantastic supervisor and mentor and I thoroughly enjoyed my time in Tucson. I really enjoyed the stimulating scientific environment and wonderful wilderness landscapes of the USA, made some life-long friends there and stole my wife, Brooke, from John’s office team. I also enjoyed seeing more of Dave, who visited Tucson on a number of occasions. Since then, John, Dave and I (often with our families) have swapped sabbatical and fellowship visits and enjoyed many great conferences and social events. I am truly indebted to John and Dave for their chemical insights, wisdom, good humour, support and friendship over many years.

After circumstances prevented me from taking up a postdoc with Dick in the early 1980s, I had to be content with seeing him at conferences, first at the RACI National Convention at UNSW (Sydney, Australia), in August 1987, where he delivered the 21st Dwyer Memorial Lecture, then many more times in the USA, Australia and Japan. I was always captivated and inspired by Dick’s seminars, which were veritable *tours de force*, and I am thankful to him for his beautiful, masterful and inspirational chemistry.

I would also like to acknowledge the passing of neurologist and author Dr Oliver Sacks, who had a life-long interest in metal chemistry (see his book *Uncle Tungsten*) and who, through personal correspondence, commended and encouraged our efforts to model Mo and W enzyme active sites. Dr Sacks was an eminent scientist, intellectual and writer as well as a kind and humble man and I am saddened by his passing.

Last but not least, I would like to thank my research group and collaborators for their hard work and contributions to our shared research and the editors for the opportunity to contribute to this monograph. I also wish to thank the Australian Research Council and the Petroleum Research Fund (administered by the American Chemical Society) for supporting our research over the years.

References

1. R. Hille, *Chem. Rev.*, 1996, **96**, 2757–2816.
2. *Molybdenum and Tungsten: Their Roles in Biological Processes*, ed. A. Sigel and H. Sigel, Metal Ions in Biological Systems, Marcel Dekker, New York, 2002, vol. 39.
3. J. M. Tunney, J. McMaster and C. D. Garner, in *Comprehensive Coordination Chemistry II*, ed. J. A. McCleverty and T. J. Meyer, Elsevier-Pergamon, Amsterdam, 2004, vol. 8, ch. 8.18, pp. 459–477.
4. R. Hille, T. Nishino and F. Bittner, *Coord. Chem. Rev.*, 2011, **255**, 1179–1205.
5. R. Hille, *Dalton Trans.*, 2013, **42**, 3029–3042.
6. M. L. Kirk and B. Stein, in *Comprehensive Inorganic Chemistry II*, ed. J. Reedijk and K. Poeppelmeier, Elsevier, Amsterdam, 2013, vol. 3, ch. 11, pp. 263–293.
7. R. Hille, J. Hall and P. Basu, *Chem. Rev.*, 2014, **114**, 3963–4038.
8. R. Hille, *Arch. Biochem. Biophys.*, 2005, **433**, 107–116.
9. R. Hille, *Eur. J. Inorg. Chem.*, 2006, 1913–1926.
10. T. Nishino, K. Okamoto, B. T. Eger and E. F. Pai, in *Handbook of Flavoproteins*, ed. R. Hille, S. M. Miller and B. Palley, de Gruyter, Berlin, 2013, vol. 2, pp. 103–124.
11. J.-H. Jeoung, J. Fesseler, S. Goetzel and H. Dobbek, *Met. Ions Life Sci.*, 2014, **14**, 37–69.
12. R. Hille, S. Dingwall and J. Wilcoxen, *JBIC, J. Biol. Inorg. Chem.*, 2015, **20**, 243–251.
13. E. I. Stiefel, in *Molybdenum and Tungsten: Their Roles in Biological Processes*, ed. A. Sigel and H. Sigel, Metal Ions in Biological Systems, Marcel Dekker, New York, 2002, vol. 39, pp. 1–29.
14. E. I. Stiefel, in *Biological Inorganic Chemistry: Structure and Reactivity*, ed. I. Bertini, H. B. Gray, E. I. Stiefel and J. S. Valentine, University Science Books, Sausalito, CA, 2007, ch. 2, pp. 7–30.
15. R. H. Holm, *Coord. Chem. Rev.*, 1990, **100**, 183–221.
16. J. H. Enemark and C. G. Young, *Adv. Inorg. Chem.*, 1993, **40**, 1–88.
17. C. G. Young, in *Biomimetic Oxidations Catalyzed by Transition Metal Complexes*, ed. B. Meunier, Imperial College Press, London, 2000, pp. 415–459.
18. J. H. Enemark, J. J. A. Cooney, J.-J. Wang and R. H. Holm, *Chem. Rev.*, 2004, **104**, 1175–1200.
19. J. McMaster, J. M. Tunney and C. D. Garner, *Prog. Inorg. Chem.*, 2004, **52**, 539–583.
20. H. Sugimoto and H. Tsukube, *Chem. Soc. Rev.*, 2008, **37**, 2609–2619.
21. S. Groysman and R. H. Holm, *Biochemistry*, 2009, **48**, 2310–2320.
22. A. Majumdar, *Dalton Trans.*, 2014, **43**, 8990–9003.
23. A. Majumdar, *Dalton Trans.*, 2014, **43**, 12135–12145.
24. C. D. Garner and J. M. Charnock, in *Comprehensive Coordination Chemistry*, ed. G. Wilkinson, R. D. Gillard and J. A. McCleverty, Pergamon, Oxford, 1987, vol. 3, ch. 36.4, pp. 1329–1374.

25. E. I. Stiefel, in *Comprehensive Coordination Chemistry*, ed. G. Wilkinson, R. D. Gillard and J. A. McCleverty, Pergamon, Oxford, 1987, vol. 3, ch. 36.5, pp. 1375–1420.
26. C. G. Young, in *Comprehensive Coordination Chemistry II*, ed. J. A. McCleverty and T. J. Meyer, Elsevier-Pergamon, Amsterdam, 2004, vol. 4, ch. 4.7, pp. 415–527.
27. *Sulfur, Its Significance for Chemistry, for the Geo-, Bio-, and Cosmosphere and Technology*, ed. A. Müller and B. Krebs, Elsevier, Amsterdam, 1984.
28. T. Shibahara, *Coord. Chem. Rev.*, 1993, **123**, 73–147.
29. J. R. Dilworth, in *Molybdenum: An Outline of its Chemistry and Uses*, ed. E. R. Braithwaite and J. Haber, Studies in Inorganic Chemistry, Elsevier, Amsterdam, 1994, vol. 19, pp. 185–250.
30. C. G. Young, *JBIC, J. Biol. Inorg. Chem.*, 1997, **2**, 810–816.
31. D. Coucouvanis, *Adv. Inorg. Chem.*, 1998, **45**, 1–73.
32. C. G. Young, *J. Inorg. Biochem.*, 2007, **101**, 1562–1585.
33. P. Pacher, A. Nivorozhkin and C. Szabó, *Pharmacol. Rev.*, 2006, **58**, 87–114.
34. A. Jurecka, *J. Inherited Metab. Dis.*, 2009, **32**, 247–263.
35. S. W. Ragsdale, *Crit. Rev. Biochem. Mol. Biol.*, 2004, **39**, 165–195.
36. G. Mörsdorf, K. Frunzke, D. Gadkari and O. Meyer, *Biodegradation*, 1992, **3**, 61–82.
37. V. Massey and C. M. Harris, *Biochem. Soc. Trans.*, 1997, **25**, 750–755.
38. E. J. Morgan, C. P. Stewart and F. C. Hopkins, *Proc. R. Soc. B*, 1922, **94**, 109–131.
39. F. Schardinger, *Z. Unters. Nahr. Genussm.*, 1902, **5**, 1113–1121.
40. D. A. Richert and W. W. Westerfeld, *J. Biol. Chem.*, 1953, **203**, 915–923.
41. D. E. Green and H. Beinert, *Biochim. Biophys. Acta*, 1953, **11**, 599–600.
42. H. Bortels, *Arch. Mikrobiol.*, 1930, **1**, 333–342.
43. E. I. Stiefel, *Prog. Inorg. Chem.*, 1977, **22**, 1–223.
44. R. C. Bray, B. G. Malmström and T. Vänngård, *Biochem. J.*, 1959, **73**, 193–197.
45. R. C. Bray, *Biol. Magn. Reson.*, 1980, **2**, 45–84.
46. R. Hille, *Biol. Magn. Reson.*, 2010, **29**, 91–120.
47. J. H. Enemark, A. V. Astashkin and A. M. Raitsimring, *Biol. Magn. Reson.*, 2010, **29**, 121–168.
48. M. J. Pushie and G. M. George, *Coord. Chem. Rev.*, 2011, **255**, 1055–1084.
49. L. S. Meriwether, W. F. Marzluff and W. G. Hodgson, *Nature*, 1966, **212**, 465–467.
50. V. Massey and D. Edmondson, *Biol. Chem.*, 1970, **245**, 6595–6598.
51. A. Szent-Györgyi, *Biochem. Z.*, 1926, **173**, 275–278.
52. A. Nason, K.-Y. Lee, S.-S. Pan and R. H. Erickson, *J. Less-Common Met.*, 1974, **36**, 449–459.
53. N. Turner, B. Barata, R. C. Bray, J. Deistung, J. Le Gall and J. J. G. Moura, *Biochem. J.*, 1987, **243**, 755–761.
54. G. N. George, *JBIC, J. Biol. Inorg. Chem.*, 1997, **2**, 790–796.

55. J. M. Berg, K. O. Hodgson, S. P. Cramer, J. L. Corbin, A. Elsberry, N. Pariyadath and E. I. Stiefel, *J. Am. Chem. Soc.*, 1979, **101**, 2774–2776.
56. J. Bordas, R. C. Bray, D. C. Garner, S. Gutteridge and S. S. Hasnain, *J. Inorg. Biochem.*, 1979, **11**, 181–186.
57. J. Bordas, R. C. Bray, C. D. Garner, S. Gutteridge and S. S. Hasnain, *Biochem. J.*, 1980, **191**, 499–508.
58. S. P. Cramer, R. Wahl and K. V. Rajagopalan, *J. Am. Chem. Soc.*, 1981, **103**, 7721–7727.
59. G. N. George and R. C. Bray, *Biochemistry*, 1988, **27**, 3603–3609.
60. S. Leimkühler, M. M. Wuebbens and K. V. Rajagopalan, *Coord. Chem. Rev.*, 2011, **255**, 1129–1144.
61. D. Collison, C. D. Garner and J. A. Joule, *Chem. Soc. Rev.*, 1996, **25**, 25–32.
62. B. Fischer and S. J. N. Burgmayer, in *Molybdenum and Tungsten: Their Roles in Biological Processes*, ed. A. Sigel and H. Sigel, Metals Ions in Biological Systems, Marcel Dekker, New York, 2002, vol. 39, pp. 265–316.
63. P. Basu and S. J. N. Burgmayer, *Coord. Chem. Rev.*, 2011, **255**, 1016–1038.
64. P. Basu and S. J. N. Burgmayer, *JBIC, J. Biol. Inorg. Chem.*, 2015, **20**, 373–383.
65. B. R. Williams, Y. Fu, G. P. A. Yap and S. J. N. Burgmayer, *J. Am. Chem. Soc.*, 2012, **134**, 19584–19587.
66. K. Clinch, D. K. Watt, R. A. Dixon, S. M. Baars, G. J. Gainsford, A. Tiwari, G. Schwarz, Y. Saotome, M. Storek, A. A. Belaïdi and J. A. Santamaria-Araujo, *J. Med. Chem.*, 2013, **56**, 1730–1738.
67. I. V. Pimkov, A. A. Peterson, D. N. Vaccarello and P. Basu, *RSC Adv.*, 2014, **4**, 19072–19076.
68. M. J. Romão, *Dalton Trans.*, 2009, 4053–4068.
69. H. Dobbek, *Coord. Chem. Rev.*, 2011, **255**, 1104–1116.
70. M. K. Chan, S. Mukund, A. Kletzin, M. W. W. Adams and D. C. Rees, *Science*, 1995, **267**, 1463–1469.
71. M. J. Romão, M. Archer, I. Moura, J. J. G. Moura, J. LeGall, R. Engh, M. Schneider, P. Hof and R. Huber, *Science*, 1995, **270**, 1170–1176.
72. R. Huber, P. Hof, R. O. Duarte, J. J. G. Moura, I. Moura, M.-Y. Liu, J. LeGall, R. Hille, M. Archer and M. J. Romão, *Proc. Natl. Acad. Sci. U. S. A.*, 1996, **93**, 8846–8851.
73. R. M. Jones, F. E. Inscore, R. Hille and M. L. Kirk, *Inorg. Chem.*, 1999, **38**, 4963–4970.
74. T. Santos-Silva, F. Ferroni, A. Thapper, J. Marangon, P. J. González, A. C. Rizzi, I. Moura, J. J. G. Moura, M. J. Romão and C. D. Brondino, *J. Am. Chem. Soc.*, 2009, **131**, 7990–7998.
75. M. C. Gómez, N. I. Neuman, S. D. Dalosto, P. J. González, J. J. G. Moura, A. C. Rizzi and C. D. Brondino, *JBIC, J. Biol. Inorg. Chem.*, 2015, **20**, 233–242.
76. O. Meyer, *J. Biol. Chem.*, 1982, **257**, 1333–1341.
77. O. Meyer and K. V. Rajagopalan, *J. Bacteriol.*, 1984, **157**, 643–648.

78. H. Dobbek, L. Gremer, R. Kiefersauer, R. Huber and O. Meyer, *Proc. Natl. Acad. Sci. U. S. A.*, 2002, **99**, 15971–15976.
79. M. Gnida, R. Ferner, L. Gremer, O. Meyer and W. Meyer-Klaucke, *Biochemistry*, 2003, **42**, 222–230.
80. M. Resch, H. Dobbek and O. Meyer, *Proc. Natl. Acad. Sci. U. S. A.*, 2005, **102**, 518–528.
81. P. G. Avis, F. Bergel and R. C. Bray, *J. Chem. Soc.*, 1955, 1100–1105.
82. C. Enroth, B. T. Eger, K. Okamoto, T. Nishino, T. Nishino and E. F. Pai, *Proc. Natl. Acad. Sci. U. S. A.*, 2000, **97**, 10723–10728.
83. I. Bonin, B. M. Martins, V. Purvanov, S. Fetzner, R. Huber and H. Dobbek, *Structure*, 2004, **12**, 1425–1435.
84. K. Okamoto, K. Matsumoto, R. Hille, B. T. Eger, E. F. Pai and T. Nishino, *Proc. Natl. Acad. Sci. U. S. A.*, 2004, **101**, 7931–7936.
85. C. J. Doonan, A. Stockert, R. Hille and G. N. George, *J. Am. Chem. Soc.*, 2005, **127**, 4518–4522.
86. J. S. Holcenberg and E. R. Stadtman, *J. Biol. Chem.*, 1969, **244**, 1194–1203.
87. N. Wagener, A. J. Pierik, A. Ibdah, R. Hille and H. Dobbek, *Proc. Natl. Acad. Sci. U. S. A.*, 2009, **106**, 11055–11060.
88. G. Schwarz and R. R. Mendel, *Annu. Rev. Plant Biol.*, 2006, **57**, 623–647.
89. R. R. Mendel and G. Schwarz, *Coord. Chem. Rev.*, 2011, **255**, 1145–1158.
90. S. Metz and W. Thiel, *Coord. Chem. Rev.*, 2011, **255**, 1085–1103.
91. M. R. A. Blomberg, T. Borowski, F. Himo, R.-Z. Liao and P. E. M. Siegbahn, *Chem. Rev.*, 2014, **114**, 3601–3658.
92. M. L. Kirk, S. Knottenbelt and A. Habtegabre, in *Computational Inorganic and Bioinorganic Chemistry*, ed. E. I. Solomon, R. A. Scott and R. B. King, Wiley, Chichester, UK, 2009, pp. 277–285.
93. B. W. Stein and M. L. Kirk, *Chem. Commun.*, 2014, **50**, 1104–1106.
94. B. W. Stein and M. L. Kirk, *JBIC, J. Biol. Inorg. Chem.*, 2015, **20**, 183–194.
95. S. Reschke, K. G. V. Sigfridsson, P. Kaufmann, N. Leidel, S. Horn, K. Gast, C. Schulzke, M. Haumann and S. Leimkühler, *J. Biol. Chem.*, 2013, **288**, 29736–29745.
96. M. L. Kirk and K. Pearson, *Curr. Opin. Chem. Biol.*, 2003, **7**, 220–227.
97. M. L. Kirk, in *Paramagnetic Resonance of Metallobiomolecules*, ACS Symposium Series 858, ed. J. Telser, American Chemical Society, Washington DC, 2003, pp. 340–357.
98. R. Hille, *Met. Ions Life Sci.*, 2009, **6**, 395–416.
99. A. Pelzmann, M. Ferner, M. Gnida, W. Meyer-Klaucke, T. Maisel and O. Meyer, *J. Biol. Chem.*, 2009, **284**, 9578–9586.
100. B. Zhang, C. F. Hemann and R. Hille, *J. Biol. Chem.*, 2010, **285**, 12571–12578.
101. M. Shanmugam, J. Wilcoxon, D. Habel-Rodriguez, G. E. Cutsail 3rd, M. L. Kirk, B. M. Hoffman and R. Hille, *J. Am. Chem. Soc.*, 2013, **135**, 17775–17782.
102. A. Cervilla, E. Llopis, A. Ribera, A. Corma, V. Fornés and F. Rey, *J. Chem. Soc., Dalton Trans.*, 1994, 2953–2957.

103. K. Heinze and A. Fischer, *Eur. J. Inorg. Chem.*, 2007, 1020–1026.
104. P. Afanasiev, *C. R. Chim.*, 2008, **11**, 159–182.
105. Y. Okamoto, *Bull. Chem. Soc. Jpn.*, 2014, **87**, 20–58.
106. Y. Yan, B. Y. Xia, Z. Xu and X. Wang, *ACS Catal.*, 2014, **4**, 1693–1705.
107. J. D. Benck, T. R. Hellstern, J. Kibsgaard, P. Chakthranont and T. F. Jaramillo, *ACS Catal.*, 2014, **4**, 3957–3971.
108. O. Peña, *Phys. C*, 2015, **514**, 95–112.
109. T. M. Trnka and G. Parkin, *Polyhedron*, 1997, **16**, 1031–1045.
110. G. Parkin, *Prog. Inorg. Chem.*, 1998, **47**, 1–165.
111. J. P. Donahue, *Chem. Rev.*, 2006, **106**, 4747–4783.
112. D. V. Partyka, R. J. Staples and R. H. Holm, *Inorg. Chem.*, 2003, **42**, 7877–7886.
113. H. Sugimoto, S. Tatemoto, K. Toyota, K. Ashikari, M. Kubo, T. Ogura and S. Itoh, *Chem. Commun.*, 2013, **49**, 4358–4360.
114. C. W. Scheele, *Chemische Abhandlung von der Luft und dem Feuer (Chemical Treatise on Air and Fire)*, Magnus Swederus, Upsala, Sweden, 1777.
115. D. C. Dittmer, in *Encyclopedia of Reagents for Organic Synthesis*, ed. L. A. Paquette, Wiley, Chichester, UK, 1995, vol. 4, pp. 2743–2749.
116. J. T. Goodman and T. B. Rauchfuss, *Inorg. Synth.*, 2002, **33**, 107–110.
117. G. Heller and W. Eysenbach, *Inorg. Chem.*, 1979, **18**, 380–383.
118. B. Haché and Y. Gareau, *Tetrahedron Lett.*, 1994, **35**, 1837–1840.
119. Y. Cai and B. P. Roberts, *Tetrahedron Lett.*, 2001, **42**, 4581–4584.
120. J.-J. Wang and R. H. Holm, *Inorg. Chem.*, 2007, **46**, 11156–11164.
121. J. J. Berzelius, *Ann. Phys. Chem.*, 1824, **78**, 113–150.
122. *Handbook of Preparative Inorganic Chemistry*, ed. G. Brauer, Academic Press, New York, 2nd edn, 1963.
123. H. Diercks and B. Krebs, *Angew. Chem., Int. Ed. Engl.*, 1977, **16**, 313.
124. D. A. Rice, *Coord. Chem. Rev.*, 1978, **25**, 199–227.
125. M. Sato, K. M. Miller, J. H. Enemark, C. E. Strouse and K. P. Callahan, *Inorg. Chem.*, 1981, **20**, 3571–3573.
126. S. Bristow, D. Collison, C. D. Garner and W. Clegg, *J. Chem. Soc., Dalton Trans.*, 1983, 2495–2499.
127. A. C. McDonell, S. G. Vasudevan, M. J. O'Connor and A. G. Wedd, *Aust. J. Chem.*, 1985, **38**, 1017–1024.
128. C. G. Young, S. A. Roberts, R. B. Ortega and J. H. Enemark, *J. Am. Chem. Soc.*, 1987, **109**, 2938–2946.
129. C. G. Young, J. H. Enemark, D. Collison and F. E. Mabbs, *Inorg. Chem.*, 1987, **26**, 2925–2927.
130. J. M. Lalancette, *Can. J. Chem.*, 1964, **42**, 2356–2357.
131. C. G. Young, I. P. McInerney, M. A. Bruck and J. H. Enemark, *Inorg. Chem.*, 1990, **29**, 412–416.
132. Z. Xiao, M. A. Bruck, C. Doyle, J. H. Enemark, C. Grittini, R. W. Gable, A. G. Wedd and C. G. Young, *Inorg. Chem.*, 1995, **34**, 5950–5962.
133. L. J. Laughlin and C. G. Young, *Inorg. Chem.*, 1996, **35**, 1050–1058.

134. S. A. Roberts, C. G. Young, W. E. Cleland Jr., K. Yamanouchi, R. B. Ortega and J. H. Enemark, *Inorg. Chem.*, 1988, **27**, 2647–2652.
135. Z. Xiao, J. H. Enemark, A. G. Wedd and C. G. Young, *Inorg. Chem.*, 1994, **33**, 3438–3441.
136. V. Polshettiwar and M. P. Kaushik, *J. Sulfur Chem.*, 2006, **27**, 353–386.
137. M. Jesberger, T. P. Davis and L. Barner, *Synthesis*, 2003, 1929–1958.
138. A. A. Eagle, E. R. T. Tiekkink and C. G. Young, *J. Chem. Soc., Chem. Commun.*, 1991, 1746–1748.
139. A. A. Eagle, S. M. Harben, E. R. T. Tiekkink and C. G. Young, *J. Am. Chem. Soc.*, 1994, **116**, 9749–9750.
140. A. A. Eagle, S. Thomas and C. G. Young, in *Transition Metal Sulfur Chemistry: Biological and Industrial Significance*, ACS Symposium Series 653, ed. E. I. Stiefel and K. Matsumoto, American Chemical Society, Washington, DC, 1996, pp. 324–335.
141. A. A. Eagle, E. R. T. Tiekkink, G. N. George and C. G. Young, *Inorg. Chem.*, 2001, **40**, 4563–4573.
142. C. Eaborn, *J. Chem. Soc.*, 1950, 3077–3089.
143. M. A. Matulenko, A. Degl'Innocenti and A. Capperucci, in *Handbook of Reagents for Organic Synthesis: Reagents for Silicon-Mediated Organic Synthesis*, ed. P. L. Fuchs, Wiley, Chichester, UK, 2011, pp. 83–84.
144. D. Gopalakrishnan, D. Damien, B. Li, H. Gullappalli, V. K. Pillai, P. M. Ajayan and M. M. Shajumon, *Chem. Commun.*, 2015, **51**, 6293–6296.
145. Y. Do, E. D. Simhon and R. H. Holm, *Inorg. Chem.*, 1983, **22**, 3809–3812.
146. J. R. Dorfman, J.-J. Girerd, E. D. Simhon, T. D. P. Stack and R. H. Holm, *Inorg. Chem.*, 1984, **23**, 4407–4412.
147. M. Minelli, J. H. Enemark, K. Wieghardt and M. Hahn, *Inorg. Chem.*, 1983, **22**, 3952–3953.
148. I. Feinstein-Jaffe, J. C. Dewan and R. R. Schrock, *Organometallics*, 1985, **4**, 1189–1193.
149. J. Sola, Y. Do, J. M. Berg and R. H. Holm, *Inorg. Chem.*, 1985, **24**, 1706–1713.
150. Y. Do, E. D. Simhon and R. H. Holm, *Inorg. Chem.*, 1985, **24**, 1831–1838.
151. Y. Do, E. D. Simhon and R. H. Holm, *Inorg. Chem.*, 1985, **24**, 2827–2832.
152. V. C. Gibson, A. Shaw and D. N. Williams, *Polyhedron*, 1989, **8**, 549–550.
153. S. A. Roberts, C. G. Young, W. E. Cleland Jr., R. B. Ortega and J. H. Enemark, *Inorg. Chem.*, 1988, **27**, 3044–3051.
154. Z. Xiao, M. A. Bruck, J. H. Enemark, C. G. Young and A. G. Wedd, *Inorg. Chem.*, 1996, **35**, 7508–7515.
155. V. N. Nemykin, S. R. Davie, S. Mondal, N. Rubie, M. L. Kirk, A. Somogyi and P. Basu, *J. Am. Chem. Soc.*, 2002, **124**, 756–757.
156. H. Liu and X. Jiang, *Chem.-Asian J.*, 2013, **8**, 2546–2563.
157. K. Dachlauer and L. Jackel, Process of preparing alkylene sulphides, US Pat. 2,094,837 and 2,094,914, 1937 (see *Chem. Abstr.*, 1936, **30**, 7122 and <http://www.google.com/patents/US2094914>).
158. K. Aarset, E. M. Page and D. A. Rice, *J. Mol. Struct.*, 2011, **1002**, 19–23.

159. M. Sander, *Chem. Rev.*, 1966, **66**, 297–339.
160. U. Zoller, in *Small Ring Heterocycles. Part 1. Aziridines, Azirines, Thiiranes, Thiirennes*, ed. A. Hassner, Wiley, New York, 1983.
161. W. Chew and D. N. Harpp, *Sulfur Rep.*, 1993, **15**, 1–39.
162. M. Rakowski DuBois, R. C. Haltiwanger, D. J. Miller and G. Glazmaier, *J. Am. Chem. Soc.*, 1979, **101**, 5245–5252.
163. W. Danzer, W. P. Fehlhammer, A. T. Liu, G. Thiel and W. Beck, *Chem. Ber.*, 1982, **115**, 1682–1693.
164. M. Rakowski DuBois, in *Catalysis by Di- and Polynuclear Metal Cluster Complexes*, ed. R. D. Adams and F. A. Cotton, Wiley-VCH, New York, 1998, pp. 127–143.
165. K. Wang, *Prog. Inorg. Chem.*, 2004, **52**, 267–314.
166. M. W. Bishop, J. Chatt and J. R. Dilworth, *J. Chem. Soc., Dalton Trans.*, 1979, 1–5.
167. J. R. Morrow, T. L. Tonker and J. L. Templeton, *Organometallics*, 1985, **4**, 745–750.
168. R. A. Fischer, H.-J. Kneuper and W. A. Herrmann, *J. Organomet. Chem.*, 1987, **330**, 365–376.
169. X. F. Yan and C. G. Young, *Aust. J. Chem.*, 1991, **44**, 361–367.
170. D. C. Gerbino, E. Hevia, D. Morales, M. E. N. Clemente, P. Pérez, L. Riera, V. Riera and D. Miguel, *Chem. Commun.*, 2003, 328–329.
171. S. Kuwata and M. Hidai, *Coord. Chem. Rev.*, 2001, **213**, 211–305.
172. M. Peruzzini, I. de los Ríos and A. Romerosa, *Prog. Inorg. Chem.*, 2001, **49**, 169.
173. A. Müller, E. Diemann, R. Jostes and H. Bögge, *Angew. Chem., Int. Ed. Engl.*, 1981, **20**, 934–955.
174. A. Müller, *Polyhedron*, 1986, **5**, 323–340.
175. C. D. Garner, in *Comprehensive Coordination Chemistry*, ed. G. Wilkinson, R. D. Gillard and J. A. McCleverty, Pergamon, Oxford, 1987, vol. 3, ch. 36.6, pp. 1421–1444.
176. H.-W. Hou, X.-Q. Xin and S. Shi, *Coord. Chem. Rev.*, 1996, **153**, 25–56.
177. J.-P. Lang, S.-J. Ji, Q.-F. Xu, Q. Shen and K. Tatsumi, *Coord. Chem. Rev.*, 2003, **241**, 47–60.
178. M. W. Degroot and J. F. Corrigan, in *Comprehensive Coordination Chemistry II*, ed. J. A. McCleverty and T. J. Meyer, Elsevier Pergamon, Amsterdam, 2004, vol. 7, ch. 7.2, pp. 57–123.
179. J.-P. Lang, W.-H. Zhang, H.-X. Li and Z.-G. Ren, in *Design and Construction of Coordination Polymers*, ed. M.-C. Hong and L. Chen, Wiley, Hoboken, NJ, 2009, pp. 267–306.
180. N. F. Suttle, *Annu. Rev. Nutr.*, 1991, **11**, 121–140.
181. S. H. Laurie, *Eur. J. Inorg. Chem.*, 2000, 2443–2450.
182. N. F. Suttle, *Adv. Nutr.*, 2012, **3**, 666–674.
183. L. Zhang, J. Lichtmannegger, K. H. Summer, S. Webb, I. J. Pickering and G. N. George, *Biochemistry*, 2009, **48**, 891–897.
184. G. Crisponi, V. M. Nurchi, D. Fanni, C. Gerosa, S. Nemolato and G. Faa, *Coord. Chem. Rev.*, 2010, **254**, 876–889.

185. H. M. Alvarez, Y. Xue, C. D. Robinson, M. A. Canalizo-Hernández, R. G. Marvin, R. A. Kelly, A. Mondragón, J. E. Penner-Hahn and T. V. O'Halloran, *Science*, 2010, **327**, 331–334.
186. M. S. P. Carepo, S. R. Pauleta, A. G. Wedd, J. J. G. Moura and I. Moura, *JBIC, J. Biol. Inorg. Chem.*, 2014, **19**, 605–614.
187. P. J. Blower and J. R. Dilworth, *Coord. Chem. Rev.*, 1987, **76**, 121–185.
188. S. Groysman and R. H. Holm, *Inorg. Chem.*, 2009, **48**, 621–627.
189. D. C. Rosenfeld, P. T. Wolczanski, K. A. Barakat, C. Buda, T. R. Cundari, F. C. Schroeder and E. B. Lobkovsky, *Inorg. Chem.*, 2007, **46**, 9715–9735.
190. J. A. McCleverty, *Prog. Inorg. Chem.*, 1968, **10**, 49–221.
191. *Dithiolene Chemistry: Synthesis, Properties and Applications*, ed. E. I. Stiefel, Progress in Inorganic Chemistry, Wiley, Hoboken, NJ, 2004, vol. 52.
192. A. Vlcek, Dithiolenes and Non-innocent Redox-active Ligands, *Coord. Chem. Rev.*, 2010, **254**(13–14), 1357–1588.
193. R. Eisenberg and H. B. Gray, *Inorg. Chem.*, 2011, **50**, 9741–9751.
194. M. L. Kirk, R. L. McNaughton and M. E. Helton, *Prog. Inorg. Chem.*, 2004, **52**, 111–212.
195. F. J. Hine, A. J. Taylor and C. D. Garner, *Coord. Chem. Rev.*, 2010, **254**, 1570–1579.
196. R. A. Rothery and J. H. Weiner, *JBIC, J. Biol. Inorg. Chem.*, 2015, **20**, 349–372.
197. R. A. Rothery, B. Stein, M. Solomonson, M. L. Kirk and J. H. Weiner, *Proc. Natl. Acad. Sci. U. S. A.*, 2012, **109**, 14773–14778.
198. T. B. Rauchfuss, *Prog. Inorg. Chem.*, 2004, **52**, 1–54.
199. D. Coucouvanis, A. Hadjikyriacou, A. Toupadakis, S.-M. Koo, O. Ileperuma, M. Draganjac and A. Salifoglou, *Inorg. Chem.*, 1991, **30**, 754–767.
200. J.-J. Wang, O. P. Kryatova, E. V. Rybak-Akimova and R. H. Holm, *Inorg. Chem.*, 2004, **43**, 8092–8101.
201. B. S. Lim, J. P. Donahue and R. H. Holm, *Inorg. Chem.*, 2000, **39**, 263–273.
202. H. Sugimoto, T. Sakurai, H. Miyake, K. Tanaka and H. Tsukube, *Inorg. Chem.*, 2005, **44**, 6927–6929.
203. J.-J. Wang, S. Groysman, S. C. Lee and R. H. Holm, *J. Am. Chem. Soc.*, 2007, **129**, 7512–7513.
204. S. Groysman, J.-J. Wang, R. Tagore, S. C. Lee and R. H. Holm, *J. Am. Chem. Soc.*, 2008, **130**, 12794–12807.
205. H. Sugimoto, K. Suyama, K. Sugimoto, H. Miyake, I. Takahashi, S. Hirota and S. Itoh, *Inorg. Chem.*, 2008, **47**, 10150–10157.
206. A. Majumdar, J. Mitra, K. Pal and S. Sarkar, *Inorg. Chem.*, 2008, **47**, 5360–5364.
207. M. Draganjac and D. Coucouvanis, *J. Am. Chem. Soc.*, 1983, **105**, 139–140.
208. C. L. Soricelli, V. A. Szalai and S. J. N. Burgmayer, *J. Am. Chem. Soc.*, 1991, **113**, 9877–9878.
209. Z.-Q. Tian, J. P. Donahue and R. H. Holm, *Inorg. Chem.*, 1995, **34**, 5567–5572.
210. B. S. Lim, M. W. Willer, M. Miao and R. H. Holm, *J. Am. Chem. Soc.*, 2001, **123**, 8343–8349.

211. D. V. Partyka and R. H. Holm, *Inorg. Chem.*, 2004, **43**, 8609–8616.
212. M. Takuma, Y. Ohki and K. Tatsumi, *Inorg. Chem.*, 2005, **44**, 6034–6043.
213. *Calixarenes 2001*, ed. Z. Asfari, V. Bohmer, J. Harrowfield and J. Vicens, Kluwer, Dordrecht, 2001.
214. C. D. Gutsche, *Calixarenes: An Introduction*, 2nd edn, Royal Society of Chemistry, London, 2008.
215. Y. Kuroda, Y. Sasaki, Y. Shiroiwa and I. Tabushi, *J. Am. Chem. Soc.*, 1988, **110**, 4049–4050.
216. W. Lo, P. Zhang, C.-C. Ling, S. Huang and R. H. Holm, *Inorg. Chem.*, 2012, **51**, 9883–9892.
217. W. F. DeGrado, C. M. Summa, V. Pavone, F. Nastri and A. Lombardi, *Annu. Rev. Biochem.*, 1999, **68**, 779–819.
218. F. Yu, V. M. Cangelosi, M. L. Zastrow, M. Tegoni, J. S. Plegaria, A. G. Tebo, C. S. Mocny, L. Ruckthong, H. Qayyum and V. L. Pecoraro, *Chem. Rev.*, 2014, **114**, 3495–3578.
219. X. Delaigue, M. W. Hosseini, N. Kyritsakas, A. De Cian and J. Fischer, *J. Chem. Soc., Chem. Commun.*, 1995, 609–610.
220. B. K. Maiti, L. B. Maia, C. M. Silveira, S. Todorovic, C. Carreira, M. S. P. Carepo, R. Grazina, I. Moura, S. R. Pauleta and J. J. G. Moura, *JBIC, J. Biol. Inorg. Chem.*, 2015, **20**, 821–829.
221. K. B. Musgrave, C. E. Laplaza, R. H. Holm, B. Hedman and K. O. Hodgson, *J. Am. Chem. Soc.*, 2002, **124**, 3083–3092.
222. F. Hapiot, S. Tilloy and E. Monflier, *Chem. Rev.*, 2006, **106**, 767–781.
223. M. Zhao, H.-B. Wang, L.-N. Ji and Z.-W. Mao, *Chem. Soc. Rev.*, 2013, **42**, 8360–8375.
224. J. P. Ward, J. M. White and C. G. Young, *Tetrahedron*, 2013, **69**, 8824–8830.
225. S. Mondal and P. Basu, *Inorg. Chem.*, 2001, **40**, 192–193.
226. J. Kofoed and J.-L. Reymond, *Curr. Opin. Chem. Biol.*, 2005, **9**, 656–664.
227. T. Hasenaka, T. Okamura and K. Onitsuka, *Dalton Trans.*, 2015, **44**, 12618–12622.
228. J. J. Berzelius, *Poggendorff's Ann. Phys. Chem.*, 1826, **7**, 262; J. J. Berzelius, *Poggendorff's Ann. Phys. Chem.*, 1827, **8**, 269.
229. A. Thapper, J. P. Donahue, K. B. Musgrave, M. W. Willer, E. Nordlander, B. Hedman, K. O. Hodgson and R. H. Holm, *Inorg. Chem.*, 1999, **38**, 4104–4114.
230. M. Miao, M. W. Willer and R. H. Holm, *Inorg. Chem.*, 2000, **39**, 2843–2849.
231. A. Müller, *Vib. Spectra Struct.*, 1986, **15**, 251–312.
232. A. Müller, E. Diemann and H. Schulze, *Z. Anorg. Allg. Chem.*, 1970, **376**, 120–124.
233. E. Hofer, W. Holzbach and K. Wieghardt, *Angew. Chem., Int. Ed.*, 1981, **20**, 282–283.
234. K. Wieghardt, M. Hahn, J. Weiss and W. Swiridoff, *Z. Anorg. Allg. Chem.*, 1982, **492**, 164–174.
235. S. F. Gheller, T. W. Hambley, P. R. Traill, R. T. C. Brownlee, M. J. O'Connor, M. R. Snow and A. G. Wedd, *Aust. J. Chem.*, 1982, **35**, 2183–2191.

236. P. R. Traill, E. R. T. Tiekkink, M. J. O'Connor, M. R. Snow and A. G. Wedd, *Aust. J. Chem.*, 1986, **39**, 1287–1295.
237. S. Bristow, C. D. Garner and C. J. Pickett, *J. Chem. Soc., Dalton Trans.*, 1984, 1617–1619.
238. J. W. Faller and Y. Ma, *Organometallics*, 1989, **8**, 609–612.
239. J. W. Faller, R. R. Kucharczyk and Y. Ma, *Inorg. Chem.*, 1990, **29**, 1662–1667.
240. H. Kawaguchi, K. Yamada, J. Lang and K. Tatsumi, *J. Am. Chem. Soc.*, 1997, **119**, 10346–10358.
241. S. Trofimenko, *Scorpionates: The Coordination Chemistry of Polypyrazolylborate Ligands*, Imperial College Press, London, 1999.
242. C. Pettinari, *Scorpionates II: Chelating Borate Ligands*, Imperial College Press, London, 2008.
243. C. G. Young, R. W. Gable, J. P. Hill and G. N. George, *Eur. J. Inorg. Chem.*, 2001, 2227–2231.
244. S. C. Drew, J. P. Hill, I. Lane, G. R. Hanson, R. W. Gable and C. G. Young, *Inorg. Chem.*, 2007, 2373–2387.
245. G. Backes, J. H. Enemark and T. M. Loehr, *Inorg. Chem.*, 1991, **30**, 1839–1842.
246. R. Singh, J. T. Spence, G. N. George and S. P. Cramer, *Inorg. Chem.*, 1989, **28**, 8–10.
247. G. N. George, W. E. Cleland Jr., J. H. Enemark, B. E. Smith, C. A. Kipke, S. A. Roberts and S. P. Cramer, *J. Am. Chem. Soc.*, 1990, **112**, 2541–2548.
248. S. C. Drew, C. G. Young and G. R. Hanson, *Inorg. Chem.*, 2007, **46**, 2388–2397.
249. A. A. Eagle, L. J. Laughlin, C. G. Young and E. R. T. Tiekkink, *J. Am. Chem. Soc.*, 1992, **114**, 9195–9197.
250. L. J. Laughlin, A. A. Eagle, G. N. George, E. R. T. Tiekkink and C. G. Young, *Inorg. Chem.*, 2007, **46**, 939–948.
251. S. Thomas, A. A. Eagle, S. A. Sproules, J. P. Hill, J. M. White, E. R. T. Tiekkink, G. N. George and C. G. Young, *Inorg. Chem.*, 2003, **42**, 5909–5916.
252. A. A. Eagle, R. W. Gable, S. Thomas, S. A. Sproules and C. G. Young, *Polyhedron*, 2004, **23**, 385–394.
253. J. P. Hill, L. J. Laughlin, R. W. Gable and C. G. Young, *Inorg. Chem.*, 1996, **35**, 3447–3448.
254. P. D. Smith, D. A. Slizys, G. N. George and C. G. Young, *J. Am. Chem. Soc.*, 2000, **122**, 2946–2947.
255. C. J. Doonan, D. J. Nielsen, P. D. Smith, J. W. White, G. N. George and C. G. Young, *J. Am. Chem. Soc.*, 2006, **128**, 305–316.
256. V. W. L. Ng, M. K. Taylor and C. G. Young, *Inorg. Chem.*, 2012, **51**, 3202–3211.
257. C. Gourlay, M. K. Taylor, P. D. Smith and C. G. Young, *Inorg. Chim. Acta*, 2010, **363**, 1126–1132.
258. C. J. Doonan, N. D. Rubie, K. Peariso, H. H. Harris, S. Z. Knottenbelt, G. N. George, C. G. Young and M. L. Kirk, *J. Am. Chem. Soc.*, 2008, **130**, 55–65.

259. N. R. Pramanik, S. Ghosh, T. K. Raychaudhuri and S. S. Mandal, *J. Indian Chem. Soc.*, 2009, **86**, 564–569.
260. A. Rana, M. Sutradhar, S. S. Mandal and S. Ghosh, *J. Coord. Chem.*, 2009, **62**, 3522–3531.
261. H. Sugimoto, H. Tano, R. Tajima, H. Miyake, H. Tsukube, H. Ohi and S. Itoh, *Inorg. Chem.*, 2007, **46**, 8460–8462.
262. H. Sugimoto, K. Hatakeyama, K. Toyota, S. Tatemoto, M. Kubo, T. Ogura and S. Itoh, *Dalton Trans.*, 2013, **42**, 3059–3070.
263. D. Dowerah, J. T. Spence, R. Singh, A. G. Wedd, G. L. Wilson, F. Farchione, J. H. Enemark, J. Kristofzski and M. Bruck, *J. Am. Chem. Soc.*, 1987, **109**, 5655–5665.
264. G. L. Wilson, M. Kony, E. R. T. Tiekkink, J. R. Pilbrow, J. T. Spence and A. G. Wedd, *J. Am. Chem. Soc.*, 1988, **110**, 6923–6925.
265. G. L. Wilson, R. J. Greenwood, J. R. Pilbrow, J. T. Spence and A. G. Wedd, *J. Am. Chem. Soc.*, 1991, **113**, 6803–6812.
266. R. J. Greenwood, G. L. Wilson, J. R. Pilbrow and A. G. Wedd, *J. Am. Chem. Soc.*, 1993, **115**, 5385–5392.
267. K. R. Barnard, M. Bruck, S. Huber, C. Grittini, J. H. Enemark, R. W. Gable and A. G. Wedd, *Inorg. Chem.*, 1997, **36**, 637–649.
268. C. J. Doonan, Novel cis-Oxo-sulfido-molybdenum Complexes Which Model Molybdenum Hydroxylases, PhD Dissertation, University of Melbourne, 2004.
269. V. W. L. Ng, J. M. White and C. G. Young, *J. Am. Chem. Soc.*, 2013, **135**, 7106–7109.
270. C. J. Doonan, C. Gourlay, D. J. Nielsen, V. W. L. Ng, P. D. Smith, D. J. Evans, G. N. George, J. M. White and C. G. Young, *Inorg. Chem.*, 2015, **54**, 6386–6396.
271. J. Mitra and S. Sarkar, *Dalton Trans.*, 2013, **42**, 3050–3058.
272. J. Mitra and S. Sarkar, *Indian J. Chem., Sect. A.*, 2011, **50**, 401–408.
273. S. Groysman, A. Majumdar, S.-L. Zheng and R. H. Holm, *Inorg. Chem.*, 2010, **49**, 1082–1089.
274. M. Bose, G. Moula, A. Begum and S. Sarkar, *Inorg. Chem.*, 2011, **50**, 3852–3854.
275. C. Gourlay, D. J. Nielsen, J. M. White, S. Z. Knottenbelt, M. L. Kirk and C. G. Young, *J. Am. Chem. Soc.*, 2006, **128**, 2164–2165.
276. C. Gourlay, Model Chemistry Relevant to the Molybdenum Copper Active Site of CO Dehydrogenase, PhD Dissertation, University of Melbourne, 2007.

Subject Index

- acetylene, catalytic/enzymatic hydration of, 84
- active site components challenges, 200–201 dithiolene complexes, 207–208 hydrosulfido-Mo species, 206 mono(dithiolene) complexes, 208–209 mononuclearity post-synthesis, 209–211 oxosulfido- and oxoselenido-Mo(vi) species, 201–206 μ -sulfido bridged oxo-Mo–Cu complexes, 206–207 aldehyde oxidases (AOs), 195
- binding energies (B.E.), 30 bond valence sum (BVS), 30, 31
- carbon monoxide dehydrogenase (CODH), 196 chalcogen-labeled cores, 154–158
- density functional theory (DFT), 85 dichlorophenolindophenol (DCIP), 23
- dimethylsulfide (DMS), 106
- dimethylsulfoxide reductase (DMSOR) family Mo^{VI}O and Mo^{IV} couple, 176–181 Mo^{VI}O₂ and Mo^{IV}O couple, 170–176 Mo^{VI}S(Se-R) and Mo^{IV}S couple, 181–182
- dimethylsulfoxide (DMSO) reduction, 24–27
- dithiolene complexes, 218–219
- dithiolene ligands, synthesis of, 36–42
- dithiolenes, chemical behavior of, 53–57
- bis(dithiolene) W complexes, 86
- DMSO reductase family, 4
- electron paramagnetic resonance (EPR), 197
- electron transfer mechanisms in molybdoenzymes, 78–80 principle, 80–87
- F-cluster, 132
- F-cluster analogues, 136–137
- Fe–Mo–S clusters, 2
- Fe₄S₄-ferredoxins, 2
- frontier orbital interaction (FMO), 85
- functional model development, 116–121
- half-reactions model complexes, 107–116 two-substrate catalytic cycle, 122–124
- N-heterocycles, chemical behavior of, 53–57
- heteroligated cores, 148–150
- heterometallic cores, 137–141
- Hille's classification, 72, 73

- imide–sulfide cores, 151–154
- ligand effects, 121
- M-Cluster, 2, 3
- Michaelis–Menten kinetics, 96–100
- Mo(IV)
- and dimethylpterin, 28
 - and flavin, 28
- Mo and pterin
- pterin-molybdenum redox chemistry, 20–23
 - pterin redox chemistry, 18–20
 - redox processes, 18–33
- Mo-dithiolene complexes
- alkynes, reactions of, 34–36
 - metal polysulfides, reactions of, 34–36
 - synthesis of, 34–36
- molecular orbitals of Moco (LUMO), 85
- molybdenum and tungsten enzymes
- active sites of, 94–96
 - Michaelis–Menten parameters determination of, 101–103
 - oxygen transfer reactions, 103–106
- molybdenum and tungsten model compounds
- role in biology, 69–70
- molybdenum cofactor (Moco), 2
- model systems, 70–78
 - proposed structure of, 17
 - structure of, 70
- tris-molybdenum dithiolene, formation of, 35
- molybdenum hydroxylases
- active sites and model targets, 199–200
 - key discoveries, 196–198
 - overview, 195–196
- molybdenum–pterin complexes, formal oxidation states in, 30–32
- molybdenum (IV) reactions
- with oxidized pterins, 27–30
- molybdoenzymes
- catalytic cycles of, 79
 - two-directional oxo-transfer reaction in, 75
- molybdopterin (MPT), 3, 196
- alternative molybdenum binding modes, 3
- $[\text{MoO}_2(\text{DTC})_2]$, 74
- N-heterocyclic groups, 2
- nitrogenase metalloclusters
- all-sulfide PN-type cores, 144–146
 - cluster assembly mechanisms, 154–158
 - F-cluster, 132
 - F-cluster analogues, 136–137
 - FeMo-cofactor, 133–134
 - heteroligated cores, 148–150
 - heterometallic cores, 137–141
 - imide–sulfide cores, 151–154
 - neutral octanuclear clusters, 146–148
 - nitrogenase superclusters, 137
 - nuclearities and sulfur-voided cubanes, 141–143
 - oxide–sulfide cores, 150–151
 - P-cluster, 132–133
 - synthetic considerations, 134–135
 - synthetic perspective, 131
 - topological analogues, 141
- oxide–sulfide cores, 150–151
- oxo-di- μ -sulfido-Mo^{VI}Cu^I dithiolene complexes, 223–224
- oxo-di- μ -sulfido-Mo^{VI}Cu^I scorpionate complexes, 224–226
- oxo(hydrosulfido)-Mo(IV) complexes, 222–223
- oxosulfido- and Oxo(hydrosulfido)-Mo(V) compounds, 219–222
- oxosulfido-Mo(VI) hard-donor complexes, 217–218

- oxosulfido-Mo(vi) scorpionate complexes, 213–217
- oxo/thiomolybdenum dithiolenes, formation of, 35
- oxygen atom transfer (OAT), 24
- oxygen transfer reactions, enzymes vs. models, 106–107
- P-cluster, 132–133
- pseudo-tetrahedral oxosulfido-Mo(vi) complexes, 212–213
- pterin chemical behavior of, 53–57 irreversible oxidation, 20 irreversible reduction, 20 19 leads, deprotonation of, 29 oxidation states of, 19 reversible redox reaction, 20 tautomerization, 20
- pterin chelating molybdenum complex, 17
- pterin dithiolene complex, 48–49
- pterindithiolene ligand synthesis of cobalt complex, 39
- pterin-inspired model compounds first-generation models, 15 Moco, 10–15 pterin ligand identity, timeline, 16 second-generation dithiolene pterins, 33 third-generation dithiolene pterins, 43
- pterin ligands, non-innocent nature of, 32–33
- pterin-molybdenum redox chemistry, 20–23
- pterin redox chemistry, 18–20
- pyranopterin system, redox state of, 49–52
- quinoxaline, 36
- reactivity ratios, 120–121
- reduced pterins, molybdenum complexes of, 23–24
- retrosynthetic analysis approach, 47–48
- spontaneous pyran ring cyclization, 48–49
- substrate reactivity trends, 121
- sulfite oxidase family, 4, 182–183
- sulfur-containing pterin molecules, synthesis of, 42–43
- synthetic pyranopterin, 44–47
- thiomolybdates, 211–212
- trimethylamine (TMA), 106
- tungsten cofactor (Wco), 2
- tungsten-dependent enzymes unidentified W center, 189–190 $W^{VI}(CO/CN)(SR)$ center, 189 $W^{VI}O(S)$ center, 186–188 $W^{VI}S(Se-R)$ center, 188–189
- tungsten enzymes, 4
- urothione synthesis from pyrazine, 42
- xanthine oxidase (XO), 81
- xanthine oxidase families, 183–185, 185–186 active site components, 200–211
- molybdenum hydroxylase models, 211–226
- molybdenum hydroxylases, 195–200
- xanthine oxidoreductase family, 4
- X-ray photoelectron spectroscopy (XPS), 20, 30